



Micropollutant dissipation at the sediment-water interface by coupling modelling and compound-specific isotope analysis

Guillaume Drouin

► To cite this version:

Guillaume Drouin. Micropollutant dissipation at the sediment-water interface by coupling modelling and compound-specific isotope analysis. Geochemistry. Université de Strasbourg, 2020. English. NNT : 2020STRAH018 . tel-03336238

HAL Id: tel-03336238

<https://theses.hal.science/tel-03336238>

Submitted on 7 Sep 2021

HAL is a multi-disciplinary open access archive for the deposit and dissemination of scientific research documents, whether they are published or not. The documents may come from teaching and research institutions in France or abroad, or from public or private research centers.

L'archive ouverte pluridisciplinaire **HAL**, est destinée au dépôt et à la diffusion de documents scientifiques de niveau recherche, publiés ou non, émanant des établissements d'enseignement et de recherche français ou étrangers, des laboratoires publics ou privés.

École Doctorale Sciences de la Terre et Environnement (ED413)
Laboratoire d'Hydrologie et de Géochimie de Strasbourg (LHyGeS)
UMR 7517 / ENGEES - CNRS

Thèse présentée par :
Guillaume DROUIN

Soutenue le 16 Novembre 2020

Pour obtenir le grade de Docteur de l'université de Strasbourg
Discipline Sciences de la Terre et de l'Univers
Spécialité Géochimie

Micropollutant dissipation at the sediment-water interface by coupling modelling and Compound-Specific Isotope Analysis

THÈSE dirigée par :

M. IMFELD Gwenaël
M. PAYRAUDEAU Sylvain

Directeur de recherche, CNRS (France)
Professeur, ENGEES (France)

RAPPORTEURS :

Mme. SAUVAGE Sabine
Mme. PASSEPORT Élodie

Ingénieure de recherche, ENSAT (France)
Professeure, Université de Toronto (Canada)

AUTRES MEMBRES DU JURY :

M. LANGE Jens
M. FAHS Marwan

Professeur, Université de Freiburg (Allemagne)
Professeur, ENGEES (France)

Aknowledgements/ Remerciements

J'ai eu l'opportunité de réaliser ce travail de doctorat au sein du Laboratoire d'Hydrologie et de Géochimie de Strasbourg (LHyGeS) dans le cadre du projet PolISO, soutenu par l'agence de l'eau Rhin-Meuse et la région Grand-Est (Projet No. 170293). Je souhaite ainsi exprimer ma gratitude envers ces deux institutions ainsi qu'au ministère de la transition écologique et solidaire au travers de l'École Nationale du Génie de l'Eau et de l'Environnement de Strasbourg (ENGEES) pour la formation académique de grande qualité qu'ils m'ont dispensé en formation d'ingénieur et la confiance qu'ils m'ont accordé pour réaliser ces travaux de recherche par la suite.

I would like to acknowledge my supervisors, Gwenaél Imfeld and Sylvain Payraudeau with whom we build this project step by step during these three intense years. Thank you for your unconditional support over the numerous scientific and human challenges we faced.

I would also like to acknowledge the members of the jury for accepting to review this thesis work and help improving it, Dr. Elodie Passeport, Dr. Sabine Sauvage, Dr. Jens Lange and Dr. Marwan Fahs. I would also like to express special thanks to Marwan with whom I was delighted to work with (early in the morning), and who taught me a lot about numerical modelling in environmental sciences.

Boris Droz played a crucial role in the achievement of this thesis work. He was my "sparring-partner" at literally every step of this work and always brought fresh and helpful opinions and ideas to make progress. Moreover, he rigorously (and patiently) introduced me to basic organic chemistry and analytical sciences that helped me a lot in acquiring a complete overview of current and future potentials of environmental sciences. From a personal point of view, I would also like to thank you Boris for all the things you shared with me (office, bicycle, music, opinions, etc.)! I will miss our

working days...

This project was made possible by the hard work of Jenna Lohmann and Margaret Johnson. Both, helped me a lot during their internships with laboratory processing of samples and fruitful discussions on diverse scientific topics and technical issues. I am also especially grateful to Benoit Guyot, Eric Pernin, Thierry Perrone and Agnès Herrmann who provided valuable day to day support at laboratory and on field.

I would also mention the precious help of Anis Younes who provided the original version of the numerical model and spent time to debug it. Collaborations with researchers outside the LHyGeS were also particularly helpful for data acquisition, interpretation and during the writing process. Thus, I would like to sincerely acknowledge Frank Leresche, Thomas Cottineau, Loic Maurer, Dimitri Heintz, Claire Villette for scientific and technical inputs and help. Also, I received a precious help from the local water resource manager Laurent Mergnac (Syndicat des Eaux et de l'Assainissement Alsace-Moselle), the hydrometry team of the DREAL Grand-Est represented for this project by Marc Klipfel, Blandine Fritsch (Chambre d'Agriculture d'Alsace) and farmers harvesting on the Avenheimerbach catchment who committed their selves to help achieving this project.

A thesis work is also made of hundreds of invaluable scientific discussions in the corridors as well as of chit-chats that help overcoming every kind of daily challenges. That being said, all members of the permanent staff of the LHyGeS as well as PhD students and post-doctorate researchers contributed somehow to this work: Jérémy Masbou, Maria De Lourdes Pietro Espinoza, Tobias Junginger, Tetyana Gilevska, Pablo Alvarez-Zaldivar, Fatima Meite, Rungroch Sungthong, Baptiste Baumlin, Charline Wiegert, Sophie Gangloff, Colin Fournet, Dimitri Rambourg, Behshad Koohbor, Aurélie Schulz, Flora Hochscheid, Coralie Ranchoux, Benjamin Jeannot, Andreas Scharmüller, Amélie Aubert, Solenn Cotel, François Lehmann, Benjamin Belfort, Sylvain Weill, Anis Younes, Florence Le Ber, Didier Baumann, Joëlle Duplay, and all others I may unfortunately forget (the list is long!)

Enfin, et non des moindres, je ne saurais remercier en quelques phrases seulement ma compagne, Мария Сивачева, à la hauteur de son soutien. Tu m'as tenu sur le droit chemin du début à la fin, et ce malgré de nombreux sacrifices pour toi. Sans toi ces trois ans de dur labeur auraient eu une tout autre saveur. Je pense aussi évidemment

à mes parents et mes soeurs qui depuis toujours m'ont incité à donner le meilleur de moi même dans ce que j'entreprends.

Résumé en Français

L'utilisation agricole des pesticides à des fins de protection des cultures contre les maladies est répandue à l'échelle planétaire. La fréquence accrue des épisodes de sécheresse liée au réchauffement climatique ainsi que la croissance pérenne de la population mondiale plaident pour une utilisation toujours plus importante des pesticides dans l'agriculture dans les années à venir [Maggi et al., 2019]. Les ressources en eau douce souffrent d'ores et déjà de pollutions par les pesticides de l'ordre du $ng.L^{-1}$ au $\mu g.L^{-1}$ [Fenner et al., 2013]. A ces niveaux, ces pollutions représentent une menace directe pour la biodiversité aquatique [Gupta and Gupta, 2020] et à plus long termes constituent un réel enjeu de santé publique [Kim et al., 2017].

Parmi l'ensemble des compartiments environnementaux pollués par les pesticides, les eaux de surface, et notamment les rivières, sont particulièrement impactées [de Souza et al., 2020]. En effet, les rivières reçoivent simultanément des flux de pesticides depuis les zones agricoles (*i.e.* pollutions diffuses) ainsi que les rejets urbains ou industriels (*i.e.* pollutions ponctuelles) [Masiol et al., 2018]. Alors que leur devenir à l'échelle des surfaces agricoles (*i.e.* sols) est largement décrit dans la littérature scientifique [Leu et al., 2004, Torabi et al., 2020], l'étude de leur dégradation et de leur transport dans les eaux de surface reste fragmentaire [Lewandowski et al., 2019]. Néanmoins, l'interface eau-sédiment (IES) est identifiée comme la zone de réactivité privilégiée à l'échelle des eaux de surface, où micro- (*e.g.* pesticides, molécules pharmaceutiques, etc.) et macro-polluants (*e.g.* nutriments, matière organique, etc.) sont rapidement transformés [Krause et al., 2017].

De la même manière que dans le cas des parcelles agricoles, une approche systémique consistant à coupler caractérisations expérimentales en laboratoire, modélisation du transport réactif et Analyse Isotopique Composé Spécifique (AICS) est un angle d'attaque prometteur pour l'étude du devenir des pesticides à l'IES [Lutz et al., 2017]. Les caractérisations expérimentales des principaux mécanismes de dégradation soutiennent l'identification des facteurs environnementaux qui contrôlent la dégradation des pesti-

cides à l'IES. Aussi, elles fournissent des valeurs de référence utiles à la prédiction de leur devenir environnemental des pesticides [Honti and Fenner, 2015]. La modélisation du transport réactif permet quant à elle d'étudier les relations complexes entre processus de dégradation et de transport à l'échelle des entités environnementales étudiées (*e.g.* nappes phréatiques [Van Breukelen, 2007, Van Breukelen and Rolle, 2012]). L'AICS permet de détecter et quantifier précisément le degré de dégradation des pesticides, indépendamment de leur transport, depuis des mesures *in-situ* ponctuelles [Elsner and Imfeld, 2016]. Finalement, l'utilisation conjointe des données de l'AICS avec les prédictions numériques augmente considérablement la robustesse et les possibilités d'interprétation du devenir des pesticides à grande échelle [Alvarez-Zaldívar et al., 2018]. Cependant, bien que ce couplage méthodologique ait été appliqué avec succès à l'échelle des parcelles agricoles, son application au contexte des eaux de surfaces reste limitée:

- I. Les protocoles expérimentaux normalisés (*i.e.* type OECD) et préconisés pour l'étude des processus de transformation des pesticides (*i.e.* biodégradation, photodégradation, hydrolyse) se révèlent bien souvent non-représentatifs des conditions environnementales réelles à l'IES (*e.g.* physico-chimie typique des eaux de surfaces en milieu agricole avec fortes teneurs en nitrates) [Katagi, 2016]. De plus, le caractère bi-phasique de l'IES (*i.e.* eau et sédiment) complexifie l'interprétation des résultats expérimentaux [Honti et al., 2016]. En somme, les indicateurs de persistance déterminés expérimentalement selon les protocoles OECD, n'apportent qu'une vision biaisée du devenir des pesticides dans les rivières [Honti et al., 2018].
- II. L'effet des processus de transport sur la dégradation des pesticides en rivière reste difficilement appréhendable. Les résultats expérimentaux *ex-* ou *in-situ* constituent une base forte révélant ces effets mais restent associés à des conditions spécifiques, peu représentatives de la diversité des conditions hydrologiques et hydrauliques qui se développent en rivière. D'autre part, le recours aux modèles numériques de transport réactif ne permet pas à l'heure actuelle de capturer précisément cette diversité de conditions et leurs variations temporelles (*e.g.* événements pluvieux transitoires) et spatiales [Boano et al., 2014].
- III. Les méthodes d'analyse de la composition isotopique des pesticides sont récentes et contraintes par des limites analytiques fortes. Les concentrations environnementales en pesticides de l'ordre du $\mu\text{g.L}^{-1}$ dans les cas les plus pollués requiert une étape de concentration des échantillons environnementaux de plus

de 1000 fois [Elsner et al., 2012]. Un tel facteur de concentration requiert nécessairement une étape de nettoyage des échantillons efficace [Bakkour et al., 2018]. Autrement, les effets de matrice (*i.e.* extraction et concentration de la matière organique de l’eau ou du sol extrait) dont le signal est amplifié proportionnellement à celui des pesticides, limitent la mesure de la composition isotopique des pesticides. Enfin, puisque plusieurs processus de dégradation peuvent intervenir simultanément dans les eaux de surface, l’AICS multi-éléments (*e.g.* C et N) pourrait-être envisagé [Hofstetter et al., 2011]. Cependant, des valeurs d’enrichissement isotopique de référence requises pour relier dégradation et variation de la composition isotopique des pesticides sont actuellement indisponibles dans la littérature.

Ces travaux de recherche s’est donc attaché à développer des méthodologies expérimentales, numériques et analytiques répondant aux attentes pré-citées, afin d’améliorer la compréhension du devenir des pesticides dans les eaux de surface. Parmi les pesticides les plus utilisés et quantifiés dans les masse d’eau, le *S*-metolachlor est une molécule phare [Maggi et al., 2019]. Cet herbicide est utilisé en agriculture conventionnelle contre les adventices en pré- et post-levée sur maïs et betterave principalement. Ainsi, le *S*-metolachlor a été utilisé comme molécule témoin pour l’ensemble des développements présentés dans ces travaux de recherche. Les chapitres II à IV présentent une suite de développements méthodologiques de complexité croissante, intégrant étape après étape les résultats précédemment acquis. L’adoption de cette méthodologie hiérarchique s’est révélée efficace pour raffiner progressivement la compréhension du devenir des pesticides à l’IES. En définitive, la méthodologie présentée dans ces travaux de recherche apparaît adaptée à l’obtention de valeurs de persistance d’un large panel de pesticides (*e.g.* plus ou moins hydrophobes et persistants) dans les eaux de surface statiques (*e.g.* lacs, bassins de rétention/dépollution, etc.) et dynamiques (*e.g.* rivières, bassins d’orage, etc.).

Le chapitre I brosse les enjeux sociétaux et scientifiques associés aux pollutions des eaux de surface par les pesticides. Il y est décrit en détails l’état de l’art associé à la compréhension de leur devenir à l’IES.

Le chapitre II présente, en introduction, une section analytique regroupant l’ensemble des éléments relatifs au traitement des échantillons et à l’analyse des concentrations et compositions isotopiques des pesticides. Par la suite, une série de protocoles expérimentaux en microcosmes permettant l’étude des principaux processus de leur trans-

formation en conditions contrôlées, à savoir, l'hydrolyse, la photodégradation et la biodégradation, est présentée. Ce chapitre dresse ainsi, le tableau des contributions respectives attendues dans les eaux de surface de chaque processus de transformation en fonction de la physico-chimie et les caractéristiques physiques du milieu étudié. La synthèse de ces résultats est proposée ci-dessous.

- I. L'hydrolyse du *S*-metolachlor dans des conditions de pH et température représentatives des eaux de surface ($6 < pH < 9$ et $T = 20^{\circ}C$) s'est révélée particulièrement lente (> 200 jours). Cependant, cette étude a révélé le potentiel de l'analyse simultanée des produits de transformations et des changements de signature isotopique pour l'identification des mécanismes de transformation des pesticides. Ainsi, l'hydrolyse du *S*-metolachlor procède par substitution nucléophile d'ordre 2. Bien que l'hydrolyse abiotique soit lente dans l'environnement, les facteurs d'enrichissement issus de cette étude sont importants et peuvent aussi être considérés comme valeurs de références pour l'étude des mécanismes de dégradation du *S*-metolachlor en conditions abiotiques ou biotiques.

- II. La photodégradation directe et indirecte du *S*-metolachlor a été étudiée dans une eau synthétique reproduisant des teneurs en nitrates (20 mg.L^{-1}) et matière organique dissoutes (DOM) ($5\text{ mg}_C.\text{L}^{-1}$) typiques des eaux de surface en contexte agricole. Les mécanismes de photodégradation directe et indirecte ont révélé des cinétiques rapides (demi vie < 7 jours). La présence de DOM a significativement réduit les vitesses de dégradation, tandis que la présence de nitrate a révélé un effet antagoniste à la DOM. L'analyse des produits de transformations a révélé la fonction charnière des radicaux hydroxyls dans la transformation du *S*-metolachlor en présence de nitrates et DOM. La source d'irradiation utilisée a influencé les changements de composition isotopique du *S*-metolachlor. Ainsi, la photodégradation du *S*-metolachlor sous lumière UV (254 nm) a engendré un fractionnement isotopique significatif en C et N de la fraction non dégradée de *S*-metolachlor. Au contraire, l'utilisation d'une source lumineuse simulant la lumière solaire (lampe Xenon) n'a pas généré de fractionnement isotopique significatif du *S*-metolachlor en C et seulement un fractionnement isotopique mineur en N. Ainsi, l'utilisation d'une source lumineuse de type Xenon est préconisée pour évaluer et obtenir des facteurs d'enrichissement isotopique représentatifs des conditions environnementales. Puisque les facteurs d'enrichissements associés à la photodégradation du *S*-metolachlor se sont révélés différents de ceux reportés précédemment pour l'hydrolyse et la biodégradation, l'AICS offre de nouvelles

opportunités pour distinguer les différents mécanismes de transformation à l'IES.

- III. La biodégradation du *S*-metolachlor a été étudiée dans un système eau-sédiment caractéristique de l'IES, en conditions oxiques et anoxiques. Pour prendre en compte les phénomènes de transfert de phase entre le sédiment et l'eau (*i.e.* sorption), un modèle mathématique a été développé, amenant à des valeurs de demi-vies indépendantes du système expérimental (*i.e.* ratio eau:sédiment). Le *S*-metolachlor a été plus rapidement dégradé en conditions oxiques que anoxiques (demi-vies de 31 ± 17 jours contre 59 ± 16 jours, respectivement). L'AICS et la présence d'acide oxalinique comme principal produit de transformation ont suggéré un processus de glutathione transférase comme voie de transformation majoritaire. A l'opposé des valeurs de demi-vie, les facteurs d'enrichissement se sont révélés indépendants du système expérimental, renforçant leur robustesse pour l'évaluation du degré de dégradation d'un pesticide *in-situ*.

Le chapitre III présente l'ensemble des développements numériques conduits au cours de ces travaux de recherche. Les modèles de transport réactif capables de capturer la complexité des flux de polluants à l'IES en rivière reste à l'heure actuelle manquants. Dans ce chapitre les échanges de polluants à l'IES ont été examinés par couplage entre maquette expérimentale de rivière à l'échelle du laboratoire et développement d'un modèle de transport réactif à base physique. Des expériences de traçage avec *NaCl* et Foron Blue 291 (molécules témoins de polluants conservatifs et modérément hydrophobe, respectivement) ont permis d'évaluer l'influence sur le transport à l'IES de la vitesse de l'eau de surface, de l'origine du polluant dans les rivières (*i.e.* sédiment ou eau de surface) ainsi que de la capacité d'un polluant à s'adsorber sur le sédiment. La comparaison des résultats expérimentaux et numériques a révélé la fiabilité du modèle de transport réactif développé. Les taux d'échange de polluant à l'IES se sont révélés indépendants de l'origine du polluant et quasi-proportionnels aux vitesses de l'eau de surface. La distribution de la masse de polluant entre l'eau et le sédiment (*i.e.* sorption) a conduit à stocker dans le sédiment jusqu'à la moitié du polluant initialement injectée dans le système expérimental et à retarder sa propagation vers les couches les plus profondes du sédiment de plus de six fois. La réalisation de cas tests numériques a démontré la capacité du modèle de transport réactif à prendre en compte les effets des flux d'eau verticaux provenant de la nappe ou vers la nappe sur le transport des polluants à l'IES. Enfin, une dernière série de traçage dans la maquette de rivière avec de la caféine (molécule témoins de polluants non-conservatifs) a permis de démontrer le potentiel du couplage expérimental/numérique à étudier de manière systématique

en conditions contrôlées le devenir des polluants dans les rivières.

Le chapitre IV constitue la phase intégrative de ces travaux et tente d'expliquer le devenir du *S*-metolachlor au sein d'un tronçon de rivière (l'Avenheimerbach, 2.2 km) de tête de bassin versant agricole au regard des enseignements issus des chapitres II et III. Une campagne de mesure du *S*-metolachlor en deux points de cette rivière a été conduite durant la saison agricole de 2019 (Mars à Octobre). L'analyse des flux de *S*-metolachlor exportés à travers les deux stations de mesure ainsi que des produits de transformation au cours de la saison ont révélé les voies dominantes de transport du *S*-metolachlor depuis les surfaces agricoles vers la rivière. Ainsi, les événements pluvieux modérés semblent favoriser le transport de sub-surface sur de longues périodes tandis que les événements pluvieux intenses génèrent un apport massif à la rivière par ruissellement de surface sur des périodes courtes. L'analyse des signatures isotopiques du *S*-metolachlor dans la rivière a permis de tracer efficacement l'état des stocks et de dégradation du *S*-metolachlor dans les sols agricoles. Enfin, l'équivalence des compositions isotopiques du *S*-metolachlor mesurées en amont et en aval du tronçon étudié ont révélé l'absence de dégradation significative le long de l'Avenheimerbach. Ainsi, l'AICS appliqué en rivière permet de démontrer la persistance des polluants au sein d'une rivière.

Le chapitre V discute transversalement l'ensemble des éléments présentés dans les principaux chapitres de cette thèse. L'ensemble des procédures expérimentales présentées en chapitre II esquissent une vision synthétique de la dégradation du *S*-metolachlor à l'IES. L'interprétation conjointe des expériences en microcosmes et maquette de rivière ainsi que les enseignements tirés de la modélisation numérique ont révélé l'importance de la sorption et de sa formalisation dans l'étude du devenir des pesticides à l'IES. La tentative de déploiement de l'AICS en rivière a révélé son potentiel à marquer la persistance des pesticides en rivière et a aussi permis d'identifier les principaux verrous conceptuels et analytiques limitant sa capacité à quantifier de faibles degrés de dégradation en rivière. Finalement, les enseignements tirés sur l'ensemble des chapitres de cette thèse quant au comportement du *S*-metolachlor en rivière sont transcrit en termes techniques dans l'optique d'une transmission du savoir aux gestionnaires de la ressource en eau. Ainsi, non seulement ces travaux ouvrent la voie à des recherches futures en termes de développement méthodologiques et numériques, mais aussi offrent une vision concrète des actions qui peuvent être mises en place dans le cadre de la reconquête du bon état des masses d'eau.

Bibliographie

- [Alvarez-Zaldívar et al., 2018] Alvarez-Zaldívar, P., Payraudeau, S., Meite, F., Masbou, J., and Imfeld, G. (2018). Pesticide degradation and export losses at the catchment scale: Insights from compound-specific isotope analysis (CSIA). *Water Research*, 139:198–207.
- [Bakkour et al., 2018] Bakkour, R., Bolotin, J., Sellergren, B., and Hofstetter, T. B. (2018). Molecularly Imprinted Polymers for Compound-Specific Isotope Analysis of Polar Organic Micropollutants in Aquatic Environments. *Analytical Chemistry*, 90(12):7292–7301.
- [Boano et al., 2014] Boano, F., Harvey, J. W., Marion, A., Packman, A. I., Revelli, R., Ridolfi, L., and Wörman, A. (2014). Hyporheic flow and transport processes: Mechanisms, models, and biogeochemical implications. *Reviews of Geophysics*, 52(4):603–679.
- [de Souza et al., 2020] de Souza, R. M., Seibert, D., Quesada, H. B., de Jesus Bassetti, F., Fagundes-Klen, M. R., and Bergamasco, R. (2020). Occurrence, impacts and general aspects of pesticides in surface water: A review. *Process Safety and Environmental Protection*, 135:22–37.
- [Elsner and Imfeld, 2016] Elsner, M. and Imfeld, G. (2016). Compound-specific isotope analysis (CSIA) of micropollutants in the environment — current developments and future challenges. *Current Opinion in Biotechnology*, 41:60–72.
- [Elsner et al., 2012] Elsner, M., Jochmann, M. A., Hofstetter, T. B., Hunkeler, D., Bernstein, A., Schmidt, T. C., and Schimmelpfennig, A. (2012). Current challenges in compound-specific stable isotope analysis of environmental organic contaminants. *Analytical and Bioanalytical Chemistry*, 403(9):2471–2491.
- [Fenner et al., 2013] Fenner, K., Canonica, S., Wackett, L. P., and Elsner, M. (2013). Evaluating Pesticide Degradation in the Environment: Blind Spots and Emerging Opportunities. *Science*, 341(6147):752–758.

- [Gupta and Gupta, 2020] Gupta, S. and Gupta, K. (2020). Bioaccumulation of Pesticides and Its Impact on Biological Systems. In *Pesticides in Crop Production*, pages 55–67. John Wiley & Sons, Ltd.
- [Hofstetter et al., 2011] Hofstetter, T. B., Bolotin, J., Skarpeli-Liati, M., Wijker, R., Kurt, Z., Nishino, S. F., and Spain, J. C. (2011). Tracking transformation processes of organic micropollutants in aquatic environments using multi-element isotope fractionation analysis. *Applied Geochemistry*, 26:S334–S336.
- [Honti et al., 2018] Honti, M., Bischoff, F., Moser, A., Stamm, C., Baranya, S., and Fenner, K. (2018). Relating degradation of pharmaceutical active ingredients in a stream network to degradation in water-sediment simulation tests. *Water Resources Research*, 54(11):9207–9223.
- [Honti and Fenner, 2015] Honti, M. and Fenner, K. (2015). Deriving Persistence Indicators from Regulatory Water-Sediment Studies – Opportunities and Limitations in OECD 308 Data. *Environmental Science & Technology*, 49(10):5879–5886.
- [Honti et al., 2016] Honti, M., Hahn, S., Hennecke, D., Junker, T., Shrestha, P., and Fenner, K. (2016). Bridging across OECD 308 and 309 Data in Search of a Robust Biotransformation Indicator. *Environmental Science & Technology*, 50(13):6865–6872.
- [Katagi, 2016] Katagi, T. (2016). Pesticide behavior in modified water-sediment systems. *Journal of Pesticide Science*, 41(4):121–132.
- [Kim et al., 2017] Kim, K.-H., Kabir, E., and Jahan, S. A. (2017). Exposure to pesticides and the associated human health effects. *Science of The Total Environment*, 575:525–535.
- [Krause et al., 2017] Krause, S., Lewandowski, J., Grimm, N. B., Hannah, D. M., Pinay, G., McDonald, K., Martí, E., Argerich, A., Pfister, L., Klaus, J., Battin, T., Larned, S. T., Schelker, J., Fleckenstein, J., Schmidt, C., Rivett, M. O., Watts, G., Sabater, F., Sorolla, A., and Turk, V. (2017). Ecohydrological interfaces as hot spots of ecosystem processes. *Water Resources Research*, 53(8):6359–6376.
- [Leu et al., 2004] Leu, C., Singer, H., Stamm, C., Müller, S. R., and Schwarzenbach, R. P. (2004). Simultaneous Assessment of Sources, Processes, and Factors Influencing Herbicide Losses to Surface Waters in a Small Agricultural Catchment. *Environmental Science & Technology*, 38(14):3827–3834.

- [Lewandowski et al., 2019] Lewandowski, J., Arnon, S., Banks, E., Batelaan, O., Betterle, A., Broecker, T., Coll, C., Drummond, J. D., Gaona Garcia, J., Galloway, J., Gomez-Velez, J., Grabowski, R. C., Herzog, S. P., Hinkelmann, R., Höhne, A., Hollender, J., Horn, M. A., Jaeger, A., Krause, S., Löchner Prats, A., Magliozzi, C., Meinikmann, K., Mojarrad, B. B., Mueller, B. M., Peralta-Maraver, I., Popp, A. L., Posselt, M., Putschew, A., Radke, M., Raza, M., Riml, J., Robertson, A., Rutere, C., Schaper, J. L., Schirmer, M., Schulz, H., Shanafield, M., Singh, T., Ward, A. S., Wolke, P., Wörman, A., and Wu, L. (2019). Is the hyporheic zone relevant beyond the scientific community? *Water*, 11(11):2230.
- [Lutz et al., 2017] Lutz, S. R., van der Velde, Y., Elsayed, O. F., Imfeld, G., Lefrancq, M., Payraudeau, S., and van Breukelen, B. M. (2017). Pesticide fate at catchment scale: conceptual modelling of stream CSIA data. *Hydrol. Earth Syst. Sci. Discuss.*, 2017:1–30.
- [Maggi et al., 2019] Maggi, F., Tang, F. H. M., Cecilia, D. I., and McBratney, A. (2019). PEST-CHEMGRIDS, global gridded maps of the top 20 crop-specific pesticide application rates from 2015 to 2025. *Scientific Data*, 6(1):1–20.
- [Masiol et al., 2018] Masiol, M., Giannì, B., and Prete, M. (2018). Herbicides in river water across the northeastern Italy: occurrence and spatial patterns of glyphosate, aminomethylphosphonic acid, and glufosinate ammonium. *Environmental Science and Pollution Research*, pages 1–11.
- [Torabi et al., 2020] Torabi, E., Wiegert, C., Guyot, B., Vuilleumier, S., and Imfeld, G. (2020). Dissipation of S-metolachlor and butachlor in agricultural soils and responses of bacterial communities: Insights from compound-specific isotope and biomolecular analyses. *Journal of Environmental Sciences*, 92:163–175.
- [Van Breukelen, 2007] Van Breukelen, B. M. (2007). Extending the Rayleigh equation to allow competing isotope fractionating pathways to improve quantification of biodegradation. *Environmental Science & Technology*, 41(11):4004–4010.
- [Van Breukelen and Rolle, 2012] Van Breukelen, B. M. and Rolle, M. (2012). Transverse Hydrodynamic Dispersion Effects on Isotope Signals in Groundwater Chlorinated Solvents’ Plumes. *Environmental Science & Technology*, 46(14):7700–7708.

Table of content

Aknowledgements/Remerciements	5
Résumé en Français	9
CHAPTER I - General introduction	31
1.1 Pesticide use, worldwide occurrence, threats and regulation.	31
1.2 State of the art: pesticide persistence in surface waters	35
1.3 Multi-scale and multi-tool approaches to assess pesticide fate at the SWI.	43
1.4 Research questions and overall approach of the thesis	53
1.5 Graphical abstract of the thesis work	56
1.6 Publications and author contributions	57
CHAPTER II - Pesticide degradation pathways at the sediment-water interface	75
2.1 Analytical section: Sample processing, Quantification and Compound-Specific Isotope Analysis	75
2.2 Pesticide hydrolysis	85
2.2.1 Introduction	86
2.2.2 Material and Methods	88
Chemicals and Solution Preparation	88
Experimental Setup	88
2.2.3 Results and Discussion	89
Hydrolysis of chloroacetanilides and isotopic fractionation	89
Mechanistic insights from AKIE values and $C-N$ isotope plots	90
2.2.4 Environmental implications	93
2.3 Pesticide photodegradation in agriculturally impacted surface waters . . .	99
2.3.1 Introduction	100
2.3.2 Material and method	102

	Chemicals and preparation of solutions	102
	Experimental Section	103
	Analytical section	104
2.3.3	Results & Discussion	105
	Effects of the Hydrochemistry on the Photodegradation	
	Rates under Simulated Sunlight	105
	Formation of Phototransformation Products	108
	C and N Isotope Fractionation to Trace Atrazine and <i>S</i> -	
	metolachlor Photodegradation	110
2.3.4	Environmental implications	112
2.4	Pesticide oxic and anoxic biodegradation in water-sediment systems . . .	121
2.4.1	Introduction	122
2.4.2	Material and method	123
	Sediment sampling and characteristics	124
	Experimental set-up	124
	Control experiments	125
	Pesticide extraction, quantification and CSIA	126
	Suspected screenings of transformation products	126
	Phase-transfer and biodegradation modelling	126
2.4.3	Results and discussion	127
	Dissipation kinetics and isotope fractionation	127
	Water-sediment phase-transfer and implications for inter-	
	preting degradation kinetics	129
	Water-sediment phase-transfer and implications for inter-	
	preting isotope signature	132
	Pesticide degradation pathways	133
2.4.4	Environmental implications for water-sediment studies	135
CHAPTER III - Pesticide transport at the sediment-water interface		145
3.1	Introduction	146
3.2	The FRT numerical model	148
3.2.1	Governing equations	148
3.2.2	Numerical resolution	151
3.3	Tracer recirculation in bench-scale river channel	152
3.3.1	Experimental setup	152
3.3.2	Conservative and sorptive tracer experiments	153

3.3.3	Data acquisition	154
3.3.4	Experiment conditions	155
3.4	Model validation <i>vs</i> experiment	156
3.4.1	Numerical simulations: Conceptual model, parameterization and domain discretization	156
3.4.2	Comparing numerical and experimental results	158
3.5	Pollutant transport at the sediment-water interface	160
3.5.1	Velocity field in the bench-scale river channel and transport processes	160
3.6	Transport processes governing mass exchange in the bench-scale river channel	162
3.6.1	Understanding and predicting the effect of sorption on mass exchange at the SWI	163
3.7	Towards a comprehensive understanding of hyporheic process at the SWI	165
3.8	Implication and perspectives for conservative and sorptive pollutant trans- port at the SWI	168
3.9	Investigation of the influence of water flow on pollutant degradation . . .	170
3.9.1	Material and Methods	171
	Adjustments to the bench-scale river channel	171
	Experimental conditions	172
	Adjustments to the FRT model	173
3.9.2	Results and discussion	175
	Influence of water flow on the depth of the oxic sediment layer	175
	Influence of water flow on caffeine degradation at the SWI	176
3.10	Implications and perspectives for pollutant degradation at the SWI	179
CHAPTER IV - <i>S</i>-metolachlor dissipation alongside a river reach		193
4.1	Introduction	193
4.2	Material and methods	195
4.2.1	Study site	195
4.2.2	<i>S</i> -metolachlor application	196
4.2.3	Soil, water and sediment collection	197
4.2.4	Chemical analyses	197
4.2.5	Data analysis	198
4.3	Results and discussion	200

4.3.1	Hydrological response and AVB hydrological functioning . . .	200
4.3.2	<i>S</i> -metolachlor sources and export to the AVB	202
4.3.3	<i>S</i> -metolachlor dissipation in the AVB: transport dominates over degradation	206
4.4	Environmental significance and outlook for CSIA use in rivers	213
CHAPTER V - General conclusions		223
5.1	Introduction	223
5.2	Laboratory testing procedures to understand pesticide fate in surface waters	225
5.2.1	General discussion	225
5.2.2	Implications and perspectives	229
5.3	A robust and parsimonious mathematical framework tailored to the stud- ied system	233
5.3.1	General discussion	233
5.3.2	Implications and perspectives	236
5.4	CSIA from molecular to river scales to characterize pesticide fate at the SWI: potential, limits and perspectives.	240
5.5	Perspectives	245
5.6	Implications for water resource managers	248
Appendices		263
CHAPTER A - Supporting information to chapter II		263
A.S1	Photodegradation	263
A.S1.1	List of chemicals	263
A.S1.2	Main Properties of Selected Pesticides and Origin of the Sub- stances Used	265
A.S1.3	Chemical Composition of Irradiation Solutions	266
A.S1.4	Organic Matter Photobleaching	267
A.S1.5	PNA/Pyr Actinometer System	268
A.S1.6	Irradiation conditions and correction of degradation rates . . .	269
A.S1.7	Light Spectrum Homogeneity within the Light-proof Box . . .	270
A.S1.8	Atrazine and <i>S</i> -metolachlor transformation products	271
A.S1.9	Optical properties of chemicals and irradiation solutions . . .	273
A.S1.10	Simulated sunlight characteristics	274
A.S1.11	Prediction of Degradation Rates and Identification of Domi- nant Photodegradation Mechanisms	275

	General methodology	275
	Calculation of Short-lived Reactive Intermediates Steady State Concentrations	275
	Identification of Main Photosensitizers	276
	Calculation of Light Absorption Rates and Screening Fac- tors	279
	Detailed Results	280
A.S1.12	Presentation of Experimental Datasets	281
A.S1.13	Comparison of C and N isotope fractionation during atrazine photodegradation, biodegradation and abiotic hydrolysis . . .	283
A.S2	Biodegradation	289
A.S2.1	Appendices for material and methods	289
	List of chemicals	289
	Sediment sampling and characteristics	289
	Hydrochemistry characterization	291
	Batch sorption isotherm	292
	Mass balance accounting for the phase-transfer process . .	293
A.S2.2	Appendices for results and discussion	298
	Sediment characteristics	298
	Hydrochemistry	299
	Control experiments	300
	Batch sorption experiments	301
	Pesticide dissipations	302
CHAPTER B - Supporting information to chapter III		305
B.S1	Current developments at the SWI	305
B.S2	Sand characterization	309
B.S3	Characterization of FB291 adsorption from the batch equilibrium method – OECD 106	311
B.S4	Compensation of tracer concentrations for evaporation and ion release . .	312
B.S5	Scaling methodology of concentrations for inter-comparison of experiments	313
B.S6	Mesh sensitivity analysis	314
B.S7	Fit of modelled velocities with the log-law profile	315
B.S8	Darcy's velocities calculation	317
B.S9	Characterization of the transport regime with Pe	318
B.S10	Characterization of the transport regime with D_{eff}	319

CHAPTER C - Supporting information to chapter IV	323
C.S1 <i>S</i> -metolachlor applications	323
C.S2 <i>S</i> -metolachlor and main TPs summary of physicochemical properties . . .	325
C.S3 Hydrochemistry of the AVB river measured at S1 and S2	327
C.S4 Example of GC-IRMS chromatogram with soil sample	330
C.S5 Riverbed sediment texture	331
C.S6 Temporal evolution of <i>S</i> -metolachlor concentrations within top soils sur- rounding S1 and S2.	332
C.S7 Test of isotopic signatures shift within the AVB river reach	334
C.S8 Averaged transit time and degradation within the AVB river reach	336
C.S9 Evidences of <i>S</i> -metolachlor release from the riverbed from monitoring of the regional water agency	338
C.S10 Temporal evolution of <i>S</i> -metolachlor concentrations in the riverbed sediment	339
C.S11 Excepted isotope fractionation with increasing residence time	340

List of Figures

I.1	Main interactions of rivers with their surrounding environment	38
I.2	Sediment-water interface (SWI) functioning with intertwined physical, chemical and biological processes and their major controls as well as scientific disciplines involved in the study of pollutant fate at the SWI	41
I.3	Example of naturally occurring stable isotopes often used as environmental tracers	46
I.4	Physics underlying mass-dependant kinetic isotope effects	48
I.5	Graphical abstract of this thesis work	56
II.1	Dual $C - N$ isotope plot for carbon and nitrogen	92
II.2	Observed and predicted half-lives of atrazine and S -metolachlor under simulated sunlight	106
II.3	Transformation products for atrazine and S -metolachlor in DIR254, DIR, NIT, SRFA, and TOT experiments.	109
II.4	Carbon isotope signature as a function of pesticide remaining fraction for acetochlor and S -metolachlor under oxic and anoxic conditions.	128
II.5	Conceptual model of the water-sediment two-phases system	130
II.6	S -metolachlor and acetochlor transformation products (TPs) under oxic and anoxic conditions	134
III.1	Conceptual description of the numerical domain decomposition	149
III.2	Bench-scale river channel setup	153
III.3	Experimental and modelled results for EHF_{NaCL} conditions	159
III.4	Experimental and modelled results for IHF_{FB291}	160
III.5	Simulated streamlines in the domain showing the pumping effect that may be caused by bedforms in rivers	161
III.6	Numerical and experimental distribution of FB291 within the sediment bed after 12 hours under IHF_{FB291} conditions	165

III.7	Effect of upwelling and downwelling velocities on conservative and sorptive pollutant penetration within the reiverbed	167
III.8	Observed and simulated oxygen gradients in the sediment bed under low and high flow	176
III.9	Observed and simulated caffeine concentrations and $\delta^{13}C$ under low and high flow	178
IV.1	Crop distribution and monitoring devices implemented in C1 and C2. Sugar beet (orange) and Maize (yellow) areas were filled with dashed lines when farmers did not provide <i>S</i> -metolachlor data. Grey areas are non-surveyed surfaces on which <i>S</i> -metolachlor was not applied.	195
IV.2	Hyetogramms used for rainfall event identification	201
IV.3	Area normalized daily discharges in S1 vs S2 and daily discharges ratios between S1 and S2	202
IV.4	Cumulative loads exported through S1 and S2	204
IV.5	Area normalized <i>S</i> -metolachlor mass loads in S1 vs S2	207
IV.6	Dissolved <i>S</i> -metolachlor $\delta^{13}C$ values in S1 and S2	209
IV.7	Rainfall, river discharge in S1 and TSS concentrations in S1 and S2, <i>S</i> -metolachlor concentration and stable isotope signatures for rainfall-runoff events 5 to 9 in S1 and S2	212
IV.8	Predicted C and N enrichment during <i>S</i> -metolachlor degradation with increasing water transit time	213
V.1	Schematic representation of the SWI functioning and reactivity	230
V.2	Bottom to top and micro to macro scale methodologies applied in this thesis work.	237
A.S1	Temporal changes of absorbance of the TOT solution caused by organic matter photobleaching	267
A.S2	Spatial distribution of irradiation intensity within the light-proof box . . .	270
A.S3	Adsorption spectra of atrazine, <i>S</i> -metolachlor, nitrates and SRFA at experimental concentrations	273
A.S4	Xenon Arc Lamp absolute light intensity as a function of the wavelength .	274
A.S5	Observed degradation kinetics and Rayleigh plots for carbon and nitrogen for atrazine	281
A.S6	Observed degradation kinetics (A) and Rayleigh plots for carbon (B) and nitrogen (C) for <i>S</i> -metolachlor	282

A.S7	Dual C and N isotope plot for atrazine reflecting contrasted enrichment patterns between biotic oxidative dealkylation by the bacterial strain <i>Rhodococcus</i> sp. NI86/21 [?], abiotic alkaline hydrolysis at pH 12 [?] and photodegradation in agriculturally impacted surface waters, with points representing the C and N enrichments observed in the presence of nitrates and DOM.	283
A.S8	Changes in hydrochemistry during biodegradation experiments	299
A.S9	Half-life dissipation for atrazine, terbutryn, acetochlor, S-metolachlor and metalaxyl under oxic and anoxic conditions in both, the water and the sediment phases	302
B.S1	Sorption isotherm of FB291	311
B.S2	Mesh sensitivity analysis, predicted tracer distribution with coarse and fine mesh and mesh size effect on the predicted tracer mass exchange as measured within the mixing beaker	314
B.S3	Regression plot for the determination of effective diffusivity	320
C.S1	Graphical summary of S-metolachlor application dates	324
C.S2	Example of GC-IRMS chromatogram from soil sample in S1	330
C.S3	Texture triangle of 7 riverbed sediment collected randomly alongside the Avenheimerbach river reach	331
C.S4	Comparison of measured and predicted S-metolachlor soil concentrations around S1 and S2	333
C.S5	Linear regressions for S1 and S2 on $\delta^{13}C$ values <i>vs</i> time	335
C.S6	Validation of the normal distribution of the regression residuals	335
C.S7	Avenheimerbach cross section in S1 and S2	337
C.S8	Avenheimerbach elevation profile between S1 and S2	337
C.S9	Temporal evolution of S-metolachlor concentrations as measured by the regional water agency	338
C.S10	Temporal evolution of S-metolachlor concentrations within the riverbed sediment in S1 and S2	339

List of Tables

II.1	Extraction yields and induced isotope fractionation (liquid-liquid and solid-liquid), analytical reproducibility, detection and quantification limits for GC-MS and GC-IRMS	78
II.2	Physico-chemical properties and chemical structures of the studied pesticides	87
II.3	Degradation rates, half-lives, fractionation factors as well as $AKIE_C$ and $AKIE_N$ values for acetochlor, alachlor, butachlor and <i>S</i> -Metolachlor at pH = 2, 4, 7, 9 and 12 and $T = 20^\circ C$ and $T = 30^\circ C$	91
II.4	C and N isotope fractionation for atrazine and <i>S</i> -metolachlor	111
II.5	Dissipation and degradation half-Lives, Carbone bulk isotopic fractionation factors and apparent kinetic isotope effect for the water and the sediment phases under oxic and anoxic conditions	129
III.1	Hydraulic properties of tracer experiments, description of experimental data used for model validation and simulated equilibrium time and riverbed length	156
III.2	Hydraulic conditions tested and associated average hydrochemical conditions	173
III.3	Hydraulic and reactive parameters for simulation of caffeine degradation in the bench-scale river channel	175
IV.1	Land-use for C1 and C2 catchments and estimated mass of applied <i>S</i> -metolachlor based on farmer surveys	196
A.S1	Main properties of atrazine and <i>S</i> -metolachlor and literature references addressing their photodegradation	265
A.S2	Chemical composition of irradiation solutions	266
A.S3	Irradiation conditions with the Xenon arc lamp and correction factors used to estimate photodegradation rates	269
A.S4	Atrazine transformation products and corresponding structures	271

A.S5	<i>S</i> -metolachlor transformation products and corresponding structures . . .	272
A.S6	Kinetic parameters for formation and consumption of short-lived reactive intermediates	277
A.S7	Comparison of predicted and observed degradation rates and presentation of the predicted contribution of each short-lived reactive intermediates to the overall photodegradation	280
A.S8	Wetland sediment characteristics	298
A.S9	changes from days 0 to 300 of the pesticide remaining fractions and carbon isotope signatures in the control experiment	300
A.S10	Comparison of pesticide sediment partitioning coefficients as derived from the batch sorption experiment and observed during the biodegradation experiments	301
B.S1	Short review of current numerical and experimental developments at the SWI (Continued on the two next pages)	306
B.S2	Sand particle size distribution	309
B.S3	Sand relative composition	310
C.S1	Physicochemical properties of <i>S</i> -metolachlor and its major transformation products	325
C.S2	Hydrochemistry over the entire monitoring campaign measured in S1 and S2	327

Chapter I

General introduction

1.1 Pesticide use, worldwide occurrence, threats and regulation.

Definition - Etymologically speaking, the word "pesticide" is derived from the English word "pest" (meaning insect or undesired animal) and "-cide" which originates from the Latin "-cida" (meaning killer). It refers to any chemical substance used to control or kill insects, small animals and other (micro)-organisms harmful to crops. As defined by the European Food Safety Agency (EFSA) it includes a myriad of different substances from insecticides, fungicides, herbicides, growth regulators, etc., where insecticides refer to substances used to control insect populations, fungicides for fungi and herbicides for vegetables (*e.g.* weeds). When used for crop protection, pesticides may be termed as Plant Protection Products (PPP). Both terms, pesticides and PPP are readily found in the literature.

Pesticide use worldwide - With a rampant population growth and an accelerated urbanization, food production has been increasingly tightening and improved crop protection is pursued via biological, mechanical and/or chemical approaches. Among available practices, pesticides have been long employed as they proved to efficiently reduce crop losses due to pest [Popp et al., 2013]. Inorganic pesticides originating from naturally occurring minerals and plant products (*e.g.* copper, zinc, pyrethrum, etc.) were long used before the 20th century (1st generation pesticides). Organic pesticides mainly synthesized from manipulations of hydrocarbons (2nd generation pesticides) boomed after the second world war [Carson et al., 1962]. Since then, about 4 million tonnes of pesticides were used in 2017 worldwide in the agricultural sector according to the FAO. This amount has been steadily increasing since the early 90s. In Europe, approximately 400 tonnes of the 500 registered pesticides are sold yearly since 2011,

corresponding to application rates varying from 1 to almost 10 kg.ha^{-1} of arable lands, depending on the countries [Eurostat (European Commission), 2017]. In addition to being used by the agricultural sector, herbicides are massively used for industrial purposes and urban amenity areas as a way to control their surrounding environment (*e.g.* weed control on railway tracks, residential settlements or industrial areas) [Sharma et al., 2019]. In the context of climate change leading to intensified water scarcities along with a continued population growth, pesticide use worldwide is likely to increase in the near future [Maggi et al., 2019]. It raises concerns of both, scientific and public communities on the pressing issue of water contaminations by pesticides and indirect derived costs expected to increase accordingly.

Already, the extensive usage of pesticides combined with the intense harnessing of water resources has led to ubiquitous contaminations of freshwaters worldwide, with concentrations ranging from ng.L^{-1} to $\mu\text{g.L}^{-1}$ [Fenner et al., 2013]. As an example, the frequency of insecticide concentrations exceeding local regulatory threshold levels (RTLs – set from ng.L^{-1} to $\mu\text{g.L}^{-1}$) is reported to be higher than 50% in surface waters worldwide [Stehle and Schulz, 2015]. Consequently, adverse effects of pesticides are broads and spread from field to surface and groundwater, thereby affecting the entire food chain, from microbial biodiversity to human health [Schwarzenbach et al., 2006, Vörösmarty et al., 2010]. For instance, in pesticide contaminated soils, microbial activity resulting in N cycling (*e.g.* nitrification, denitrification, ammonification, methanogenesis, etc.) and organic matter (OM) mineralization is weakened, hence delivering to their connected freshwaters, effluents of altered qualities [Hussain et al., 2009]. Later on, in fresh waters, the taxa richness of stream invertebrates is almost halved in the presence of pesticides even at concentrations below the RTLs, hence threatening biodiversity development [Beketov et al., 2013]. Finally, as regards to human health, direct exposure from occupational, agricultural, and household use as well as indirect exposure through digestion of contaminated food (*i.e.* biomagnification and bioaccumulation in fish for examples [Gupta and Gupta, 2020]) correlate with outbreaks of cancers, asthma or even Parkinson’s disease [Kim et al., 2017].

Of particular interest is the chloroacetanilide herbicide ***S*-metolachlor** as it ranks among the top five of most used active ingredients worldwide in maize and sugar beet harvesting [Maggi et al., 2019]. Its racemic mixture (R- and *S*-metolachlor) was banned in Europe in 2002 and enriched the active ingredient *S*-metolachlor. As a consequence, it is detected worldwide at ng to $\mu\text{g.L}^{-1}$ concentrations in surface wa-

ters [de Souza et al., 2020]. It is frequently detected in surface waters due to its moderate solubility and sorptive behaviour with high octanol-water partition coefficient ($\log(K_{ow}) = 3.05$) and a moderate organic carbon-water partition coefficient with soils ($K_{oc} = 120 \text{ L.kg}^{-1}/g_{oc}.g^{-1}$) [Alvarez-Zaldívar et al., 2018, Lefrancq et al., 2017]. However, to the best of our knowledge, no specific studies on *S*-metolachlor dissipation in surface waters have been conducted so far. Accordingly, all experimental procedures were conducted for a mix of pesticides including atrazine, terbutryn, acetochlor, metalaxyl and systematically *S*-metolachlor, with a **special focus on *S*-metolachlor which was transversally studied across the different chapters of this thesis.**

Main regulatory levers - In response to these high exposures to pesticides, globally harmonized and comprehensive pesticide regulations at all levels of the supply chain (*i.e.* registration, usage, labelling, storage, etc.) would enhance the ability to protect the public health and the environment [Handford et al., 2015]. However, high disparities still exist between developed and developing countries with a quarter of African and Southeast Asian countries lacking of such regulations, whereas developed countries already enacted the most severe legislations according to their national priorities and capabilities [Matthews et al., 2011]. On the one hand, at the highest level of the regulation are the restrictions/prohibitions of selected pesticides, but it only comes *a posteriori* to damages. A noteworthy example is the United Nations Environment Programme (UNEP) Stockholm convention on persistent organic pollutants (POPs). It restricted and/or banned the use in 2001 of nine 2nd generation pesticides highly persistent (several years), widespread throughout the environment, strongly bio-accumulative and toxic for human kind (*e.g.* aldrin, chlordane, DDT, dieldrin, etc.). Since then, the list originally adopted was amended several times, bringing to seventeen the number of pesticides currently accounted for. On the other hand, registration procedures constitute *a priori* regulatory measures but strongly differ from one country to the others.

Nonetheless, a striking example of harmonized procedure is proposed by the Organisation for Economic Co-operation and Development (OECD) and relies on normalized tiered testing strategies. Normalized tiered testing assessments enable reliable and inter-comparable environmental risk assessments [Honti and Fenner, 2015]. Finally, slightly aside from the pesticide regulation itself is the individual or collective commitment of nations to achieve reduction of pollution by any suited means. For instance,

the EU Water Framework Directive 2000/60/EC (WFD) was drawn in 2000 as an ambitious and substantial environmental legislation aiming at ecologically and chemically restoring Europe’s waters by 2027. To that end, reduction of surface water contaminations by pesticides arose as a critical aspect to achieve [Carvalho et al., 2019]. However, twenty years after the WFD implementation, progress remain slow and the WFD struggles with the little understanding of water ecosystem complexities, their interactions at different scales as well as monitoring issues [Voulvoulis et al., 2017].

Context of the PolISO project – At European scale, France is a major food producer with about 25% of the total maize, wheat and sugar beet harvested in its territory in 2015 [Eurostat (European Commission), 2017]. This optimized harvesting system is supported by intense use of fertilizers and pesticides, ensuring constant yields and quality of crops. As a consequence, high pesticide concentrations are measured in French ground and surface waters, threatening drinking water resources and aquatic biodiversity [European Environment Agency, 2018]. Along with previously standing water legislations, notably the nitrates directive - 91/676/CEE, the French declination of the WFD imposed from 2009 to the six national water agencies to quickly implement efficient actions aiming at restoring and protecting quality of pre-identified water bodies [Carvalho et al., 2019]. In this context, the Souffel catchment and particularly its uttermost upstream river branch, namely the Avenheimerbach (see map of the Avenheimerbach subcatchment in Chapter IV) was established as a severely impacted water body (bad ecological and chemical status) particularly struggling with high pesticide contaminations. Although first attempts to minimize the impact of agriculture and urban waste water discharges within the Souffel river, good status of the water-body could not be met by 2015 as required by the WFD. Consequently, the EU granted the water agency to postpone the deadline to 2027 considering the ambitious management plan proposed, named “Souffel 2027”. This plan gathers with the water agency, additional local stakeholders including the region Grand-Est, the departmental water resource manager (SDEA - Syndicat des Eaux et de l’Assainissement Alsace-Moselle) as well as the chamber of agriculture. Considering economic and environmental stakes, the plan outlined the need to reduce fertilizer and pesticide use over the whole catchment and to renature the Souffel geomorphology. However, few is known about 1) pesticide source areas and their propensity to migrate toward the Avenheimerbach from field (*i.e.* periods and dominant transport) and 2) the specific role of the Souffel river to attenuate, store or transport downstream pesticides. Accordingly, gaining knowledge on these specific points would help refining and implementing an highly

efficient restoration plan and achieve better water quality by 2027. It mostly relies on the implementation and the evaluation of the potential of Compound-Specific Isotope Analysis (CSIA) and modelling tools at river reach scale to assess pesticide dissipation in the Avenheimerbach. This work falls within the PolISO project (2 PhDs over 4 years) which was financed by the water agency Rhin-Meuse and the region Grand-Est. My PhD thesis, carried out within the PolISO framework, was supported by the French ministry of environment.

1.2 State of the art: pesticide persistence in surface waters

Why focusing on headwater catchments and surface waters? – At catchment scale, surface waters (*e.g.* rivers, ponds, lakes, etc.) constitute the compartment that interacts the most with its ecological environment. It receives water fluxes from precipitations, surface runoff, subsurface flow as well as punctual anthropogenic discharges [Fryirs and Brierley, 2012] (see Figure I.1). As a consequence, surface waters easily integrate pollution from different sources and potentially propagate them to their surrounding compartments [Engelhardt et al., 2014]. Among all surface waters, headcatchment rivers (Strahler order < 2) constitute a specific entity, accounting for almost 96% of the world river number, covering 77% of the world stream length although draining water from small catchments (mean river length $< 3.7\text{ km}$, mean river width $< 1.8\text{ m}$) [Downing, 2012]. Due to their small sizes, low Strahler order rivers are strongly connected to their catchments and their associated anthropogenic activities. It makes them more likely to receive high loads of pollutants (*i.e.* agricultural areas, industrial and urban discharges which may concentrate around lower-order streams, etc.) [Honti et al., 2018, Meyer and Elsner, 2013]. In Switzerland, a national survey conducted from 2005 to 2012 revealed that in low Strahler order rivers, pesticide pollution exceeding the regulatory threshold of $0.1\text{ }\mu\text{g.L}^{-1}$ were 40 times more frequent in rivers with a Strahler order less than two (accounting for $\approx 75\%$ of the national stream length) than in larger rivers [Munz et al., 2013]. In addition, as pollutant travel time from field to surface waters is relatively short as compared with the route from field to groundwater (*e.g.* surface runoff vs leaching), in-field pollutant attenuation is likely mitigated (*e.g.* dilution, degradation or adsorption to soil and aquifer material) while direct transport toward surface waters is favoured. This results in occurrence levels and frequencies of pollution in surface waters generally higher than in groundwaters [Luo et al., 2014]. Malaj et al. (2014) observed that at European scale, sensitive

fish, invertebrate and algae species suffered from acute lethal and chronic long-term effects due to anthropogenic pollution in up to 42% of 4000 monitored surface waters [Malaj et al., 2014]. This clearly illustrates the high sensitivity of surface waters to anthropogenic pollution.

Accordingly, it is of great importance to understand factors controlling pesticide fate at headwater catchment scale to protect biodiversity and human health [Fenner et al., 2013]. To that end, as headwater surface waters are especially prone to pollutant inputs from their surrounding environment, seeking for deep understanding of pesticide inputs in surface waters is a valuable starting point [Ouyang et al., 2017].

Routes of contaminations from catchment to surface waters - Pesticide contaminations in rivers reflect both their application in fields (*i.e.* agricultural areas) and their direct discharge into streams (*i.e.* industrial or domestic effluent discharges). While field applications constitute a diffuse source of pesticides and is generally associated to extended spatial and temporal contaminations at tolerable levels, direct discharges discontinuously bring pesticides into rivers at potentially higher loads [Masiol et al., 2018]. Interestingly, export from both sources are similarly hydrologically controlled [Skark et al., 2004] with surface runoff (*e.g.* from agricultural fields or impervious urban areas) and subsurface flow playing critical roles during wet seasons (*e.g.* from leaching to groundwater in fields or urban drainage) [Chen et al., 2017]. Intense rainfalls generating surface runoff mostly contribute to the total pesticide input in rivers although it represents a minor fraction of the whole period. In contrast, light and moderate rainfall events only generating long term subsurface flow contribute less to the total pesticide input [Alvarez-Zaldívar et al., 2018, Chen et al., 2017, Gerecke et al., 2002, Huber et al., 2000, Skark et al., 2004]. The proportion of pesticides transported from overland flow and subsurface flow is catchment specific and highly depends on soil physico-chemical properties (*i.e.* compaction, texture), the pesticide application date as well as rainfall frequencies, intensities and date of occurrence (*e.g.* long/short after pesticide applications) [Meite et al., 2018]. **It is thus necessary to differentiate from surface runoff and subsurface flow to describe pesticide inputs in surface waters.** While both pathways transport freely dissolved pesticides in surface water, surface runoff also transport soil-bounded pesticides in rivers [Clark and Siu, 2008, Jarsjö et al., 2017]. Mobility of pesticides bounded to soil particles in rivers is then determined by the transport of soil particles themselves (*i.e.* sedimentation, re-suspension, bioavailability, etc.), greatly affecting pesticide fate in streams [Ren and

Packman, 2004a].

Pesticide degradation in surface waters – For organic contaminants, the predominant degradation processes in surface waters include biotic (*e.g.* aerobic and anaerobic microbial biodegradation) and abiotic (*e.g.* chemical hydrolysis, direct and indirect photodegradation) processes [Fenner et al., 2013]. Once in surface waters, pesticides may either be quickly transported downstream and consequently slightly affected by degradation, or undergo intense mixing and degradation within the riverbed or the overlying water [Ciffroy, 2018]. Indeed, in surface waters, the sediment-water interface (SWI) is a recognized hot-spot degradation. While the riverbed sediment mostly hosts biodegradation, shallow overlying water mostly hosts photodegradation [Lewandowski et al., 2019]. In addition, while mixing within the riverbed, pesticides may undergo partitioning onto sediment grains. Then, depending on ambient conditions, the riverbed may either act as a sink (*i.e.* incorporation, adsorption and degradation) or a secondary source of pesticides, releasing fractions accumulated from prior pollution events (*i.e.* desorption, storage in porewater) [Knapp and Cirpka, 2017]. Figure I.1 summarises main interactions identified and studied by the scientific community to date.

Biodegradation - The SWI is characterized by an intense and continuous mixing of surface, subsurface and groundwater caused by hyporheic flow [Boano et al., 2014]. Hyporheic flow drives mass exchanges supplying dissolved oxygen, nutrients and dissolved organic carbon to the riverbed, hence favouring intense biogeochemical activities [Krause et al., 2017, Lewandowski et al., 2019]. Various and steep redox gradients develop at the SWI and support myriads of biochemigeocal processes at high transformation rates (*e.g.* organic matter mineralization, nitrification, denitrification, organic contaminant removal, etc.) [Akbarzadeh et al., 2018, Paraska et al., 2014]. Indeed, from a biological point of view, the narrow stratification of physicochemical parameters at the SWI supports richness and abundance of microbial and macro-invertebrates communities supporting high microbial and enzyme activity within the sediment bed [Brune et al., 2000, Posselt et al., 2020]. Consequently, the SWI has a strong potential to remove a wide panel of organic pollutant from rivers, as already evidenced for fragrances and pharmaceuticals [Jüttner, 1999, Lewandowski et al., 2011]. Mersie et al. (2004) showed that *S*-metolachlor can be biodegraded in both, aerobic (oxidizing conditions) and anaerobic (reducing conditions) sediment bed with an average half-life value of 34 days ($k = 2 \cdot 10^{-7} \cdot s^{-1}$, aerobic sediment progressively shifting

to anaerobic in 30 days) [Mersie et al., 2004]. In addition, from a theoretical perspective, the presence of oxygen (O_2/H_2O , $E^0 = +818\text{ mV}$) in aerobic conditions is most likely a favourable energetic situation for microorganisms leading to the quickest degradation rates. These rates are decreasing along the sequence of terminal electron acceptors developing under anaerobic conditions (sulphate reduction or methanogenesis, CO_2/CH_4 , $E^0 = -244\text{ mV}$) [Sims and Kanissery, 2019].

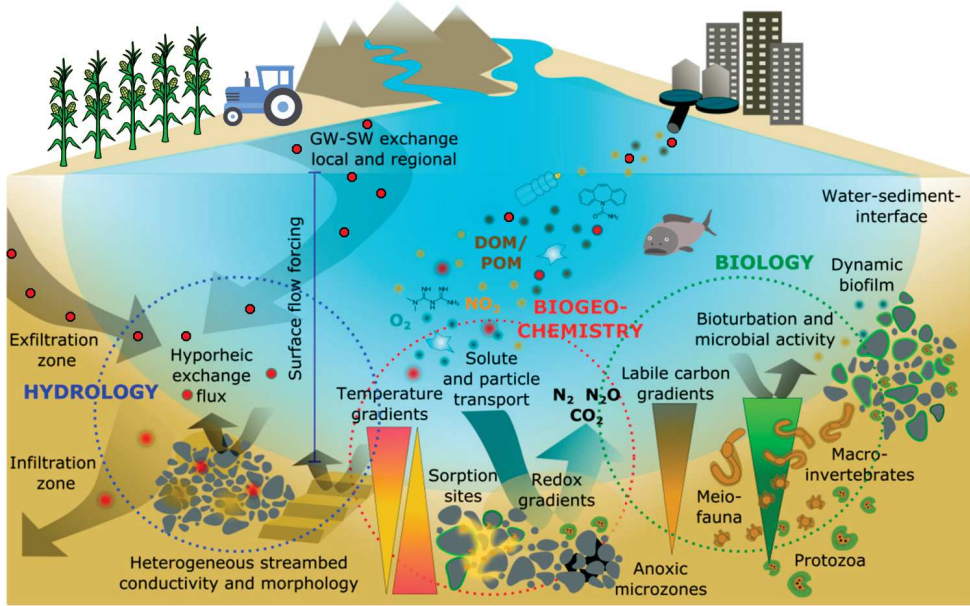


Figure I.1 – Main interactions of rivers with their surrounding environment. Shaded arrows represent water fluxes entering and leaving rivers. Pesticides are represented by red dots and macro-pollutants (e.g. nutrients, organic material) by yellow to brown dots. Main degradation processes represented within the dotted circles locate at the sediment-water interface. GW: groundwater, SW: surface water, DOM: dissolve organic matter, POM: particulate organic matter. Adapted from [Lewandowski et al., 2019].

Photodegradation - Direct and indirect photodegradation is restricted to the upper part of the overlying water directly exposed to sunlight [Fono et al., 2006]. As a matter of fact, in Prairie potholes lakes, direct and indirect photodegradation proved fast degrading processes for myriad of pesticides including metolachlor ($10^{-6} < k < 10^{-4}\text{ s}^{-1}$) [Zeng and Arnold, 2013]. Nonetheless, a direct extrapolation to different environmental conditions is hampered as photodegradation mechanisms are affected

by the presence of dissolved ions (*i.e.* nitrates, carbonates and DOM) which may either act as inhibitors or sensitizers of photodegradation [Remucal, 2014]. In addition, laboratory procedures to study photodegradation are highly sensitive to experimental conditions, which may lead to biased pesticide photodegradation rates (*e.g.* UV light *vs* solar light) [Willach et al., 2018].

Abiotic hydrolysis - Chemical hydrolysis can theoretically occur throughout the whole SWI, either in the overlying water or in the sediment porewater. Chemical hydrolysis of pesticides highly depends on pH and temperature [Katagi, 2002]. At typical pH of world rivers ($6 < pH < 8.2$) [Meybeck, 2003] at $20^{\circ}C$, acetanilides, including *S*-metolachlor, recently revealed unaffected by abiotic hydrolysis, with a DT_{50} higher than 200 days ($k < 10^{-8} s^{-1}$) [Masbou et al., 2018]. Nonetheless, hydrolysis may also be biotically-mediated at higher degradation rates and reflect similar characteristics (*e.g.* transformation products formation, isotope fractionation) than abiotic hydrolysis [Meyer et al., 2009]. Thus, characterisations of abiotic hydrolysis as a surrogate of biotic-hydrolysis is worthy.

Formation of transformation products - Worth of note, pesticide degradation in surface waters leads to the formation of transformation products (TPs) that are often more polar and generally hydrophilic than their parent compounds (PCs), thereby increasing their potential to reach underground drinking water resources [Fenner et al., 2013]. Notably, non-selective radical reactions and rearrangements involved in photodegradation have a strong propensity to produce plethora of TPs. This has been exemplified with the formation of more than 10 very persistent TPs during *S*-metolachlor photodegradation [Dimou et al., 2005, Gutowski et al., 2015]. In the case of *S*-metolachlor biodegradation in sediment, the formation of *S*-metolachlor oxalinic acid (OXA) was indicative of aerobic conditions while *S*-metolachlor ethanesulfonic acid (ESA) could be produced in aerobic and anaerobic conditions, though in minimal amounts [Mersie et al., 2004]. Besides, a precise characterization of patterns of TPs formation for each relevant degradation process may prove useful in pinpointing pesticide route of degradation and transport toward rivers. For instance, as previously demonstrated at field scale, the dominating presence of OXA in rivers is indicative of transport via surface runoff while ESA characterizes slower flowpaths such as subsurface flow [Lefrancq et al., 2017].

However, although *S*-metolachlor biodegradation in soils has already been extensively

studied, knowledge on biodegradation mechanisms in fully saturated sediment bed remain scarce [Accinelli et al., 2001, Anhalt et al., 2000, Katagi, 2004]. Also, mechanistic investigations focusing on photodegradation mechanisms in agriculturally impacted surface waters with high nitrate and dissolved organic carbon (DOC) concentrations are still lacking [Remucal, 2014].

The crucial control of hyporheic flow on pesticide fate within surface waters -

At river scale, hyporheic flow (*i.e.* horizontal and vertical water flows within and across the SWI) is driven by hydrostatic forces (*i.e.* pressure gradients developing across the SWI) [Cardenas and Wilson, 2007b] and hydrodynamic forces (*i.e.* turbulent motion from the overlying water crossing the interface) [Grant and Marusic, 2011]. While the first one controls both hydro- static and -dynamic forces at spatial scale ranging from cm to km, hydrodynamic forces only scales over the first mm of sediment bed below which turbulences vanish [Boano et al., 2014]. Hydrostatic forces arise from natural geomorphologic structures at catchment scale (*e.g.* steepening channel slope, meanders, in-stream gravel bars, etc.) [Binley et al., 2013, Dwivedi et al., 2018, Trauth et al., 2015] as well as anthropogenic obstacles (*e.g.* dams, steps, weirs etc.) [Briggs et al., 2012, Hester et al., 2009, Menichino and Hester, 2014] which locally generate head gradients alternatively forcing water to leave and return into the sediment bed from the overlying water [Hester and Doyle, 2008]. At regional scale, vertical hyporheic flow may also be generated by head gradients arising from water height differences between the water surface and the water table [Binley et al., 2013]. At sediment bed scale, overlying water flowing over bed forms (*e.g.* dunes, pool riffles, coarse gravel bed, instream wood, etc.) also generates oscillatory pressure gradients favouring hyporheic flow at a centimetre spatial scale in a process referred to as “pumping flow” [Cardenas and Wilson, 2007a, Elliott and Brooks, 1997a, Kaufman et al., 2017, Mutz et al., 2007, Packman et al., 2004].

The variety of mechanisms involved in hyporheic flow genesis makes it highly dynamic. On the one hand, alongside river reaches, spatial heterogeneity of the sediment bed with alternatively low and high permeable sediments (*e.g.* fine/clogged sand *vs* gravel), gentle and steep slopes (*e.g.* headwater *vs* plain rivers) or even with or without bed-forms would lead to varying magnitude of hyporheic flow [Binley et al., 2013, Elliott and Brooks, 1997b, Jin et al., 2019]. On the other hand, for a specific river reach with a stable geometry, temporal variability may arise from hydrogeological forcing. For instance, hyporheic flow increases as a function of increasing overlying water velocities

and turbulences penetrating within the riverbed [Voermans et al., 2017]. In addition, the temporally delayed responses of river stages and water table height to precipitations may exacerbate upwelling or downwelling fluxes, hence favouring or hampering hyporheic exchanges [Byrne et al., 2014].

Contaminant mixing and degradation within the SWI is intrinsically related to hyporheic flow, and *de facto* displays similar spatial and temporal variabilities as depicted in Figure I.2 [Flipo et al., 2014].

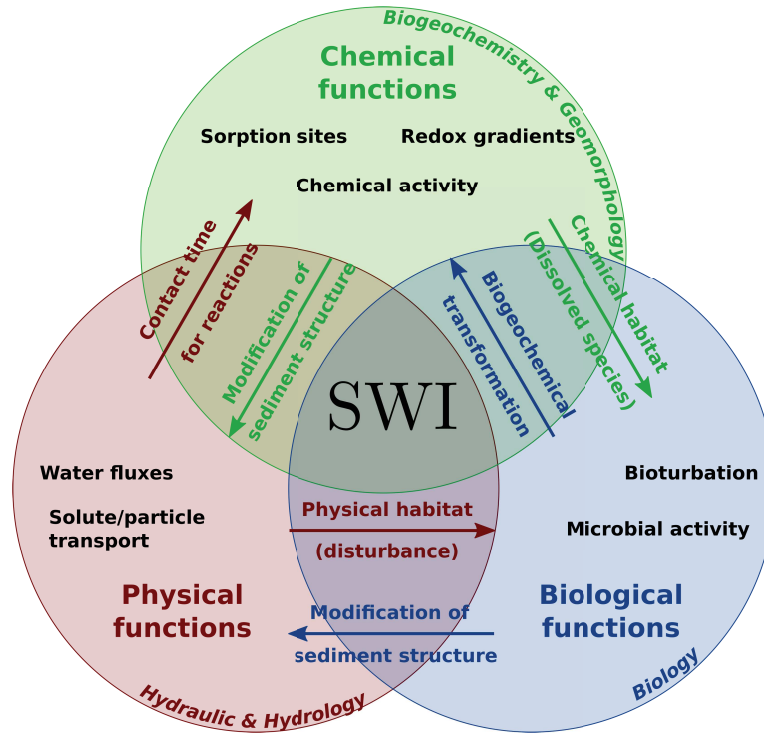


Figure I.2 – Sediment-water interface (SWI) functioning as a location of intertwined physical, chemical and biological processes (referred as "functions" and detailed alongside the arrows) with their major controls (black writing) and disciplines involved (color writing alongside the circles). Adapted from [Ward, 2016, Lewandowski et al., 2019].

The extent of redox gradients developing within the SWI and controlling biodegradation are affected accordingly. Hindered hyporheic flow with low sediment permeability can reduce microbial diversity and activity within the SWI [Nogaro et al., 2013]. In groundwater-fed rivers, nitrate removal within the sediment bed was inhibited under upwelling conditions due to a depleted organic matter apportionment from surface

water, whereas it was favoured at higher river stages promoting more intense mixing of surface water within the sediment bed [Byrne et al., 2015, Lansdown et al., 2015]. At the sediment bed scale, the availability of dissolved oxygen is usually limited to the first mm or cm of sediment bed [Shrestha et al., 2016]. Dissolved oxygen availability is, however, enhanced in the presence of bedforms and with increasing flow, leaving potential for both aerobic and anaerobic microbial processes [Brune et al., 2000, Kaufman et al., 2017]. In addition, further interactions such as contaminant partitioning (*i.e.* sorption) onto the sediment grain surfaces also affect contaminant mixing at the SWI [Eylers et al., 1995]. Rivers with slow overlying water velocities and sediment bed with elevated fraction of organic carbon (f_{oc}) revealed delayed penetration within the sediment bed or even immobilized contaminant at the top of the sediment bed [Ren and Packman, 2004b]. Together with increased biological activity at river bottom, sorption was conjectured to increase residence time and thus transformation of organic contaminants at the SWI [Liao et al., 2013]. In contrast, geochemical and biological activities at the SWI affect hyporheic flow and consequently the SWI degradation potential through sediment clogging by fine particle deposition [Jin et al., 2019] or biofilm formation limiting porewater velocities [Vervier et al., 1992]. Figure I.2 exemplifies existing feedback existing on pollutant transport at the SWI between hydraulic forcing, geochemical and biological activities concomitantly developing at the SWI. Due to this complexity, to our knowledge, no systematic relationships between hyporheic flow and pesticide degradation potential at the SWI have been established yet.

1.3 Multi-scale and multi-tool approaches to assess pesticide fate at the SWI.

The previous description of pesticide fate at the SWI underscored the complexity and the intertwined character of involved processes. Degradation processes are co-occurring at the SWI and are spatially distributed between the overlying water (*e.g.* photodegradation), the oxic and anoxic layers (*e.g.* aerobic/anaerobic biodegradation) and the redox gradients (*e.g.* hydrolysis) developing in the riverbed. Meanwhile, complex transport processes control both, the oxic zonation within the riverbed (*i.e.* interactions at multi-scales and temporal variations), as well as the pesticide penetration and contact time with the highly reactive layers of the SWI. Thus, investigating pesticide fate in rivers requires to understand the scale-dependant transport and degradation processes that lead to the observed high reactivity of the SWI [Krause et al., 2017]. To that end, coupling laboratory and modelling approach is a first-class combination to mechanistically investigate pesticide fate at the SWI. [Lewandowski et al., 2019].

Laboratory conceptualization of the SWI functioning under static (*i.e.* individual degradation processes) and dynamic (*i.e.* transport and degradation processes together) conditions may also support field investigations [Soulsby et al., 2008]. A physically-based modelling approach coupled with CSIA can support the interpretation of laboratory experiments as well as pesticide fate assessment at river scale [Van Breukelen, 2007b, Alvarez-Zaldívar et al., 2018]. In the following section we highlight currently available experimental and numerical methods that can be applied in the future to assess pesticide fate at the SWI.

Mechanistic investigation of degradation under static conditions - In multifactorial systems such as the SWI, pesticide persistence assessment and exposure modelling requires a specific characterisation of individual degradation processes affecting pesticide fate. To date, the OECD tier-testing strategy offers a unique way to achieve the relevant characterizations needed to assess pesticide fate in static surface waters. It presents different laboratory standardized procedures to provide a comprehensive understanding of pesticide fate in the environment as well as a consistent set of parameters for pesticide fate modelling [Honti et al., 2018]. For instance, the OECD 308 test [OECD, 2002] simulates shallow and deep static surface waters, respectively associated with aerobic and anaerobic conditions. The OECD 316 test [OECD, 2008] is intended to derive direct photodegradation behaviour in surface waters. The OECD

111 test [OECD, 2004] focuses on abiotic hydrolysis as a function of pH. Although these protocols are convenient to assess pesticide fate in surface waters (*i.e.* derive specific DT_{50} , monitor and identify TPs, etc.), they are particularly expensive (≈ 100 k€/molecule), long (> 3 months) and raise concerns about their representativeness of surface water conditions [Honti and Fenner, 2015, Katagi, 2016].

The main concern on the OECD 308 protocol incriminates the design of the test system (*i.e.* a sediment layer overlaid by water with a volume ratio comprised between 1 : 3 to 1 : 4). It is thought to influence the observations and hamper a strict characterisation of isolated processes. The rapid consumption of oxygen within the first mm of the riverbed favours the simultaneous occurrence of aerobic and anaerobic degradation. Besides, the diffusion of pesticides within the sediment bed blurs the limits between actual degradation and dilution. Finally, the excess of sediment over water as compared with natural surface waters abnormally shifts the mass distribution toward the sediment phase [Shrestha et al., 2016]. Thus, concentrations from the overlying water most likely reflect the contaminant dissipation rather than its actual degradation. This may lead to overestimations of process-specific degradation half-lives [Ericson et al., 2014]. Nonetheless, recent improvements of this experimental procedure includes homogenised systems instead of separated sediment and overlying water and adapted sediment-water ratio to avoid excessive sorption. This system is accompanied with a specific mathematical framework dedicated to interpret data allow for a more systematic and robust derivation of system-independent and process specific degradation rates [Honti et al., 2016]. Detailed implications on this specific issue are described in the recent suite of papers: Honti and Fenner (2015), Shrestha et al. (2016), Honti et al. (2016) [Honti et al., 2016, Honti and Fenner, 2015, Shrestha et al., 2016]. As regards to the OECD 316 protocol, the main concern lies in the fact that direct and indirect photodegradation mechanisms are not studied separately in laboratory. Thus, capturing the effects of varying DOM, nitrates, carbonates and dissolved oxygen concentrations on the extent of direct and indirect photodegradation is hardly achievable in actual riverine systems from these laboratory characterizations [Remucal, 2014].

Experimental gaps of knowledge - Available normalized experimental protocols aiming at providing primary information on pesticide behaviour at the SWI are facing representativeness and complexity issues [Katagi, 2016]. Although pesticides mostly originate from agricultural areas, typical hydrochemistry of agriculturally-impacted surface waters is not accounted for when studying photodegradation [Remucal, 2014]. In addition, within the bi-phasic system which represents the SWI, the effect of phase partitioning on the quantification of pesticide persistence has been introduced recently [Honti and Fenner, 2015], questioning the validity of previously derived persistence indicators.

Accordingly, a key solution toward improved characterizations of pesticide fate at the SWI is to seek for system-independent indicators (i.e. degradation vs dissipation half-lives), exclusively encompassing pesticide degradation regardless dilution processes (i.e diffusion, advection and phase partitioning) and variations in environmental conditions [Elsayed et al., 2014]. To that end, CSIA may prove relevant [Maier et al., 2016].

Identification of exclusive degradation footprints with compound-specific isotope analysis (CSIA) - In environmental geochemistry, natural and anthropogenic stable isotopes are relevant tracers of contaminant fate that capture molecular scale transformation mechanisms occurring in large scales environmental systems (*i.e.* catchment, rivers, etc.) [Kendall and Caldwell, 1998]. Complementary to the usual concentration and transformation products (TPs) analyses, compound-specific isotope analysis (CSIA) allows to follow-up the isotopic composition of organic pollutants in the field. This approach is currently used to identify contaminant sources, to evidence the occurrence of degradation independently from dilution processes (*i.e.* diffusion, advection, sorption, volatilization, etc.) as well as to quantify the extent of degradation in field [Hunkeler et al., 2008]. A recent demonstration of this versatility is emphasised by the ability of environmental stable isotopes to identify nitrate processing (*i.e.* molecular scale), sources (*i.e.* field scale) and transport pathways to rivers (*i.e.* sub-catchment to catchment scale) at the scale of highly dynamic large catchments (Bode catchment, Germany - $3200km^2$) [Mueller et al., 2016].

Isotopes are atoms of the same element that have different number of neutrons (neutron number N) and the same number of protons (atomic number Z) (see Figure I.3). While

both unstable (*i.e.* radioactive – isotopes with no fill in Figure I.3) and stable isotopes (isotopes with a fill pattern) naturally occur in the environment, stable isotopes are of greatest interest for contaminant fate assessment. In general, it exists two dominant stable isotopes naturally occurring for each atom, with average terrestrial abundance from 1:22 for $^{34}\text{S}/^{36}\text{S}$ to 1:6410 for $^2\text{H}/^1\text{H}$. The isotopic composition of an organic compound is usually reported in δ values and expressed in ‰, as expressed in Eq.I.1:

$$\delta^h X = \left(\frac{R_s}{R_{std}} - 1 \right) \cdot 1000 \quad (\text{I.1})$$

R denotes the ratio of heavy to light isotopes of element X ($R = \frac{^hX}{^lX}$) within the measured sample (R_s) or in a standard material (R_{std}). The normalisation of measurements to a reference material allows for inter-comparison of results obtained in different laboratories (*e.g.* atmospheric nitrogen standard for $\delta^{15}\text{N}$ or the heavy to light ratio of carbon contained in the shell of a cretaceous marine fossil for $\delta^{13}\text{C}$) [Mariotti, 1983].

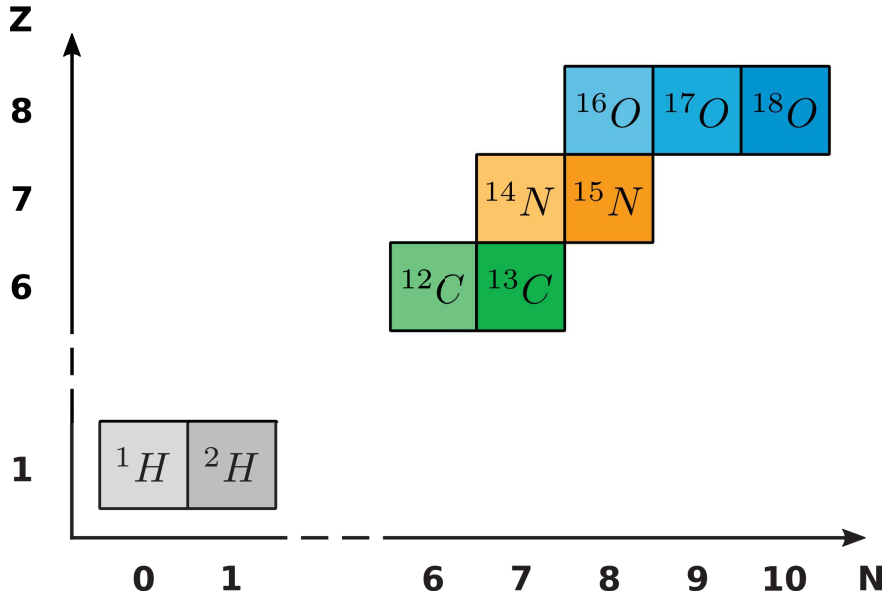


Figure I.3 – Example of naturally occurring stable isotopes often used as environmental tracers. N and Z stand for the number of neutrons and protons respectively. Light and heavy isotopes are filled with light and bright colors, respectively.

Isotopes with the highest number of neutrons are heavier (*i.e.* termed heavy isotopes such as ^{13}C or ^{15}N) than the ones with the lowest number (*i.e.* termed light isotopes such as ^{12}C or ^{14}N), resulting in slightly different bonding strength to other atoms

(Figure I.3) [Sharp, 2017]. These slight differences in bonding strength are responsible for mass-dependant kinetic isotope effect (KIE) accompanying chemical and biological reactions (Figure I.4). The KIE mostly leads to preferential degradation of organic compounds containing light isotopes, resulting in a progressive enrichment of the non-degraded fraction of organic compound in heavy isotopes [Elsner, 2010]. Even more than a footprint of the occurrence of degradation, changes in isotopic composition of an organic compound can even be related to the extent of degradation a compound undergone. To that end, the Rayleigh equation (Eq. I.2) is used to link degradation-induced isotopic shifts with the extent of degradation in closed systems [Rayleigh, 1896].

$$\frac{R_t}{R_0} = \frac{\delta^h X_t + 1}{\delta^h X_0 + 1} = \left(\frac{C_t}{C_0} \right)^\epsilon \quad (\text{I.2})$$

Variables with the subscript t and 0 refer to the present and initial states. $\frac{C_t}{C_0} = f$ refers to the non degraded and remaining fraction of the organic compound at time t and ϵ is the enrichment factor expressed in ‰. In addition, isotope fractionation and enrichment factors are mechanism- and molecule-specifics [Elsner et al., 2005]. Thus, ϵ values have to be experimentally determined in laboratory for each molecule and degradation pathway of interest.

The applicability of the Rayleigh equation relies on the assumption of a closed and well mixed system which may not be fulfilled in the environment. In heterogeneous aquifers, hydrodynamic dispersion causes contaminant molecules to be exposed to different travel time and the original closed-system Rayleigh equation becomes unappropriated to directly assess degradation extent [Hunkeler et al., 2008]. Still in aquifers, competing degradation pathways simultaneously or phase-occurring (*e.g.* aerobic *vs* anaerobic degradation, sorption and formation of non-extractable residues) also break the closed-system assumption [Van Breukelen, 2007a]. Under such conditions, direct estimations of degradation extents in natural environments requires an extension of the original Rayleigh equation. For instance a dilution factor may be used to account for dispersion of pollutant alongside its transport (see Eq. I.3) or an equivalent ϵ value may be used to account for co-occurring degradation processes (see Eq. I.4). Thus, at the SWI similar corrections are needed.

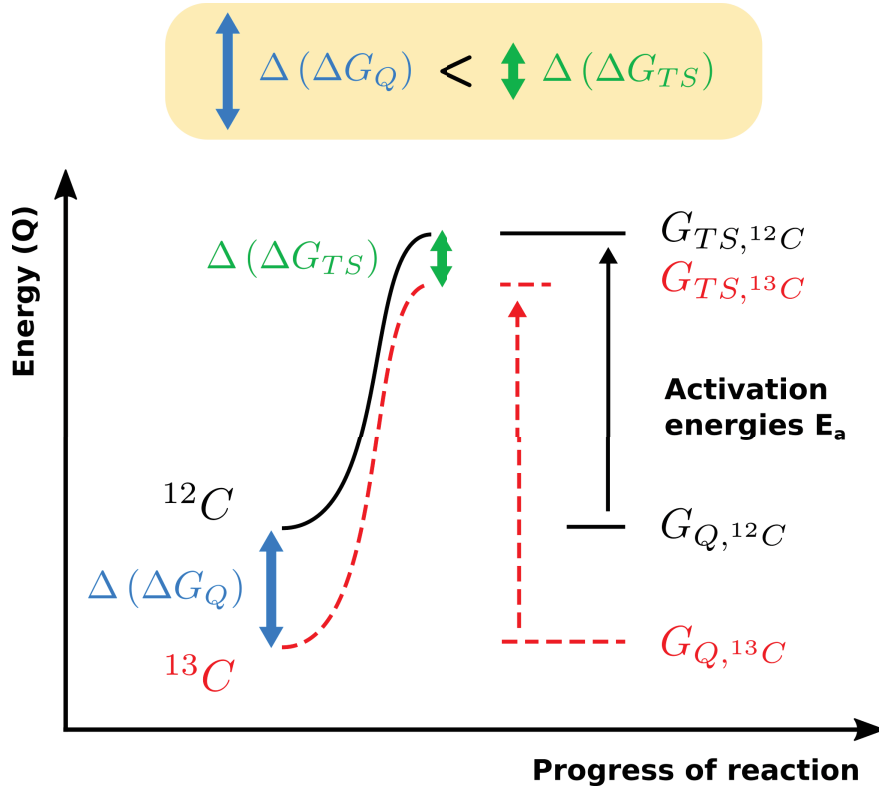


Figure I.4 – Physics underlying mass-dependant kinetic isotope effects. Heavier isotopologues have lower ground state energies G_Q than the lighter ones and require higher activation energies to reach their transition state G_{TS} . KIE occurs solely at the rate limiting step. This illustration exemplify the case of a one step reaction (e.g. SN-2) constituting the rate-limiting step. Adapted from [Elsner, 2010]

$$\frac{R_t}{R_0} = (f \cdot F)^\epsilon \quad (\text{I.3})$$

$$\frac{R_t}{R_0} = f^{\left(\frac{k_1 \epsilon_1 + k_2 \epsilon_2}{k_1 + k_2}\right)} \quad (\text{I.4})$$

with F the dilution factor undergone by the pollutant from its source to the measurement location. k_i and ϵ_i refer respectively to the degradation rates and the enrichment factors of degradation processes i with for instance $i = 1$ for biodegradation and $i = 2$ for photodegradation in the overlying water.

Analytical gaps of knowledge - Although petroleum and chlorinated hydrocarbons CSIA is a time-tested method that can provide strong line of evidence of contaminant degradation in environmental systems at varying temporal and spatial scales [Meckenstock et al., 2004], pesticide CSIA is a relatively new field of investigations which still struggles with analytical and conceptual challenges [Elsner and Imfeld, 2016]. From an analytical point of view, the resolution of gas- or liquid-chromatography (LC or GC) and the sensitivity of isotope-ratio mass spectrometers (IRMS) limit field applications. First, while hydrocarbons may be found in the environment at $g.L^{-1}$ concentrations, pesticides mostly range 10^{-6} to 10^{-9} order of magnitudes below. In addition, as both heavy and light isotopes must be quantified with high precision (*e.g.* $^{13}C/^{12}C \approx 10^{-2}$), for instance compound-specific carbon isotope analysis is only possible for compound concentrations typically two or three orders of magnitude larger than for conventional analysis of organic compound concentrations [Elsner et al., 2012]. This is even more limited for 2H or ^{15}N whose relative abundance and relative mass in pesticides are lower than for carbon. Second, the presence of complex matrices hardly separated from the organic compounds in environmental samples may bias the isotope analysis [Elsner et al., 2012, Bakkour et al., 2018]. Besides, from a conceptual point of view, enrichment factors of pesticides characterizing relevant degradation mechanisms (*e.g.* enzymatic degradation, photodegradation) occurring in surface waters are mostly lacking [Elsner and Imfeld, 2016]. In addition, in context where co-occurring degradation mechanisms exist, multi-element CSIA (mostly N and C) becomes vital to accurately quantify degradation and should be further developed for pesticides [Hofstetter et al., 2011]. Altogether, CSIA appears promising to track pesticide fate at river scale but has not been applied yet.

To our knowledge no analytical correction of the Rayleigh equation exists for surface waters due to the system complexity, with dilution and co-occurring degradation processes as well as the existence of steep redox gradients gradually segregating aerobic and anaerobic degradation. Complementarily, physically-based reactive transport modelling, handling transport induced fractionation (*e.g.* dispersion, multiple flow path mixing) may be a more versatile and promising way to extend CSIA to new environmental compartments, including surface waters [Van Breukelen and Rolle, 2012, Lutz et al., 2013].

Numerical modelling to resolve the interplay between pesticide transport and degradation under dynamic conditions - While the pre-cited experimental designs at the laboratory scale are suited to reproduce pesticide dissipation in static surface waters, they fail to explain and predict dissipation patterns observed in rivers, mostly because of complex interactions between transport and degradation processes under dynamic conditions [Honti et al., 2018]. In addition to experimental characterizations, the effect of hyporheic flow on pesticide degradation can be examined with flow reactive transport (FRT) models [Kaufman et al., 2017].

FRT models capture different degrees of complexity depending on the spatial scales they cover (*i.e.* from cm to km) and the underlying physics (*i.e.* physically-based, conceptual or empirical) they integrate. A top to bottom methodology starting with *in-situ* tracer experiments at river scale (*e.g.* river reaches $\sim 100\text{ m}$ to $\sim 10\text{ km}$) and ended by numerical modelling can help to infer pesticide degradation within specific rivers (*e.g.* degradation and exchange rates or even sorption capacity). To that end, transient storage models (TSM) can be used. TSM formulation is generally conceptual and rely on a 1D longitudinal advection-dispersion equation to which appropriate terms are added to account for lateral fluxes (see Eq. I.5). Additionally, a transfer term is used to account for pollutant mixing and degradation within the sediment bed (generally named “storage zone”) represented by a second equation coupled to Eq. I.5 (see Eq. I.6) [Workshop, 1990].

$$\frac{\partial C}{\partial t} = -\frac{Q}{A} \frac{\partial C}{\partial x} + \frac{1}{A} \frac{\partial}{\partial x} \left[AD \frac{\partial C}{\partial x} \right] + \underbrace{\frac{Q_L}{A} (C_L - C)}_{\text{Lateral input}} + \underbrace{\alpha (C_s - C)}_{\text{Transient storage}} \quad (\text{I.5})$$

$$\frac{\partial C_s}{\partial t} = -\alpha \frac{A}{A_s} (C_s - C) \quad (\text{I.6})$$

Where C , C_L and C_s [M/L^3] represent the contaminant concentrations within the overlying water, the lateral input and the sediment bed, A_s [L^2] is the cross-sectional area of the sediment bed, D is the dispersion coefficient [L^2/T] and α is a coefficient controlling storage zone exchange. This simplest form of TSM formulation is valid for conservative tracers but can also be modified to account for contaminant degradation or sorption to the sediment bed [Liao et al., 2013]. In addition, the advective term may also be modulated to account for additional bedform-driven mass exchanges [Fox et al., 2014]. These models proved useful to identify and quantify the overall mixing and degradation rates (*i.e.* tracer mass recovery) as well as sorption (*i.e.* retardation)

of probe contaminants over long river reaches [Bencala et al., 1990, Haggerty et al., 2009, Liao et al., 2013]. However, the TSM dependency on *in-situ* tracer experiments makes it hardly applicable to real contaminants (*i.e.* physico-chemical properties of the tracer such as hydrophobicity and sensitivity to degradation processes). In addition, as they do not explicitly account for hyporheic flow, they struggle to demonstrate the underlying mechanisms linking contaminant retention and degradation, and are unable to capture short-term variations caused by varying hydrological forcing [Cardenas, 2015, Runkel et al., 2003].

Alternatively, a bottom to top methodology starting with laboratory characterizations of individual degradation reactions and transport processes subsequently used to feed physically-based FRT models. FRT models coupling flow, transport and degradation can virtually resolve all temporal and spatial variabilities, including among the vertical dimension. These are useful in deriving fundamental relationships for a wide range of physical and chemical forcing between mass exchanges, sediment bed geometry and water flow. In addition, FRT models allow to predict contaminant fate under varying conditions independently from experimental labour [Cardenas and Wilson, 2007b, Voermans et al., 2018]. This category of model is principally composed of i) the empirical diffusive model that mostly relies on the Fick's law (Eq. I.7), and ii) the 2D and 3D FRT models that relies on the coupling of three operators representing flow, mass transport and reactive processes (Eq. I.8, Eq. I.9 and Eq. I.10) continuously computed within and across the SWI [Angot et al., 2017].

$$\epsilon \frac{\partial C}{\partial t} = -D_{eff} \frac{\partial^2 C}{\partial z^2} + v \frac{\partial C}{\partial z} \quad (\text{I.7})$$

Fickian's type models have been long used for studying nutrient exchanges and processing at the SWI (*e.g.* sediment diagenesis) [Akbarzadeh et al., 2018, Berner, 1980]. However, up to now they mostly focused on steady state simulations with no specific account for hyporheic exchanges driven by the overlying water velocity [Paraska et al., 2014]. Recent improvements in modelling hyporheic flow induced mass exchange at the SWI with Fickian's type models proved promising. Nonetheless, it may not be systematically applicable to diverse environmental conditions [Chandler et al., 2016, Voermans et al., 2018].

Where z [L] refers to the vertical dimension of the SWI, D_{eff} is an effective diffusivity expressing the combined effects of diffusion and hyporheic flow driven mass exchanges

and v the vertical flow velocity relative to the sediment bed.

Contrarily to the Fickian's type models, 2D/3D FRT models recently proved capable of capturing transient evolution of oxic zonation within the SWI over a few bed forms (5 to 30 m) associated with varying streamflow [Kaufman et al., 2017, Trauth et al., 2013]. Therefore, these models assisted mechanistic investigations of the relationship between streamflow and mass exchanges at the SWI. However, these models also face numerical challenges due to steep permeability gradient at the SWI. This constrains them to limited scale applications (*e.g.* laboratory flume experiments, $\sim 1\text{ m} - 10\text{ m}$) with limited forcing from the surrounding compartments (*e.g.* upwelling/downwelling fluxes) [Bars and Worster, 2006, Kaufman et al., 2017].

$$\frac{\rho}{\epsilon} \frac{\partial \mathbf{u}}{\partial t} + \frac{\mu}{K} \mathbf{u} + \frac{\rho}{\epsilon^2} (\mathbf{u} \cdot \nabla) \mathbf{u} - \frac{\mu}{\epsilon} \nabla \cdot (\nabla \mathbf{u}) + \nabla P = -\rho g \nabla z \quad (\text{I.8})$$

$$\nabla \mathbf{u} = \mathbf{0} \quad (\text{I.9})$$

$$\epsilon \frac{\partial C}{\partial t} + \mathbf{u} \cdot \nabla C - \nabla \cdot (\mathbf{D} \cdot \nabla C) = r \quad (\text{I.10})$$

Numerical gaps of knowledge - Previous numerical developments brought deep understanding and accurate identification of factors controlling flow and pollutant transport at the SWI. However, most of these results are case-specific and only suit specific experimental or *in-situ* conditions. Furthermore, developed methodologies mostly focus on pollutant transport rather than on degradation. When accounted for, pollutant degradation is almost exclusively treated as an average process homogeneously occurring across the entire SWI without considering vertical variations of redox conditions. Also, the effect of sorption on pollutant distribution, residence time and degradation at the SWI is not considered yet. Altogether, current methodologies can hardly be extrapolated to understand and predict pollutant fate at the SWI under a representative panel of hydrological forcing typical of rivers. A short review of available models, their mathematical approach, scale, potential and validity field is presented in appendix B.S1.

1.4 Research questions and overall approach of the thesis

The above introduction emphasizes the global pressure exerted by pesticide pollution of surface and groundwater resources on biodiversity and public health [de Souza et al., 2020]. Despite a strong regulation aiming at constraining these pollution to an environmentally acceptable level, harmonized procedures used to predict pesticide degradation in surface waters do not capture the entire complexity of the SWI functioning [Katagi, 2016]. Accordingly, the occurrence of legacy compounds and their transformation products in surface and groundwater several years after their prohibition remains partly unexplained whereas official persistence indicators generally point to moderate pesticide half-life values of few weeks only (see for example the Pesticide Properties DataBase - PPDB - <https://sitem.herts.ac.uk/aeru/ppdb>). This highlights that the fate of pesticides in the central elements of every catchments, namely the rivers remains poorly understood so far:

- Where pesticides mainly degrade at the SWI (*i.e.* overlying water or sediment)?
- What are main factors controlling pesticide degradation at the SWI (*i.e.* redox conditions, hydrological forcing, pesticide chemical properties) and which degradation mechanisms are involved?
- Does the sediment layer acts as a sink or source of pesticides, and under which conditions?
- At river scale, which factors control the apparition of hot-spots or hot-moments of degradation (*i.e.* specific instream or geomorphologic features, low or high flow conditions)?
- How surface water and groundwater are inter-connected in terms of pollution and how do they influence each other accros the SWI?
- How the degradation potential of a river reach can be observed *in-situ* or inferred from laboratory or numerical modelling insights?

To answer these questions, this thesis work aimed at improving the interpretation of pesticide dissipation at the SWI as an essential feature of surface waters such as ponds, lakes or event rivers. To do so, **three main research questions** were addressed in this thesis, addressing fundamental micro- to meso-scale characteristics of the SWI and the large scale functioning at river scale:

- I. What are the main degradation mechanisms involved at the SWI? Which environmental factors (*i.e.* hydrochemistry, molecular descriptors such as dissociation constant, light absorption or affinity with the sediment) control their extent? Do specific patterns of transformation products formation and stable isotope fractionation help distinguishing between each mechanisms?
- II. How pesticides are transported across the SWI? How hydrological conditions and pesticide partitioning to sediment affect its transport? What is the interplay between transport and degradation at the SWI?
- III. What is the pesticide dissipation and attenuation potential of a low Strahler order river and what characterizes hot-spots and hot-moments of degradation? To what extent insights from laboratory procedures including CSIA data and numerical modelling may help investigating pesticide fate in river?

The methodology developed to answer these questions has been established according to decades of intense scientific research on pollutant fate in the environment and increasing availability of cutting edge analytical (*e.g.* High Resolution-Isotope Ratio Mass Spectrometer) and modelling tools (*e.g.* large scale multimedia environmental fate models [Di Guardo et al., 2018] that may be optimally coupled to improve evaluation of pesticide behaviour in river systems [Lutz et al., 2017].

The methodology used in this thesis relies on a bottom to top approach [Lewandowski et al., 2019] (*i.e.* from laboratory scale to field scale) and develops around three main pillars:

- I. **Microcosms and bench-scale river channel experiments** allowed to study pesticide degradation under simplified conditions. First, individual characterizations of hydrolysis, photodegradation and biodegradation at the SWI brought elementary descriptions (*i.e.* degradation half-lives, transformation products formation, C and N isotope fractionation factors) of main degradation processes expected at the SWI (**Chapter II**). Second, experiments in a recirculated bench-scale river channel highlighted the distribution of these processes at the SWI and the interplay with transport generated by overlying water flow, typical of headwater rivers (**Chapter III**).
- II. **A comprehensive mathematical framework** was built to improve the interpretation of laboratory data and initiate the projection towards river-scale studies. This framework is original because it captures and reveals the interplay

between degradation and transport processes under all theoretical hydrological conditions typical of surface water (**Chapter III**).

- III. **S-metolachlor degradation at river-reach scale** was monitored over an agricultural season with CSIA. It is a first attempt for upscaling laboratory and numerical insights at river scale. Doing so main analytical, monitoring and numerical locks still holding were revealed with associated potential and limits (**Chapter IV**)

1.5 Graphical abstract of the thesis work

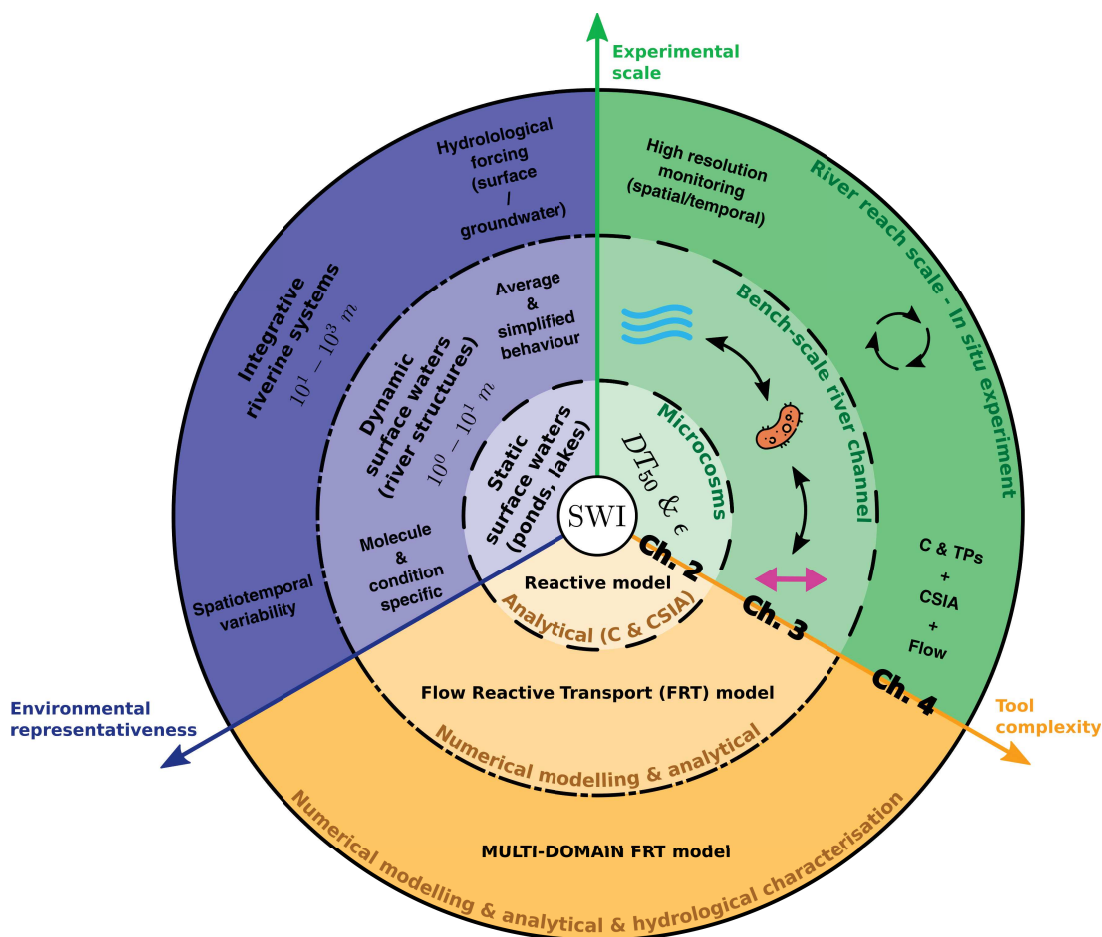


Figure I.5 – General thesis framework highlighting the coupling between experimental and model developments and the step by step up-scaling toward a better representativeness of riverine systems. From the inner to the outer parts of the diagram, steps of developments are separated by lines reflecting the different nature of work carried out (i.e. experimental, modelling and field study). Long-dash contours stand for achieved transitions during this work from simplified to more environmental representations of pesticide degradation at the SWI. Short-dash contours represent partly achieved transitions still subject to improvements.

1.6 Publications and author contributions

Published articles

Masbou, J., **Drouin, G.**, Payraudeau, S., & Imfeld, G. (2018). Carbon and nitrogen stable isotope fractionation during abiotic hydrolysis of pesticides. *Chemosphere*, doi.org/10.1016/j.chemosphere.2018.09.056

Submitted articles

Drouin, G., Droz, B., Leresche, F., Payraudeau, S., Masbou, J. & Imfeld, G. (expected 2020 - 2021). Direct and Indirect Photodegradation of Atrazine and S-metolachlor in Agriculturally Impacted Surface Water and Associated C and N Isotope Fractionation, *Environmental Science & Technology*.

Drouin, G., Fahs, M., Droz, B., Younes, A., Imfeld, G. & Payraudeau, S. (expected 2020 - 2021). Pollutant dissipation at the sediment-water-interface: a robust discrete continuum numerical model and recirculating laboratory experiments, *Water Resources Research*.

Droz, B., **Drouin, G.**, Maurer, L., Payraudeau, S. & Imfeld, G. (expected 2020 - 2021). Mass-Transfer and Biodegradation of Acetochlor and S-Metolachlor in Water–Sediment Systems, *Environmental Science & Technology*.

In preparation

Droz, B., **Drouin, G.**, Payraudeau, S. & Imfeld, G. (expected 2021). Insights on pollutant degradation in rivers by coupling bench-scale river channel experiments, CSIA and flow reactive transport modelling.

Droz, B. & Drouin, G., Imfeld, G & Payraudeau, S. (expected 2021 - 2022). Identifying point and non-point sources of *S*-metolachlor and its degradation in a headwater catchment river of East-France.

Bibliography

- [Accinelli et al., 2001] Accinelli, C., Dinelli, G., Vicari, A., and Catizone, P. (2001). Atrazine and metolachlor degradation in subsoils. *Biology and Fertility of Soils*, 33(6):495–500.
- [Akbarzadeh et al., 2018] Akbarzadeh, Z., Laverman, A. M., Rezanezhad, F., Raimonet, M., Viollier, E., Shafei, B., and Van Cappellen, P. (2018). Benthic nitrite exchanges in the Seine River (France): An early diagenetic modeling analysis. *Science of The Total Environment*, 628-629:580–593.
- [Alvarez-Zaldívar et al., 2018] Alvarez-Zaldívar, P., Payraudeau, S., Meite, F., Masbou, J., and Imfeld, G. (2018). Pesticide degradation and export losses at the catchment scale: Insights from compound-specific isotope analysis (CSIA). *Water Research*, 139:198–207.
- [Angot et al., 2017] Angot, P., Goyeau, B., and Ochoa-Tapia, J. A. (2017). Asymptotic modeling of transport phenomena at the interface between a fluid and a porous layer: Jump conditions. *Physical Review E*, 95(6).
- [Anhalt et al., 2000] Anhalt, J. C., Arthur, E. L., Anderson, T. A., and Coats, J. R. (2000). Degradation of atrazine, metolachlor, and pendimethalin in pesticide-contaminated soils: effects of aged residues on soil respiration and plant survival. *Journal of Environmental Science and Health. Part. B, Pesticides, Food Contaminants, and Agricultural Wastes*, 35(4):417–438.
- [Bakkour et al., 2018] Bakkour, R., Bolotin, J., Sellergren, B., and Hofstetter, T. B. (2018). Molecularly Imprinted Polymers for Compound-Specific Isotope Analysis of Polar Organic Micropollutants in Aquatic Environments. *Analytical Chemistry*, 90(12):7292–7301.
- [Bars and Worster, 2006] Bars, M. L. and Worster, M. G. (2006). Interfacial conditions between a pure fluid and a porous medium: implications for binary alloy solidification. *Journal of Fluid Mechanics*, 550:149–173.

- [Beketov et al., 2013] Beketov, M. A., Kefford, B. J., Schäfer, R. B., and Liess, M. (2013). Pesticides reduce regional biodiversity of stream invertebrates. *Proceedings of the National Academy of Sciences of the United States of America*, 110(27):11039–11043.
- [Bencala et al., 1990] Bencala, K. E., McKnight, D. M., and Zellweger, G. W. (1990). Characterization of transport in an acidic and metal-rich mountain stream based on a lithium tracer injection and simulations of transient storage. *Water Resources Research*, 26(5):989–1000.
- [Berner, 1980] Berner, R. A. (1980). *Early Diagenesis: A Theoretical Approach*.
- [Binley et al., 2013] Binley, A., Ullah, S., Heathwaite, A. L., Heppell, C., Byrne, P., Lansdown, K., Trimmer, M., and Zhang, H. (2013). Revealing the spatial variability of water fluxes at the groundwater-surface water interface. *Water Resources Research*, 49(7):3978–3992.
- [Boano et al., 2014] Boano, F., Harvey, J. W., Marion, A., Packman, A. I., Revelli, R., Ridolfi, L., and Wörman, A. (2014). Hyporheic flow and transport processes: Mechanisms, models, and biogeochemical implications. *Reviews of Geophysics*, 52(4):603–679.
- [Briggs et al., 2012] Briggs, M. A., Lautz, L. K., McKenzie, J. M., Gordon, R. P., and Hare, D. K. (2012). Using high-resolution distributed temperature sensing to quantify spatial and temporal variability in vertical hyporheic flux. *Water Resources Research*, 48(2).
- [Brune et al., 2000] Brune, A., Frenzel, P., and Cypionka, H. (2000). Life at the oxic-anoxic interface: microbial activities and adaptations. *FEMS microbiology reviews*, 24(5):691–710.
- [Byrne et al., 2014] Byrne, P., Binley, A., Heathwaite, A. L., Ullah, S., Heppell, C. M., Lansdown, K., Zhang, H., Trimmer, M., and Keenan, P. (2014). Control of river stage on the reactive chemistry of the hyporheic zone. *Hydrological Processes*, 28(17):4766–4779.
- [Byrne et al., 2015] Byrne, P., Zhang, H., Ullah, S., Binley, A., Heathwaite, A. L., Heppell, C. M., Lansdown, K., and Trimmer, M. (2015). Diffusive equilibrium in thin films provides evidence of suppression of hyporheic exchange and large-scale nitrate transformation in a groundwater-fed river. *Hydrological Processes*, 29(6):1385–1396.

- [Cardenas, 2015] Cardenas, M. B. (2015). Hyporheic zone hydrologic science: A historical account of its emergence and a prospectus. *Water Resources Research*, 51(5):3601–3616.
- [Cardenas and Wilson, 2007a] Cardenas, M. B. and Wilson, J. L. (2007a). Dunes, turbulent eddies, and interfacial exchange with permeable sediments. *Water Resources Research*, 43(8).
- [Cardenas and Wilson, 2007b] Cardenas, M. B. and Wilson, J. L. (2007b). Hydrodynamics of coupled flow above and below a sediment–water interface with triangular bedforms. *Advances in Water Resources*, 30(3):301–313.
- [Carson et al., 1962] Carson, R., Darling, L., Darling, L., Houghton Mifflin Company, and Riverside Press (Cambridge, M. (1962). *Silent spring*.
- [Carvalho et al., 2019] Carvalho, L., Mackay, E. B., Cardoso, A. C., Baattrup-Pedersen, A., Birk, S., Blackstock, K. L., Borics, G., Borja, A., Feld, C. K., Ferreira, M. T., Globevnik, L., Grizzetti, B., Hendry, S., Hering, D., Kelly, M., Langaas, S., Meissner, K., Panagopoulos, Y., Penning, E., Rouillard, J., Sabater, S., Schmedtje, U., Spears, B. M., Venohr, M., van de Bund, W., and Solheim, A. L. (2019). Protecting and restoring Europe’s waters: An analysis of the future development needs of the Water Framework Directive. *Science of The Total Environment*, 658:1228–1238.
- [Chandler et al., 2016] Chandler, I. D., Guymer, I., Pearson, J. M., and Egmond, R. v. (2016). Vertical variation of mixing within porous sediment beds below turbulent flows. *Water Resources Research*, 52(5):3493–3509.
- [Chen et al., 2017] Chen, H., Luo, Y., Potter, C., Moran, P. J., Grieneisen, M. L., and Zhang, M. (2017). Modeling pesticide diuron loading from the San Joaquin watershed into the Sacramento-San Joaquin Delta using SWAT. *Water Research*, 121:374–385.
- [Ciffroy, 2018] Ciffroy, P. (2018). Modelling the Fate of Chemicals in Surface Waters. In Ciffroy, P., Tediosi, A., and Capri, E., editors, *Modelling the Fate of Chemicals in the Environment and the Human Body*, pages 77–99. Springer International Publishing, Cham.
- [Clark and Siu, 2008] Clark, S. E. and Siu, C. Y. S. (2008). Measuring Solids Concentration in Stormwater Runoff: Comparison of Analytical Methods. *Environmental Science & Technology*, 42(2):511–516.

- [de Souza et al., 2020] de Souza, R. M., Seibert, D., Quesada, H. B., de Jesus Bassetti, F., Fagundes-Klen, M. R., and Bergamasco, R. (2020). Occurrence, impacts and general aspects of pesticides in surface water: A review. *Process Safety and Environmental Protection*, 135:22–37.
- [Di Guardo et al., 2018] Di Guardo, A., Gouin, T., MacLeod, M., and Scheringer, M. (2018). Environmental fate and exposure models: advances and challenges in 21st century chemical risk assessment. *Environmental Science: Processes & Impacts*, 20(1):58–71.
- [Dimou et al., 2005] Dimou, A. D., Sakkas, V. A., and Albanis, T. A. (2005). Metolachlor Photodegradation Study in Aqueous Media under Natural and Simulated Solar Irradiation. *Journal of Agricultural and Food Chemistry*, 53(3):694–701.
- [Downing, 2012] Downing, J. (2012). Global abundance and size distribution of streams and rivers. *Inland Waters*, 2(4):229–236.
- [Dwivedi et al., 2018] Dwivedi, D., Steefel, C. I., Arora, B., Newcomer, M., Moulton, J. D., Dafflon, B., Faybishenko, B., Fox, P., Nico, P., Spycher, N., Carroll, R., and Williams, K. H. (2018). Geochemical exports to river from the intramountain hyporheic zone under transient hydrologic conditions: east river mountainous watershed, Colorado. *Water Resources Research*, 54(10):8456–8477.
- [Elliott and Brooks, 1997a] Elliott, A. H. and Brooks, N. H. (1997a). Transfer of nonsorbing solutes to a streambed with bed forms: Laboratory experiments. *Water Resources Research*, 33(1):137–151.
- [Elliott and Brooks, 1997b] Elliott, A. H. and Brooks, N. H. (1997b). Transfer of non-sorbing solutes to a streambed with bed forms: Theory. *Water Resources Research*, 33(1):123–136.
- [Elsayed et al., 2014] Elsayed, O. F., Maillard, E., Vuilleumier, S., Nijenhuis, I., Richnow, H. H., and Imfeld, G. (2014). Using compound-specific isotope analysis to assess the degradation of chloroacetanilide herbicides in lab-scale wetlands. *Chemosphere*, 99:89–95.
- [Elsner, 2010] Elsner, M. (2010). Stable isotope fractionation to investigate natural transformation mechanisms of organic contaminants: principles, prospects and limitations. *Journal of Environmental Monitoring*, 12(11):2005–2031.

- [Elsner and Imfeld, 2016] Elsner, M. and Imfeld, G. (2016). Compound-specific isotope analysis (CSIA) of micropollutants in the environment — current developments and future challenges. *Current Opinion in Biotechnology*, 41:60–72.
- [Elsner et al., 2012] Elsner, M., Jochmann, M. A., Hofstetter, T. B., Hunkeler, D., Bernstein, A., Schmidt, T. C., and Schimmelmann, A. (2012). Current challenges in compound-specific stable isotope analysis of environmental organic contaminants. *Analytical and Bioanalytical Chemistry*, 403(9):2471–2491.
- [Elsner et al., 2005] Elsner, M., Zwank, L., Hunkeler, D., and Schwarzenbach, R. P. (2005). A new concept linking observable stable isotope fractionation to transformation pathways of organic pollutants. *Environmental Science & Technology*, 39(18):6896–6916.
- [Engelhardt et al., 2014] Engelhardt, I., Barth, J. a. C., Bol, R., Schulz, M., Ternes, T. A., Schüth, C., and van Geldern, R. (2014). Quantification of long-term wastewater fluxes at the surface water/groundwater-interface: an integrative model perspective using stable isotopes and acesulfame. *The Science of the Total Environment*, 466-467:16–25.
- [Ericson et al., 2014] Ericson, J. F., Smith, R. M., Roberts, G., Hannah, B., Hoeger, B., and Ryan, J. (2014). Experiences with the OECD 308 transformation test: A human pharmaceutical perspective. *Integrated Environmental Assessment and Management*, 10(1):114–124.
- [European Environment Agency, 2018] European Environment Agency (2018). *Chemicals in European waters knowledge developments*.
- [Eurostat (European Commission), 2017] Eurostat (European Commission) (2017). Agriculture, forestry and fishery statistics — 2016 edition.
- [Eylers et al., 1995] Eylers, H., Brooks, N. H., and Morgan, J. J. (1995). Transport of adsorbing metals from stream water to a stationary sand-bed in a laboratory flume. *Marine and Freshwater Research*, 46(1):209–214.
- [Fenner et al., 2013] Fenner, K., Canonica, S., Wackett, L. P., and Elsner, M. (2013). Evaluating Pesticide Degradation in the Environment: Blind Spots and Emerging Opportunities. *Science*, 341(6147):752–758.
- [Flipo et al., 2014] Flipo, N., Mouhri, A., Labarthe, B., Biancamaria, S., Rivière, A., and Weill, P. (2014). Continental hydrosystem modelling: the concept of nested

- stream–aquifer interfaces. *Hydrology and Earth System Sciences*, 18(8):3121–3149.
- [Fono et al., 2006] Fono, L. J., Kolodziej, E. P., and Sedlak, D. L. (2006). Attenuation of Wastewater-Derived Contaminants in an Effluent-Dominated River. *Environmental Science & Technology*, 40(23):7257–7262.
- [Fox et al., 2014] Fox, A., Boano, F., and Arnon, S. (2014). Impact of losing and gaining streamflow conditions on hyporheic exchange fluxes induced by dune-shaped bed forms. *Water Resources Research*, 50(3):1895–1907.
- [Fryirs and Brierley, 2012] Fryirs, K. A. and Brierley, G. J. (2012). Catchment Hydrology. *Geomorphic Analysis of River Systems*, pages 44–64.
- [Gerecke et al., 2002] Gerecke, A. C., Schärer, M., Singer, H. P., Müller, S. R., Schwarzenbach, R. P., Sägesser, M., Ochsenbein, U., and Popow, G. (2002). Sources of pesticides in surface waters in Switzerland: pesticide load through waste water treatment plants—current situation and reduction potential. *Chemosphere*, 48(3):307–315.
- [Grant and Marusic, 2011] Grant, S. B. and Marusic, I. (2011). Crossing turbulent boundaries: interfacial flux in environmental flows. *Environmental Science & Technology*, 45(17):7107–7113.
- [Gupta and Gupta, 2020] Gupta, S. and Gupta, K. (2020). Bioaccumulation of Pesticides and Its Impact on Biological Systems. In *Pesticides in Crop Production*, pages 55–67. John Wiley & Sons, Ltd.
- [Gutowski et al., 2015] Gutowski, L., Olsson, O., Leder, C., and Kümmerer, K. (2015). A comparative assessment of the transformation products of S-metolachlor and its commercial product Mercantor Gold(®) and their fate in the aquatic environment by employing a combination of experimental and in silico methods. *The Science of the Total Environment*, 506-507:369–379.
- [Haggerty et al., 2009] Haggerty, R., Martí, E., Argerich, A., von Schiller, D., and Grimm, N. B. (2009). Resazurin as a “smart” tracer for quantifying metabolically active transient storage in stream ecosystems. *Journal of Geophysical Research: Biogeosciences*, 114(G3).
- [Handford et al., 2015] Handford, C. E., Elliott, C. T., and Campbell, K. (2015). A review of the global pesticide legislation and the scale of challenge in reaching the

- global harmonization of food safety standards. *Integrated Environmental Assessment and Management*, 11(4):525–536.
- [Hester and Doyle, 2008] Hester, E. T. and Doyle, M. W. (2008). In-stream geomorphic structures as drivers of hyporheic exchange. *Water Resources Research*, 44(3).
- [Hester et al., 2009] Hester, E. T., Doyle, M. W., and Poole, G. C. (2009). The influence of in-stream structures on summer water temperatures via induced hyporheic exchange. *Limnology and Oceanography*, 54(1):355–367.
- [Hofstetter et al., 2011] Hofstetter, T. B., Bolotin, J., Skarpeli-Liati, M., Wijker, R., Kurt, Z., Nishino, S. F., and Spain, J. C. (2011). Tracking transformation processes of organic micropollutants in aquatic environments using multi-element isotope fractionation analysis. *Applied Geochemistry*, 26:S334–S336.
- [Honti et al., 2018] Honti, M., Bischoff, F., Moser, A., Stamm, C., Baranya, S., and Fenner, K. (2018). Relating degradation of pharmaceutical active ingredients in a stream network to degradation in water-sediment simulation tests. *Water Resources Research*, 54(11):9207–9223.
- [Honti and Fenner, 2015] Honti, M. and Fenner, K. (2015). Deriving Persistence Indicators from Regulatory Water-Sediment Studies – Opportunities and Limitations in OECD 308 Data. *Environmental Science & Technology*, 49(10):5879–5886.
- [Honti et al., 2016] Honti, M., Hahn, S., Hennecke, D., Junker, T., Shrestha, P., and Fenner, K. (2016). Bridging across OECD 308 and 309 Data in Search of a Robust Biotransformation Indicator. *Environmental Science & Technology*, 50(13):6865–6872.
- [Huber et al., 2000] Huber, A., Bach, M., and Frede, H. (2000). Pollution of surface waters with pesticides in Germany: modeling non-point source inputs. *Agriculture, Ecosystems & Environment*, 80(3):191–204.
- [Hunkeler et al., 2008] Hunkeler, D., Meckenstock, R. U., Sherwood Lollar, B., Schmidt, T. C., and Wilson, J. T. (2008). A guide for assessing biodegradation and source identification of organic ground water contaminants using Compound Specific Isotope Analysis (CSIA). page 82.
- [Hussain et al., 2009] Hussain, S., Siddique, T., Saleem, M., Arshad, M., and Khalid, A. (2009). Chapter 5 Impact of Pesticides on Soil Microbial Diversity, Enzymes,

and Biochemical Reactions. In *Advances in Agronomy*, volume 102, pages 159–200. Academic Press.

- [Jarsjö et al., 2017] Jarsjö, J., Chalov, S. R., Pietroni, J., Alekseenko, A. V., and Thorslund, J. (2017). Patterns of soil contamination, erosion and river loading of metals in a gold mining region of northern Mongolia. *Regional Environmental Change*, 17(7):1991–2005.
- [Jin et al., 2019] Jin, G., Chen, Y., Tang, H., Zhang, P., Li, L., and Barry, D. A. (2019). Interplay of hyporheic exchange and fine particle deposition in a riverbed. *Advances in Water Resources*, 128:145–157.
- [Jüttner, 1999] Jüttner, F. (1999). Efficacy of bank filtration for the removal of fragrance compounds and aromatic hydrocarbons. *Water Science and Technology*, 40(6):123–128.
- [Katagi, 2002] Katagi, T. (2002). Abiotic hydrolysis of pesticides in the aquatic environment. *Reviews of Environmental Contamination and Toxicology*, 175:79–261.
- [Katagi, 2004] Katagi, T. (2004). Photodegradation of Pesticides on Plant and Soil Surfaces. In Ware, G. W., editor, *Reviews of Environmental Contamination and Toxicology*, number 182 in Continuation of Residue Reviews, pages 1–78. Springer New York.
- [Katagi, 2016] Katagi, T. (2016). Pesticide behavior in modified water-sediment systems. *Journal of Pesticide Science*, 41(4):121–132.
- [Kaufman et al., 2017] Kaufman, M. H., Cardenas, M. B., Buttles, J., Kessler, A. J., and Cook, P. L. M. (2017). Hyporheic hot moments: Dissolved oxygen dynamics in the hyporheic zone in response to surface flow perturbations. *Water Resources Research*, 53(8):6642–6662.
- [Kendall and Caldwell, 1998] Kendall, C. and Caldwell, E. A. (1998). Chapter 2 - Fundamentals of Isotope Geochemistry. In Kendall, C. and McDONNELL, J. J., editors, *Isotope Tracers in Catchment Hydrology*, pages 51–86. Elsevier, Amsterdam.
- [Kim et al., 2017] Kim, K.-H., Kabir, E., and Jahan, S. A. (2017). Exposure to pesticides and the associated human health effects. *Science of The Total Environment*, 575:525–535.

- [Knapp and Cirpka, 2017] Knapp, J. L. A. and Cirpka, O. A. (2017). Determination of hyporheic travel time distributions and other parameters from concurrent conservative and reactive tracer tests by local-in-global optimization. *Water Resources Research*, 53(6):4984–5001.
- [Krause et al., 2017] Krause, S., Lewandowski, J., Grimm, N. B., Hannah, D. M., Pinay, G., McDonald, K., Martí, E., Argerich, A., Pfister, L., Klaus, J., Battin, T., Larned, S. T., Schelker, J., Fleckenstein, J., Schmidt, C., Rivett, M. O., Watts, G., Sabater, F., Sorolla, A., and Turk, V. (2017). Ecohydrological interfaces as hot spots of ecosystem processes. *Water Resources Research*, 53(8):6359–6376.
- [Lansdown et al., 2015] Lansdown, K., Heppell, C. M., Trimmer, M., Binley, A., Heathwaite, A. L., Byrne, P., and Zhang, H. (2015). The interplay between transport and reaction rates as controls on nitrate attenuation in permeable, streambed sediments. *Journal of Geophysical Research: Biogeosciences*, 120(6):1093–1109.
- [Lefrancq et al., 2017] Lefrancq, M., Payraudeau, S., Guyot, B., Millet, M., and Imfeld, G. (2017). Degradation and Transport of the Chiral Herbicide S-Metolachlor at the Catchment Scale: Combining Observation Scales and Analytical Approaches. *Environmental Science & Technology*, 51(22):13231–13240.
- [Lewandowski et al., 2019] Lewandowski, J., Arnon, S., Banks, E., Batelaan, O., Betterle, A., Broecker, T., Coll, C., Drummond, J. D., Gaona Garcia, J., Galloway, J., Gomez-Velez, J., Grabowski, R. C., Herzog, S. P., Hinkelmann, R., Höhne, A., Hollender, J., Horn, M. A., Jaeger, A., Krause, S., Löchner Prats, A., Magliozzi, C., Meinikmann, K., Mojarrad, B. B., Mueller, B. M., Peralta-Maraver, I., Popp, A. L., Posselt, M., Putschew, A., Radke, M., Raza, M., Riml, J., Robertson, A., Rutere, C., Schaper, J. L., Schirmer, M., Schulz, H., Shanafield, M., Singh, T., Ward, A. S., Wolke, P., Wörman, A., and Wu, L. (2019). Is the hyporheic zone relevant beyond the scientific community? *Water*, 11(11):2230.
- [Lewandowski et al., 2011] Lewandowski, J., Putschew, A., Schwesig, D., Neumann, C., and Radke, M. (2011). Fate of organic micropollutants in the hyporheic zone of a eutrophic lowland stream: Results of a preliminary field study. *Science of The Total Environment*, 409(10):1824–1835.
- [Liao et al., 2013] Liao, Z., Lemke, D., Osenbrück, K., and Cirpka, O. A. (2013). Modeling and inverting reactive stream tracers undergoing two-site sorption and decay in the hyporheic zone. *Water Resources Research*, 49(6):3406–3422.

- [Luo et al., 2014] Luo, Y., Guo, W., Ngo, H. H., Nghiem, L. D., Hai, F. I., Zhang, J., Liang, S., and Wang, X. C. (2014). A review on the occurrence of micropollutants in the aquatic environment and their fate and removal during wastewater treatment. *Science of The Total Environment*, 473–474:619–641.
- [Lutz et al., 2017] Lutz, S. R., van der Velde, Y., Elsayed, O. F., Imfeld, G., Lefrancq, M., Payraudeau, S., and van Breukelen, B. M. (2017). Pesticide fate at catchment scale: conceptual modelling of stream CSIA data. *Hydrol. Earth Syst. Sci. Discuss.*, 2017:1–30.
- [Lutz et al., 2013] Lutz, S. R., van Meerveld, H. J., Waterloo, M. J., Broers, H. P., and van Breukelen, B. M. (2013). A model-based assessment of the potential use of compound-specific stable isotope analysis in river monitoring of diffuse pesticide pollution. *Hydrol. Earth Syst. Sci.*, 17(11):4505–4524.
- [Maggi et al., 2019] Maggi, F., Tang, F. H. M., Cecilia, D. I., and McBratney, A. (2019). PEST-CHEMGRIDS, global gridded maps of the top 20 crop-specific pesticide application rates from 2015 to 2025. *Scientific Data*, 6(1):1–20.
- [Maier et al., 2016] Maier, M. P., Prasse, C., Pati, S. G., Nitsche, S., Li, Z., Radke, M., Meyer, A., Hofstetter, T. B., Ternes, T. A., and Elsner, M. (2016). Exploring Trends of C and N Isotope Fractionation to Trace Transformation Reactions of Diclofenac in Natural and Engineered Systems. *Environmental Science & Technology*, 50(20):10933–10942.
- [Malaj et al., 2014] Malaj, E., Ohe, P. C. v. d., Grote, M., Kühne, R., Mondy, C. P., Usseglio-Polatera, P., Brack, W., and Schäfer, R. B. (2014). Organic chemicals jeopardize the health of freshwater ecosystems on the continental scale. *Proceedings of the National Academy of Sciences*, 111(26):9549–9554.
- [Mariotti, 1983] Mariotti, A. (1983). Atmospheric nitrogen is a reliable standard for natural ^{15}N abundance measurements. *Nature*, 303(5919):685–687.
- [Masbou et al., 2018] Masbou, J., Drouin, G., Payraudeau, S., and Imfeld, G. (2018). Carbon and nitrogen stable isotope fractionation during abiotic hydrolysis of pesticides. *Chemosphere*, 213:368–376.
- [Masiol et al., 2018] Masiol, M., Giannì, B., and Prete, M. (2018). Herbicides in river water across the northeastern Italy: occurrence and spatial patterns of glyphosate, aminomethylphosphonic acid, and glufosinate ammonium. *Environmental Science and Pollution Research*, pages 1–11.

- [Matthews et al., 2011] Matthews, G., Zaim, M., Yadav, R. S., Soares, A., Hii, J., Ameneshewa, B., Mnzava, A., Dash, A. P., Ejov, M., Tan, S. H., and van den Berg, H. (2011). Status of Legislation and Regulatory Control of Public Health Pesticides in Countries Endemic with or at Risk of Major Vector-Borne Diseases. *Environmental Health Perspectives*, 119(11):1517–1522.
- [Meckenstock et al., 2004] Meckenstock, R. U., Morasch, B., Griebler, C., and Richnow, H. H. (2004). Stable isotope fractionation analysis as a tool to monitor biodegradation in contaminated aquifers. *Journal of Contaminant Hydrology*, 75(3–4):215–255.
- [Meite et al., 2018] Meite, F., Alvarez-Zaldívar, P., Crochet, A., Wiegert, C., Payraudeau, S., and Imfeld, G. (2018). Impact of rainfall patterns and frequency on the export of pesticides and heavy-metals from agricultural soils. *Science of The Total Environment*, 616-617:500–509.
- [Menichino and Hester, 2014] Menichino, G. T. and Hester, E. T. (2014). Hydraulic and thermal effects of in-stream structure-induced hyporheic exchange across a range of hydraulic conductivities. *Water Resources Research*, 50(6):4643–4661.
- [Mersie et al., 2004] Mersie, W., McNamee, C., Seybold, C., Wu, J., and Tierney, D. (2004). Degradation of metolachlor in bare and vegetated soils and in simulated water-sediment systems. *Environmental Toxicology and Chemistry*, 23(11):2627–2632.
- [Meybeck, 2003] Meybeck, M. (2003). Global Occurrence of Major Elements in Rivers. *Treatise on Geochemistry*, 5:605.
- [Meyer and Elsner, 2013] Meyer, A. H. and Elsner, M. (2013). $^{13}\text{C}/^{12}\text{C}$ and $^{15}\text{N}/^{14}\text{N}$ Isotope Analysis To Characterize Degradation of Atrazine: Evidence from Parent and Daughter Compound Values. *Environmental Science & Technology*, 47(13):6884–6891.
- [Meyer et al., 2009] Meyer, A. H., Penning, H., and Elsner, M. (2009). C and N Isotope Fractionation Suggests Similar Mechanisms of Microbial Atrazine Transformation Despite Involvement of Different Enzymes (AtzA and TrzN). *Environmental Science & Technology*, 43(21):8079–8085.
- [Mueller et al., 2016] Mueller, C., Zink, M., Samaniego, L., Krieg, R., Merz, R., Rode, M., and Knöller, K. (2016). Discharge Driven Nitrogen Dynamics in a Mesoscale

- River Basin As Constrained by Stable Isotope Patterns. *Environmental Science & Technology*, 50(17):9187–9196.
- [Munz et al., 2013] Munz, N., Leu, C., and Wittmer, I. (2013). Pesticides dans les cours d’eau Suisses. *Aqua & Gas*, 7/8:78–87.
- [Mutz et al., 2007] Mutz, M., Kalbus, E., and Meinecke, S. (2007). Effect of instream wood on vertical water flux in low-energy sand bed flume experiments. *Water Resources Research*, 43(10).
- [Nogaro et al., 2013] Nogaro, G., Datry, T., Mermillod-Blondin, F., Foulquier, A., and Montuelle, B. (2013). Influence of hyporheic zone characteristics on the structure and activity of microbial assemblages. *Freshwater Biology*, 58(12):2567–2583.
- [OECD, 2002] OECD (2002). *Test No. 308: Aerobic and Anaerobic Transformation in Aquatic Sediment Systems*. Organisation for Economic Co-operation and Development, Paris.
- [OECD, 2004] OECD (2004). *Test No. 111: Hydrolysis as a Function of pH*. Organisation for Economic Co-operation and Development, Paris.
- [OECD, 2008] OECD (2008). *Test No. 316: Phototransformation of Chemicals in Water – Direct Photolysis*. Organisation for Economic Co-operation and Development, Paris.
- [Ouyang et al., 2017] Ouyang, W., Gao, X., Wei, P., Gao, B., Lin, C., and Hao, F. (2017). A review of diffuse pollution modeling and associated implications for watershed management in China. *Journal of Soils and Sediments*, 17(6):1527–1536.
- [Packman et al., 2004] Packman, A. I., Salehin, M., and Zaramella, M. (2004). Hyporheic Exchange with Gravel Beds: Basic Hydrodynamic Interactions and Bedform-Induced Advective Flows. *Journal of Hydraulic Engineering*, 130(7):647–656.
- [Paraska et al., 2014] Paraska, D. W., Hipsey, M. R., and Salmon, S. U. (2014). Sediment diagenesis models: Review of approaches, challenges and opportunities. *Environmental Modelling & Software*, 61:297–325.
- [Popp et al., 2013] Popp, J., Pető, K., and Nagy, J. (2013). Pesticide productivity and food security. A review. *Agronomy for Sustainable Development*, 33(1):243–255.

- [Posselt et al., 2020] Posselt, M., Mechelke, J., Rutere, C., Coll, C., Jaeger, A., Raza, M., Meinikmann, K., Krause, S., Sobek, A., Lewandowski, J., Horn, M. A., Hollender, J., and Benskin, J. P. (2020). Bacterial Diversity Controls Transformation of Wastewater-Derived Organic Contaminants in River-Simulating Flumes. *Environmental Science & Technology*, 54(9):5467–5479.
- [Rayleigh, 1896] Rayleigh, R. (1896). L. Theoretical considerations respecting the separation of gases by diffusion and similar processes. *The London, Edinburgh, and Dublin Philosophical Magazine and Journal of Science*, 42(259):493–498.
- [Remucal, 2014] Remucal, C. K. (2014). The role of indirect photochemical degradation in the environmental fate of pesticides: a review. *Environmental Science-Processes & Impacts*, 16(4):628–653.
- [Ren and Packman, 2004a] Ren, J. and Packman, A. I. (2004a). Modeling of simultaneous exchange of colloids and sorbing contaminants between streams and streambeds. *Environmental Science & Technology*, 38(10):2901–2911.
- [Ren and Packman, 2004b] Ren, J. and Packman, A. I. (2004b). Stream-subsurface exchange of zinc in the presence of silica and kaolinite colloids. *Environmental Science & Technology*, 38(24):6571–6581.
- [Runkel et al., 2003] Runkel, R. L., McKnight, D. M., and Rajaram, H. (2003). Modeling hyporheic zone processes. *Advances in Water Resources*, 26(9):901–905.
- [Schwarzenbach et al., 2006] Schwarzenbach, R. P., Escher, B. I., Fenner, K., Hofstetter, T. B., Johnson, C. A., Gunten, U. v., and Wehrli, B. (2006). The Challenge of Micropollutants in Aquatic Systems. *Science*, 313(5790):1072–1077.
- [Sharma et al., 2019] Sharma, A., Kumar, V., Shahzad, B., Tanveer, M., Sidhu, G. P. S., Handa, N., Kohli, S. K., Yadav, P., Bali, A. S., Parihar, R. D., Dar, O. I., Singh, K., Jasrotia, S., Bakshi, P., Ramakrishnan, M., Kumar, S., Bhardwaj, R., and Thukral, A. K. (2019). Worldwide pesticide usage and its impacts on ecosystem. *SN Applied Sciences*, 1(11):1446.
- [Sharp, 2017] Sharp, Z. (2017). Principles of Stable Isotope Geochemistry, 2nd Edition. *Open Educational Resources*.
- [Shrestha et al., 2016] Shrestha, P., Junker, T., Fenner, K., Hahn, S., Honti, M., Bakkour, R., Diaz, C., and Hennecke, D. (2016). Simulation studies to explore

- biodegradation in water–sediment systems: From OECD 308 to OECD 309. *Environmental Science & Technology*, 50(13):6856–6864.
- [Sims and Kanissery, 2019] Sims, G. K. and Kanissery, R. G. (2019). Anaerobic Biodegradation of Pesticides. In Arora, P. K., editor, *Microbial Metabolism of Xenobiotic Compounds*, Microorganisms for Sustainability, pages 33–54. Springer, Singapore.
- [Skark et al., 2004] Skark, C., Zullei-Seibert, N., Willme, U., Gatzemann, U., and Schlett, C. (2004). Contribution of non-agricultural pesticides to pesticide load in surface water. *Pest Management Science*, 60(6):525–530.
- [Soulsby et al., 2008] Soulsby, C., Neal, C., Laudon, H., Burns, D. A., Merot, P., Bonell, M., Dunn, S. M., and Tetzlaff, D. (2008). Catchment data for process conceptualization: simply not enough? *Hydrological Processes*, 22(12):2057–2061.
- [Stehle and Schulz, 2015] Stehle, S. and Schulz, R. (2015). Agricultural insecticides threaten surface waters at the global scale. *Proceedings of the National Academy of Sciences*, 112(18):5750–5755.
- [Trauth et al., 2013] Trauth, N., Schmidt, C., Maier, U., Vieweg, M., and Fleckenstein, J. H. (2013). Coupled 3-D stream flow and hyporheic flow model under varying stream and ambient groundwater flow conditions in a pool-riffle system. *Water Resources Research*, 49(9):5834–5850.
- [Trauth et al., 2015] Trauth, N., Schmidt, C., Vieweg, M., Oswald, S. E., and Fleckenstein, J. H. (2015). Hydraulic controls of in-stream gravel bar hyporheic exchange and reactions. *Water Resources Research*, 51(4):2243–2263.
- [Van Breukelen, 2007a] Van Breukelen, B. M. (2007a). Extending the Rayleigh equation to allow competing isotope fractionating pathways to improve quantification of biodegradation. *Environmental Science & Technology*, 41(11):4004–4010.
- [Van Breukelen, 2007b] Van Breukelen, B. M. (2007b). Quantifying the Degradation and Dilution Contribution to Natural Attenuation of Contaminants by Means of an Open System Rayleigh Equation. *Environmental Science & Technology*, 41(14):4980–4985.
- [Van Breukelen and Rolle, 2012] Van Breukelen, B. M. and Rolle, M. (2012). Transverse Hydrodynamic Dispersion Effects on Isotope Signals in Groundwater Chlorinated Solvents’ Plumes. *Environmental Science & Technology*, 46(14):7700–7708.

- [Vervier et al., 1992] Vervier, P., Gibert, J., Marmonier, P., and Dole-Olivier, M.-J. (1992). A Perspective on the Permeability of the Surface Freshwater-Groundwater Ecotone. *Journal of the North American Benthological Society*, 11(1):93–102.
- [Voermans et al., 2017] Voermans, J. J., Ghisalberti, M., and Ivey, G. N. (2017). The variation of flow and turbulence across the sediment–water interface. *Journal of Fluid Mechanics*, 824:413–437.
- [Voermans et al., 2018] Voermans, J. J., Ghisalberti Marco, and Ivey Gregory N. (2018). A model for mass transport across the sediment-water interface. *Water Resources Research*, 0(0).
- [Voulvoulis et al., 2017] Voulvoulis, N., Arpon, K. D., and Giakoumis, T. (2017). The EU Water Framework Directive: From great expectations to problems with implementation. *Science of The Total Environment*, 575:358–366.
- [Vörösmarty et al., 2010] Vörösmarty, C. J., McIntyre, P. B., Gessner, M. O., Dudgeon, D., Prusevich, A., Green, P., Glidden, S., Bunn, S. E., Sullivan, C. A., Liermann, C. R., and Davies, P. M. (2010). Global threats to human water security and river biodiversity. *Nature*, 467(7315):555–561.
- [Ward, 2016] Ward, A. S. (2016). The evolution and state of interdisciplinary hyporheic research. *WIREs Water*, 3(1):83–103.
- [Willach et al., 2018] Willach, S., Lutze, H. V., Eckey, K., Löppenberg, K., Lüling, M., Wolbert, J.-B., Kujawinski, D. M., Jochmann, M. A., Karst, U., and Schmidt, T. C. (2018). Direct Photolysis of Sulfamethoxazole Using Various Irradiation Sources and Wavelength Ranges—Insights from Degradation Product Analysis and Compound-Specific Stable Isotope Analysis. *Environmental Science & Technology*, 52(3):1225–1233.
- [Workshop, 1990] Workshop, S. S. (1990). Concepts and Methods for Assessing Solute Dynamics in Stream Ecosystems. *Journal of the North American Benthological Society*, 9(2):95–119.
- [Zeng and Arnold, 2013] Zeng, T. and Arnold, W. A. (2013). Pesticide Photolysis in Prairie Potholes: Probing Photosensitized Processes. *Environmental Science & Technology*, 47(13):6735–6745.

Preface to Chapter II

As a first step to improve the understanding of pesticide fate at the sediment-water interface, the individual characterization of pesticide degradation mechanisms is mandatory. This chapter describes a complete laboratory procedure to identify factors controlling pesticide photodegradation, biodegradation and hydrolysis at the sediment-water interface. Accordingly, 3 sub-chapters cover laboratory insights gained for each mechanism.

- I. Results on **pesticide hydrolysis** are first presented. It occurs in the water phase only (*i.e.* overlying water or porewater) and is consequently easily investigated with simple experimental setup (*i.e.* aqueous solutions). This offers the opportunity to enter into molecular investigations of degradation mechanisms. It also underscores the interest of coupling concentration, transformation products analysis and CSIA to resolve degradation mechanisms at laboratory scale and evidence degradation at catchment scale.
- II. Results on **pesticide photodegradation** are then presented (reformatted from a submitted paper to EST) since photodegradation is the main abiotic degradation mechanism occurring in the overlying water of surface waters.
- III. Finally the interplay between **biodegradation and phase partitioning** in the sediment is addressed (reformatted from a submitted paper to EST as second author).

Altogether these results constitute a necessary background to develop a mathematical framework integrating the most relevant pesticide degradation mechanisms and interactions with the sediment at the SWI. These chapters are preceded by a sub-chapter gathering all information about samples laboratory processing, analytical methods and procedures.

Chapter II

Pesticide degradation pathways at the sediment-water interface

2.1 Analytical section: Sample processing, Quantification and Compound-Specific Isotope Analysis

The information provided in this section stand throughout the entire thesis manuscript. It presents the general extraction and analytical procedures (quantification, transformation products analysis and CSIA) for pesticides used over this work. When required, information specific to each experiment are described in their corresponding appendix section.

Pesticide extraction

Extraction from liquid samples - Solid Phase Extraction (SPE) on water samples was carried out using a SolEx C18 cartridges (1 g, Dionex®, CA, USA) and an AutoTrace 280 SPE system (Dionex®, CA, USA) [Elsayed et al., 2014]. SPE cartridges were sequentially rinsed with 5 mL of ethanol and ACN before being conditioned with 10 mL of deionized water. Liquid samples were then loaded at 10 mL/min and cartridges were dried afterwards under nitrogen flux for 10 minutes. Then, a sequential elution with 5 mL of EtOAc and ACN allowed pesticide elution before concentration up to the last droplet under nitrogen flux and resuspension in 1000 µL of ACN for storage at -20°C .

Extraction from solid samples - Pesticides were extracted from sediment samples by solid-liquid extraction modified from Ivdra et al. (2014) [Ivdra et al., 2014]. The wet sediment (5 g dry mass) was extracted in a centrifuge tube with 3 mL of a mix

pentane:dichloromethane (3 : 1 in volume/volume), vortexed for 5 s, followed by 5 minutes of sonication in a bath (Branson 5510, 40 *kHz*) and vortexed again for 1 minute before a final centrifugation at 2400 *RCF* for 20 minutes to separate the liquid from the solid phase. Then, the supernatant was transferred into an amber glass vial. This extraction procedure was performed in total 3 times per sample. The 3 supernatants were pooled together, concentrated up to the last droplet under nitrogen flux, resuspended in 1000 μL of ACN in glass vials. Residual humidity and impurities were removed by adding in each vial about 75 *mg* of anhydrous MgSO_4 and 13 *mg* of primary-secondary amine (PSA; P/N 52738, bonded silica). Finally, vials were vortexed for 30 seconds, centrifuged at 2400 *RCF* for 5 minutes and the supernatant was transferred into a 1.5 *mL* glass GC vials for storage at -20°C before measurement.

Extraction yields and extraction-induced stable isotope fractionation - Extraction yields and induced stable isotope fractionation by the extraction procedures were evaluated for liquid and solid samples by performing control extractions. For the water samples, 100 *mL* of synthetic freshwater was spiked with pesticides in the range 1 to 1500 $\mu\text{g.L}^{-1}$. Six successive concentrations were tested, including 1, 5, 10, 50, 500 and 1500 $\mu\text{g.L}^{-1}$. Water samples were then extracted as described above. For sediment samples, 5 *g* of dry sediment (40°C for 24 hours) were mixed in a 15 *mL* centrifuge tube with ultrapure water up to water saturation. Sediment samples were spiked with pesticides in the range 0.5 to 150 $\mu\text{g.g}^{-1}$. Ten successive concentrations were tested, including 0.5, 5, 10, 20, 30, 40, 50, 75, 100, 125 and 150 $\mu\text{g.g}^{-1}$. Sediment samples were then vortexed for 3 minutes to ensure complete homogenization. Sediment samples were incubated for 7 days in the dark at 4°C before extraction to ensure pesticide penetration within the sediment matrix. Sediment samples were then extracted as described above. Each tested concentration was duplicate. Additionally, a blank series with no sediment was spiked as previously described to evaluate whether pesticide sorption on centrifuge tubes occurred over the 7 days incubation period. A series of abiotic control experiments was conducted in parallel to quantify potential abiotic degradation or volatilization losses over the 7 days incubation period. In this case, sediment samples were autoclaved twice (24 hours intervals).

For *S*-metolachlor, the **liquid extraction** procedure led to quantitative extraction at environmental $\text{pH} \in [7; 9]$ ($\eta > 100\%$) and did not result in significant C and N stable isotope fractionation $|\Delta\delta^{13}\text{C}| = |\delta^{13}\text{C}_{\text{EA-IRMS}} - \delta^{13}\text{C}_{\text{GC-IRMS}}| = 0.1 \pm 0.4\text{‰}$ and $|\Delta\delta^{15}\text{N}| = 0.9 \pm 0.9\text{‰}$. See Masbou et al. (2018) for more details on the effect of pH [Masbou et al., 2018]. See Table II.1 for details on other molecules.

For *S*-metolachlor, **the solid-liquid extraction** procedure led to quantitative extraction ($\eta > 97 \pm 23\%$) and resulted in acceptable C and N stable isotope fractionation ($|\Delta\delta^{13}C| = 0.1 \pm 0.4\text{‰}$ and $|\Delta\delta^{15}N| = 0.9 \pm 0.9\text{‰}$). The solid-liquid extraction was tested on a wetland sediment used for the biodegradation experiment (Rouffach - France - $47^{\circ}57'43''N, 07^{\circ}17'26''E$, sediment characteristics in Appendix A.S2.2) as well as on the Avenheimerbach sediment (sediment characteristics in Appendix C.S5). Reported values represent the arithmetic means on both sediments. See Table II.1 for details on other molecules.

Pesticide quantification

Pesticides were quantified by Gas-Chromatography (GC, Trace 1300, Thermo Fisher Scientific) coupled with a Mass-Spectrometer (MS, ISQTM, Thermo Fisher Scientific) in selected-ion-monitoring mode (SIM). Each sample was injected twice to ensure analytical reproducibility and was diluted to fall within the linearity range of the MS, estimated according to the calibration curve to lie between 50 and 1000 $\mu\text{g.L}^{-1}$. 1 μL of metolachlor-d11 at 300 $\mu\text{g.L}^{-1}$ was systematically added to the 1 μL of sample as an Internal Standard (IS) by the autosampler (TriPlus RSHTM, Thermo Fisher Scientific) and was used to normalize peak area of the molecules of interest. The combined 2 μL were then injected in split mode with a split flow of 6 mL.min^{-1} at 280°C . Separation happened through a TG-5MS column (30 m x 0.25 mm internal diameter, 0.25 μm film thickness) well suited for slightly polar molecules with a helium flow of 1.5 mL.min^{-1} . Heat ramp started after 1 minute at 50°C and raised up to 160°C at a rate of $30^{\circ}\text{C.min}^{-1}$, continued up to 220°C at $4^{\circ}\text{C.min}^{-1}$ and finally reached 300°C at $30^{\circ}\text{C.min}^{-1}$ to be held for 1 minute. The MS transfer line and the source were kept at 320°C for the entirety of the analysis. Detection limits (DLs) and quantification limits (QLs) were estimated according to the multiple injection method as described in Olivier et al. (2006) and are reported in Table II.1 [Olivieri et al., 2006].

Transformation Products Quantification

During the photodegradation and biodegradation experiments, transformation products (TPs) were analyzed in samples displaying similar extent of degradation, following the general methodology presented in Villette et al. (2019) and summarized below [Villette et al., 2019]. Samples were analyzed by a Dionex Ultimate 3000 (Thermo-Fischer Scientific, USA) liquid chromatograph (LC) coupled with an Impact-II (Bruker, Ger-

Table II.1 – Extraction yields and induced isotope fractionation (liquid-liquid and solid-liquid), analytical reproducibility, detection and quantification limits for GC-MS and GC-IRMS. Uncertainties correspond to the standard deviation (SD) from n replicate measurements.

Pesticide	Atrazine	Terbutryn	Acetochlor	S-metolachlor	Metalaxyl
Solid-liquid extraction (averages for wetland and river sediments)					
Recovery (%) , n=22	92.8 ± 20.0	92.0 ± 21.5	97.0 ± 23.0	95.5 ± 22.5	88.0 ± 20.0
$\Delta\delta^{13}C$ (‰), n=12) ^a	-0.28 ± 0.5	0.1 ± 1.9	-0.17 ± 0.2	-0.55 ± 1.0	0.6 ± 0.9
$\Delta\delta^{15}N$ (‰), n=5) ^a	-0.10 ± 1.1	0.7 ± 0.9	1.2 ± 0.4	1.6 ± 0.6	1.9 ± 0.4
Solid phase extraction (SPE)					
Recovery (%) , n=4	108.3 ± 11.7	107.7 ± 12.6	121.9 ± 14.2	115.9 ± 12.2	125.4 ± 14.4
$\Delta\delta^{13}C$ (‰), n=4) ^a	0.4 ± 0.6	0.1 ± 0.2	-0.1 ± 0.4	0.1 ± 0.4	0.9 ± 0.7
$\Delta\delta^{15}N$ (‰), n=4) ^a	0.5 ± 1.0	2.0 ± 1.3	0.7 ± 0.7	0.9 ± 0.9	1.1 ± 1.1
Gas chromatography mass spectrometer (GC-MS)					
IDLs ($mg.L^{-1}$) ^b	4.5 ± 0.1	2.5 ± 0.4	2.3 ± 0.6	7.4 ± 0.4	0.8 ± 0.1
IQLs ($mg.L^{-1}$) ^b	41.6 ± 1.3	45.3 ± 1.2	33.2 ± 1.6	30.5 ± 1.1	39.3 ± 2.6
anal. rep. (%) ^c	2.3 ± 0.0	4.4 ± 0.0	5.6 ± 0.0	4.3 ± 0.0	7.2 ± 0.2
wat. anal. prec. (%) ^d	11.7 ± 0.1	12.6 ± 0.1	14.2 ± 0.2	12.2 ± 0.1	14.4 ± 0.2
sed. anal. prec. (%) ^d	19.9 ± 0.1	21.9 ± 0.1	23.6 ± 0.2	23.7 ± 0.1	23.1 ± 0.2
Gas chromatography isotopic ratio mass spectrometer (GC-IRMS)					
C range lin. (ng_C) ^e	10 – 300	10 – 300	20 – 300	20 – 300	20 – 300
($mg.L^{-1}$)	11 – 336	10 – 321	16 – 240	15 – 236	15 – 232
N range lin. (ng_N) ^e	40 – 300	40 – 300	40 – 300	40 – 300	40 – 300
($mg.L^{-1}$)	72 – 538	86 – 642	449 – 3366	472 – 3541	465 – 3486

^a $\Delta\delta$ values are reported as $\Delta\delta = \delta_{EA-IRMS} - \delta_{GC-IRMS}$. It accounts for isotope fractionation induced by the gas chromatography and the extraction. It was compared to a pure pesticide reference determined independently from gas chromatography and the extraction by an elemental analyzer IRMS (EA-IRMS - Flash EA IsoLinkTM CN IRMS, Thermo Fisher Scientific).

^b Instrumental detection limits (IDLs) and instrumental quantification limits (IQLs) were determined by multiple blank and standard injection ($n = 5$), respectively, at the lowest concentration giving a signal-to-noise (S/N) ratio of three.

^c Analytical reproducibility is determined as the ratio of SD and concentrations of five standard injections at $500 \mu g.L^{-1}$ over five independent GC runs [Huntscha et al., 2012].

^d Analytical precisions associated with the matrix effect of water (wat.) and sediment (sed.) samples were evaluated by five independent GC runs ($n = 5$) of the similar spike sample at $300 \mu g.L^{-1}$ and reported as the ratio between measured and spiked values.

^e Range of linearity with the lowest values corresponding to the limit for precise isotope analysis (LPIA) was calculated using a moving window procedure [Jochmann et al., 2006] with intervals of $\pm 0.5\text{‰}$ and $\pm 1\text{‰}$ for C and N, respectively. Corresponding concentration values are given in $mg.L^{-1}$ for a $2 \mu L$ injection.

many) quadrupole time of flight (Q-TOF) high resolution mass spectrometer (HR-MS/MS). Molecule fragments generated during positive and negative ionization were scanned over a range of 30 to 1000 m/z with a resolving power of 54 000 defined at 400 m/z . A list of suspected molecules used for screening of TPs was generated using the pathway prediction systems Metabolite Predict 2.0 (Brucker, Germany), META Ultra 1.2 and Meta PC 1.8.1 (MultiCASE, Beachwood, OH, US) and by reviewing the literature. When available, suspected molecules were confirmed by matching residence times using analytical standards (L1). Tentative candidates were assigned using a mass deviation criteria ($\Delta m/Z$) of 3 *ppm* as compared with mass spectra from the literature (L3) [Schymanski et al., 2014].

For the hydrolysis experiment, TPs were identified using a TSQ Quantum ACCESS LC/MS equipped with an Accela autosampler (Thermo Fisher Scientific) fitted with a temperature-controlled sample tray (10°C). Xcalibur (version 2.1.0) was used for data acquisition. Injection volume was 20 μL . The analytical column was an EC 150/3 Nucleodur Polar Tec (particle size 3 μm , length 150 *mm*, internal diameter 3 *mm*) fitted with a precolumn EC 4/3 Polar Tec, 30 *mm* (Macherey Nagel). The mobile phase consisted of 0.1% formic acid/acetonitrile (A) and 0.1% formic acid/high-purity water (B). The program (flow rate 0.3 $mL \cdot min^{-1}$) included an initial step at 30% A (2 minutes) followed by gradients from 30% to 95% A in 16 minutes and then 3 minutes at 95% A, prior to column regeneration (95 – 30% A (1 minute), 30% A (6 minutes)). Column oven temperature was set at 60°C. The mass spectrometer (MS) was a TSQ Quantum triple quadrupole mass spectrometer (Thermo Scientific) operated using a heated electrospray ionization (HESI) source. Mass spectra were recorded in the positive (spray voltage: 4250 *V*) and negative ion mode (spray voltage: 3500 *V*) and in the positive mode (spray voltage: 4250 *V*) for the internal standard Alachlor-d13. The vaporizer temperature was 300°C, with sheath gas N_2 pressure setting 10 (arbitrary units), auxiliary gas pressure 20, ion sweep gas pressure 0; and ion transfer capillary temperature 300°C. Best sensitivity in multiple reaction monitoring operation (MRM) mode was achieved through acquisition of selected reaction monitoring (SRM) transitions. For compound identification, two SRM transitions and a correct ratio between the abundances of two optimized SRM transitions (SRM1/SRM2) were required along with retention time matching. Mass spectrometry parameters for the detection of (TPs) by LC-MS are available in Masbou et al. (2018).

C- and N-CSIA of Pesticides

A GC-C-IRMS device fitted with a TRACE™ ultra Gas Chromatograph (ThermoFisher Scientific) coupled via a GC IsoLink/Conflow IV interface to an Isotope Ratio Mass Spectrometer (DeltaV plus, ThermoFisher Scientific) allowed for measurements of carbon and nitrogen isotope composition of pesticides. Samples were injected in split mode with a split flow of $30 \text{ mL} \cdot \text{min}^{-1}$ at 250° . Chromatographic separation happened through a TG-5MS column ($60 \text{ m} \times 0.25 \text{ mm}$ internal diameter, $0.25 \mu\text{m}$ film thickness) with helium as the carrier gas at a flow rate of 1.5 mL/min according to the following method. The heat ramp started after 1 min at 50°C and raised up to 150°C at a rate of $15^\circ\text{C} \cdot \text{min}^{-1}$, continued up to 250°C at $2^\circ\text{C} \cdot \text{min}^{-1}$ and finally reached 300°C at $20^\circ\text{C} \cdot \text{min}^{-1}$ to be held for 3 minutes. The oxidation oven consisted of a single combined reactor (P/N 1255321, NiO tube and CuO-NiO-Pt wires, Thermo Fischer Scientific) and was set at 1000°C . A cold finger filled with liquid nitrogen trapped CO_2 formed during the combustion for N measurements.

$\delta^{13}\text{C}$ and $\delta^{15}\text{N}$ values were normalized by the Vienna Pee Dee Belemnite (VPDB) standard for carbon and by the international AIEA600 air standard for nitrogen as follows:

$$\delta^h X [\text{‰}] = 1000 \cdot \left(\frac{R_{\text{sample}}}{R_{\text{standard}}} - 1 \right) \quad (\text{II.1})$$

where $\delta^h X$ is expressed in per thousand (‰) and R refers to the ratio of heavy (h) to light (l) isotopes of the element X ($\frac{^h X}{^l X}$) in the analysed samples and the international standards. Samples were injected in triplicate and $\delta^{13}\text{C}$ and $\delta^{15}\text{N}$ values are reported as the associated arithmetic mean. Each measurement was checked to remain within the linearity ranges for C and N (see Table II.1). A set of in-house BTEX (for C), caffeine (AIEA 600, for N) and pesticide (for C and N) standards with known isotopic composition (determined by EA-IRMS) was measured at least every ten injections to control the measurement quality. Reference $\delta^{13}\text{C}$ and $\delta^{15}\text{N}$ compositions of BTEX and pesticide standards were determined at our isotope facility using an elemental analyser-isotopic ratio mass spectrometer (Flash EA IsoLinkTMCN IRMS, Thermo Fisher Scientific, Bremen, Germany). An analytical uncertainty of $1\sigma_{\delta^{13}\text{C}} \leq 0.5\%$ (n=43) and $1\sigma_{\delta^{15}\text{N}} \leq 0.6\%$ (n=72) was attributed to each measurement, corresponding to the long term accuracy and reproducibility of pesticide standards measured across the analytical sessions.

CSIA data processing

For all experiments, the Rayleigh equation (Eq. II.2) was used to relate pesticide degradation to changes in stable isotope ratios of the non-degraded fraction of pesticides. Bulk isotope fractionation factors (ϵ_{bulk}) for C and N (ϵ_C and ϵ_N) were derived from the linearized Rayleigh equation and was not forced through the origin [Scott et al., 2004]. Isotopic fractionation factors were only reported when the regression with the linearized Rayleigh equation was significant ($p < 0.05$).

$$\frac{\delta^h X_t + 1000}{\delta^h X_0 + 1000} = \frac{X_t}{X_0}^{\frac{\epsilon_{bulk}}{1000}} \quad (\text{II.2})$$

$\delta^h X_0$ and $\delta^h X_t$ are expressed in ‰ and refer to the initial and current isotope composition of pesticides (Eq. II.1), and $\frac{X_t}{X_0}$ to the non-degraded fraction. Correction of ϵ_{bulk} values accounting for repetitive sampling in batch hydrolysis and photodegradation experiments was deemed irrelevant as it systematically fell within the regression confidence interval [Buchner et al., 2017].

In addition to ϵ_{bulk} values, dual element isotope plots of $\delta^{15}N$ against $\delta^{13}C$ values ($\Lambda_{N/C}$, Eq. II.3) were established to relate possible specific transformation mechanisms in the laboratory to photodegradation pathways in the environment [Elsner and Imfeld, 2016, Wijker et al., 2013].

$$\Lambda_{N/C} = \frac{\ln\left(\frac{\delta^{15}N+1}{\delta^{15}N_0+1}\right)}{\ln\left(\frac{\delta^{13}C+1}{\delta^{13}C_0+1}\right)} \approx \frac{\epsilon_N}{\epsilon_C} \quad (\text{II.3})$$

To interpret and compare ϵ_{bulk} values in terms of underlying degradation pathways, apparent kinetic isotope effects (AKIE) were calculated for each element to correct ϵ_{bulk} for isotope dilution, number of reactive sites and intramolecular isotopic competition (Eq. II.4):

$$AKIE \approx \frac{1}{1 + z \cdot \left(\frac{n}{x}\right) \cdot \frac{\epsilon_{bulk}}{1000}} \quad (\text{II.4})$$

where n is the total number of atoms of an element, x the number of atoms in reactive positions and z the number of atoms [Elsner et al., 2005].

Statistical analysis

All statistical analysis and regressions were performed in R using the “stats” package, version 3.6.3. Data from linear regression (*i.e.* k_{eff} , ϵ_C and ϵ_N) are reported with their confidence interval at level 95%.

Bibliography

- [Buchner et al., 2017] Buchner, D., Jin, B., Ebert, K., Rolle, M., Elsner, M., and Haderlein, S. B. (2017). Experimental Determination of Isotope Enrichment Factors - Bias from Mass Removal by Repetitive Sampling. *Environmental Science & Technology*, 51(3):1527–1536.
- [Elsayed et al., 2014] Elsayed, O. F., Maillard, E., Vuilleumier, S., Nijenhuis, I., Richnow, H. H., and Imfeld, G. (2014). Using compound-specific isotope analysis to assess the degradation of chloroacetanilide herbicides in lab-scale wetlands. *Chemosphere*, 99:89–95.
- [Elsner and Imfeld, 2016] Elsner, M. and Imfeld, G. (2016). Compound-specific isotope analysis (CSIA) of micropollutants in the environment — current developments and future challenges. *Current Opinion in Biotechnology*, 41:60–72.
- [Elsner et al., 2005] Elsner, M., Zwank, L., Hunkeler, D., and Schwarzenbach, R. P. (2005). A new concept linking observable stable isotope fractionation to transformation pathways of organic pollutants. *Environmental Science & Technology*, 39(18):6896–6916.
- [Huntscha et al., 2012] Huntscha, S., Singer, H. P., McArdell, C. S., Frank, C. E., and Hollender, J. (2012). Multiresidue analysis of 88 polar organic micropollutants in ground, surface and wastewater using online mixed-bed multilayer solid-phase extraction coupled to high performance liquid chromatography–tandem mass spectrometry. *Journal of Chromatography A*, 1268:74–83.
- [Ivdra et al., 2014] Ivdra, N., Herrero-Martín, S., and Fischer, A. (2014). Validation of user- and environmentally friendly extraction and clean-up methods for compound-specific stable carbon isotope analysis of organochlorine pesticides and their metabolites in soils. *Journal of Chromatography A*, 1355:36–45.
- [Jochmann et al., 2006] Jochmann, M. A., Blessing, M., Haderlein, S. B., and Schmidt, T. C. (2006). A new approach to determine method detection limits for compound-

- specific isotope analysis of volatile organic compounds. *Rapid communications in mass spectrometry: RCM*, 20(24):3639–3648.
- [Masbou et al., 2018] Masbou, J., Drouin, G., Payraudeau, S., and Imfeld, G. (2018). Carbon and nitrogen stable isotope fractionation during abiotic hydrolysis of pesticides. *Chemosphere*, 213:368–376.
- [Olivieri et al., 2006] Olivieri, A. C., Faber, N. M., Ferré, J., Boqué, R., Kalivas, J. H., and Mark, H. (2006). Uncertainty estimation and figures of merit for multivariate calibration (IUPAC Technical Report). *Pure and Applied Chemistry*, 78(3):633–661.
- [Schymanski et al., 2014] Schymanski, E. L., Jeon, J., Gulde, R., Fenner, K., Ruff, M., Singer, H. P., and Hollender, J. (2014). Identifying Small Molecules via High Resolution Mass Spectrometry: Communicating Confidence. *Environmental Science & Technology*, 48(4):2097–2098.
- [Scott et al., 2004] Scott, K. M., Lu, X., Cavanaugh, C. M., and Liu, J. S. (2004). Optimal methods for estimating kinetic isotope effects from different forms of the Rayleigh distillation equation. *Geochimica et Cosmochimica Acta*, 68(3):433–442.
- [Villette et al., 2019] Villette, C., Maurer, L., Wanko, A., and Heintz, D. (2019). Xenobiotics metabolism in *Salix alba* leaves uncovered by mass spectrometry imaging. *Metabolomics*, 15(9):122.
- [Wijker et al., 2013] Wijker, R. S., Adamczyk, P., Bolotin, J., Paneth, P., and Hofstetter, T. B. (2013). Isotopic Analysis of Oxidative Pollutant Degradation Pathways Exhibiting Large H Isotope Fractionation. *Environmental Science & Technology*, 47(23):13459–13468.

2.2 Pesticide hydrolysis

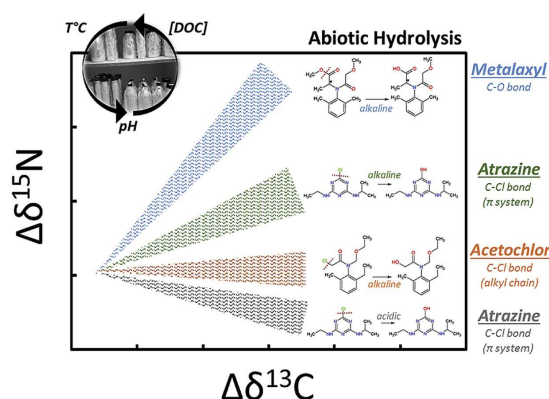
This section presents an extended summary of a previously published paper [Masbou et al., 2018]. This work started before the PhD and was published during. Specific results from this publication are part of the interpretation of S-metolachlor degradation at the SWI. While hydrolysis of triazine (atrazine), acylalanine (metalaxyl) and chloroacetanilide pesticides (alachlor, acetochlor, butachlor and S-Metolachlor) were investigated in this study, the results presented here voluntarily focus on chloroacetanilide pesticides. Sections on the enantio-selectivity of metalaxyl hydrolysis and isotope fractionation of transformation products are not presented. Only hydrolysis degradation rates, TPs formation and induced isotope fractionation are reported in this manuscript, for the sake of consistency with other chapters of this thesis.

From published paper:

Masbou, J., Drouin, G., Payraudeau, S., Imfeld, G. (2018). Carbon and nitrogen stable isotope fractionation during abiotic hydrolysis of pesticides. *Chemosphere*, 213, 368–376.

Abstract

Compound-specific Stable Isotope Analysis (CSIA) has been recently established as a tool to study pesticide degradation in the environment. Among degradative processes, hydrolysis is environmentally relevant as it can be chemically or enzymatically mediated. Here, CSIA was used to examine stable carbon and nitrogen isotope fractionation during abiotic hydrolysis of legacy or currently used chloroacetanilide herbicides (Acetochlor, Alachlor, S-Metolachlor and Butachlor). Degradation products analysis and C-N dual-CSIA allowed to infer hydrolytic degradation pathways from carbon and nitrogen isotopic fractionation. Carbon isotopic fractionation for alkaline hydrolysis revealed similar apparent kinetic isotope effects ($AKIE_C = 1.03 - 1.07$) for all pesticides, which were consistent with SN2 type nucleophilic substitutions. Reference values for abiotic versus biotic SN2 reactions derived from carbon and nitrogen CSIA may be used to untangle pesticide degradation pathways and evaluate in situ degradation during natural and engineered remediation.



2.2.1 Introduction

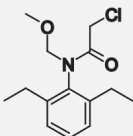
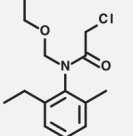
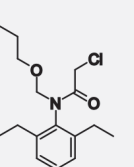
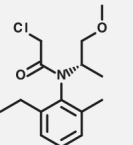
The frequent and ubiquitous detection of pesticides in ground and surface-waters reflects their extensive use and persistence [Fenner et al., 2013]. In the environment, pesticide concentrations mainly decrease by degradation, but also by non-degradative processes, such as dilution or sorption. This hinders the estimation of degradation extent in the field without detection of transformation products, which are often unknown, or establishment of mass balances. Hydrolysis is a major pathway of pesticide degradation, which can be abiotically or biologically-mediated [Meyer et al., 2009], depending on pH, temperature [Mill and Mabey, 1988] or dissolved organic matter (Larson and Weber, 1994). However, degradation pathways, such as hydrolysis, first have to be related to specific transformation mechanisms to tease them apart in laboratory experiments, and to eventually evaluate dissipation pathways under field conditions.

In this context, Compound-specific Stable Isotope Analysis (CSIA) is useful to evaluate in situ pesticide degradation because it may provide independent estimates of pesticide degradation [Elsner, 2010, Elsner and Imfeld, 2016]. Pesticide CSIA relies on the kinetic isotope effect (KIE) caused by slightly different cleavage rates of molecule's bonds containing light and heavy isotopes. In contrast, non-degradative processes, such as dilution, volatilization or sorption generally result in insignificant isotopic fractionation [Schüth et al., 2003, Imfeld et al., 2014, Elsner and Imfeld, 2016]. The isotope fractionation (ϵ) relates changes of isotope ratios to the extent of degradation following a Rayleigh approach [Hoefs, 2009]. Some reference ϵ values for specific biotic or abiotic transformation mechanisms of pesticides, were retrieved from laboratory experiments [Hartenbach et al., 2008, Meyer et al., 2009]. Changes in carbon isotope ratios are, however, smaller for larger molecules and may not be easily detected under

field conditions because non-reactive positions ‘dilute’ isotope effects at the reacting bond [Elsner, 2010]. In this case, dual element isotope plots of, for instance Nitrogen *vs* Carbon, reveal the footprint of underlying isotope effects [Elsner and Imfeld, 2016]. For example, N and C dual element isotope patterns enabled to discriminate bond cleavage mechanisms during abiotic (acidic and alkaline) and biotic hydrolysis of Atrazine in experimental [Meyer et al., 2008, Meyer et al., 2009] and theoretical [Grzybewska et al., 2014] studies. However, C and N isotope fractionation during hydrolysis of anilide pesticides have yet to be evaluated.

Among anilide pesticides, S-Metolachlor, Acetochlor and Alachlor are the most applied herbicides worldwide [Maggi et al., 2019] and Butachlor is commonly used in Indian rice fields [Armanpour and Bing, 2015]. Anilide pesticides are mainly made of carbon ($\approx 60\%$, Table II.2) and changes in $\delta^{13}C$ values have been used to evaluate chloroacetanilide degradation [Elsayed et al., 2014, Alvarez-Zaldívar et al., 2018]. Due to high detection limits of isotope ratio mass spectrometry and small contribution of nitrogen (*i.e.*, only one N heteroatom in the chloroacetanilides) challenge multi-element CSIA of anilide pesticides at environmental concentrations [Lutz et al., 2017], sample pre-concentration (> 1000 times) recently allowed dual N and C-CSIA of S-Metolachlor at an agricultural catchment [Alvarez-Zaldívar et al., 2018]. However, reference C and N isotopic fractionation ϵ for transformation reactions involving anilides are lacking so far. In addition, $C - N$ isotope dual plots derived during hydrolysis may help to tease apart aqueous hydrolysis from other pathways of pesticide dissipation.

Table II.2 – *Physico-chemical properties and chemical structures of the studied pesticides.* ¹ Data from [Lewis et al., 2016].

	Chloroacetanilide			
	Alachlor	Acetochlor	Butachlor	S-Metolachlor
Molecular formula	$C_{14}H_{20}ClNO_2$	$C_{14}H_{20}ClNO_2$	$C_{17}H_{26}ClNO_2$	$C_{15}H_{22}ClNO_2$
Molecular structure				
Molar mass ($g.mol^{-1}$) ¹	269.8	269.8	311.8	283.8
Solubility in water (20 – 25°C, $mg.L^{-1}$) ¹	240	282	20	530
Dissociation constant (pKa) ¹	Non-ionizable	Non-ionizable	Non-ionizable	Non-ionizable

The objectives of this study were (i) to evaluate reaction kinetic rate constants for abiotic hydrolysis of chloroacetanilide herbicides (Alachlor, Acetochlor, S-Metolachlor, Butachlor) as a function of pH, Temperature and dissolved organic carbon concentrations that may occur in natural water, (ii) to derive reference carbon (ϵ_C) and nitrogen (ϵ_N) isotope fractionation actors during pesticide hydrolysis and (iii) to identify degradation mechanisms of pesticide degradation during abiotic hydrolysis using AKIE values and $C - N$ dual isotope plots. Gas chromatography combustion isotope ratio mass spectrometry (GC-C-IRMS) methods were developed for $\delta^{13}C$ and $\delta^{15}N$ analysis of pesticides and used together with parent compounds and degradation products analysis to evaluate isotope fractionation during abiotic hydrolysis as a function of pH (from 2 to 12), temperature (T, from $20^\circ C$ and $30^\circ C$) and dissolved organic carbon concentration (DOC, from 0 to $20\text{ mg}_C.L^{-1}$).

2.2.2 Material and Methods

Chemicals and Solution Preparation

Chloroacetanilides (Alachlor, Acetochlor, Butachlor, S-Metolachlor) standards (analytical grade purity: 99.6%), Metolachlor-d11 (analytical grade purity, > 97%), solvents (dichloromethane DCM, acetonitrile CAN, ethyl acetate EtOAc; HPLC grade purity, > 99.9%) were purchased from Sigma-Aldrich (St. Louis, MO, USA). Sodium hydroxide (BioUltra, > 98.0%), potassium phthalate (> 99.5%), potassium chloride (BioReagent, > 99.0%), potassium phosphate (> 99.0%), boric acid (BioReagent, > 99.5%), calcium chloride dehydrate (> 99.0%) and humic acid sodium salt (technical grade) were purchased from Sigma-Aldrich (St. Louis, MO, USA).

Stock solutions for water spiking and standards for chromatographic analysis were prepared at $5\text{ g}.L^{-1}$ as individual pesticide or mix solutions in DCM and ACN, respectively. Aliquots of the solutions were stored at $-20^\circ C$ until use and/or analysis. Physicochemical properties of the pesticides used in the experiment are listed in Table II.2.

Experimental Setup

Hydrolysis depends on pH and temperature [Mill and Mabey, 1988], but dissolved organic carbon in aquatic environment may also alter pesticide hydrolytic patterns [Larson, 2018]. Duplicate abiotic hydrolysis experiments were carried out in 1 L Schott glass bottles under dark and sterile conditions [OECD, 2004]. Five aqueous buffer so-

lutions (1 L) were prepared at $pH = 2, 4, 7, 9$ and 12 , sterilized by filtration through a $0.22 \mu m$ cellulose membrane (Rotilabo®), Carl Roth®, France) and split in autoclaved Schott bottles. Experiments with dissolved organic carbon (DOC) were carried out at $pH = 7$ for approaching environmental conditions. Briefly, humic acid salts dissolved in $0.1 mol.L^{-1}$ NaOH solution by 45 minutes sonication [Mazzuoli et al., 2003] were filtered on $0.22 \mu m$ cellulose membranes (Rotilabo®, Carl Roth®, France) and adjusted to $pH = 7$ to reach final DOC concentrations of $4.9, 10.7$ and $20.3 \pm 0.1 mg_C.L^{-1}$. Buffer solutions were spiked with $3.2 mg.L^{-1}$ ($\approx 12 \mu mol.L^{-1}$) of Alachlor, Ace-tochlor, Metalaxyl and S-Metolachlor, $4.3 mg.L^{-1}$ ($\approx 20 \mu mol.L^{-1}$) for Atrazine and $2.4 mg.L^{-1}$ ($\approx 8 \mu mol.L^{-1}$) for Butachlor from a $5 g.L^{-1}$ stock solution in DCM. The solutions were stirred at $20^\circ C$ until total DCM evaporation. Intermolecular effects between pesticides were negligible at those concentrations as confirmed by very similar results obtained for Atrazine in our study compared to previous studies with Atrazine only [Meyer et al., 2008]. Bottles were tightly capped with screw caps (Schott), covered with aluminum foil and incubated separately at $20 \pm 1^\circ C$ and $30 \pm 1^\circ C$. From $20 mL$ to $100 mL$ of different buffers were sampled at $t = 0$ (all conditions), $t = 9$ (all), $t = 22$ ($pH = 12$), $t = 30$ ($pH = 12$), $t = 36$ (all), $t = 44$ ($pH = 12$), $t = 57$ ($pH = 12$), $t = 94$ (all), $t = 200$ days (all), depending on pH conditions and dissipation kinetics.

Analytical methods are provided in Section 2.1 of this thesis.

2.2.3 Results and Discussion

Hydrolysis of chloroacetanilides and isotopic fractionation

Hydrolysis of chloroacetanilides was only observed under alkaline conditions ($pH=12$) and DOC addition did not influenced hydrolysis at $pH = 7$ (see Table II.3). All chloroacetanilide molecules underwent hydrolysis at $30^\circ C$ with similar degradation kinetics ($k = 0.038 \pm 0.003 d^{-1}$ for Acetochlor, $k = 0.038 \pm 0.004 d^{-1}$ for Alachlor, $k = 0.027 \pm 0.005 d^{-1}$ for Butachlor), with the exception of S-Metolachlor ($k = 0.006 \pm 0.001 d^{-1}$ at $30^\circ C$ and insignificant hydrolysis at $20^\circ C$). Hydrolysis kinetics for Acetochlor, Alachlor and Butachlor in experiment at $30^\circ C$ were 3 to 4 fold faster compared to those in experiments at $20^\circ C$. Except for S-Metolachlor, for which no degradation products were identified, mass spectra interpretation and comparison with literature [Zheng and Ye, 2001] indicates the formation of the hydroxylated products N-(2,6-diethylphenyl)-2-hydroxy-N-(methoxymethyl) acetamide, N-(ethoxymethyl)eN-(2-ethyl-6-methylphenyl)-2- hydroxyacetamide and N-(2,6-diethylphenyl)-2-hydroxy-

N- (butoxymethyl)acetamide as degradation products for Alachlor, Acetochlor and Butachlor hydrolysis, respectively. Inspection of mass spectra obtained by both GC-MS and LC-MS running in full-scan mode did not allow to detect other degradation products. The occurrence of hydroxylated degradation products in all experiments revealed nucleophilic substitution at the $C - Cl$ bond position of the chloroacetanilide pesticides. Our results are consistent with those obtained during alkaline ($NaOH$ 2 N) hydrolysis of chloroacetanilides [Carlson et al., 2006]. In few cases, however, an additional pathway involving amide cleavage was observed, that we could not exclude for S-Metolachlor under alkaline hydrolysis as no degradation products were unequivocally identified.

Acetochlor, Alachlor and Butachlor displayed similar carbon isotopic fractionation during abiotic hydrolysis ($\epsilon_C = -4.0 \pm 0.8\text{‰}$, $\epsilon_C = -4.9 \pm 0.4\text{‰}$ and $\epsilon_C = -3.7 \pm 0.7\text{‰}$, respectively), whereas ϵ_C for S-metolachlor was lower ($-2.8 \pm 0.6\text{‰}$) (see Table II.3). In comparison, ϵ_C values have been obtained for biotic degradation of metolachlor ($\epsilon_C \approx 0\text{‰}$, degradation $\leq 30\%$), alachlor ($\epsilon_C = -2.0 \pm 0.3\text{‰}$, degradation $\leq 60\%$) and acetochlor ($\epsilon_C = -3.4 \pm 0.5\text{‰}$, degradation $\leq 65\%$) in a constructed wetland [Elsayed et al., 2014] or for S-metolachlor biotic degradation ($\epsilon_C = -1.5 \pm 0.5\text{‰}$, degradation $\geq 80\%$) in soil incubation experiments [Alvarez-Zaldívar et al., 2018]. Small differences in isotopic fractionation during chloroacetanilide hydrolysis and biotic degradation may reflect distinct mechanisms, which is supported by the formation of different degradation products. For instance, oxanilic (OXA) and ethanesulfonic acids (MESA) prevailed in wetlands [Maillard et al., 2016] but were not detected in this study.

Weak nitrogen isotopic fractionation ($\Delta\delta^{15}N \approx 1.5\text{‰}$) for Alachlor, Acetochlor and Butachlor did not allow to derive ϵ_N values given the analytical precision ($\approx 1.0\text{‰}$). In contrast, S-Metolachlor displayed small but significant $\epsilon_N = -2.0 \pm 1.3\text{‰}$. Since S-Metolachlor contains a single nitrogen heteroatom, nitrogen isotope effect is position specific and secondary.

Mechanistic insights from AKIE values and $C - N$ isotope plots

$AKIE_C$ values derived from isotopic fractionation for both alkaline and acidic hydrolysis (Table II.3) ranged from 1.043 to 1.073 for all pesticides, which is consistent with primary isotope effect during $SN - 2$ type mechanisms ($AKIE_C$ from 1.03 to 1.07 [Elsner et al., 2005]). Despite the occurrence of primary isotope effects and $AKIE_C$ calculation that limit isotopic dilution effects, carbon isotope fractionations lack of sensitivity to tease apart hydrolysis mechanisms.

Table II.3 – Degradation rates ($k - d^{-1}$), Half-lives ($DT_{50} - d$), fractionation factors (ϵ_C and ϵ_N - ‰) as well as $AKIE_C$ and $AKIE_N$ values for Acetochlor, Alachlor, Butachlor and S-Metolachlor at pH = 2, 4, 7, 9 and 12 and $T = 20^\circ C$ and $T = 30^\circ C$. Results indicate mean $\pm \sigma$. The results obtained for the experiments with DOC (5 $mg_C.L^{-1}$, 10 $mg_C.L^{-1}$, 20 $mg_C.L^{-1}$) at pH=7 are not displayed as they did not differ from the condition without DOC (i.e. $DT_{50} \geq 200$ days, and ϵ insignificants). *n.s.* stands for not significant.

pH		2		4		7		9		12	
Temperature		30°C	20°C	30°C	20°C	30°C	20°C	30°C	20°C	30°C	20°C
Acetochlor	k	\leq 0.004	\leq 0.004	\leq 0.004	\leq 0.004	\leq 0.004	\leq 0.004	\leq 0.004	\leq 0.004	-0.009 ± 0.002	-0.038 ± 0.003
	DT_{50}	\geq 200	\geq 200	\geq 200	\geq 200	\geq 200	\geq 200	\geq 200	\geq 200	74.6 ± 17.2	18.4 ± 1.6
	$\Delta\delta^{13}C$	<i>n.s.</i>	<i>n.s.</i>	<i>n.s.</i>	<i>n.s.</i>	<i>n.s.</i>	<i>n.s.</i>	<i>n.s.</i>	<i>n.s.</i>	-3.9 ± 1.9	-3.6 ± 0.9
	ϵ_C (AKIE _C)	<i>n.s.</i>	<i>n.s.</i>	<i>n.s.</i>	<i>n.s.</i>	<i>n.s.</i>	<i>n.s.</i>	<i>n.s.</i>	<i>n.s.</i>	-4.0 ± 0.8	(1.060 ± 0.012)
	ϵ_N (AKIE _N)	-	-	-	-	-	-	-	-	<i>n.s.</i>	
Alachlor	k	\leq 0.004	\leq 0.004	\leq 0.004	\leq 0.004	\leq 0.004	\leq 0.004	\leq 0.004	\leq 0.004	-0.011 ± 0.002	-0.038 ± 0.004
	DT_{50}	\geq 200	\geq 200	\geq 200	\geq 200	\geq 200	\geq 200	\geq 200	\geq 200	63.2 ± 14.3	18.1 ± 2.0
	$\Delta\delta^{13}C$	<i>n.s.</i>	<i>n.s.</i>	<i>n.s.</i>	<i>n.s.</i>	<i>n.s.</i>	<i>n.s.</i>	<i>n.s.</i>	<i>n.s.</i>	-4.6 ± 0.9	-4.9 ± 0.6
	ϵ_C (AKIE _C)	<i>n.s.</i>	<i>n.s.</i>	<i>n.s.</i>	<i>n.s.</i>	<i>n.s.</i>	<i>n.s.</i>	<i>n.s.</i>	<i>n.s.</i>	-4.9 ± 0.4	(1.073 ± 0.005)
	ϵ_N (AKIE _N)	-	-	-	-	-	-	-	-	<i>n.s.</i>	
Butachlor	k	\leq 0.004	\leq 0.004	\leq 0.004	\leq 0.004	\leq 0.004	\leq 0.004	\leq 0.004	\leq 0.004	-0.010 ± 0.002	-0.027 ± 0.005
	DT_{50}	\geq 200	\geq 200	\geq 200	\geq 200	\geq 200	\geq 200	\geq 200	\geq 200	70.1 ± 17.2	25.3 ± 4.5
	$\Delta\delta^{13}C$	<i>n.s.</i>	<i>n.s.</i>	<i>n.s.</i>	<i>n.s.</i>	<i>n.s.</i>	<i>n.s.</i>	<i>n.s.</i>	<i>n.s.</i>	-3.2 ± 0.6	-4.3 ± 1.3
	ϵ_C (AKIE _C)	<i>n.s.</i>	<i>n.s.</i>	<i>n.s.</i>	<i>n.s.</i>	<i>n.s.</i>	<i>n.s.</i>	<i>n.s.</i>	<i>n.s.</i>	-3.7 ± 0.7	(1.067 ± 0.013)
	ϵ_N (AKIE _N)	-	-	-	-	-	-	-	-	<i>n.s.</i>	
S-Metolachlor	k	\leq 0.004	\leq 0.004	\leq 0.004	\leq 0.004	\leq 0.004	\leq 0.004	\leq 0.004	\leq 0.004		-0.006 ± 0.001
	DT_{50}	\geq 200	\geq 200	\geq 200	\geq 200	\geq 200	\geq 200	\geq 200	\geq 200	≥ 200	122.1 ± 26.0
	ϵ_C (AKIE _C)	<i>n.s.</i>	<i>n.s.</i>	<i>n.s.</i>	<i>n.s.</i>	<i>n.s.</i>	<i>n.s.</i>	<i>n.s.</i>	<i>n.s.</i>	-	-2.8 ± 0.6 (1.043 ± 0.008)
	ϵ_N (AKIE _N)	-	-	-	-	-	-	-	-	-	-2.0 ± 1.3 (1.002 ± 0.001)

As anilide pesticides contain 1 – 3 N heteroatoms, dual $C - N$ isotope analysis may circumvent the issue of isotope effect ‘dilution’ encountered with C isotopes and show sufficient sensitivity to distinguish hydrolysis mechanisms. Secondary nitrogen isotope effect occurred for all molecules, except for S-Metolachlor. Despite low $AKIE_N$ values ranging from 0.994 to 1.003, dual plot of $\delta^{13}C$ versus $\delta^{15}N$ values suggests that degradation mechanism for Acetochlor and Butachlor during hydrolysis differ from that of S-Metolachlor (Figure II.1). Isotope fractionation patterns in dual plots thus revealed

the footprint of underlying isotope effects for Acetochlor, Alachlor and Butachlor which undergo $SN_2 C - Cl$ bond breaking in alkyl chain. Altogether, these results highlight that further work is needed to minimize analytical uncertainties and enhance interpretation when degradation extent and/or isotope fractionation are modest.

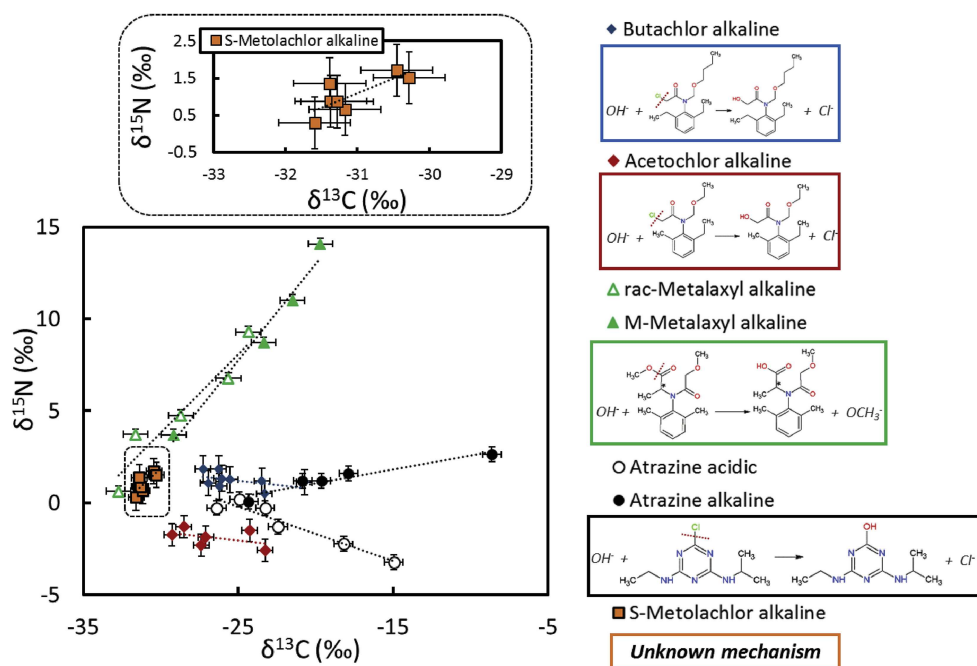


Figure II.1 – $C - N$ isotope plot for carbon and nitrogen for Atrazine, Metalaxyl (racemic and R enantiomer formulation (M-Metalaxyl)) and S-Metolachlor during acidic and/or alkaline hydrolysis. S-Metolachlor data are zoomed at the top of the figure. Error bars correspond to the analytical uncertainty of triplicate measurements ($\pm\sigma$). Displayed linear regression are significant except for Butachlor and Acetochlor ($p > 0.05$)

2.2.4 Environmental implications

Abiotic hydrolysis of Acetochlor, Alachlor, S-Metolachlor, Butachlor, Metalaxyl, and Atrazine at most common environmental pH ($4 < pH < 9$) is a slow process ($DT_{50} > 200$ days) associated with insignificant isotopic fractionation ($\Delta\delta^{13}C \leq 0.5\text{‰}$). Abiotic hydrolysis of studied pesticides thus may be neglected in most CSIA studies when pH of surface and groundwater systems range between 6 and 8.5, although hydrolysis may also occur locally at water-mineral interface in aquifers [Smolen and Stone, 1997]. In contrast, significant hydrolysis occurred at $pH > 9$. For instance, at $30^{\circ}C$ chloroacetanilide degradation ranged from a few days (Acetochlor, $pH = 12$) to several months (S-Metolachlor, $pH = 12$). Such alkaline conditions may locally occur in carbonate-rich minerals drainage ($pH \approx 10 - 12$, [Khoury et al., 1992, Möller and Bau, 1993]). Most importantly, the combination of degradation products analysis and C-N dual-CSIA allowed to elucidate degradation mechanisms of chloroacetanilide pesticides. These first reference isotopic fractionation values for hydrolysis of anilide pesticides can be compared in the future with ^{15}N and ^{13}C fractionation patterns during microbial degradation, and eventually used to tease apart degradation pathways in the field.

Bibliography

- [Alvarez-Zaldívar et al., 2018] Alvarez-Zaldívar, P., Payraudeau, S., Meite, F., Masbou, J., and Imfeld, G. (2018). Pesticide degradation and export losses at the catchment scale: Insights from compound-specific isotope analysis (CSIA). *Water Research*, 139:198–207.
- [Armanpour and Bing, 2015] Armanpour, S. and Bing, L. (2015). Adsorption of Herbicide Butachlor in Cultivated Soils of Golestan Province, Iran. *Journal of Geoscience and Environment Protection*, 3(3):15–24.
- [Carlson et al., 2006] Carlson, D. L., Than, K. D., and Roberts, A. L. (2006). Acid- and Base-Catalyzed Hydrolysis of Chloroacetamide Herbicides. *Journal of Agricultural and Food Chemistry*, 54(13):4740–4750.
- [Elsayed et al., 2014] Elsayed, O. F., Maillard, E., Vuilleumier, S., Nijenhuis, I., Richnow, H. H., and Imfeld, G. (2014). Using compound-specific isotope analysis to assess the degradation of chloroacetanilide herbicides in lab-scale wetlands. *Chemosphere*, 99:89–95.
- [Elsner, 2010] Elsner, M. (2010). Stable isotope fractionation to investigate natural transformation mechanisms of organic contaminants: principles, prospects and limitations. *Journal of Environmental Monitoring*, 12(11):2005–2031.
- [Elsner and Imfeld, 2016] Elsner, M. and Imfeld, G. (2016). Compound-specific isotope analysis (CSIA) of micropollutants in the environment — current developments and future challenges. *Current Opinion in Biotechnology*, 41:60–72.
- [Elsner et al., 2005] Elsner, M., Zwank, L., Hunkeler, D., and Schwarzenbach, R. P. (2005). A new concept linking observable stable isotope fractionation to transformation pathways of organic pollutants. *Environmental Science & Technology*, 39(18):6896–6916.

- [Fenner et al., 2013] Fenner, K., Canonica, S., Wackett, L. P., and Elsner, M. (2013). Evaluating Pesticide Degradation in the Environment: Blind Spots and Emerging Opportunities. *Science*, 341(6147):752–758.
- [Grzybkowska et al., 2014] Grzybkowska, A., Kaminski, R., and Dybala-Defratyka, A. (2014). Theoretical predictions of isotope effects versus their experimental values for an example of uncatalyzed hydrolysis of atrazine. *Physical Chemistry Chemical Physics*, 16(29):15164–15172.
- [Hartenbach et al., 2008] Hartenbach, A. E., Hofstetter, T. B., Tentscher, P. R., Canonica, S., Berg, M., and Schwarzenbach, R. P. (2008). Carbon, Hydrogen, and Nitrogen Isotope Fractionation During Light-Induced Transformations of Atrazine. *Environmental Science & Technology*, 42(21):7751–7756.
- [Hoefs, 2009] Hoefs, J. (2009). *Stable Isotope Geochemistry*. Springer-Verlag, Berlin Heidelberg, 6 edition.
- [Imfeld et al., 2014] Imfeld, G., Kopinke, F. D., Fischer, A., and Richnow, H. H. (2014). Carbon and hydrogen isotope fractionation of benzene and toluene during hydrophobic sorption in multistep batch experiments. *Chemosphere*, 107:454–461.
- [Khoury et al., 1992] Khoury, H., Salameh, E., Clark, I., Fritz, P., Bajjali, W., Milodowski, A., Cave, M., and Alexander, W. (1992). A natural analogue of high pH cement pore waters from the Maqarin area of northern Jordan. I: introduction to the site. *Journal of Geochemical Exploration*, 46(1):117–132.
- [Larson, 2018] Larson, R. (2018). *Reaction Mechanisms in Environmental Organic Chemistry*. Routledge.
- [Lewis et al., 2016] Lewis, K. A., Tzilivakis, J., Warner, D. J., and Green, A. (2016). An international database for pesticide risk assessments and management. *Human and Ecological Risk Assessment: An International Journal*, 22(4):1050–1064.
- [Lutz et al., 2017] Lutz, S. R., van der Velde, Y., Elsayed, O. F., Imfeld, G., Lefrancq, M., Payraudeau, S., and van Breukelen, B. M. (2017). Pesticide fate at catchment scale: conceptual modelling of stream CSIA data. *Hydrol. Earth Syst. Sci. Discuss.*, 2017:1–30.
- [Maggi et al., 2019] Maggi, F., Tang, F. H. M., Cecilia, D. I., and McBratney, A. (2019). PEST-CHEMGRIDS, global gridded maps of the top 20 crop-specific pesticide application rates from 2015 to 2025. *Scientific Data*, 6(1):1–20.

- [Maillard et al., 2016] Maillard, E., Lange, J., Schreiber, S., Dollinger, J., Herbstritt, B., Millet, M., and Imfeld, G. (2016). Dissipation of hydrological tracers and the herbicide S-metolachlor in batch and continuous-flow wetlands. *Chemosphere*, 144:2489–2496.
- [Masbou et al., 2018] Masbou, J., Drouin, G., Payraudeau, S., and Imfeld, G. (2018). Carbon and nitrogen stable isotope fractionation during abiotic hydrolysis of pesticides. *Chemosphere*, 213:368–376.
- [Mazzuoli et al., 2003] Mazzuoli, S., Loiselle, S., Hull, V., Bracchini, L., and Rossi, C. (2003). The Analysis of the Seasonal, Spatial, and Compositional Distribution of Humic Substances in a Subtropical Shallow Lake. *Acta hydrochimica et hydrobiologica*, 31(6):461–468.
- [Meyer et al., 2009] Meyer, A. H., Penning, H., and Elsner, M. (2009). C and N Isotope Fractionation Suggests Similar Mechanisms of Microbial Atrazine Transformation Despite Involvement of Different Enzymes (AtzA and TrzN). *Environmental Science & Technology*, 43(21):8079–8085.
- [Meyer et al., 2008] Meyer, A. H., Penning, H., Lowag, H., and Elsner, M. (2008). Precise and Accurate Compound Specific Carbon and Nitrogen Isotope Analysis of Atrazine: Critical Role of Combustion Oven Conditions. *Environmental Science & Technology*, 42(21):7757–7763.
- [Mill and Mabey, 1988] Mill, T. and Mabey, W. (1988). Hydrolysis of Organic Chemicals. In *Reactions and Processes*, number 2 / 2D in The Handbook of Environmental Chemistry, pages 71–111. Springer Berlin Heidelberg.
- [Möller and Bau, 1993] Möller, P. and Bau, M. (1993). Rare-earth patterns with positive cerium anomaly in alkaline waters from Lake Van, Turkey. *Earth and Planetary Science Letters*, 117:671–676.
- [OECD, 2004] OECD (2004). *Test No. 111: Hydrolysis as a Function of pH*. Organisation for Economic Co-operation and Development, Paris.
- [Schüth et al., 2003] Schüth, C., Taubald, H., Bolaño, N., and Maciejczyk, K. (2003). Carbon and hydrogen isotope effects during sorption of organic contaminants on carbonaceous materials. *Journal of Contaminant Hydrology*, 64(3):269–281.

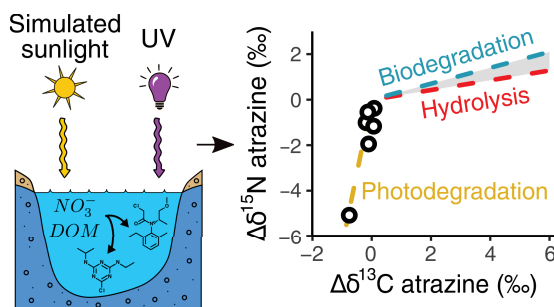
- [Smolen and Stone, 1997] Smolen, J. M. and Stone, A. T. (1997). Divalent Metal Ion-Catalyzed Hydrolysis of Phosphorothionate Ester Pesticides and Their Corresponding Oxonates. *Environmental Science & Technology*, 31(6):1664–1673.
- [Zheng and Ye, 2001] Zheng, H. H. and Ye, C. M. (2001). Identification of UV photo-products and hydrolysis products of butachlor by mass spectrometry. *Environmental Science & Technology*, 35(14):2889–2895.

2.3 Pesticide photodegradation in agriculturally impacted surface waters

From submitted paper: Drouin, G., Droz, B., Leresche, F., Payraudeau, S., Masbou, J. & Imfeld, G., Direct and Indirect Photodegradation of Atrazine and S-metolachlor in Agriculturally Impacted Surface Water and Associated C and N Isotope Fractionation, Environmental Science & Technology.

Abstract

Limited knowledge of photodegradation-induced isotope fractionation hampers the application of compound-specific isotope analysis (CSIA) to trace pesticide degradation in surface waters. Here, we investigated carbon and nitrogen isotope fractionation during direct and indirect photodegradation of the herbicides atrazine and *S*-metolachlor in synthetic water mimicking agriculturally impacted surface waters containing nitrates ($20\text{ mg}\cdot\text{L}^{-1}$) and dissolved organic matter (DOM - $5.4\text{ mg}_C\cdot\text{L}^{-1}$). Atrazine and *S*-metolachlor were quickly photodegraded by direct and indirect mechanisms (half-lives < 5 and < 7 days, respectively). DOM slowed down photodegradation while nitrates increased degradation rates. Transformation products analysis showed that oxidation mediated by hydroxyl radicals predominate during indirect photodegradation. UV light (254 nm) caused significant C and N isotope fractionation, yielding fractionation factors $\epsilon_C = 2.7 \pm 0.3$ and $0.8 \pm 0.1\text{‰}$ and $\epsilon_N = 2.4 \pm 0.3$ and $-2.6 \pm 0.7\text{‰}$ for atrazine and *S*-metolachlor respectively. In contrast, photodegradation under simulated sunlight led to negligible C and slight N isotope fractionation. As the radiation wavelength influenced the direct photodegradation-induced isotope fractionation, the use of simulated sunlight is recommended to evaluate photodegradation mechanisms in the environment. Since C and N isotope fractionation patterns for atrazine and *S*-metolachlor photodegradation differed from those reported for biodegradation and hydrolysis, CSIA offers new opportunities to distinguish between photodegradation and other dissipation pathways in surface waters.



2.3.1 Introduction

The ever-increasing use of pesticides, mainly for agricultural purposes, has led to ubiquitous contamination of surface waters, [de Souza et al., 2020] which may affect environmental biodiversity and human health [Stehle and Schulz, 2015]. Understanding pesticide transformation in surface waters is thus crucial for predicting their persistence, the formation of transformation products (TPs) and mitigating detrimental effects of further pollution. While biodegradation is an important process of pesticide degradation in the environment, photodegradation also plays a prominent role in surface waters [Fenner et al., 2013]. Pesticide photodegradation is compound- and condition-specific, which often limits the interpretation of photodegradation kinetics and mechanisms in various types of surface water [Remucal, 2014, Zeng and Arnold, 2013]. In particular, the influence of the hydrochemical composition, the nature of dissolved organic matter (DOM) as well as the light spectrum on pesticide photodegradation remains poorly understood [Celeiro et al., 2017].

Pesticides undergo photodegradation by direct and indirect mechanisms. During direct photodegradation, pesticide molecules absorb light resulting in bond cleavage. Indirect photodegradation involves reactions with short-lived reactive intermediates, such as hydroxyl radical ($HO\bullet$) or DOM excited triplet states (${}^3DOM^*$) [Schwarzenbach et al., 2003]. Nitrate photolysis produces $HO\bullet$ that can react with pesticides in surface waters, even at nitrate concentrations as low as 0.02 mg.L^{-1} [Zeng and Arnold, 2013]. DOM has both inhibitory and/or photosensitizing effects, depending on its concentration and composition. [Leresche et al., 2016]. On the one hand, DOM absorbs light, reducing direct photodegradation of pesticides and $HO\bullet$ generation from nitrate photolysis. On the other hand, upon absorbing light, DOM generates ${}^3DOM^*$ that is the precursor of $({}^1O_2)$ in surface waters. Both ${}^3DOM^*$ and $({}^1O_2)$ can react with pesticides. DOM is also a major sink of HO in surface waters, reducing HO reactions with pesticides. DOM can also reduce pesticide oxidation intermediates back to the parent compounds, and limit pesticide photodegradation [Rosario-Ortiz and Canonica, 2016]. The effects of DOM on pesticide photodegradation are, however, compound-specific and involve mostly unknown mechanisms [Karpuzcu et al., 2016]. While the combined effect of nitrates and DOM on pesticide photodegradation is relevant for surface waters in agricultural areas, few studies on the subject have been carried out to date [Dimou et al., 2005, Remucal, 2014].

The ability of compound-specific isotope analysis (CSIA) to specifically evaluate micropollutant degradation, including pesticides and pharmaceuticals, has already been exploited in diverse environmental compartments [Elsner and Imfeld, 2016]. Pollutant molecules displaying different ratios of light over heavy isotopes are degraded at slightly different rates, resulting in a kinetic isotope effect (KIE) quantifiable by CSIA [Elsner et al., 2005]. However, dilution processes, such as transport or sorption, generally do not alter stable isotope ratios (e.g., $^2H/^1H$, $^{13}C/^{12}C$, and $^{15}N/^{14}N$) within pesticides [Thullner et al., 2012]. As the KIE reflects the rate-limiting step of the involved mechanism, each degradation pathway displays a specific isotope fractionation pattern, which may allow to differentiate co-occurring degradation processes in the environment. For example, CSIA was used to distinguish the contribution of direct photodegradation from other processes, including biodegradation, abiotic oxidation and dilution, affecting the dissipation of the pharmaceutical diclofenac in riverine systems [Maier et al., 2016]. Although CSIA has been recently applied to characterize pesticide degradation in the environment, [Torabi et al., 2020] little is known about stable isotope fractionation of pesticides during direct and indirect photodegradation in surface waters.

To the best of our knowledge, only Hartenbach et al. (2008) have evaluated isotope fractionation for direct and indirect photodegradation of atrazine under specific conditions of irradiation and water chemistry [Hartenbach et al., 2008]. However, stable isotope fractionation may depend on the irradiation source and the DOM nature. Negligible enrichment in ^{13}C of the antibiotic sulfamethoxazole was observed in experiments with UV-C light, while significant isotopic fractionation ($\epsilon_C = -4.8 \pm 0.1\text{‰}$) was observed when UV-B and UV-A prevailed [Willach et al., 2018]. Slight C isotopic fractionation ($\epsilon_C = -0.7 \pm 0.2\text{‰}$) has also been observed during direct photodegradation of diclofenac under sunlight [Maier et al., 2016]. Differences in $\delta^{13}C$ vs. $\delta^{15}N$ enrichment trends suggest distinct mechanisms associated with photodegradation of the nitrile herbicide bromoxynil when irradiated either with a UV lamp or exposed to sunlight under environmental conditions [Knossow et al., 2020]. Isotope fractionation may also depend on the nature of DOM and its propensity to favour $HO\bullet$ and $^3DOM^*$ short-lived reactive intermediates oxidation, as observed for methyl *tert-butyl* ether and ethyl *tert-butyl* ether [Zhang et al., 2015]. Although these results emphasize the potential of CSIA to evaluate photodegradation in laboratory and in natural systems, reference isotopic fractionation factors to characterize pesticide photodegradation in agriculturally impacted surface waters are currently missing.

In this context, the purpose of this study was to examine typical patterns of photodegradation and associated isotope fractionation for atrazine and *S*-metolachlor in agriculturally impacted surface waters. We irradiated atrazine and *S*-metolachlor with a simulated sunlight (λ from 270 to 720 nm) under hydrochemical conditions representative of agriculturally impacted surface waters ($DOM = 5.4 \text{ mg}_C.L^{-1}$, $NO_3^- = 20 \text{ mg}.L^{-1}$). We hypothesized that the hydrochemical composition of surface waters differently affect pesticide photodegradation and associated isotopic fractionation through direct and indirect mechanisms. In particular irradiation of nitrates and DOM may lead to the formation of short-lived reactive intermediates controlling underlying photodegradation mechanisms. Direct and indirect photodegradation of pesticides were thus tested, separately and concomitantly, in the presence of nitrates and DOM. C and N isotopic fractionation factors were derived for direct and indirect photodegradation of atrazine and *S*-metolachlor. Complementary experiments were conducted with an ultraviolet (UV) light ($\lambda = 254 \text{ nm}$) to evaluate the influence of irradiation wavelength on C and N isotopic fractionation during pesticide photodegradation.

2.3.2 Material and method

Chemicals and preparation of solutions

All chemicals were at least HPLC grade ($> 97\%$) (see Appendix A.S1.1). Atrazine and *S*-metolachlor (Pestanal, $> 99.9\%$) stock solutions were individually prepared at $5 \text{ g}.L^{-1}$ in dichloromethane (DCM) and aliquots were stored at $-20^\circ C$ in brown glass vials. Before irradiations, pesticide stock solutions were spiked and stirred for one hour, up to complete evaporation of DCM. Suwannee river fulvic acid (SRFA - 2S101F) was purchased from the International Humic Substances Society (IHSS) and selected as a source of DOM representative of headwater rivers [Zhang et al., 2015]. Stock solutions of SRFA were prepared at a concentration of $50 \text{ mg}_C.L^{-1}$ by dissolving 10 mg of SRFA in 100 mL of ultrapure water (UW) ($> 15 \text{ M}\Omega$; $DOC < 0.2 \text{ mg}_C.L^{-1}$), followed by 15 min sonication (Branson 5510, 40 kHz). The solutions were then filtered through a $0.22 \mu m$ pore diameter cellulose acetate membrane pre-conditioned with UW ensuring sterile conditions and stored at $4^\circ C$ in brown glass vial. Synthetic fresh water was prepared following Smith et al. (2002) to target the ionic composition of typical soft surface waters [Smith et al., 2002].

Experimental Section

Atrazine and *S*-metolachlor were selected as representatives of widely used and ubiquitously detected triazine and chloroacetanilide pesticides [de Souza et al., 2020] and based on existing degradation rates (including for photodegradation) and isotope fractionation factors (see Appendix A.S1.2). Direct photolysis experiments were carried out independently for atrazine and *S*-metolachlor in UW with a 50 mM phosphate buffer (KH_2PO_4/Na_2HPO_4) at $pH = 7.9 \pm 0.2$, as it has no significant effects on photodegradation rates and isotope fractionation [Ratti et al., 2015b]. The effect of nitrates on pesticide photodegradation was investigated in buffered synthetic fresh water by adding $331 \pm 2 \mu M$ of sodium nitrate salts (*i.e.* $[NO_3^-] = 20 mg.L^{-1}$), considered as representative of agriculturally impacted surface waters in Europe [Agency, 2019]. The effect of DOM was studied by adding $5.4 \pm 0.2 mg_C.L^{-1}$ of SRFA considered as a representative concentration of rivers worldwide [Raymond and Spencer, 2015]. The concomitant effect of nitrates and DOM was investigated in synthetic fresh water, spiked with sodium nitrates, SRFA and atrazine ($5 \mu M$) or *S*-metolachlor ($3 \mu M$) (final hydrochemistry in Appendix A.S1.3). DIR, NIT, SRFA, and TOT notations stand for irradiation conditions to test under simulated sunlight, respectively, direct photodegradation (DIR), the effect of nitrates (NIT), dissolved organic matter (SRFA), and the combined effect of nitrates and dissolved organic matter (TOT). Finally, DIR254 refers to direct photodegradation experiments conducted with a low-pressure mercury lamp (LP Hg) (Philips, TUV 6W G6T5 - $\lambda = 254 nm$).

Experiments were conducted in a single 500 mL quartz tube (5 cm diameter) beyond 90% degradation of atrazine and *S*-metolachlor, and lasted from 7 to 600 hours irradiation. Aliquots from 15 to 200 mL were sequentially collected during the experiments. No significant degradation ($< 5\%$) in sterile and dark controls for all experimental conditions indicated insignificant hydrolysis and biodegradation during the photodegradation experiments. Photo-bleaching of DOM by $HO\bullet$ only slightly decreased the initial dissolved organic carbon (DOC) concentrations ($< 18\%$) after more than 310 hours of irradiation (see Appendix A.S1.4). Accordingly, irradiation conditions in experiments containing DOM were assumed steady across the experiments.

Direct and indirect irradiations were carried out under simulated sunlight consisting in a stand-alone lightning system (Sutter Instrument® - Lambda LS) fitted with a 300 W xenon (Xe) arc lamp (Cermax® - PE300BUV). A liquid optic fibre transmitted the light to a quartz tube covered with aluminium foils and cut-off ultra-violet

(UV) radiations below $\lambda = 270 \text{ nm}$. The light spectrum obtained through the quartz tube fell in the range $[270, 720] \text{ nm}$ (see Appendix A.S1.10) as characterized with a calibrated spectroradiometer ILT 900C (International Light®). Mean photon fluence rate was estimated at $E_0 = 7 \mu\text{E} \cdot \text{m}^{-2} \cdot \text{s}^{-1}$ in the range 290 to 400 nm with a PNA (30 μM)/pyridine (10 mM) actinometer system prepared as previously described [Dulin and Mill, 1982]. Up to date values of quantum yields independent from wavelength for PNA, $\Phi_{PNA} = 3.19 \bullet 10^{-3} \text{ mol.einstein}^{-1}$ [Laszakovits et al., 2017] were used (see Appendix A.S1.5). Due to long irradiation times, fluctuations of light intensity were followed-up for the ranges UVA ($320 < \lambda < 400 \text{ nm}$), UVB ($280 < \lambda < 320 \text{ nm}$) and visible light (VIS, $360 < \lambda < 830 \text{ nm}$) using a calibrated SOLAR® light PMA2200 radiometer. Xe arc lamps were systematically replaced when total light intensity dropped or as soon as shifts in the ratios UVA/UVB/VIS exceeded 5% of the original value (see Appendix A.S1.6).

The effect of the irradiation wavelength on direct photodegradation of pesticides was examined using a light-proof box with black material equipped with the LP Hg lamp providing a monochromatic light source ($\lambda = 254 \text{ nm}$). Open 3.3 borosilicate beakers were filled with 50 mL of buffered solution and spiked either with atrazine (90 μM) or S-metolachlor (70 μM). Beakers were placed into the black-box, irradiated on the top, and sequentially removed to measure pesticide degradation rates. Light intensity within the box was homogeneous ($83 < I_{average} < 121\%$, see Appendix A.S1.7). Control experiments without pesticides showed no cross-contamination. In this case photon fluence rate was not determined since these experiments were solely designed to evaluate the effect of the irradiation wavelength on atrazine and S-metolachlor isotope fractionation induced by photodegradation and not to derive degradation rates.

Analytical section

For analytical details, we refer to section 2.1.

Data analysis - Pesticide degradation followed the linearized pseudo-first order equation ($R^2 > 82\%$, $p < 0.05$, $n \leq 5$). Degradation rates (k_{deg}) were normalized by the mean irradiation intensity (see Appendix A.S1.6) according to Eq. II.5, allowing comparison among experiments. Degradation rates presented below refer to the normalized value, k_{eff} .

$$k_{eff} = \frac{I_{exp}}{I_{max}} \cdot k_{deg} \quad (\text{II.5})$$

where I_{exp} and I_{max} stand for the light intensities measured during each experiment and the maximal inter-experiment value used as the reference for normalization.

All statistical analysis and regressions were performed in R using the “stats” package, version 3.6.3. Data from linear regression (i.e. k_{eff} , ϵ_C and ϵ_N) are reported with their confidence interval at level 95%.

2.3.3 Results & Discussion

Effects of the Hydrochemistry on the Photodegradation Rates under Simulated Sunlight

Nitrates and DOM under simulated sunlight affected atrazine and *S*-metolachlor photodegradation rates. Direct photodegradation in UW (DIR) exhibited the quickest degradation rates for both pesticides with $k_{ATZ,DIR} = (6.6 \pm 0.4) \cdot 10^{-6} \text{ s}^{-1}$ (i.e. $DT_{50} = 29.0 \pm 1.7 \text{ h}^{-1}$) and $k_{SMET,DIR} = (3.3 \pm 0.2) \cdot 10^{-6} \text{ s}^{-1}$ (i.e. $DT_{50} = 58.8 \pm 3.2 \text{ h}^{-1}$). Although atrazine was slightly more sensitive to direct photodegradation than *S*-metolachlor, degradation rates were in the same order of magnitude as those previously reported [Dimou et al., 2005, Zeng and Arnold, 2013]. The strong light absorption of atrazine and *S*-metolachlor in the near UV range overlaps the Xe lamp radiation spectrum ($< 320 \text{ nm}$) and explains their high reactivity. The simulated sunlight spectrum is provided in Appendix A.S1.10).

In contrast, the addition of 5.4 mgC.L^{-1} of DOC, with or without 20 mg.L^{-1} of nitrates, decreased the photodegradation rates of atrazine and *S*-metolachlor, respectively, compared to the UW experiments. This supports the idea that SRFA decreases atrazine and *S*-metolachlor photodegradation in surface waters with typical DOC concentrations. However, photodegradation rates in experiments with nitrates only were similar to rates in direct photodegradation experiments ($\frac{k_{ATZ,NIT}}{k_{ATZ,DIR}} = 0.8$ and $\frac{k_{SMET,NIT}}{k_{SMET,DIR}} = 1.0$). Addition of nitrates to the SRFA solution enhanced the reaction ($\frac{k_{ATZ,TOT}}{k_{ATZ,SRFA}} = 2.1$ and $\frac{k_{SMET,TOT}}{k_{SMET,SRFA}} = 1.2$), highlighting oxidation of atrazine and *S*-metolachlor with $HO\bullet$ originating from nitrate irradiation. DOM and nitrates in surface waters thus display similar photosensitizing or inhibitory effects on atrazine and *S*-metolachlor photodegradation. Similar effects can be explained by absorption spectra of atrazine and *S*-metolachlor in the near UV range, and similar one-electron oxidation potentials ($E1_{SMET} = -2.40 \text{ V vs NHE}$ and $E1_{ATZ} = -2.41 \text{ V vs NHE}$). One-electron oxidation potentials are often used as a reliable indicator of the poten-

tial of organic contaminants to react with ${}^3DOM^*$ and $HO\bullet$ [Arnold, 2014, Karpuzcu et al., 2016, Leresche et al., 2016].

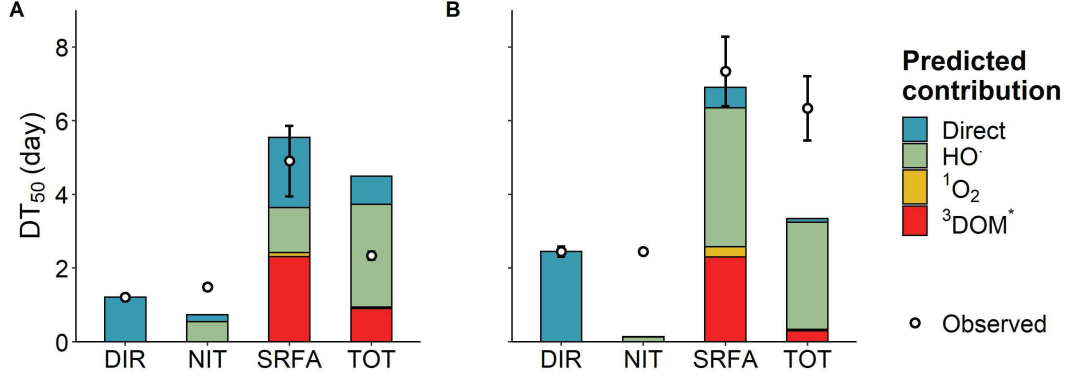


Figure II.2 – Observed and predicted half-lives of A) atrazine and B) S-metolachlor under simulated sunlight. Predicted contributions of direct and indirect mechanisms ($HO\bullet$, ${}^3DOM^*$ and 1O_2) to the total pesticide photodegradation is displayed within the stacked bars. DIR, NIT, SRFA, and TOT stand for conditions used to test, respectively, the direct photodegradation, the effect of nitrates, the effect of DOM and the combined effects of nitrates and DOM together. Half-lives values were calculated from degradation rates according to $DT_{50} = \frac{\ln(2)}{k}$. Error bars correspond to the 95% confidence interval.

The contributions of direct and indirect mechanisms to photodegradation were inferred from photochemical predictions using Eq. II.6. This equation decomposes observed degradation rates as the sum of contributions of direct and indirect photodegradation mechanisms (*i.e.* $HO\bullet$ and ${}^3DOM^*$ mediated) [Bodrato and Vione, 2014, Janssen et al., 2014, Zeng and Arnold, 2013]. Carbonate radicals ($CO_3^{\bullet-}$) were not included as potential relevant photosensitizers because oxidation of atrazine and anilines with $CO_3^{\bullet-}$ under simulated sunlight remains limited, even in carbonate-rich surface waters ($[HCO_3^-]$ and $[CO_3^{2-}] \approx 10$ times higher than in our conditions) [Vione et al., 2009]. Carbonates were, however, considered as potential quenchers of $HO\bullet$ [Zeng and Arnold, 2013]. The calculation procedure and required parameters from the literature are summarized in Appendix A.S1.11.

$$\begin{aligned} \frac{dC}{dt} &= -k_{obs} \bullet C \\ &= -\left(k_{dir} + k_{HO\bullet} \bullet [HO\bullet]_{SS} + k_{3DOM^*} \bullet [{}^3DOM^*]_{SS} + k_{1O_2} \bullet [{}^1O_2]_{SS}\right) \end{aligned} \quad (II.6)$$

C stands for pesticide concentration, and k_{obs} the observed degradation rate [s^{-1}], which can be expressed as the sum of direct (k_{dir}) and selected indirect processes ($k_{HO\bullet}$, $k_{^3DOM^*}$ and $k_{^1O_2}$). The latter degradation rates are second order and depend on the steady state concentrations of associated radicals and short live species ($[HO\bullet]_{SS}$, $[^3DOM^*]_{SS}$ and $[^1O_2]_{SS}$).

Observed and predicted degradation rates were consistent, suggesting that dominant photodegradation pathways could be identified in all experiments (Figure II.2 and Appendix A.S1.11). Nitrate-mediated photodegradation contributed to 60% of atrazine and 90% of *S*-metolachlor photodegradation in TOT conditions, and is thus expected to dominate in agriculturally impacted surface waters. Although competing for UV light and limiting direct photodegradation, SRFA favoured indirect photodegradation with $^3DOM^*$ and $HO\bullet$. Accordingly, atrazine was slightly more sensitive than *S*-metolachlor to oxidation by $^3DOM^*$, whereas $HO\bullet$ mostly affected *S*-metolachlor. Nitrate mediated photodegradation was, however, partly hampered in the TOT experiment as compared with the DIR experiment. Indeed, DOC at $5.4\text{ mg}_C.L^{-1}$ not only competes for light irradiance with nitrates but also quenches $HO\bullet$ radicals, reducing the photosensitizing effect of nitrates as observed in the NIT condition [Garbin et al., 2007, Leresche et al., 2016]. Direct photodegradation contributed less in SRFA than in DIR experiments because UV light absorption by DOM limited direct photodegradation. Consequently, direct photodegradation rates were 10 to 30 times slower in SRFA than in DIR experiments for atrazine and *S*-metolachlor. Finally, 1O_2 stemming from reactions between dissolved oxygen and $^3DOM^*$, contributed to less than 2% for atrazine and 4% for *S*-metolachlor of observed degradation rates. In aqueous solution, water immediately scavenges most of the produced 1O_2 , limiting its reaction with pesticides [Cory et al., 2009].

While direct and nitrate mediated photodegradation have strong potentials to transform atrazine and *S*-metolachlor in agriculturally impacted surface waters, DOM greatly reduces their potential by competing for UV light with pesticides and nitrates. Thus, pesticides with the strongest light absorption spectrum in the near UV, such as atrazine, are likely less impacted by UV light competition caused by DOM. However, nitrates with concentrations about $20\text{ mg}.L^{-1}$ would partly compensate for UV light competition caused by DOM by promoting $HO\bullet$ oxidation. As discussed below, specific patterns of TPs formation and stable isotope fractionation further confirmed the

predominance of nitrate- and DOM-mediated indirect pathways in NIT, SRFA and TOT experiments.

Formation of Phototransformation Products

TPs were analyzed in samples displaying similar extent of degradation ($\approx 80\%$). Analysed TP structures are provided in Appendix A.S1.8). Atrazine irradiation led to desethylatrazine (DEA) and desisopropylatrazine (DIA) in all experiments, whereas 2-hydroxyatrazine (A-OH) was specific to direct photodegradation (Figure II.3A). Indirect photolysis may proceed through atrazine oxidation at the N-ethyl and N-isopropyl group by $^3DOM^*$ and $HO\bullet$ [Torrents et al., 1997]. Non-selective attacks of $HO\bullet$ on the N-ethyl and N-isopropyl groups may thermodynamically favour the formation of DEA since weaker N-C bond dissociation energy is associated to the N-ethyl group [Vollhardt and Peter, 2009]. A steric effect is also expected to favour the formation of DEA as the isopropyl group is less reactive than the ethyl group [Smith and March, 2006]. On the other hand, the intermediate formed during the hydrogen abstraction by $HO\bullet$ would electronically favour DIA formation due to the weaker C-H bond, and weaker intermediate stabilization by the isopropyl group than by the ethyl group [Hapeman et al., 1995].

Four TPs of *S*-metolachlor were identified (Figure II.3B). Hydroxymetolachlor was observed in neither DIR254 nor DIR, although it was reported in previous studies [Dimou et al., 2005, Gutowski et al., 2015a, Gutowski et al., 2015b] as the major TP formed during direct photodegradation of (S)-metolachlor. We postulate that after 80% degradation of *S*-metolachlor, hydroxymetolachlor was further degraded into secondary TPs. In the SRFA and DIR experiments, only metolachlor oxalinic acid (OXA) was observed, whereas in NIT and TOT experiments, no TPs were detected. This suggests that *S*-metolachlor was easily oxidized by $^3DOM^*$ and $HO\bullet$ into *S*-metolachlor OXA, its acidic form. In the presence of nitrates, the large and constant generation of non-selective $HO\bullet$ may favour fast *S*-metolachlor OXA degradation [Dimou et al., 2005], explaining the absence of TPs in the NIT and TOT experiments. The absence of TPs in the NIT and TOT experiments also supports the idea that nitrates mainly contribute to *S*-metolachlor photodegradation, even with $5.4\text{ mg}_C.L^{-1}$ of DOC.

It is also worth noting that the number of detected TPs was maximum for both compounds during irradiations at $\lambda = 254\text{ nm}$ in DIR254 experiments (Figure II.3). In the case of *S*-metolachlor, Metolachlor CGA 37735, Metolachlor CGA 50267 and MET-GLiu were specific suspected TPs in DIR254 experiments, although only Metolachlor

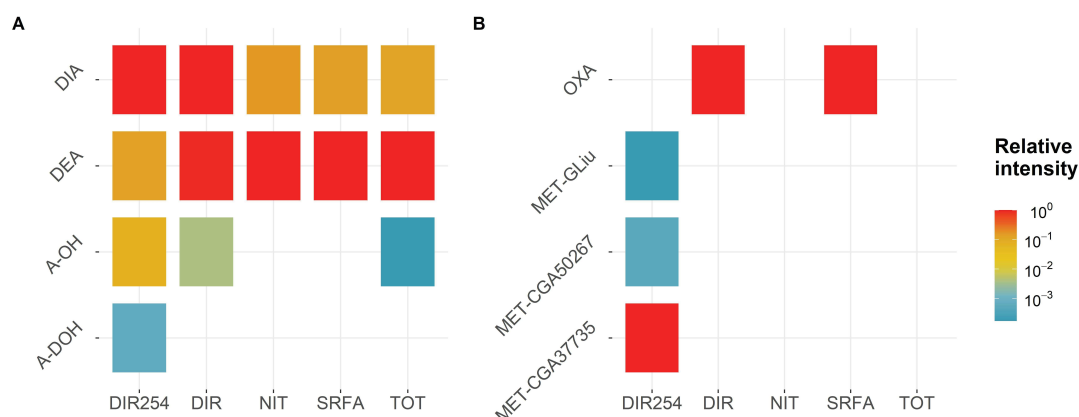


Figure II.3 – Transformation products for (a) atrazine and (b) *S*-metolachlor in DIR254, DIR, NIT, SRFA, and TOT experiments. DIR254, DIR, NIT, SRFA, and TOT stand for conditions used to test, respectively, direct photodegradation with the Hg and the Xe lamp, the effect of nitrates, the effect of DOM and the concomitant effects of nitrates and DOM together. DIA, DEA, A-OH and A-DOH stand, respectively, for desisopropyl atrazine, desethyl atrazine, hydroxyl atrazine and desethyl 2 hydroxy atrazine. OXA, MET-Gliu, MET-CGA37735 and MET-CGA50267 stand, respectively, for metolachlor oxalinic acid, MET-GLiu, Metolachlor CGA 37735 and Metolachlor CGA 50267. Relative intensity refers to the peak amplitude of transformation product normalized by the intensity of the dominant transformation product peak for each sample.

CGA 37735 could be confirmed with analytical standards. This suggests that the spectrum of degradation mechanisms associated with monochromatic UV light is wider than that with simulated sunlight, and/or that the specific TPs result from further degradation of the first generation of TPs.

Altogether, patterns of TPs formation slightly differed between direct and indirect photodegradation. While the dechlorinated compound A-OH feature direct photodegradation for atrazine, oxidized compounds (e.g. atrazine DEA and DIA and *S*-metolachlor OXA) are likely to predominate in agriculturally impacted surface waters. TPs are likely transient and rapidly degraded into secondary and unidentified TPs, as shown during *S*-metolachlor photodegradation. Nonetheless, TPs patterns were identical for atrazine in NIT and SRFA experiments, although $^3\text{DOM}^*$ oxidation was predicted to prevail over $\text{HO}\bullet$. Similarly, indirect photodegradation of *S*-metolachlor did not

generate specific patterns of TPs. Interestingly, *S*-metolachlor ESA was not detected. Since *S*-metolachlor ESA is frequently measured in the environment and is neither a transformation product associated with hydrolysis [Masbou et al., 2018] nor photodegradation, its detection might indicate *S*-metolachlor biodegradation.

C and N Isotope Fractionation to Trace Atrazine and *S*-metolachlor Photodegradation

Direct photolysis of atrazine in the DIR254 experiment with a low-pressure mercury lamp caused inverse isotope fractionation for both C and N ($\Lambda_{N/C} = 0.9 \pm 0.1$), in agreement with previous results from Hartenbach et al. (2005) ($\Lambda_{N/C} = 1.05 \pm 0.14$) [Hartenbach et al., 2008]. In contrast, *S*-metolachlor featured a less pronounced and inverse C fractionation and stronger N fractionation ($\Lambda_{N/C} = -3.2 \pm 1.0$).

An inverse C fractionation for direct photolysis of atrazine and *S*-metolachlor is a priori inconsistent with a nucleophilic substitution of the chlorine atom by a hydroxyl group at the C-Cl bond expected for the formation of the TPs A-OH or MET-OH. In addition, an inverse C fractionation cannot be explained by the cleavage of the C-N bond at the N-ethyl or N-isopropyl group. Indeed, a cleavage at the N-ethyl or N-isopropyl group leading to DEA and DIA should reflect a normal primary isotopic effect [Elsner et al., 2005]. Two non-exclusive hypotheses may explain the isotopic patterns obtained in DIR254 experiments. First, successive steps of intersystem crossing before atrazine dechlorination can lead to inverse fractionation during direct photolysis of atrazine [Hartenbach et al., 2008]. Second, a magnetic mass-independent isotope effect (MIE) involving spin carrying nuclei and unpaired electrons may cause an inverse isotope fractionation [Buchachenko, 2013, Hartenbach et al., 2008, Ratti et al., 2015b].

In contrast, direct photodegradation under simulated sunlight (DIR experiment) was characterized by non-significant C and N isotope fractionation for both pesticides (Table II.4). Together with preliminary evidence from diclofenac photolysis [Maier et al., 2016], our results suggest that C isotope fractionation associated with direct photodegradation under simulated sunlight of organic micropollutants remains limited.

Most importantly, our results indicate that photo-induced C and N isotope fractionation depends on the irradiation wavelength. Similar results have been reported by Willach et al. (2018) for the antibiotic sulfamethoxazole under broad and cut off light spectrums [Willach et al., 2018]. Instead of generating a single-band UV light as with

the Hg lamp ($\lambda = 254 \text{ nm}$), the Xe lamp emits light over a broad and continuous range of wavelengths and energies from the near UV ($\lambda > 270 \text{ nm}$) to the near infrared ($\lambda < 600 \text{ nm}$). Xe lamp emission may thus generate a miscellaneous population of excited triplet states, which affected photolytic dechlorination of 4-Cl-aniline and led to varying C and N isotope fractionation caused by a spin selective isotope effect [Ratti et al., 2015a]. Hence, the average isotope value of the residual fraction of atrazine and *S*-metolachlor may indicate multiple and co-occurring underlying photodegradation reactions under simulated sunlight.

Table II.4 – C and N isotope fractionation for atrazine and *S*-metolachlor ($\Delta\delta^{13}\text{C}$ and $\Delta\delta^{15}\text{N}$ - $\Delta\delta$ values stand for the difference between initial and final stable isotope ratios). Isotopic fractionation factors are reported with their uncertainties corresponding to the 95% confidence interval from the regression analysis. *n.s.*: Not significant ($p > 0.05$). *n.c.*: Not calculated. Rayleigh plots are presented in Appendix A.S1.12

Compound	Experiment	$\Delta\delta^{13}\text{C}$	$\Delta\delta^{15}\text{N}$	ϵ_{C}	ϵ_{N}
	(Degradation extent - %)	(‰)	(‰)	(‰)	(‰)
atrazine	DIR254 (99)	8.9	11	2.7 ± 0.3	2.4 ± 0.3
	DIR (90)	1.2	1.4	n.s.	n.s.
	NIT (99)	1.7	2	n.s.	0.7 ± 0.3
	SRFA (97)	< 1.0	2.1	n.c.	0.6 ± 0.2
	TOT (98)	1	4.8	0.1 ± 0.1	0.9 ± 0.6
<i>S</i> -metolachlor	DIR254 (99)	2.6	-8.4	0.8 ± 0.1	-2.6 ± 0.7
	DIR (80)	-2.0.	-1	n.s.	n.s.
	NIT (98)	1.2	-3.4	n.s.	-0.8 ± 0.1
	SRFA (94)	< 1.0	-2.3	n.c.	-0.7 ± 0.4
	TOT (94)	< 1.0	-1.9	n.c.	-0.7 ± 0.1

In the case of indirect photodegradation with simulated sunlight, insignificant C and significant N isotope fractionations for both pesticides were systematically observed in NIT and TOT experiments with nitrates. Inverse and normal N fractionations were observed for atrazine and *S*-metolachlor, respectively ($\frac{\epsilon_{\text{N}}^{\text{TOT}}}{\epsilon_{\text{N}}^{\text{NIT}}} = 1.3 \pm 0.5$ for atrazine

and ($\frac{\epsilon_N^{TOT}}{\epsilon_N^{NIT}} = 0.9 \pm 0.2$ for *S*-metolachlor). Similar N isotope fractionation in NIT and TOT experiments further confirms the predominance of nitrate-mediated photodegradation in agriculturally impacted surface waters, even in the presence of $5.4 \text{ mg}_C.L^{-1}$ of DOM. Accordingly, ϵ_N values for atrazine and *S*-metolachlor in the NIT experiments represent reference values, specific for $HO\bullet$ oxidation in the presence of nitrates.

In the SRFA experiments, where ${}^3DOM^*$ oxidation presumably drove indirect photodegradation along with $HO\bullet$, only N isotope fractionation was observed for both pesticides ($\epsilon_N = 0.6 \pm 0.2\text{‰}$ for atrazine and $\epsilon_N = 0.7 \pm 0.4\text{‰}$ for *S*-metolachlor). Low N fractionation through ${}^3DOM^*$ oxidation is consistent with the absence C-N bond cleavage during *S*-metolachlor dechlorination leading to OXA. In addition, similar N enrichments in NIT and SRFA experiments ($\frac{\epsilon_N^{SRFA}}{\epsilon_N^{NIT}} = 0.9 \pm 0.5$) confirms the predicted significant contribution of $HO\bullet$ radicals generated by DOM irradiation ($HO\bullet = 54\%$ and ${}^3DOM^* = 33\%$). A similar conclusion can be drawn for atrazine as $\frac{\epsilon_N^{SRFA}}{\epsilon_N^{NIT}} = 0.9 \pm 0.5$. The inverse N fractionation observed also agrees with oxidation by ${}^3DOM^*$ at the N-ethyl or N-isopropyl side chain leading to either DEA or DIA proceeding through single electron transfer [Meyer et al., 2014, Zhang et al., 2015]. Accordingly, inverse C fractionation should also have been observed, which was not the case. The large collection of chromophores occurring in natural DOM (i.e. SRFA) can be promoted to their singlet or triplet states under simulated sunlight, thereby providing a wide range of energies, enabling oxidation at bonds involving irrespectively heavy and light isotopes [Rosario-Ortiz and Canonica, 2016]. This could be confirmed experimentally using Cs^+ as a quencher of excited singlet states to enhance the contribution of excited triplet states and by evaluating the corresponding decrease of ϵ_C and ϵ_N values, as previously observed for 2-Cl-anilines [Ratti et al., 2015a].

2.3.4 Environmental implications

Depending on hydrochemistry and the targeted pesticides, photodegradation can contribute to pesticide degradation to a similar or greater extent than biodegradation [Fenner et al., 2013] in static surface waters (e.g. ponds, lakes, etc.) and rivers with long transit time [Fono et al., 2006]. Direct photodegradation of atrazine and *S*-metolachlor was particularly fast, and was slowed down due to UV light absorption caused by DOM. However, nitrate concentrations higher than $20 \text{ mg}.L^{-1}$ can significantly enhance oxidation with $HO\bullet$ and level off the photodegradation inhibition caused by DOM in surface waters. Under simulated sunlight and environmentally-relevant hydrochem-

istry ($\text{pH}=8$; 20 mg.L^{-1} of nitrates and $5.4 \text{ mg}_C.\text{L}^{-1}$ of DOC), half-lives of atrazine and *S*-metolachlor were as short as a few days ($1 < DT_{50} < 10$ days). However, strong variations of solar irradiance in the UV region due to gaseous light absorption by ozone, altitude or geographic location or rapid absorption of UV lights in water, restrict our findings to shallow surface waters (i.e. $< 50 \text{ cm}$ deep) [Schwarzenbach et al., 2003]. Altogether, this advocates for a more systematic account of local irradiation spectrum and hydrochemistry to estimate the contribution and half-lives of pesticide photodegradation [Apell and McNeill, 2019].

While CSIA offers a new opportunity to evaluate pesticide degradation in surface waters, identifying photodegradation mechanisms of micropollutants in the field remains challenging, as also confirmed by recent studies [Maier et al., 2016, Willach et al., 2018]. Under sunlight irradiation, C isotope composition of atrazine and *S*-metolachlor are likely not affected by photodegradation, although photodegradation can significantly contribute to the pesticide degradation. Accordingly, changes in C stable isotopic ratios may almost exclusively reflect atrazine or *S*-metolachlor biodegradation. Indeed, biodegradation is typically characterized by significant isotope fractionation (e.g. biotic oxidative dealkylation of atrazine, $\Lambda_{N/C} = 0.35$) [Meyer and Elsner, 2013] in contaminated surface waters with high nitrate and DOM concentrations, as illustrated by the C/N dual plot comparing fractionation factors determined in this study with others from the literature (see Appendix A.S1.13). However, an opposite and similar absolute ϵ_N value for atrazine photodegradation and biodegradation would hamper a specific evaluation of photodegradation relying solely on changes of N isotope ratios. Since photodegradation mechanisms of atrazine and *S*-metolachlor mostly involve C-H and C-Cl bonds, [Hartenbach et al., 2008, Maier et al., 2016] multi-element isotope analysis (e.g. H, C, N and Cl) of pesticides by CSIA from environmental samples may help in the future to tease apart photodegradation mechanisms and evaluate their contribution among degradative processes. In contrast, abiotic hydrolysis is a slow process at pH of most surface waters (e.g. half-life value for alkaline abiotic hydrolysis of atrazine at $\text{pH} = 9$ and 20°C higher than 200 days), [Masbou et al., 2018] and is thus unlikely to significantly contribute to pesticide degradation in surface waters.

Most importantly, the irradiation source strongly influences C and N enrichment patterns. Our results advocate for a more systematic use of simulated sunlight when characterizing photodegradation mechanisms using CSIA in laboratory experiments. In addition, the nature of DOM under different environmental contexts can affect the

production of $HO\bullet$, and thus alter changes of the stable isotope composition of pesticides [Ratti et al., 2015a, Zhang et al., 2015]. Although SRFA serves as a model DOM representative of headwater rivers, [Leresche et al., 2016] site-specific studies should be deployed to address the specific role of DOC during pesticide photodegradation. Altogether, this study highlights the relevance of pesticide photodegradation in agriculturally impacted surface waters with nitrates and DOM.

Bibliography

- [Agency, 2019] Agency, E. E. (2019). Indicator assessment - Nutrients in freshwater in Europe. CSI 020(WAT 003).
- [Apell and McNeill, 2019] Apell, J. N. and McNeill, K. (2019). Updated and validated solar irradiance reference spectra for estimating environmental photodegradation rates. *Environmental Science: Processes & Impacts*, 21(3):427–437.
- [Arnold, 2014] Arnold, W. A. (2014). One electron oxidation potential as a predictor of rate constants of N-containing compounds with carbonate radical and triplet excited state organic matter. *Environ. Sci.: Processes Impacts*, 16(4):832–838.
- [Bodrato and Vione, 2014] Bodrato, M. and Vione, D. (2014). APEX (Aqueous Photochemistry of Environmentally occurring Xenobiotics): a free software tool to predict the kinetics of photochemical processes in surface waters. *Environmental Science. Processes & Impacts*, 16(4):732–740.
- [Buchachenko, 2013] Buchachenko, A. L. (2013). Mass-Independent Isotope Effects. *The Journal of Physical Chemistry B*, 117(8):2231–2238.
- [Celeiro et al., 2017] Celeiro, M., Facorro, R., Dagnac, T., Vilar, V. J. P., and Llompart, M. (2017). Photodegradation of multiclass fungicides in the aquatic environment and determination by liquid chromatography-tandem mass spectrometry. *Environmental Science and Pollution Research*, 24(23):19181–19193.
- [Cory et al., 2009] Cory, R. M., Cotner, J. B., and McNeill, K. (2009). Quantifying Interactions between Singlet Oxygen and Aquatic Fulvic Acids. *Environmental Science & Technology*, 43(3):718–723.
- [de Souza et al., 2020] de Souza, R. M., Seibert, D., Quesada, H. B., de Jesus Bassetti, F., Fagundes-Klen, M. R., and Bergamasco, R. (2020). Occurrence, impacts and general aspects of pesticides in surface water: A review. *Process Safety and Environmental Protection*, 135:22–37.

- [Dimou et al., 2005] Dimou, A. D., Sakkas, V. A., and Albanis, T. A. (2005). Metolachlor Photodegradation Study in Aqueous Media under Natural and Simulated Solar Irradiation. *Journal of Agricultural and Food Chemistry*, 53(3):694–701.
- [Dulin and Mill, 1982] Dulin, D. and Mill, T. (1982). Development and evaluation of sunlight actinometers. *Environmental Science & Technology*, 16(11):815–820.
- [Elsner and Imfeld, 2016] Elsner, M. and Imfeld, G. (2016). Compound-specific isotope analysis (CSIA) of micropollutants in the environment — current developments and future challenges. *Current Opinion in Biotechnology*, 41:60–72.
- [Elsner et al., 2005] Elsner, M., Zwank, L., Hunkeler, D., and Schwarzenbach, R. P. (2005). A new concept linking observable stable isotope fractionation to transformation pathways of organic pollutants. *Environmental Science & Technology*, 39(18):6896–6916.
- [Fenner et al., 2013] Fenner, K., Canonica, S., Wackett, L. P., and Elsner, M. (2013). Evaluating Pesticide Degradation in the Environment: Blind Spots and Emerging Opportunities. *Science*, 341(6147):752–758.
- [Fono et al., 2006] Fono, L. J., Kolodziej, E. P., and Sedlak, D. L. (2006). Attenuation of Wastewater-Derived Contaminants in an Effluent-Dominated River. *Environmental Science & Technology*, 40(23):7257–7262.
- [Garbin et al., 2007] Garbin, J. R., Milori, D. M. B. P., Simões, M. L., da Silva, W. T. L., and Neto, L. M. (2007). Influence of humic substances on the photolysis of aqueous pesticide residues. *Chemosphere*, 66(9):1692–1698.
- [Gutowski et al., 2015a] Gutowski, L., Baginska, E., Olsson, O., Leder, C., and Kümmerer, K. (2015a). Assessing the environmental fate of S-metolachlor, its commercial product Mercantor Gold® and their photoproducts using a water–sediment test and in silico methods. *Chemosphere*, 138(Supplement C):847–855.
- [Gutowski et al., 2015b] Gutowski, L., Olsson, O., Leder, C., and Kümmerer, K. (2015b). A comparative assessment of the transformation products of S-metolachlor and its commercial product Mercantor Gold(®) and their fate in the aquatic environment by employing a combination of experimental and in silico methods. *The Science of the Total Environment*, 506-507:369–379.
- [Hapeman et al., 1995] Hapeman, C. J., Karns, J. S., and Shelton, D. R. (1995). Total mineralization of aqueous atrazine in the presence of ammonium nitrate using ozone

- and *Klebsiella terrigena* (strain drs-i): mechanistic considerations for pilot scale disposal. *Journal of Agricultural and Food Chemistry*, 43(5):1383–1391.
- [Hartenbach et al., 2008] Hartenbach, A. E., Hofstetter, T. B., Tentscher, P. R., Canonica, S., Berg, M., and Schwarzenbach, R. P. (2008). Carbon, Hydrogen, and Nitrogen Isotope Fractionation During Light-Induced Transformations of Atrazine. *Environmental Science & Technology*, 42(21):7751–7756.
- [Janssen et al., 2014] Janssen, E. M.-L., Erickson, P. R., and McNeill, K. (2014). Dual Roles of Dissolved Organic Matter as Sensitizer and Quencher in the Photooxidation of Tryptophan. *Environmental Science & Technology*, 48(9):4916–4924.
- [Karpuzcu et al., 2016] Karpuzcu, M. E., McCabe, A. J., and Arnold, W. A. (2016). Phototransformation of pesticides in prairie potholes: effect of dissolved organic matter in triplet-induced oxidation. *Environmental Science: Processes & Impacts*, 18(2):237–245.
- [Knossow et al., 2020] Knossow, N., Siebner, H., and Bernstein, A. (2020). Isotope analysis method for the herbicide bromoxynil and its application to study photo-degradation processes. *Journal of Hazardous Materials*, 388:122036.
- [Laszakovits et al., 2017] Laszakovits, J. R., Berg, S. M., Anderson, B. G., O’Brien, J. E., Wammer, K. H., and Sharpless, C. M. (2017). p-Nitroanisole/Pyridine and p-Nitroacetophenone/Pyridine Actinometers Revisited: Quantum Yield in Comparison to Ferrioxalate. *Environmental Science & Technology Letters*, 4(1):11–14.
- [Leresche et al., 2016] Leresche, F., von Gunten, U., and Canonica, S. (2016). Probing the Photosensitizing and Inhibitory Effects of Dissolved Organic Matter by Using N,N-dimethyl-4-cyanoaniline (DMABN). *Environmental Science & Technology*, 50(20):10997–11007.
- [Maier et al., 2016] Maier, M. P., Prasse, C., Pati, S. G., Nitsche, S., Li, Z., Radke, M., Meyer, A., Hofstetter, T. B., Ternes, T. A., and Elsner, M. (2016). Exploring Trends of C and N Isotope Fractionation to Trace Transformation Reactions of Diclofenac in Natural and Engineered Systems. *Environmental Science & Technology*, 50(20):10933–10942.
- [Masbou et al., 2018] Masbou, J., Drouin, G., Payraudeau, S., and Imfeld, G. (2018). Carbon and nitrogen stable isotope fractionation during abiotic hydrolysis of pesticides. *Chemosphere*, 213:368–376.

- [Meyer et al., 2014] Meyer, A. H., Dybala-Defratyka, A., Alaimo, P. J., Geronimo, I., Sanchez, A. D., Cramer, C. J., and Elsner, M. (2014). Cytochrome P450-catalyzed dealkylation of atrazine by *Rhodococcus* sp. strain NI86/21 involves hydrogen atom transfer rather than single electron transfer. *Dalton Trans.*, 43(32):12175–12186.
- [Meyer and Elsner, 2013] Meyer, A. H. and Elsner, M. (2013). $^{13}\text{C}/^{12}\text{C}$ and $^{15}\text{N}/^{14}\text{N}$ Isotope Analysis To Characterize Degradation of Atrazine: Evidence from Parent and Daughter Compound Values. *Environmental Science & Technology*, 47(13):6884–6891.
- [Ratti et al., 2015a] Ratti, M., Canonica, S., McNeill, K., Bolotin, J., and Hofstetter, T. B. (2015a). Isotope Fractionation Associated with the Indirect Photolysis of Substituted Anilines in Aqueous Solution. *Environmental Science & Technology*, 49(21):12766–12773.
- [Ratti et al., 2015b] Ratti, M., Canonica, S., McNeill, K., Bolotin, J., and Hofstetter, T. B. (2015b). Isotope Fractionation Associated with the Photochemical Dechlorination of Chloroanilines. *Environmental Science & Technology*, 49(16):9797–9806.
- [Raymond and Spencer, 2015] Raymond, P. A. and Spencer, R. G. (2015). Riverine DOM. In *Biogeochemistry of Marine Dissolved Organic Matter*, pages 509–533. Elsevier.
- [Remucal, 2014] Remucal, C. K. (2014). The role of indirect photochemical degradation in the environmental fate of pesticides: a review. *Environmental Science-Processes & Impacts*, 16(4):628–653.
- [Rosario-Ortiz and Canonica, 2016] Rosario-Ortiz, F. L. and Canonica, S. (2016). Probe Compounds to Assess the Photochemical Activity of Dissolved Organic Matter. *Environmental Science & Technology*, 50(23):12532–12547.
- [Schwarzenbach et al., 2003] Schwarzenbach, R. P., Gschwend, P. M., Imboden, D. M., and Imboden, M. (2003). *Environmental Organic Chemistry / Edition 2*.
- [Smith et al., 2002] Smith, E. J., Davison, W., and Hamilton-Taylor, J. (2002). Methods for preparing synthetic freshwaters. *Water Research*, 36(5):1286–1296.
- [Smith and March, 2006] Smith, M. B. and March, J. (2006). *March’s Advanced Organic Chemistry: Reactions, Mechanisms, and Structure, Sixth Edition*.

- [Stehle and Schulz, 2015] Stehle, S. and Schulz, R. (2015). Agricultural insecticides threaten surface waters at the global scale. *Proceedings of the National Academy of Sciences*, 112(18):5750–5755.
- [Thullner et al., 2012] Thullner, M., Centler, F., Richnow, H.-H., and Fischer, A. (2012). Quantification of organic pollutant degradation in contaminated aquifers using compound specific stable isotope analysis – Review of recent developments. *Organic Geochemistry*, 42(12):1440–1460.
- [Torabi et al., 2020] Torabi, E., Wiegert, C., Guyot, B., Vuilleumier, S., and Imfeld, G. (2020). Dissipation of S-metolachlor and butachlor in agricultural soils and responses of bacterial communities: Insights from compound-specific isotope and biomolecular analyses. *Journal of Environmental Sciences*, 92:163–175.
- [Torrents et al., 1997] Torrents, A., Anderson, B. G., Bilboulia, S., Johnson, W. E., and Hapeman, C. J. (1997). Atrazine Photolysis: Mechanistic Investigations of Direct and Nitrate-Mediated Hydroxy Radical Processes and the Influence of Dissolved Organic Carbon from the Chesapeake Bay. *Environmental Science & Technology*, 31(5):1476–1482.
- [Vione et al., 2009] Vione, D., Maurino, V., Minero, C., Carlotti, M. E., Chiron, S., and Barbati, S. (2009). Modelling the occurrence and reactivity of the carbonate radical in surface freshwater. *Comptes Rendus Chimie*, 12(8):865–871.
- [Vollhardt and Peter, 2009] Vollhardt, K. and Peter, C. (2009). Organic Chemistry - Structure Function.
- [Willach et al., 2018] Willach, S., Lutze, H. V., Eckey, K., Löppenberg, K., Lüling, M., Wolbert, J.-B., Kujawinski, D. M., Jochmann, M. A., Karst, U., and Schmidt, T. C. (2018). Direct Photolysis of Sulfamethoxazole Using Various Irradiation Sources and Wavelength Ranges—Insights from Degradation Product Analysis and Compound-Specific Stable Isotope Analysis. *Environmental Science & Technology*, 52(3):1225–1233.
- [Zeng and Arnold, 2013] Zeng, T. and Arnold, W. A. (2013). Pesticide Photolysis in Prairie Potholes: Probing Photosensitized Processes. *Environmental Science & Technology*, 47(13):6735–6745.
- [Zhang et al., 2015] Zhang, N., Schindelka, J., Herrmann, H., George, C., Rosell, M., Herrero-Martín, S., Klán, P., and Richnow, H. H. (2015). Investigation of Humic

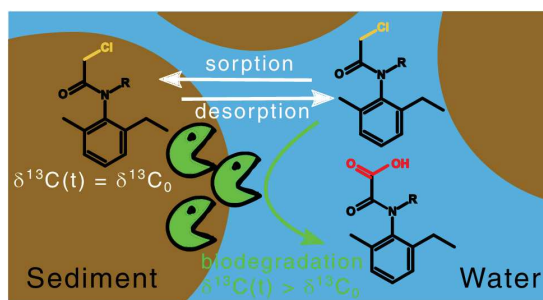
Substance Photosensitized Reactions via Carbon and Hydrogen Isotope Fractionation. *Environmental Science & Technology*, 49(1):233–242.

2.4 Pesticide oxic and anoxic biodegradation in water-sediment systems

From submitted paper: Droz, B., Drouin, G., Maurer, L., Payraudeau, S. & Imfeld, G., Mass-Transfer and Biodegradation of Acetochlor and S-Metolachlor in Water-Sediment Systems, Environmental Science & Technology.

Abstract

Current approaches are limited in their ability to evaluate the contribution of pesticide dissipation processes in water-sediment systems since both degradation and phase-transfer (*i.e.* sorption-desorption), contribute to apparent decrease of pesticide concentration. Here the dissipation of widely used herbicides acetochlor and S-metolachlor was examined in laboratory water-sediment batch experiments under oxic and anoxic conditions. Degradation pathways were elucidated using compound-specific isotopes analysis (CSIA), phase-transfer model to evaluate biodegradation, and high-resolution tandem mass spectrometry (HR-MS/MS) to identify transformation products. Biodegradation half-life of acetochlor and S-metolachlor in water were slower under anoxic ($DegT_{50,w} = 59 \pm 16$ and 199 ± 48 days) than under oxic conditions ($DegT_{50,w} = 31 \pm 17$ and 29 ± 8 days). Carbon apparent kinetic isotope effects ($AKIE_C$) ranged from 1.018 ± 0.001 to 1.075 ± 0.008 , suggesting degradation via nucleophilic substitution. Together with the predominance of the oxalinic acids transformation product, this suggests that the glutathione transferase pathway prevailed under both anoxic and oxic conditions in the water-sediment batch experiments. CSIA coupled with transformation product identification and an adapted phase-transfer model is a promising approach to support fat assessment pesticide in water-sediment systems under laboratory conditions.



2.4.1 Introduction

Up to $2.6 \cdot 10^6$ tons of pesticides are applied yearly on about 10% of the global land surface [Maggi et al., 2019]. Off-site export of pesticides from agricultural or urbanized areas and potential persistence in surface waters are frequently observed [Burri et al., 2019]. Pesticides raise considerable toxicological concerns as they may impact surface waters and decrease drinking water supply quality [Schwarzenbach et al., 2010, Malaj et al., 2014]. Pesticide biodegradation in surface waters is a prevailing degradation process in water–sediment system [Fenner et al., 2013]. At surface water, biodegradation is located in the oxic water column and the anoxic sediment bed. Contrasted biogeochemical conditions in these two environments may favor distinct biodegradation pathways and kinetics [Ericson et al., 2014, Shrestha et al., 2016]. Pesticide biodegradation studies have focused mainly on oxic conditions and associated pathways [Ghattas et al., 2017]. In comparison, only few studies have addressed biodegradation pathways under anoxic conditions in the water–sediment system [Vandermaesen et al., 2016].

Pesticide dissipation processes in water–sediment systems include biodegradation, phase-transfer (*i.e.* adsorption–desorption) and transport (*i.e.* diffusion, advection). Pesticide biodegradation rates derived from laboratory experiments usually serve to predict pesticide behavior in the environment [Moser et al., 2018]. Recent works have raised concerns about the representativeness of study conditions, claiming that derived pesticide biodegradation rates may be biased when co-occurring dissipation processes are not considered [Latino et al., 2017, Katagi, 2016]. Recently, conceptual model to evaluate processes contributing to pesticide dissipation has been validated for a broad spectrum of compounds and study conditions [Shrestha et al., 2016, Honti et al., 2016]. The model considers phase-transfer between the water phase with freely dissolved species, and the sediment phase including species sorbed on particles or dissolved organic carbon (DOC). However, knowledge of the contribution of pesticide biodegradation and phase-transfer to the overall pesticide dissipation in surface waters remains scarce, although this information is crucial for sediment and water management.

As a direct evidence of degradation, high resolution tandem mass spectrometry (HR-MS/MS) allows identifying known and unknown transformation product (TPs) in water–sediment system, and then approaching degradation pathways [Escher et al., 2020]. Complementarily, compound-specific isotope analysis (CSIA) may help teasing apart pesticide biodegradation from other dissipation processes and identifying degradation pathways. The degradation rate of pesticide molecules with light isotopes is slightly

faster than that of pesticides with heavy isotopes at the reactive site, resulting in a kinetic isotope effect (KIE) [Elsner and Imfeld, 2016]. Within KIE, primary isotope effect results in larger isotope fractionation as it corresponds to degradative processes involving bond cleavage atoms. In addition, pesticide biodegradation pathway generally modifies their stable isotope signature in a systematic way, and the extent of isotope fractionation may indicate the underlying biodegradation pathway. In contrast, pesticide sorption is likely associated with minor isotope fractionation, even after successive sorption-desorption steps in water–sediment systems [Kopinke et al., 2005]. The applicability of CSIA to evaluate pesticide dissipation in water–sediment systems, accounting for phase-transfer and biodegradation, still needs to be demonstrated.

Here, we examined pesticide dissipation in surface waters using laboratory water–sediment batch experiments. The widely used chloroacetanilide herbicides acetochlor and *S*-metolachlor, ranking twelve and eight among the most sold pesticides worldwide [Maggi et al., 2019] were selected as representative pesticides in surface waters [Kiefer et al., 2019]. The purpose of this study was to examine degradation of acetochlor and *S*-metolachlor and associated pathways under contrasted oxic and anoxic conditions in relation to phase-transfer in water–sediment systems. CSIA, transformation product identification, and a simplified version of a phase-transfer model [Honti and Fenner, 2015] were used together to improve interpretation of pesticide degradation in water–sediment systems.

2.4.2 Material and method

The list of chemicals including suppliers and purities is provided in Appendix A.S2.1. Five currently used or legacy pesticides (acetochlor, *S*-metolachlor, atrazine, terbutryn, and metalaxyl) were initially selected for the study (see the Appendix A.S2.1 for details on the mixture). Results and discussion were, however, restricted to acetochlor and *S*-metolachlor since low concentrations or limited degradation in the water phase hampered CSIA measurements of atrazine, terbutryn, and metalaxyl. The pesticide mixture was prepared in a 5 g.L^{-1} stock solution in acetonitrile (ACN) and stored at -20°C . Experiments were carried out using a soft ($< 10\text{ mg.L}^{-1}$ of inorganic carbon) synthetic water [Smith et al., 2002] mimicking an average surface water content of $\text{DOC} = 1.6 \pm 0.2\text{ mgC.L}^{-1}$ [Raymond and Spencer, 2015]. Details on the synthetic water preparation and hydrochemistry are provided in Appendix A.S2.1.

Sediment sampling and characteristics

Sediment was collected (details in Appendix A.S2.1) in an experimental stormwater wetland located at the outlet of a vineyard catchment (Rouffach, France, 47°57'43" N, 7°17'26" E) [Maillard and Imfeld, 2014], wet-sieved at 2 mm and stored wet at 4°C before experiment and analysis. Sediment physico-chemical parameters were measured following standard analytical procedure (NF/ISO; methods detailed in Appendix A.S2.1) and were characterized as follows (average \pm standard deviation, $n = 3$): $pH = 7.5 \pm 0.5$, cation exchange capacities (CEC) $14.3 \pm 2.8 \text{ cmol.kg}^{-1}$, residual humidity (RH, w/w) $37 \pm 3\%$, clay ($< 2 \mu\text{m}$) $21.2 \pm 2.5\%$, silt (2 to 50 μm) $67.4 \pm 2.5\%$, sand (50 to 2000 μm) $11.4 \pm 4.3\%$, organic carbon (f_{oc}) $2.3 \pm 2.1\%$ and mineral carbon (C_{min}) $3.9 \pm 0.5\%$. Sediment partitioning coefficients (K_d) were determined under batch sorption experiments [OECD, 2000]: $K_{(d, acetolachlor)} = 5.8 \pm 2.3 \text{ L.kg}^{-1}$ and $K_{d,S-metolachlor} = 6.6 \pm 1.7 \text{ L.kg}^{-1}$. The sediment and the synthetic water did not introduce redox-reactive elements, and iron and manganese remained below 1 mg.g^{-1} in both phase (Appendix A.S2.2). Abiotic degradation associated with reactive solid phases [Borch et al., 2010] and/or with bisulfide [Loch et al., 2002] were thus assumed insignificant.

Experimental set-up

Two series of biodegradation batch experiments were conducted in duplicate under oxic and anoxic conditions to evaluate pesticide dissipation in water-sediment systems. The biodegradation experiment preparation followed the original OECD Test No. 308: Aerobic and Anaerobic Transformation in Aquatic Sediment Systems [OECD, 2004] and the modified OECD 309 test [Shrestha et al., 2016] to ensure homogeneous redox conditions and an optimal balance between pesticide degradation and phase partitioning ($K_d < 2000 \text{ L.kg}^{-1}$). The sediment-water ratio represented conditions in settled sediment from ponds or riverbed systems [Honti et al., 2016]. Shaking was preferred over stirring to limit the impact of grain size change over time (Appendix A.S2.2) [Shrestha et al., 2016].

Biodegradation batch experiments were prepared with 5 g equivalent dry mass of wet sediment in 50 mL head-space glass vials. Filtered and sterilized synthetic water (0.2 μm cellulose acetate; CA) was spiked with the pesticide mixture (5 g.L^{-1}) stock solution in ACN to reach a concentration of 25 mg.L^{-1} of each pesticide. The solution was under-saturated with respect to the pesticide mixture, as calculated on

phreeqc-v3.0 (USGS) [Charlton and Parkhurst, 2011] with stability constants from the MINQEL+ v4.6 [Schecher and McAvoy, 1992] thermodynamic database and solubility correction of each pesticide for ionic strength. The solution was stirred until complete ACN evaporation. The sediment was then mixed with the pesticide solution to reach a sediment-water ratio (w/w) of 1:6, corresponding to a concentration of total suspended solid (TSS) of 0.2 g.L^{-1} . All batch experiments were crimped with butyl/PTFE caps. Under oxic conditions (6 to $9 \text{ mg.L}^{-1} \text{ O}_2$), a $0.2 \text{ }\mu\text{m}$ PTFE syringe filter was mounted on a needle and inserted through the vial caps to allow gas exchange in the vials while limiting water loss and avoiding bacterial contaminations from air [Alvarez-Zaldívar et al., 2018]. Anoxic batch experiments were flushed with N_2 (5.0) and vortexed three times to maintain an atmosphere below $0.02 \text{ mg.L}^{-1} \text{ O}_2$.

The oxic and anoxic batch experiments were incubated in the dark at $20 \pm 5^\circ\text{C}$ on an orbital shaker (80 rpm; reax-2, Heidolph). Degradation kinetics were assumed to comply with the pseudo first-order conditions. Batch experiments were sacrificed on days 2, 5, 15, 50, 80, 100, 150, 200, 250 and 300. At each sampling time, dissolved oxygen was measured with a fiber optic oxygen meter (SP-PSt3-YAU with a Fibox3, PreSens). pH was recorded with an electrode (pH/cond multi 350i, WTW) and remained constant across the experiments (7.6 ± 0.4). Cation-anion concentrations were analyzed from a water aliquot (Appendix A.S2.1). Water and sediment phases were collected for pesticide analysis.

Control experiments

Abiotic controls were prepared and incubated as biodegradation batch experiments with the same sediment which was autoclaved twice at 24 hours interval (steam under 103 kPa at 125°C for 20 minutes) to evaluate abiotic pesticide degradation during the experiment. Hydrolysis experiments were conducted in autoclaved synthetic water amended with a 50 mM phosphate buffer ($\text{KH}_2\text{PO}_4/\text{Na}_2\text{HPO}_4$) at $\text{pH} = 8$. Blank experiments without pesticide allowed to evaluate the initial background concentration of pesticides. Control and blank experiments were sacrificed on days 15, 50, 200 and 300. Abiotic controls confirmed insignificant pesticide dissipation at the end of the experiment ($< 10\%$, Appendix A.S2.2) associated to insignificant isotope fractionation in water ($|\Delta\delta^{13}\text{C}_{\text{obs},w}| < |\Delta\delta^{13}\text{C}_{\text{min},w}|$ with $|\Delta\delta^{13}\text{C}_{\text{min},w}|$ the minimal change of isotope signature before which isotope fractionation was considered as degradation, calculation method detailed below). The initial background concentration of pesticides in the

sediment phase was below the limit of detection ($< 0.1 \mu g.L^{-1}$). Biodegradation and sorption batch experiments for individual pesticides confirmed the absence of inhibitory or synergistic effects of the mix of pesticides on degradation rates and partitioning coefficients (Appendix A.S2.2) [Hammershøj et al., 2019].

Pesticide extraction, quantification and CSIA

For analytical and data processing details, we refer to section 2.1.

Specific details about CSIA data processing The minimal change of isotope signature ($\Delta\delta^{13}C_{min}$) before which isotope fractionation was considered as degradation was determined with the propagation of uncertainties associated with measurements and sample preparation as follow [Alvarez-Zaldívar et al., 2018]:

$$\Delta\delta^h E_{min} = \sqrt{\sigma_{EA}^2 + \sigma_s^2 + \sigma_{AU}^2} + \Delta\delta^h E_{extraction} \quad (II.7)$$

where σ_{EA} , σ_s and σ_{AU} are the uncertainty associate with the triplicate measurement of the initial product by an elemental analyzer IRMS (0.5‰ and 0.7‰ for C and N respectively), the sample uncertainty associated with the triplicate measurement and the maximal analytical uncertainty of the GC-IRMS (0.5‰ and 1.0‰ for C and N respectively), respectively. $\delta^h E_{extraction}$ is the trueness of the isotope composition measurement associated with the extraction procedure (see Section 2.1, Table II.1). $\Delta\delta^{13}C_{min}$ for water (w) and sediment (s) were, respectively, 0.94‰ and 0.91‰ for acetochlor, and 0.95‰ and 1.77‰ for *S*-metolachlor. $\Delta\delta^{15}N_{min,w}$ was 1.70‰ and 1.99‰ for acetochlor and *S*-metolachlor, respectively.

Suspected screenings of transformation products

Some selected water and sediment samples on days 50, 150, 200 and 250 were screened for TPs identification from oxic and anoxic experiments, and blank samples on days 0 and 200 to evaluate background of pesticides and TPs. TPs identification methodology is described in section 2.1.

Phase-transfer and biodegradation modelling

Pesticide concentrations and associated isotope fractionation were interpreted using an adapted version of the phase-transfer model developed previously [Honti and Fenner,

2015]. The model concepts and assumptions are detailed in Appendix A.S2.1. Data treatment and model-assisted interpretation including CSIA data are discussed below.

2.4.3 Results and discussion

Partitioning coefficients and hydrochemistry indicated steady-state conditions over time in the batch experiments. Partitioning coefficients of pesticides between the sediment phase (P_s) and the water phase (P_w) during the experiments were similar to the sediment partitioning coefficients derived during batch sorption experiments (average $|\log(P_s/P_w - K_d)| = 0.5 \pm 0.2$, Appendix A.S2.2). $P_s - P_w$ ratios indicated that phase partitioning equilibrium was reached within two days and maintained over time. Stable redox hydrochemistry (Ca^{2+} , Mg^{2+} , NO_3^- , SO_4^{2-} , Cl^- , pH) in all experiments indicated constant conditions for biodegradation over time, although sulfate concentrations slightly increased over time under oxic conditions ($\Delta SO_4^{2-}{}_{t=0-300 \text{ days}} = 0.20 \pm 0.05 \text{ mmol.L}^{-1}$). Under anoxic conditions, depletion of NO_3^- and SO_4^{2-} in the aqueous phase within two days indicated reducing conditions. DOC content and properties (ultraviolet absorbance and oxidation state) did not change over time (oxic: 10 ± 5 and anoxic $19 \pm 4 \text{ mgC.L}^{-1}$).

Dissipation kinetics and isotope fractionation

Pesticide dissipation followed pseudo first-order kinetics in both oxic and anoxic batch experiments (Table II.5). Dissipation half-lives in water and sediment for acetochlor and *S*-metolachlor under oxic and anoxic conditions (DT_{50} , Table 1) were in ranges reported in the literature [Graham et al., 1999, Lewis et al., 2016]. Worthy of note, DT_{50} values in water were higher under anoxic than under oxic conditions. Higher DT_{50} values under anoxic conditions supports the assumption that oxic degradation of pesticides is more energetically favorable than anoxic degradation using weaker electron acceptors (*e.g.* Mn , NO_3^- , Fe , SO_4^{2-}) than oxygen [Ghattas et al., 2017]. Acetochlor dissipation is faster than *S*-metolachlor, which is consistent with previous studies [Lewis et al., 2016]. The comparatively large *S*-metolachlor headgroup may sterically reduce the enzyme access to the *C-Cl* bond, thereby reducing *S*-metolachlor degradation rates [Graham et al., 1999].

Isotope fractionation for acetochlor and *S*-metolachlor in the water phase confirmed that biodegradation contributed to dissipation (Figure II.4a and b). $\epsilon_{bulk,C}$ under oxic and anoxic conditions ranged, respectively, from $-4.97 \pm 1.62\text{‰}$ and $-3.62 \pm 0.70\text{‰}$ for

acetochlor to $-1.20 \pm 0.35\text{‰}$ and $-1.87 \pm 0.58\text{‰}$ for *S*-metolachlor (Table II.5).

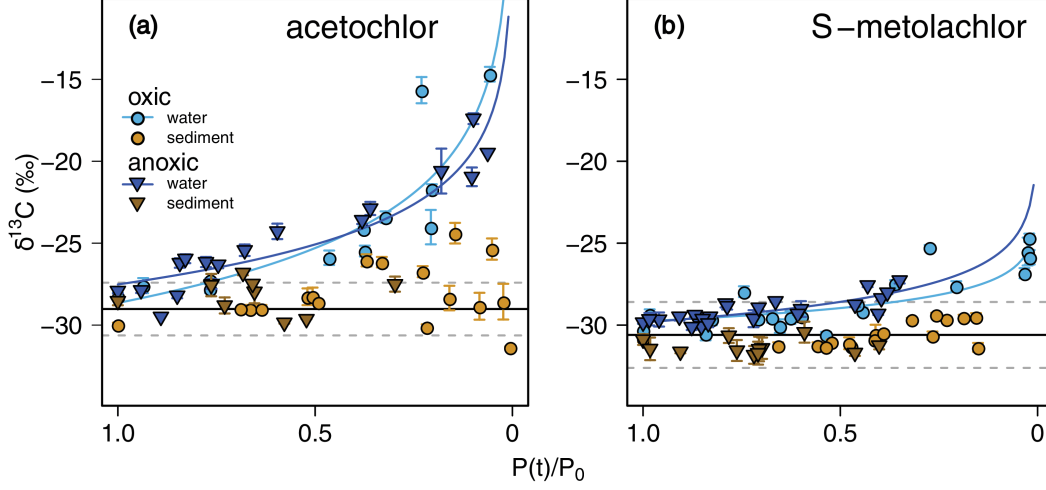


Figure II.4 – Carbon isotope signature ($\delta^{13}\text{C}$) as a function of pesticide remaining fraction ($P(t)/P_0$) of (a) acetochlor and (b) *S*-metolachlor in oxic and anoxic water–sediment systems. Error bars indicate the 95% confidence intervals of $\delta^{13}\text{C}$ values. Black lines indicate the reference carbon isotope signatures of standards measured with an elemental analyzer–isotope ratio mass spectrometer (EA-IRMS). Grey dotted lines represent the $\Delta\delta^{13}\text{C}_{\min,w}$. Color lines represent the fit based on the logarithmic expression of the Rayleigh equation.

Similar DT_{50} values (t-test, $p < 0.05$) for acetochlor and *S*-metolachlor in the water and the sediment phases suggest similar degradation rates in both phases (Table II.5, Appendix A.S2.2). However, insignificant isotope fractionation was observed in the sediment ($0.9\text{‰} < |\Delta\delta^{13}\text{C}_{\min,s}|$, Figure II.4). Hence, CSIA data indicated prevailing degradation in water, and low or insignificant degradation in sediment since CSIA is limited to detect low extent of biodegradation. For instance, to reliably detect biodegradation with CSIA in sediment, at least 16% of acetochlor and 40% of *S*-metolachlor should be degraded assuming a similar degradation pathway. We thus hypothesized that pesticides did not degrade significantly in sediment, but rather desorbed from sediment to water to fulfill the phase-transfer equilibrium during pesticide degradation in water. Pesticide dissipation rate constants in sediment were close to those in water, and dissipation rates in water ($k_{\text{obs},w}$) reflected both pesticide mass removal during biodegradation and phase-transfer from sediment to water. As a re-

sult, phase-transfer should be accounted for to quantify pesticide biodegradation rate constants irrespective to the effect of phase-transfer (k_{deg}) in the system.

Table II.5 – Dissipation Half-Life (DT_{50}), Degradation Half-Life ($DegT_{50}$), Carbon Bulk Isotopic Enrichment Factor ($\epsilon_{bulk,C}$) and Apparent Kinetic Isotope Effect (AKIE) for the Bulk, Water (w) and Sediment (s) Phase under Oxic and Anoxic Experiments.

	$DT_{50,w}^1$ (days)	$DT_{50,s}^1$ (days)	$DegT_{50,w}$ (days)	$\epsilon_{bulk,C}^2$ (‰)	$\epsilon_{bulk,corr,C}^2$ (‰)	$AKIE_C^3$ (-)
Oxic						
acetochlor	47 ± 25	53 ± 27	31 ± 17	-4.97 ± 1.62	-5.23 ± 1.09	1.075 ± 0.008
<i>S</i> -metolachlor	61 ± 10	151 ± 83	29 ± 8	-1.20 ± 0.35	-1.19 ± 0.19	1.018 ± 0.001
Anoxic						
acetochlor	69 ± 16	47 ± 12	59 ± 16	-3.62 ± 0.7	-3.51 ± 0.38	1.053 ± 0.003
<i>S</i> -metolachlor ⁴	249 ± 56	182 ± 41	199 ± 48	-1.87 ± 0.58	-1.83 ± 0.32	1.029 ± 0.001

¹ Half-life time were calculated following a pseudo first-order kinetics $DT_{50} = \ln(2)/k_{obs}$.

Goodness of the linear fit were $R^2 > 0.7$ for dissipation and $R^2 > 0.8$ for degradation.

² ϵ derived from the Raleigh plot. Goodness of the linear fit were $R^2 > 0.7$.

³ Calculated with Eq. II.4 where $n = 14$ and 15 for acetochlor and *S*-metolachlor, respectively, and $z = x = 1$.

⁴ Experiment reaching $P(t)/P_0 = 0.66$.

Water–sediment phase-transfer and implications for interpreting degradation kinetics

The biodegradation rate constant (k_{deg}) for each phase was estimated from pesticide dissipation using the conceptual model developed and validated by Honti et al. [Honti and Fenner, 2015]. The concept, described in details in Appendix A.S2.1, is that pesticides are either freely dissolved in the water phase (P_w), or sorbed to the organic fraction of sediment (P_s) consisting in dissolved and particulate organic carbon (Figure II.5). The original conceptual model presented in Figure II.5a has been developed according to OECD protocols, validated for a wide range of experimental conditions (TOC between 10^{-3} to $300 \text{ mg}_C.L^{-1}$ and sediment-water ratio 1:3 to 1:1000) and molecules ($\log K_{oc}$ from 1 to 5) [Honti and Fenner, 2015, Shrestha et al., 2016, Honti et al., 2016]. Here, this model was simplified to handle pesticide and TPs

concentrations only, and adapted using CSIA observation to interpret dissipation and biodegradation processes (Figure II.5b).

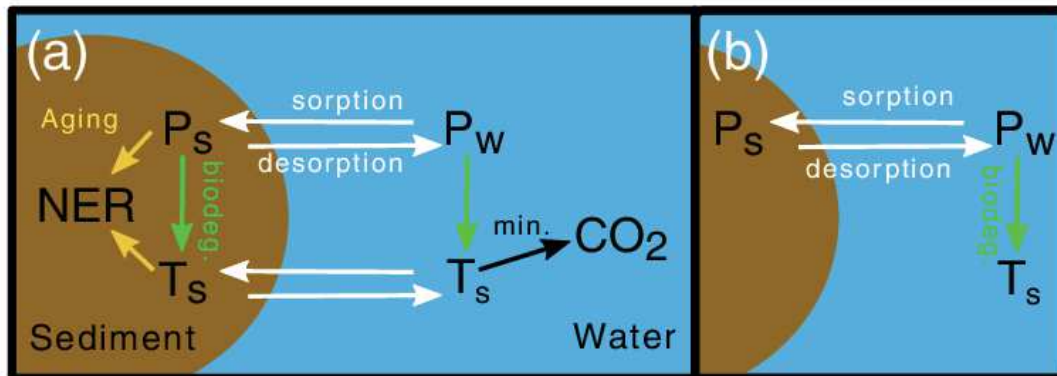


Figure II.5 – Conceptual model of the two-phases system: water (*w*) – sediment (*s*). (a) Original model [Honti et al., 2016]. (b) simplified model adopted in the present study. Species are P_s : pesticide in the sediment phase (i.e. sorbed to the sum of dissolved and particulate organic carbon), P_w : freely dissolved pesticide concentration in the water phase, T_s : sum of transformation products sorbed on total organic carbon, T_w : sum of *T* freely dissolved in water phase, *NER*: non-extractable residues and CO_2 : carbon dioxide. Arrows with the same color express the same processes.

The model arose from the assumption that biodegradation exclusively occurs in water. This assumption has been used since decades in regulatory testing [European Chemicals Agency, 2016] and simple pollutant fate modeling for a broad scale of molecules and conditions [Schwarzenbach et al., 2003]. It relies on the fact that sediment-bound pesticides are assumed to be non-available to biodegradation [Knauer et al., 2017]. In the present study, this assumption is comforted by the absence of significant carbon isotope fractionation in the sediment showed in the previous part. However, degrading microorganisms are also attached on the sediment surface and pesticide degradation may occur at the interface between sediment and water [Zumstein and Helbling, 2019]. In our case, TPs sorption was neglected because TPs of acetochlor and *S*-metolachlor were not detected in the sediment phase, in agreement with TPs physico-chemical properties (octanol–water partition coefficient, $P_{ow,p} > P_{ow,TPs}$ and $K_{oc,p} > K_{oc,TPs}$) [Lewis et al., 2016]. Finally, our model focuses on parent pesticides and the first generation of TPs to specifically derive phase-specific degradation rates and isotopic enrichment factors of parent pesticides. Comparatively, the OECD protocol also aims at identifying and quantifying TPs persistence, pesticide mineralization

and formation of NERs, justifying a specific account for additional phases [Honti and Fenner, 2015].

Pesticide mass balance under closed system and steady-state condition was established from the simplified framework (see Figure II.5b), and detailed in Appendix A.S2.1) The mass balance equation was rearranged to express pseudo first-order degradation rates ($k_{deg,w}$) as a function of observed dissipation rates ($k_{obs,w}$) (Eq. II.8):

$$k_{deg,w} = k_{obs,w} \cdot [1 + K_{oc} \cdot (f_{oc} \cdot TSS + DOC)] \quad (\text{II.8})$$

where K_{oc} is the sediment organic carbon–water partitioning coefficient.

Since $DOC \ll POC = f_{oc} \cdot TSS$ ($\frac{DOC}{POC} = 0.3\%$) in our system, Eq. II.8 simplifies to Eq. II.9:

$$k_{deg,w} = k_{obs,w} \cdot [1 + K_{oc} \cdot (f_{oc} \cdot TSS)] \quad (\text{II.9})$$

This assumption remains valid for water–sediment systems with DOC concentrations lower than the threshold value defined in Eq. II.10:

$$DOC \leq \frac{CI \cdot (1 + K_{oc} \cdot f_{oc} \cdot TSS)}{K_{oc}} \quad (\text{II.10})$$

where CI is the 95% confidence interval associated to $k_{obs,w}$. In our case, this simplification is valid for DOC concentrations lower than 70 mg.L^{-1} , which is ten to seventy times higher than typical average river concentrations [Raymond and Spencer, 2015]. For higher DOC concentrations, Eq. II.8 remains valid but measured pesticide concentrations in water should be corrected to account for partitioning between the freely dissolved fraction, feeding P_w , and the fraction sorbed to DOC, feeding P_s .

Corrections of $k_{obs,w}$ to retrieve $k_{deg,w}$ in our system are provided in Table II.5. $k_{deg,w}$ are higher than $k_{obs,w}$ because $1 + K_{oc} \cdot f_{oc} \cdot TSS > 1$ (Eq. II.9), and depends on the TSS and/or the partitioning coefficient of pesticides [Honti and Fenner, 2015]. Without consideration of phase-transfer, pesticide degradation would be underestimated by a factor of 1.2 ± 0.2 to 1.5 ± 0.5 for acetochlor (ratio between $k_{obs,w}$ and $k_{deg,w}$), and from 1.3 ± 0.2 to 2.1 ± 0.1 for *S*-metolachlor in oxic and anoxic condition, respectively. This emphasizes the need to account for phase-transfer when estimating $k_{deg,w}$ of pesticides in water–sediment systems.

Water–sediment phase-transfer and implications for interpreting isotope signature

In addition, the observed isotope signatures of pesticides in water ($\delta^{13}C_{obs,w}$) may also be affected by phase-transfer. A sorption-based isotope effects may occur when the non-degraded pesticide fraction that is sorbed to the sediment progressively desorbs and mixes in water, while partitioning equilibrium is not achieved over degradation. This would decrease $\delta^{13}C_{obs,w}$ during degradation and justify a correction of $\delta^{13}C_{obs,w}$. To evaluate the potential effect of desorption on ϵ_{bulk} values, we corrected acetochlor and *S*-metolachlor concentration and CSIA data accounting for the effect of phase-transfer (Eq. A.S24 to A.S30) (see Table II.5).

In our case, the corrected enrichment factors ($\epsilon_{bulk,corr}$) and ϵ_{bulk} values did not significantly change ($< 0.3\text{‰}$, Table II.5). A negligible effect of pesticide desorption from sediment on ϵ_{bulk} supports the notion that partitioning equilibrium is quasi-instantaneously achieved over degradation and isotope fractionation is limited through equilibrium [Kopinke et al., 2005] for ratios of degradation to desorption rate constant (k_{deg}/k_{des}) lower than 0.02 ($k_{des} < 2 \text{ d}^{-1}$). (Site 2001) We anticipate that the model remains valid under a ratio of k_{deg}/k_{des} lower than 0.1 [Anslyn and Dougherty, 2006]. Outside this domain, sorption-desorption kinetics have to be addressed in the model. To evaluate the impact of various types sediment on the $\epsilon_{bulk,corr}$, a sensitivity analysis was carried out for a large range of pesticides conditions (ϵ_{bulk} between -0.5 to -40‰ , $\log K_{oc}$ between 1 to 6 and TOC between 0.5 to 500 mg.L^{-1}) [Lewis et al., 2016]. The analysis showed insignificant effect of pesticide phase-transfer between sediment and water on isotope fractionation ($\epsilon_{bulk,corr} - \epsilon_{bulk} < 0.5\text{‰}$). This supports the idea that phase-transfer is associated with negligible isotope fractionation in water–sediment systems, and correction of ϵ_{bulk} is not needed under environmental conditions.

However, a correction of $\delta^{13}C_{obs,w}$ may be necessary to follow the model terminology P_w and P_s (see above) when DOC concentrations are high and significantly contribute to the isotope mass balance. The threshold for a correction that accounts for DOC concentrations can be determined with an isotope mass balance as follows:

$$\delta^{13}C_{obs,w} = x_{p,DOC} \cdot \delta^{13}C_{DOC} + (1 - x_{p,DOC}) \cdot \delta^{13}C_w \quad (\text{II.11})$$

where $x_{p,DOC}$ is the mass fraction and $\delta^{13}C_{DOC}$ the isotope signature of DOC-bound pesticides. Under the model assumption, the limit of model validity to avoid considering the isotope signature of DOC can be expressed using partitioning equations (Eq.

A.S12) and Eq. II.11:

$$DOC \leq \frac{\Delta}{(\delta^{13}C_{DOC} - \Delta) \cdot K_{oc} \cdot f_{oc}} \quad (\text{II.12})$$

where Δ is the minimal isotope signature threshold under which isotope signature of DOC-bound pesticides ($\delta^{13}C_{DOC}$) does not significantly influence pesticide isotope signature in the water ($\Delta = 0.5\text{‰}$). From Eq. II.12, using the physico-chemical properties of the pesticides, with $\log K_{oc}$ between 1 to 6 [Lewis et al., 2016], and realistic DOC surface waters concentration between 5 and 20 mg.L^{-1} [Raymond and Spencer, 2015], a correction of the DOC term is not required to interpret CSIA data. However, for the same range of pesticide physico-chemical properties, a correction of the DOC term is needed for DOC concentrations larger than 300 mg.L^{-1} , which can be reached in active sludge of wastewater treatment plants (Mann et al. 2012).

Pesticide degradation pathways

The carbon apparent kinetic isotope effects of acetochlor and *S*-metolachlor ($AKIE_C$) were calculated to compare isotope fractionation between different compounds and to interpret degradation pathways using ϵ_{bulk} values. Similar $AKIE_C$ values and TP patterns under oxic and anoxic conditions suggest an identical prevailing degradation pathway for acetolachlor and *S*-metolachlor.

Acetolachlor $AKIE_C$ values (oxic: 1.075 ± 0.008 and anoxic: 1.053 ± 0.003) and *S*-metolachlor (oxic: 1.018 ± 0.001 and anoxic: 1.029 ± 0.001) fit in the range of experimentally derived $AKIE_C$ for nucleophilic substitution degradations [Elsner et al., 2005]. This is also in agreement with the predominance of acetolachlor and *S*-metolachlor oxalinic acids as the major TPs (Figure II.6). Nucleophile substitution pathway of acetolachlor and *S*-metolachlor, primarily leading to the formation of oxalinic acids (Figure II.6), has been previously elucidated via the Glutathione-S-transferase followed by an oxidation [Feng, 1991]. Ethanosulfonic acids, also produced via the Glutathione-S-transferase, were identified as second TPs produced under different environmental conditions [Feng, 1991, Mersie et al., 2004, Graham et al., 1999]. Similar $AKIE_C$ values observed in a wetland column experiment ($AKIE_C$, acetolachlor = 1.051 ± 0.007) [Elsayed et al., 2014], and soil batch experiment ($AKIE_C$, *S*-metolachlor = 1.023 ± 0.001) [Alvarez-Zaldívar et al., 2018], suggest a similar degradation pathway or similar co-occurring pathways under various environmental conditions. N isotope signatures of acetochlor and *S*-metolachlor in water phase did not significantly change

under oxic and anoxic conditions ($1.2\text{‰} < |\Delta\delta^{15}N_{min,w}|$), which supports the proposed pathway. Indeed, N in acetochlor and *S*-metolachlor is positioned three atoms away from the reactive site, and only secondary isotope effect may be expected.

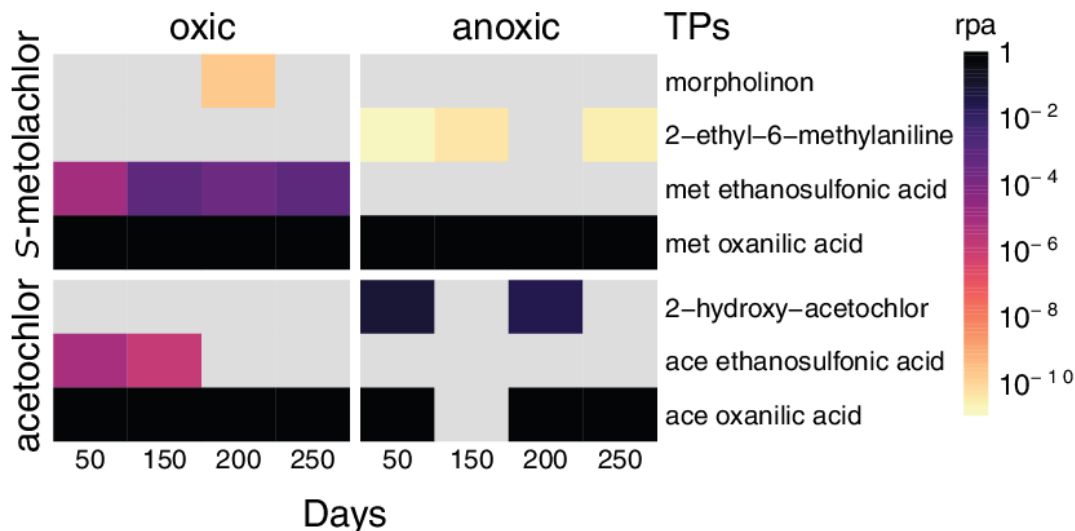


Figure II.6 – *S*-metolachlor and acetochlor transformation products (TPs) under oxic and anoxic conditions. Confirmed structures (Level 1) are presented. The relative peak area (rpa) is defined for each TPs as the ratio of the peak area normalized by the response factor for one TP to the main TP for the same pesticide. Grey indicates absence of the TPs.

The contribution of acetolachlor and *S*-metolachlor ethanosulfonic acids was low (relative peak area between 10^{-2} to 10^{-5}) compared to previous studies showing that production of ethanosulfonic acid was only two to five times lower than production of oxalinic acid [Feng, 1991, Graham et al., 1999]. Semi-quantitative analysis of HR-MS/MS data showed that TPs patterns under oxic and anoxic conditions slightly differed (Figure II.6).

Under anoxic conditions, acetolachlor and *S*-metolachlor ethanosulfonic acids were not detected, although its formation also involves a S-cysteine conjugate intermediate, as for acetolachlor and *S*-metolachlor oxalinic acids [Feng, 1991]. We hypothesize that some microorganisms may use acetolachlor and *S*-metolachlor ethanosulfonic acid as an alternative source of sulfur to grow under sulfate limiting conditions, such as those found in our anoxic batch experiments (Appendix A.S2.2) [Zürcher et al., 1987, Uria-

Nickelsen et al., 1994]. This idea is also supported by the confirmed formation of hydroxy acetochlor and the suggested formation of N-ethyl-N-(2-ethyl-6-methylphenyl)-2-hydroxyacetamide (L3; $m/z [M - H]^- = 221.1415$). Both may be formed as secondary hydroxy-TPs during microorganism sulfur assimilation, as observed previously with ethanesulfonate metazachlor (chloroacetanilide). (Laue, Field, and Cook 1996) However, a previous study with *S*-metolachlor under oxic nutrient-limiting conditions suggested the formation of the N-ethyl-N-(2-ethyl-6-methylphenyl)-2-hydroxyacetamide without any detection of the ethanesulfonic acid [Gutowski et al., 2015]. Specific conditions of microbial consumption of ethanesulfonate as a sulfur source remain unclear, although environmental implications are important since ethanesulfonic acids are more mobile than their parent pesticides and other TP [Huntscha et al., 2008].

2.4.4 Environmental implications for water–sediment studies

Here we examined the dissipation of the two widely used pesticides acetochlor and *S*-metolachlor in water–sediment batch experiments under contrasted oxic and anoxic conditions. $\delta^{13}C$ data and TP identification complementarily allowed to identify possible degradation pathways and associated mechanisms. In water–sediment systems with two main phases, dissipation reflects the contribution of both biodegradation and phase-transfer. A simplified version of a conceptual model validated over a broad range of conditions and molecules facilitated the estimation and the interpretation of degradation rate constants and bulk isotopic enrichment factors (ϵ_{bulk}) associated with each phase. The simplified model is valid in closed steady-state laboratory systems when the studied pesticide has the similar sorption affinity on dissolved (DOC) and particulate (POC) forms of organic carbon. Steady-state conditions are fulfilled and the model remains valid when sorption kinetics are faster than biodegradation ($k_{deg}/k_{des} < 0.1$). This ratio should carefully be estimated from experimental data before using this model. However, a k_{deg}/k_{des} ratios lower than 0.1 is satisfied in 82% of experiments derived from pesticide degradation in the envPath ($n = 4716$) database [Latino et al., 2017], considering cases when k_{des} is lower than $2 d^{-1}$ [Delle Site, 2001].

Most importantly, we anticipate negligible effects of phase-transfer on measured isotope signatures ($< 0.5\text{‰}$) for a broad spectrum of environmental conditions. Insignificant isotope fractionation during phase-transfer is crucial to apply CSIA to evaluate *in situ* degradation in water–sediment systems (*i.e.* ponds, wastewater treatment plant, rivers, etc.). ϵ_{bulk} determined under representative conditions in laboratory experiments can be applied *in situ* to estimate $DegT_{50,w}$ in different environmental systems.

This can facilitate pesticide dissipation studies and follow-up of pesticides in surface waters because pesticide degradation can be evaluated with pesticide CSIA, with limited or without information on pesticide concentrations or TPs. Moreover, CSIA data can improve predictions of pesticide degradation in reactive-transport model and provide direct information of the extent of degradation.

From a methodological point of view, we anticipate that sample preparation to limit the matrix effect (*e.g.* the dissolved or particulate carbon or nitrogen) before GC-IRMS measurements is necessary to apply CSIA in water–sediment systems. Bakkour et al. (2018) evaluate that GC-IRMS injected sample containing DOC to pesticide ratio (*mol/mol*) higher than 80 might create a too large background signal for accurate isotope ratios measurements. However, this limitation can be overcome in the future with additional cleaning steps, including molecularly imprinted polymers [Bakkour et al., 2018], or preparative high pressure liquid chromatography [Torrentó et al., 2019, Schreglmann et al., 2013] to selectively extract the compound of interest. Altogether, we anticipate that CSIA can help in the future to elucidate under laboratory and field conditions pesticide degradation in specific phases of the water–sediment to eventually improve predictive models of pesticide behavior in rivers.

Bibliography

- [Alvarez-Zaldívar et al., 2018] Alvarez-Zaldívar, P., Payraudeau, S., Meite, F., Masbou, J., and Imfeld, G. (2018). Pesticide degradation and export losses at the catchment scale: Insights from compound-specific isotope analysis (CSIA). *Water Research*, 139:198–207.
- [Anslyn and Dougherty, 2006] Anslyn, E. V. and Dougherty, D. A. (2006). *Modern physical organic chemistry*. University Science, Sausalito, CA.
- [Bakkour et al., 2018] Bakkour, R., Bolotin, J., Sellergren, B., and Hofstetter, T. B. (2018). Molecularly Imprinted Polymers for Compound-Specific Isotope Analysis of Polar Organic Micropollutants in Aquatic Environments. *Analytical Chemistry*, 90(12):7292–7301.
- [Borch et al., 2010] Borch, T., Kretzschmar, R., Kappler, A., Cappellen, P. V., Ginder-Vogel, M., Voegelin, A., and Campbell, K. (2010). Biogeochemical redox processes and their impact on contaminant dynamics. *Environmental Science & Technology*, 44(1):15–23.
- [Burri et al., 2019] Burri, N. M., Weatherl, R., Moeck, C., and Schirmer, M. (2019). A review of threats to groundwater quality in the anthropocene. *The Science of the Total Environment*, 684:136–154.
- [Charlton and Parkhurst, 2011] Charlton, S. R. and Parkhurst, D. L. (2011). Modules based on the geochemical model PHREEQC for use in scripting and programming languages. *Computers & Geosciences*, 37(10):1653–1663.
- [Delle Site, 2001] Delle Site, A. (2001). Factors Affecting Sorption of Organic Compounds in Natural Sorbent/Water Systems and Sorption Coefficients for Selected Pollutants. A Review. *Journal of Physical and Chemical Reference Data*, 30(1):187–439.
- [Elsayed et al., 2014] Elsayed, O. F., Maillard, E., Vuilleumier, S., Nijenhuis, I., Richnow, H. H., and Imfeld, G. (2014). Using compound-specific isotope analysis to

- assess the degradation of chloroacetanilide herbicides in lab-scale wetlands. *Chemosphere*, 99:89–95.
- [Elsner and Imfeld, 2016] Elsner, M. and Imfeld, G. (2016). Compound-specific isotope analysis (CSIA) of micropollutants in the environment — current developments and future challenges. *Current Opinion in Biotechnology*, 41:60–72.
- [Elsner et al., 2005] Elsner, M., Zwank, L., Hunkeler, D., and Schwarzenbach, R. P. (2005). A new concept linking observable stable isotope fractionation to transformation pathways of organic pollutants. *Environmental Science & Technology*, 39(18):6896–6916.
- [Ericson et al., 2014] Ericson, J. F., Smith, R. M., Roberts, G., Hannah, B., Hoeger, B., and Ryan, J. (2014). Experiences with the OECD 308 transformation test: A human pharmaceutical perspective. *Integrated Environmental Assessment and Management*, 10(1):114–124.
- [Escher et al., 2020] Escher, B. I., Stapleton, H. M., and Schymanski, E. L. (2020). Tracking complex mixtures of chemicals in our changing environment. *Science (New York, N.Y.)*, 367(6476):388–392.
- [European Chemicals Agency, 2016] European Chemicals Agency (2016). *Guidance on information requirements and chemical safety assessment Chapter R.16: environmental exposure assessment*. ECHA, Helsinki.
- [Feng, 1991] Feng, P. (1991). Soil transformation of acetochlor via glutathione conjugation. *Pesticide Biochemistry and Physiology*, 40(2):136–142.
- [Fenner et al., 2013] Fenner, K., Canonica, S., Wackett, L. P., and Elsner, M. (2013). Evaluating Pesticide Degradation in the Environment: Blind Spots and Emerging Opportunities. *Science*, 341(6147):752–758.
- [Ghattas et al., 2017] Ghattas, A.-K., Fischer, F., Wick, A., and Ternes, T. A. (2017). Anaerobic biodegradation of (emerging) organic contaminants in the aquatic environment. *Water Research*, 116:268–295.
- [Graham et al., 1999] Graham, W. H., Graham, D. W., deNoyelles, F., Smith, V. H., Larive, C. K., and Thurman, E. M. (1999). Metolachlor and Alachlor Breakdown Product Formation Patterns in Aquatic Field Mesocosms. *Environmental Science & Technology*, 33(24):4471–4476.

- [Gutowski et al., 2015] Gutowski, L., Olsson, O., Leder, C., and Kümmerer, K. (2015). A comparative assessment of the transformation products of S-metolachlor and its commercial product Mercantor Gold(®) and their fate in the aquatic environment by employing a combination of experimental and in silico methods. *The Science of the Total Environment*, 506-507:369–379.
- [Hammershøj et al., 2019] Hammershøj, R., Birch, H., Redman, A. D., and Mayer, P. (2019). Mixture Effects on Biodegradation Kinetics of Hydrocarbons in Surface Water: Increasing Concentrations Inhibited Degradation whereas Multiple Substrates Did Not. *Environmental Science & Technology*, 53(6):3087–3094.
- [Honti and Fenner, 2015] Honti, M. and Fenner, K. (2015). Deriving Persistence Indicators from Regulatory Water-Sediment Studies – Opportunities and Limitations in OECD 308 Data. *Environmental Science & Technology*, 49(10):5879–5886.
- [Honti et al., 2016] Honti, M., Hahn, S., Hennecke, D., Junker, T., Shrestha, P., and Fenner, K. (2016). Bridging across OECD 308 and 309 Data in Search of a Robust Biotransformation Indicator. *Environmental Science & Technology*, 50(13):6865–6872.
- [Huntscha et al., 2008] Huntscha, S., Singer, H., Canonica, S., Schwarzenbach, R. P., and Fenner, K. (2008). Input Dynamics and Fate in Surface Water of the Herbicide Metolachlor and of its Highly Mobile Transformation Product Metolachlor ESA. *Environmental Science & Technology*, 42(15):5507–5513.
- [Katagi, 2016] Katagi, T. (2016). Pesticide behavior in modified water-sediment systems. *Journal of Pesticide Science*, 41(4):121–132.
- [Kiefer et al., 2019] Kiefer, K., Müller, A., Singer, H., and Hollender, J. (2019). New relevant pesticide transformation products in groundwater detected using target and suspect screening for agricultural and urban micropollutants with LC-HRMS. *Water Research*, 165:114972.
- [Knauer et al., 2017] Knauer, K., Homazava, N., Junghans, M., and Werner, I. (2017). The influence of particles on bioavailability and toxicity of pesticides in surface water. *Integrated Environmental Assessment and Management*, 13(4):585–600.
- [Kopinke et al., 2005] Kopinke, F.-D., Georgi, A., Voskamp, M., and Richnow, H. H. (2005). Carbon isotope fractionation of organic contaminants due to retardation on humic substances: implications for natural attenuation studies in aquifers. *Environmental Science & Technology*, 39(16):6052–6062.

- [Latino et al., 2017] Latino, D. A. R. S., Wicker, J., Gütlein, M., Schmid, E., Kramer, S., and Fenner, K. (2017). Eawag-Soil in enviPath: a new resource for exploring regulatory pesticide soil biodegradation pathways and half-life data. *Environmental Science: Processes & Impacts*, 19(3):449–464.
- [Lewis et al., 2016] Lewis, K. A., Tzilivakis, J., Warner, D. J., and Green, A. (2016). An international database for pesticide risk assessments and management. *Human and Ecological Risk Assessment: An International Journal*, 22(4):1050–1064.
- [Loch et al., 2002] Loch, A. R., Lippa, K. A., Carlson, D. L., Chin, Y. P., Traina, S. J., and Roberts, A. L. (2002). Nucleophilic Aliphatic Substitution Reactions of Propachlor, Alachlor, and Metolachlor with Bisulfide (HS-) and Polysulfides (Sn2-). *Environmental Science & Technology*, 36(19):4065–4073.
- [Maggi et al., 2019] Maggi, F., Tang, F. H. M., Cecilia, D. l., and McBratney, A. (2019). PEST-CHEMGRIDS, global gridded maps of the top 20 crop-specific pesticide application rates from 2015 to 2025. *Scientific Data*, 6(1):1–20.
- [Maillard and Imfeld, 2014] Maillard, E. and Imfeld, G. (2014). Pesticide Mass Budget in a Stormwater Wetland. *Environmental Science & Technology*, 48(15):8603–8611.
- [Malaj et al., 2014] Malaj, E., Ohe, P. C. v. d., Grote, M., Kühne, R., Mondy, C. P., Usseglio-Polatera, P., Brack, W., and Schäfer, R. B. (2014). Organic chemicals jeopardize the health of freshwater ecosystems on the continental scale. *Proceedings of the National Academy of Sciences*, 111(26):9549–9554.
- [Mersie et al., 2004] Mersie, W., McNamee, C., Seybold, C., Wu, J., and Tierney, D. (2004). Degradation of metolachlor in bare and vegetated soils and in simulated water-sediment systems. *Environmental Toxicology and Chemistry*, 23(11):2627–2632.
- [Moser et al., 2018] Moser, A., Wemyss, D., Scheidegger, R., Fenicia, F., Honti, M., and Stamm, C. (2018). Modelling biocide and herbicide concentrations in catchments of the Rhine basin. *Hydrology and Earth System Sciences*, 22(8):4229–4249.
- [OECD, 2000] OECD (2000). *Test No. 106: Adsorption – Desorption Using a Batch Equilibrium Method*. Organisation for Economic Co-operation and Development, Paris.
- [OECD, 2004] OECD (2004). *Test No. 111: Hydrolysis as a Function of pH*. Organisation for Economic Co-operation and Development, Paris.

- [Raymond and Spencer, 2015] Raymond, P. A. and Spencer, R. G. (2015). Riverine DOM. In *Biogeochemistry of Marine Dissolved Organic Matter*, pages 509–533. Elsevier.
- [Schecher and McAvoy, 1992] Schecher, W. D. and McAvoy, D. C. (1992). MINEQL+: A software environment for chemical equilibrium modeling. *Computers, Environment and Urban Systems*, 16(1):65–76.
- [Schreglmann et al., 2013] Schreglmann, K., Hoeche, M., Steinbeiss, S., Reinnicke, S., and Elsner, M. (2013). Carbon and nitrogen isotope analysis of atrazine and desethylatrazine at sub-microgram per liter concentrations in groundwater. *Analytical and Bioanalytical Chemistry*, 405(9):2857–2867.
- [Schwarzenbach et al., 2010] Schwarzenbach, R. P., Egli, T., Hofstetter, T. B., von Gunten, U., and Wehrli, B. (2010). Global Water Pollution and Human Health. *Annual Review of Environment and Resources*, 35:109–136.
- [Schwarzenbach et al., 2003] Schwarzenbach, R. P., Gschwend, P. M., Imboden, D. M., and Imboden, M. (2003). *Environmental Organic Chemistry / Edition 2*.
- [Shrestha et al., 2016] Shrestha, P., Junker, T., Fenner, K., Hahn, S., Honti, M., Bakkour, R., Diaz, C., and Hennecke, D. (2016). Simulation studies to explore biodegradation in water–sediment systems: From OECD 308 to OECD 309. *Environmental Science & Technology*, 50(13):6856–6864.
- [Smith et al., 2002] Smith, E. J., Davison, W., and Hamilton-Taylor, J. (2002). Methods for preparing synthetic freshwaters. *Water Research*, 36(5):1286–1296.
- [Torrentó et al., 2019] Torrentó, C., Bakkour, R., Glauser, G., Melsbach, A., Ponsin, V., Hofstetter, T. B., Elsner, M., and Hunkeler, D. (2019). Solid-phase extraction method for stable isotope analysis of pesticides from large volume environmental water samples. *The Analyst*, 144(9):2898–2908.
- [Uria-Nickelsen et al., 1994] Uria-Nickelsen, M. R., Leadbetter, E. R., and Godchaux, W. (1994). Comparative aspects of utilization of sulfonate and other sulfur sources by *Escherichia coli* K12. *Archives of Microbiology*, 161(5):434–438.
- [Vandermaesen et al., 2016] Vandermaesen, J., Horemans, B., Bers, K., Vandermeeren, P., Herrmann, S., Sekhar, A., Seuntjens, P., and Springael, D. (2016).

Application of biodegradation in mitigating and remediating pesticide contamination of freshwater resources: state of the art and challenges for optimization. *Applied Microbiology and Biotechnology*, 100(17):7361–7376.

[Zumstein and Helbling, 2019] Zumstein, M. T. and Helbling, D. E. (2019). Biotransformation of antibiotics: Exploring the activity of extracellular and intracellular enzymes derived from wastewater microbial communities. *Water Research*, 155:115–123.

[Zürcher et al., 1987] Zürcher, D., Cook, A. M., and Leisinger, T. (1987). Microbial desulfonation of substituted naphthalenesulfonic acids and benzenesulfonic acids. *Applied and Environmental Microbiology*, 53(7):1459–1463.

Preface to Chapter III

Pesticide transport and degradation at the SWI as derived from results of Chapter 4.1 are expected to vary under dynamic conditions. Pollutant transport driven by overlying water flow and surface-groundwater exchanges developing at the SWI may influence the occurrence, extent and pathways of pollutant degradation. Since these effects are molecule- and case-specific, in this chapter we present a generic procedure capable of accurately capturing the effect of pollutant transport on pollutant degradation at the SWI.

An experimental recirculated bench-scale river channel was used to examine the effect of overlying water velocity on pollutant transport, sorption in the sediment and degradation. Concomitantly, we developed a flow-reactive-transport (FRT) model to quantify and interpret the effect of pollutant transport under varying hydraulic forcing typical of rivers, on pollutant degradation. The combined experimental setup and FRT model may help refining knowledge of pesticide fate in rivers.

Chapter III

Pesticide transport at the sediment-water interface

From submitted paper: Drouin, G., Fahs, M., Droz, B., Younes, A., Imfeld, G. & Payraudeau, S. Pollutant dissipation at the sediment-water-interface: a robust discrete continuum numerical model and recirculating laboratory experiments, Water Resources Research.

Abstract

Pollutant exchange in the hyporheic zone is a major process controlling its degradation in riverine systems, although knowledge of mass transfer processes at the sediment-water interface (SWI) remain scarce. Accurate predictive modelling of complex horizontal and vertical flows driving pollutant fluxes at the SWI is currently limited. Here we examined mass exchange at the SWI by combining laboratory bench-scale experiments and the development of a physically-based flow reactive transport (FRT) model. NaCl and Foron Blue 291 tracers were used as surrogates of conservative and moderately sorptive organic pollutants, respectively. Tracer experiments in the bench-scale river channel reproduced the influence of overlying water velocities, the source of the pollutant (*i.e.* overlying water or sediment bed), and its sorption capacity on pollutant exchange at the SWI. A methodological framework to calibrate the FRT model against a lab-scale experiment was developed. Good agreement between the experimental and numerical results confirmed the robustness of the experimental setup and the numerical model. The pollutant origin, either from the sediment or the overlying water, did not influence the pollutant exchange rates at the SWI. The exchange rates were quasi-proportional to the overlying water velocity. The tracer partitioning retarded the equilibrium up to 6 times compared with the conservative tracer NaCl. Numerical tests involving both overlying and vertical velocities showed that the latter is the main factor controlling pollutant exchange at the SWI. Altogether, the model helps capture complex interactions between transport and pollutant partitioning to the sediment in rivers, thus paving the way for

more systematic investigations of pollutant fate in rivers.

3.1 Introduction

More than one-third of the global available freshwater resource is used for human activities, and freshwater contaminations by macro- and micro-pollutants are recurring and widespread [Sousa et al., 2018]. Rivers are the most sensitive environmental compartments to pollution hazards, especially low Strahler order rivers, which may receive proportionally larger loads of pollutants relatively to their water discharge [Honti et al., 2018, Munz et al., 2011]. Hyporheic zone processes in rivers enhance both pollutant mixing and biogeochemical activity in the sediment bed [Boano et al., 2014]. Despite decades of intense research on hyporheic zone, the dynamics of hyporheic zone processes remain partly unresolved, and current approaches often fail to identify predominant factors controlling the interactions between pollutants and river sediment beds.

Hyporheic processes occur at the sediment water interface (SWI) where the mixing of dissolved pollutants in sediment bed sustains the development of various redox gradients [Byrne et al., 2014]. Hydrological forcing conditions in rivers, including succession of low flow and floods, vertical surface-groundwater exchanges, and geomorphological variations of river reaches mainly affect the transport of dissolved pollutants at the SWI [Briggs et al., 2014, Dwivedi et al., 2018, Lansdown et al., 2015]. In addition, the propensity of a pollutant to sorb and degrade within the sediment bed controls its accumulation in the hyporheic zone [Liao et al., 2013]. Sorption typically increases the pollutant residence time within the sediment bed and alters its distribution across the hyporheic zone [Ren and Packman, 2004a, Ren and Packman, 2004b]. Altogether, the complex interplay between hydraulic forcing and pollutant partitioning currently limits our understanding of pollutant fate in riverine systems [Krause et al., 2017].

In this context, the characterization of hyporheic exchanges in rivers can rely on laboratory tracer experiments [Liao et al., 2013]. Tracers can be used as surrogate of pollutants that may ease investigations of pollutant fate at the SWI. The experimental procedures generally involve intense logistics, including technical constraints and space, and may be expensive (see Appendix B.S1). Chandler et al. (2016) and Fox et al. (2014) examined the effect of varying hydraulic forcing on tracer exchange at the SWI [Chandler et al., 2016, Fox et al., 2014]. Different riverbed geometries were

studied by Cardenas and Wilson (2007) [Cardenas and Wilson, 2007b]. The effect of pollutant physico-chemical properties on the mass flux at the SWI was investigated by Ren and Packman (2004b) [Ren and Packman, 2004b]. While previous studies often relied on large scale experimental setups ($\sim m$), small-scale experiments ($\sim cm$) in recirculating flumes also demonstrated to be promising to study transport in rivers, as they allow for repetitive testing [Malverti et al., 2008].

Although adapted experimental flumes can be designed, characterizing the processes governing pollutant transport at the SWI remains delicate because the direct observation of velocity fields in the sediment bed is often limited. In this context, conceptual and physically based reactive transport modelling can help to characterize and interpret transport processes in the sediment bed [Voermans et al., 2017]. Conceptual diffusive models rely on the Fick’s law with an effective diffusivity featuring the combined effect of diffusion, dispersion and small scale advective processes. Although diffusive models provide a computationally inexpensive way to simulate pollutant mass exchange at the SWI [Voermans et al., 2018], they rely on systematic and site-specific experimental characterizations of the effective diffusivity. These characterizations severely limit the extrapolation of diffusive models to different river conditions. On the other hand, physically based flow-reactive-transport (FRT) models coupling three operators representing flow, pollutant transport and reactive processes across the SWI [Angot et al., 2017, Kaufman et al., 2017]. The FRT models intrinsically overcome the limitations of the diffusive models and allow more generic representation of pollutant exchange at the SWI. However, one major drawback of FRT models is the lack of accuracy of flow simulation at the SWI. Using Darcy’s law for both fluid and porous regions ensures continuity of the primary variables and yields to a consistent mathematical system. However, the velocity in the fluid layer (and also in a layer of high permeable sediment) cannot be accurately simulated with the Darcy’s model [Salim Joodi et al., 2010, Xu et al., 2018]. The classical approach, which uses the Navier-Stokes equation within the overlying water and the Darcy’s equation within the porous sediment bed, leads to a more robust representation of flows but requires coupling the conservation equations at the interface using appropriate boundary conditions [Ehrhardt, 2012], because the continuity of normal and tangential velocities, stress and pressure at the interface cannot be simultaneously ensured. This challenges the selection of the most suited interface conditions and makes it case-specific [Bars and Worster, 2006, Lācis and Bagheri, 2017, Valdés-Parada et al., 2013]. Interface conditions are also required when the Brinkman model is used instead of Darcy’s law [Ehrhardt, 2012].

The purpose of this study is to improve the mechanistic interpretation of pollutant exchange at the SWI. We developed a FRT model based on the combination of Navier-Stokes and Brinkman models, for the fluid (*i.e.* overlying water) and the porous region (*i.e.* sediment bed), respectively, and a cost-effective and recirculating laboratory bench-scale tracer experiment. The FRT model relies on numerical schemes that continuously solve the governing flow and pollutant transport equations for both the fluid and porous regions. The bench-scale river channel enables repetitive tests under a large panel of hydraulic conditions and allows NaCl and Foron Blue 291 tracers to be used as surrogates of conservative and moderately sorptive organic pollutants, respectively. We present a methodology to calibrate the numerical model against experimental data to evaluate the suitability of the new numerical model and the experimental device. Finally, we investigated numerically the impact of losing and gaining rivers on pollutant exchange at the river scale, which paves the way for future studies of pollutant transport in complex river systems.

3.2 The FRT numerical model

The novelty of the conceptualization and the resolution of the physically-based discrete continuum FRT model presented here lies in the continuity of all state variables at the fluid-porous interface; *i.e.* between the overlying water and the riverbed sediment (Figure III.1). This continuity allows the generic resolution of pollutant transport at the SWI under various hydrological conditions.

3.2.1 Governing equations

The Navier-Stokes and Brinkman equations were merged into a single equation (Eq. III.1 and III.2). The set of logical coefficients (s_1, s_2, s_3, s_4) was used to switch from the fluid to the high and low permeable porous domains in the sediment layer as depicted in Figure III.1. The continuity of all variables was thus ensured while empirical interfacial conditions were not necessary to compute the flow or transport as it would be with classical multi-domain approaches [Bars and Worster, 2006].

$$s_1 \cdot \frac{\rho}{\epsilon} \frac{\partial \mathbf{u}}{\partial t} + s_2 \cdot \frac{\mu}{K} \mathbf{u} + s_3 \cdot \frac{\rho}{\epsilon^2} (\mathbf{u} \cdot \nabla) \mathbf{u} - s_4 \cdot \frac{\mu}{\epsilon} \nabla \cdot (\nabla \mathbf{u}) + \nabla P = -\rho g \nabla z \quad (\text{III.1})$$

$$\nabla \mathbf{u} = \mathbf{0} \quad (\text{III.2})$$

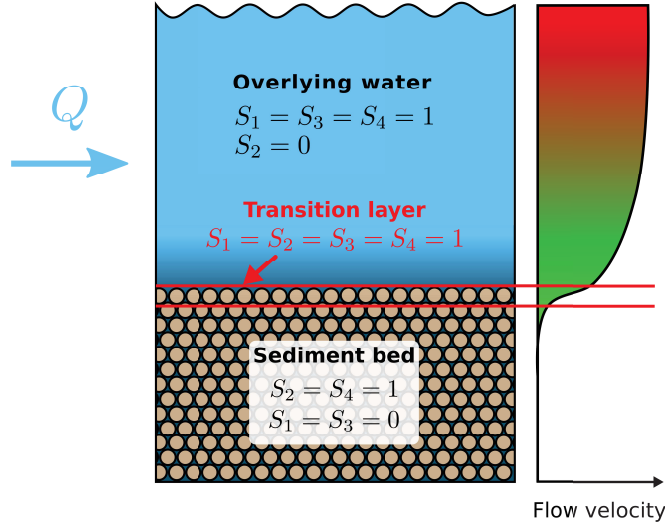


Figure III.1 – Conceptual description of the domain decomposition with parameters used in Eq. III.1 for the three layers configuration

where \mathbf{u} [L/T] is the fluid velocity, including horizontal and vertical components, and P is the water pressure [$M/L/T^2$]. ρ and μ are the water volumetric mass density [M/L^3] and the dynamic viscosity [$M/L/T$], ϵ is the sediment porosity [L^3/L^3], g is the gravity [L/T^2] and z is the vertical position [L].

In the overlying water, the flow was described using the Navier-Stokes equations by setting coefficients s_1 , s_3 and s_4 to be 1 and coefficient s_2 to be 0. In the porous medium of low permeability (*i.e.* sediment bed layer), Darcy's law was applied by suppressing the transient effect and the convective term of the Brinkman equation, corresponding to s_1 and s_3 equal to 0 and s_2 and s_4 equal to 1. A transition layer with a high permeability was introduced between the fluid and the porous region. The occurrence of a transition layer at the fluid-porous interface [Nield, 1983] has been experimentally validated by Goharzadeh et al. (2005) [Goharzadeh et al., 2005]. The thickness of the transition layer was in the same size order as the grain size of the porous medium. In this transition layer all coefficients of the Brinkman equation were set to 1.

The FRT model is based on the advection – dispersion – reaction equations (Eq. III.3):

$$\epsilon \frac{\partial C_i}{\partial t} + \rho_{bulk} \cdot \frac{\partial S_i}{\partial t} + \mathbf{u} \cdot \nabla C_i - \nabla \cdot (\mathbf{D}_i \cdot \nabla C_i) = r_i \quad (\text{III.3})$$

$$\mathbf{D}_i = D_{m,i} \cdot \mathbf{I} + \mathbf{D}_{\text{disp}} = (\alpha_T \cdot |\mathbf{u}| + D_m) \cdot \delta_{lm} + (\alpha_L - \alpha_T) \cdot \frac{u_l \cdot u_m}{|\mathbf{u}|} \quad (\text{III.4})$$

where C_i [M/L^3] represents the dissolved pollutant concentration, subscript i indicates the chemical species i , S_i [M/M] is the sorbed concentration, ρ_{bulk} is the bulk density of the porous medium [M/L^3], D_i is the related dispersion tensor [L^2/T] accounting for pollutant molecular diffusion ($D_{m,i}$) [L^2/T] and longitudinal (α_L) and transversal (α_T) dispersion [L], δ_{lm} is the Kronecker function with $l, m = 1, 2$ and r_i is the reactive term representing either sorption or degradation of specie i .

The model application was limited in our case to laminar flow, although the proposed approach can be extended to turbulent flow. While turbulent flow in the overlying water may enhance mass exchange at the SWI [Grant and Marusic, 2011], turbulences may not penetrate within the sediment bed except in conditions of high velocities, and/or very coarse and permeable sediment [Boano et al., 2014, Voermans et al., 2017]. The model applications to laminar flow is justified here by the predominance of low Strahler order rivers (< 2) accounting for 75% of the global river length [Downing, 2012]. The limited velocity in low Strahler order rivers favours laminar flow, except during floods, and sediment bed clogging even from coarse sand riverbed [Jin et al., 2019], thereby limiting turbulent flow penetration in the sediment bed. The model is thus valid below the critical Reynolds number above which laminar flow transforms to turbulent in rectangular channels. This number is generally observed around $Re = 3000$ [Suga et al., 2010] and may theoretically even ranks higher, up to $Re = 15000$, with decreasing sediment bed permeability [Sparrow et al., 1973].

Kinetic sorption was considered since the residence times of pollutants at the SWI vary from minutes to days [Liao et al., 2013]. A one site reversible sorption was adopted, as previously recommended in sorption studies involving metal ions and quartz sand sediment bed [Eylers et al., 1995]. Adsorption and desorption were thus implemented with the one-site first order kinetic sorption described in Van Genuchten and Wagenet (1989) [van Genuchten and Wagenet, 1989]. The sorption isotherm followed a reversible linear relationship (Eq. III.5). Sorption equilibrium was assumed to be fully established after 12 hours (99.3% of the equilibrium value) [OECD, 2000].

$$\frac{\partial S_i}{\partial t} = \alpha_i \cdot (K_{d,i} \cdot C_i - S_i) \quad (\text{III.5})$$

where $K_{d,i}$ is the phase partitioning coefficient of specie i in [L^3/M] and α_i is the first

order rate of adsorption $[T^{-1}]$.

3.2.2 Numerical resolution

Equations were solved using numerical techniques for space discretization and time integration. Specific numerical methods were implemented for flow, advection, dispersion and reaction operators to obtain efficient simulations while maintaining high accuracy and continuity of state variables and mass fluxes between the water and sediment layers. The developed model relies on the numerical scheme suggested by Younes et al. (2014) to solve the coupled Navier Stokes and heat transfer equations [Younes et al., 2014]. The same numerical scheme was adopted here to solve the merged form of Navier-Stokes and Brinkman model (Eq. III.1) coupled with the mass transport equations of the reactive system (Eq. III.3). Flow, transport and reactive operators were sequentially solved. The flow equation was solved with the non-conforming Crouzeix-Raviart (CR) finite element method [Burman and Hansbo, 2005]. In contrast to the standard conforming finite element method, the non-conforming method deals with the velocity at the edges of elements of the computational mesh. This important property ensures local mass conservation and yields continuous fluxes at the SWI without any specific treatment.

Solving the advection dominated transport is a challenging task. Standard Eulerian methods are known to introduce unphysical oscillations or numerical diffusion. Avoiding these numerical artefacts requires demanding computational requirements with dense computational grids and small time steps. We used here the Discontinuous-Galerkin (DG) finite element method [Miller et al., 2013] to overcome these difficulties and discretize the advection term of the transport equation. The DG method is superior to existing finite element methods [Miller et al., 2013]. DG is suitable for our specific SWI application because it accurately couples to the CR finite element method, and can capture strong concentration gradients and physical discontinuities (*e.g.* permeability gradient at the SWI). The diffusion-dispersion term of the transport equation was discretized using the Multi-Point Flux Approximation (MPFA) method. This method was selected because of its local mass conservation property. Further, MPFA was condensed in a single system with the DG method to reduce numerical errors when solving advection and dispersion separately (see Younes et al. (2014) for more details). The reactive term was included by an operator splitting approach using results of the transport operator as initial values to update specie concentrations based on chemical reactivity. The kinetic reactive transport was solved using the backward

differentiation formula [Fahs et al., 2011].

An adaptive, non-iterative time stepping was used for time integration to ensure numerical model accuracy and performance [Hirthe and Graf, 2012]. This technique adapts the time step during simulation from an estimation of the local truncation error due to time discretization. The time stepping procedure also controls intrinsic error caused by the operator splitting approach when dealing with chemical reactions [Fahs et al., 2008].

The developed numerical scheme combining previously described methods was validated against Fourier series solutions for problems of free fluids (Navier-Stokes equation) in Fahs and Younes (2014) [Fahs and Younes, 2014]. The correctness of the developed code was further checked by comparison with COMSOL® multi-physics for cases including either pure Darcy or Brinkman model (results not shown).

3.3 Tracer recirculation in bench-scale river channel

The experimental laboratory bench-scale river channel allowed to test the relationship between hydrological conditions and the transport of tracers as surrogates of pollutants at the SWI.

3.3.1 Experimental setup

The tracer experiments were conducted in a closed and recirculated bench-scale river channel (Figure III.2). Recirculated systems allow studying dissolved pollutant transport as it mimics long river reaches ($> km$) in space as limited as a laboratory bench ($< 30 cm$) while running with a constant water volume ($\approx 2 L$).

The bench-scale river channel was made of glass and composed of a channel and a mixing beaker (Figure III.2). All materials were selected to limit organic tracers and pollutant sorption. The sediment bed defining the SWI was 15 *cm* long (L_{sb}) and centred around a 28 *cm* long channel allowing flow stabilization up- and downstream of the interface. Water was pumped by a centrifuge pump (Iwaki MD-15R) through Isoversinic® tubing at the outlet of the channel up to the mixing beaker and fed back by gravity to the channel. Flow restrictors at the inlet of the pump and of the channel allowed setting the water flow and water height constant over time. The sand bed was 10 *cm* deep and made of thoroughly washed homogeneous sand (Kaltenhouse K30 –

France, $\Phi_{50} = 493 \mu m$, $\Phi_{95} = 786 \mu m$, detailed composition in Text B.S2). The sand porosity ($\epsilon = 0.35 \pm 0.01$) did not change across experiments. The sediment apparent density ($\rho_{bulk} = 1700 kg.m^{-3}$) was determined from sand density provided by the manufacturer. A mean sand saturated conductivity of $K_0 = 7.4 \pm 2.2 \cdot 10^{-4} m.s^{-1}$ was determined from 6 replicates using the constant-head method.

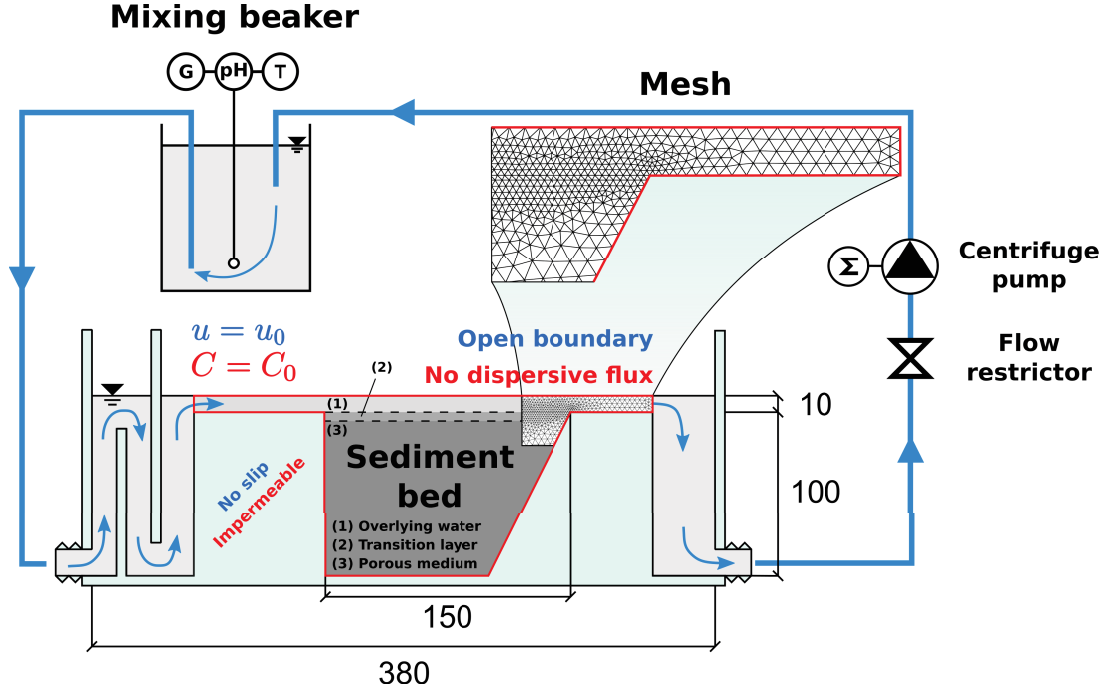


Figure III.2 – Bench-scale river channel setup. Quotations are in mm. Water was recirculated over the sediment bed with a centrifuge pump. A mixing beaker was placed in the circulating loop to measure tracer concentrations, pH, temperature (T) and conductivity (G). A flow restrictor controlled the water height within the channel. Water flow was controlled with the height difference between the channel and the mixing beaker. The computational domain is delineated by red lines. Boundary conditions are shown in blue for flow (no slip or open boundary) and in red for mass transport (impermeable or no dispersive flux). An example of extracted computational mesh is represented with smaller elements at the SWI interface.

3.3.2 Conservative and sorptive tracer experiments

Tracer experiments were carried out to study the relationship between pollutant transport patterns at the SWI (*i.e.* pollutant originating from the sediment or the over-

lying water), water flow and sorption. Saline solution (NaCl) was used as a conservative tracer and the dye Foron blue 291 (FB291) was used as a strongly sorptive molecule [Berez et al., 2016]. The combination of tracers with different sorptive properties was recently demonstrated to be suited to differentiate between organic pollutant transport and phase partitioning in lab-scale constructed wetlands [Fernandez-Pascual et al., 2020]. Initial tracer concentrations were adjusted to prevent density driven flow during mixing with NaCl (500 mg.L^{-1}) [Nagaoka and Ohgaki, 1990] or to avoid precipitation of FB291 (150 mg.L^{-1}). Tracers were injected in ultrapure water ($> 15 \text{ MOhm}$) alone for NaCl and with the adjunction of 0.01 M CaCl_2 for FB291 to reproduce a typical solution ionic strength [OECD, 2000]. The pH remained constant at 7 ± 0.5 across the experiment. Twenty four hours of equilibration were conducted after the addition of the tracer solutions to the sediment to ensure establishment of sorption equilibrium with FB291. The tracer experiments lasted between 1 and 12 days and were ended when no significant variation of concentrations was observed in the mixing beaker or the sediment bed.

The adsorption properties of FB291 were derived from the batch adsorption equilibrium method [OECD, 2000] (Text B.S3), which was used previously in similar experiments [Eylers et al., 1995, Ren and Packman, 2004a]. The linear adsorption isotherm was most suited for FB291, yielding a $K_d = 7.7 \pm 0.2 \text{ mL.g}^{-1}$. The adsorption of FB291 on sand occurs by the electrostatic interaction forces between the cationic form of the organic pollutant and the negatively charge surface of quartz at experimental $pH = 7.5 \pm 0.5$ [Jada and Ait Akbour, 2014]. A reversible adsorption/desorption process with no hysteresis (*i.e.* no significant non-extractable residual fraction and degradation) was thus assumed.

3.3.3 Data acquisition

The pollutant transport was analysed from in-bed and overlying water concentration dynamics. The tracer concentrations in the mixing beaker were continuously monitored at a sampling frequency of 30 seconds. The concentration variations over time within the mixing beaker reflected the global mass exchange. The NaCl concentration was followed-up by conductivity measurements (WTW 350i), converted into concentration with a previously established linear relationship. The FB291 concentration was continuously monitored by a spectrophotometric method (Avantes AvaLight-D5) at $\lambda = 304 \text{ nm}$, in which the FB291 concentrations showed a strongly linear relationship with the absorbance in the range from 1 to 150 mg.L^{-1} .

The NaCl concentrations in the sediment bed were followed-up by collecting during each experiments 0.8 to 1 *mL* of pore water samples from a depth of 0.5 to 7.5 *cm* depth with pore water samplers (MicroRhizons®). The sample volumes were adjusted to allow sufficient measurement accuracy while limiting the impact of porewater removal on the experiment. The tracer concentrations were immediately measured. MicroRhizon samplers could not be used for the experiment with FB291 since the tracer sorbed to the samplers. A beaker filled with water, with a similar shape as the mixing beaker, was placed along with the channel and weighted over time to estimate the evaporation. Blank experiments were also conducted for low and high flow without tracer to quantify any unexpected release of ions from the sand which could potentially bias NaCl quantification by conductivity measurements. The raw time-series of tracer concentrations were corrected for evaporation and ions release before comparison with the modelled data (TextB.S4). The measured concentrations were normalized by the theoretical equilibrium concentration (C_{eq}) to compare the experiments (methodology described in Text B.S5).

3.3.4 Experiment conditions

Riverbed sediments can alternatively act as sources or sinks of pollutants dissolved in the overlying water depending on hyporheic flows [Krause et al., 2017]. Cases of pollutant incorporation (I), with the tracer originating from the overlying water (*e.g.* surface contamination), and solute export (E), with the tracer released from the sediment bed (*e.g.* groundwater contamination or historical contamination by the river), were examined. In the case of solute incorporation, the sediment bed was filled with ultrapure water, and the tracer was spiked in the mixing beaker. In the case of solute export, the sediment bed was filled with the tracer solution and the mixing beaker was filled with ultrapure water.

The effect of water flow on mass exchange was tested for each case with low (LF) and high flow (HF) conditions. The targeted flow velocities were 1.5 and 5.0 *cm.s*⁻¹, corresponding to $Re \approx 100$ and 400 for LF and HF conditions, respectively. The velocities were below the critical Reynolds number for laminar flow and transitional regimes in rectangular open channels [Allen, 1965]. The Flows were adjusted with the flow pump and water height was kept at 1 *cm* over the sediment bed. NaCl was used to investigate the effect of solute origin (ILF_{NaCl} vs ELF_{NaCl} and IHF_{NaCl} vs EHF_{NaCl}) and the overlying water velocity (ILF_{NaCl} vs IHF_{NaCl} and EHF_{NaCl} vs IHF_{NaCl}) on

its transport. Additional experiments with FB291 were conducted under high flow for incorporation and export cases to investigate the effect of sorption on transport at the SWI (IHF_{FB291} vs IHF_{NaCL} and EHF_{FB291} vs EHF_{NaCL}). Experimental conditions are summarized in Table III.1. Except for the experiments IHF_{FB291} and EHF_{FB291} , the experiment duration was sufficient to establish equilibrium in the first 8 cm of the sediment bed.

Table III.1 – Hydraulic properties of tracer experiments (left side): V_{ch} stands for the water velocity set in the canal, Re for the associated Reynolds number and t_{max} for the experimental duration. Experimental data used for model validation (middle of the table). For ILF_{NaCL} , excessive ion release hampered $t_{80\%}$ stands for the time required to reach 80% of the theoretical equilibrium concentration within the mixing beaker and $L_{eq,80\%}$ for the associated equivalent length. $t_{80\%}$ and $L_{eq,80\%}$ arise from numerical computations (right side).

Hydraulic properties						Datasets		Numerical results	
Case	Tracer	Configuration	V_{ch}	Re	t_{max}	Global mass ex-change	Vertical distribution	$t_{80\%}$	$L_{eq,80\%}$
Units			$cm.s^{-1}$		h			h	km
ELF_{NaCL}	NaCl	Export	1.5 (1.2 ; 1.9)	107	92	Yes	Yes	140 (92; 175)	7.5
ILF_{NaCL}		Incorporation	1.4 (1.2 ; 1.8)	102	70	No	Yes	/	/
EHF_{NaCL}		Export	4.7 (3.9 ; 5.8)	335	92	Yes	Yes	30	5
IHF_{NaCL}		Incorporation	4.6 (3.8 ; 5.8)	329	23	Yes	Yes	31	5.1
$EHFFB291$	FB291	Export	5.4	385	287	Yes	No	138	27
$IHFFB291$		Incorporation	4.7 (3.9 ; 5.8)	335	187	Yes	No	186	31

3.4 Model validation vs experiment

3.4.1 Numerical simulations: Conceptual model, parameterization and domain discretization

The SWI was split in three areas with distinct physical properties, namely, the overlying water, the transition layer and the porous medium (see Figure III.1). Navier-Stokes

was solved in the overlying water while Brinkman was applied in the transition layer and the porous medium. The size of the transition layer thickness was assumed to correspond to that of the maximum grain diameter ($D_{max} \approx 0.001 \text{ m}$, Table B.S2) [Goharzadeh et al., 2005]. The porosity of the transition layer (ϵ_{TL}) corresponded to the geometric mean between porosities of the overlying water and the porous medium, giving $\epsilon_{TL} = 0.67$ [Goharzadeh et al., 2005, Voermans et al., 2017]. The Carman-Kozeny equation (Eq. III.6, [Carman, 1997]) predicted the sediment bed permeability well ($K_0^{CK} = 10.2 \cdot 10^{-4} \text{ m.s}^{-1}$ vs $K_0 = 7.4 \pm 2.2 \cdot 10^{-4} \text{ m.s}^{-1}$ as measured). The permeability of the transition layer (K_{TL}) was thus assumed to vary accordingly with a fixed $D_{50} = 0.494 \text{ mm}$.

$$K_{TL} = \frac{\epsilon_{TL}^3}{180 \cdot (1 - \epsilon_{TL})^2} \cdot D_{50}^2 = 28.7 \cdot K_0 = 2.13 \cdot 10^{-2} \text{ m.s}^{-1} \quad (\text{III.6})$$

No-slip boundary conditions were set at the boundary edge except at the inlet and outlet of the channel. Water was forced through the system with an inlet horizontal velocity (Dirichlet condition) and free to flow at the outlet (open boundary). At the free surface, slip condition allowed horizontal but no vertical velocities. Zero flux Neumann boundary conditions were imposed for transport everywhere except at the inlet where the concentrations are imposed. The boundary conditions are also represented in Figure III.2. Water recirculation was addressed in the model with an external subroutine actualizing transport boundary conditions for the inlet at each time step.

Model validation was performed sequentially with data from the conservative (*i.e.* NaCl) and sorptive (*i.e.* FB291) tracer experiments. Both tracer concentrations were used in the mixing beaker and at different depths of the sediment bed. Experimental inaccuracies originating from uncertainties in the determination of K_0 and u^* were accounted for, through a simulated confidence interval, computed with the set of parameters $(K_0 + \delta_{K_0}; u^* + \delta_{u^*})$ and $(K_0 - \delta_{K_0}; u^* - \delta_{u^*})$ as upper and lower limits ($\delta_{u^*} = 2 \text{ mm}$). This methodology revealed the ability of the model to predict mass exchange at the SWI for solutes with various physicochemical properties.

The validation procedure minimized the calibration steps. Thus, for transport of non-reactive species (*i.e.* NaCl), the dispersion coefficients were exclusively used as the calibrated parameters as they could not be experimentally determined. Longitudinal and transverse dispersivities were set at $\alpha_L = 0.01 \text{ m}$ and $\alpha_T = \alpha_L/10$ after a manual optimization procedure. The molecular diffusion coefficient for NaCl was set at $D_{NaCl}(25^\circ\text{C}) = 1.612 \cdot 10^{-9} \text{ m}^2.\text{s}^{-1}$ [Harned and Hildreth, 1951]. For FB291, no

experimental value was found in the literature. Thus, it was set to $D_{FB291}(25^{\circ}C) = 5 \cdot 10^{-10} \text{ m}^2.s^{-1}$ as a reference value for similar azo dyes [Santos et al., 2008].

The computational domain was gridded with a triangular mesh with a maximal size of 0.004 m (5606 elements in total). A local mesh refinement defined a transition layer between the overlying water and the porous medium (see Figure III.2). A mesh sensitivity analysis was performed to ensure mesh independency of flow and transport solutions (Text B.S6).

3.4.2 Comparing numerical and experimental results

The fit between the observed and modelled results was tested in all conditions with both tracers. EHF_{NaCL} and IHF_{FB291} experiments are presented here as representative results.

The model satisfactorily reproduced the dynamics of NaCl concentrations after calibration of the dispersion coefficients ($\alpha_L = 0.01 \text{ m}$ and $\alpha_T = 0.001 \text{ m}$). The observed and simulated mass fluxes through the SWI interface (ϕ_O and ϕ_M) generally ranged around the identity line (*i.e.* $\phi_O = \phi_M$, Figure III.3C), with residual differences close to zero ($|\overline{\Delta\phi}| = |\overline{\phi_O - \phi_M}| = 0.10 \text{ mg.h}^{-1}$ and $\sigma_{\Delta\phi} = 0.79 \text{ mg.h}^{-1}$, Figure III.3D).

The sorptive tracer concentrations better fit with the experimental data than the experiments with NaCl. The modelled and simulated mass fluxes fitted well after adjustment with a K_d value of 3.0 mL.g^{-1} , rather than using the experimental 7.7 mL.g^{-1} (Figure III.4A), ($|\overline{\Delta\phi}| = |\overline{\phi_O - \phi_M}| = 0.010 \text{ mg.h}^{-1}$) and $\sigma_{\Delta\phi} = 0.54 \text{ mg.h}^{-1}$) (Figure III.4B and C). While no in-bed measurements were possible with FB291, similar observed and simulated tracer penetration into the sediment bed confirmed the validity of simulations in the case of IHF_{FB291} (Figure III.6A and III.6B).

Some offsets reflected transient experimental conditions. Equilibrium was reached within the sediment bed after hours in the EHF_{NaCL} experiment. However, at the end of the experiments with NaCl, the slight and steady increases of NaCl concentrations in the mixing beaker could be attributed to the unintended release of ions from the sand, although it was thoroughly washed. For instance, this caused the residual differences of simulated and observed mass fluxes to shift from neutral values in the end of the experiment EHF_{NaCL} . In contrast, the spectrophotometric measurements of FB291 were found insensitive to experimental bias. For further tests, fluorescent conservative tracers (*e.g.* fluorescein sodium salt – CAS Number: 518-47-8) also measured

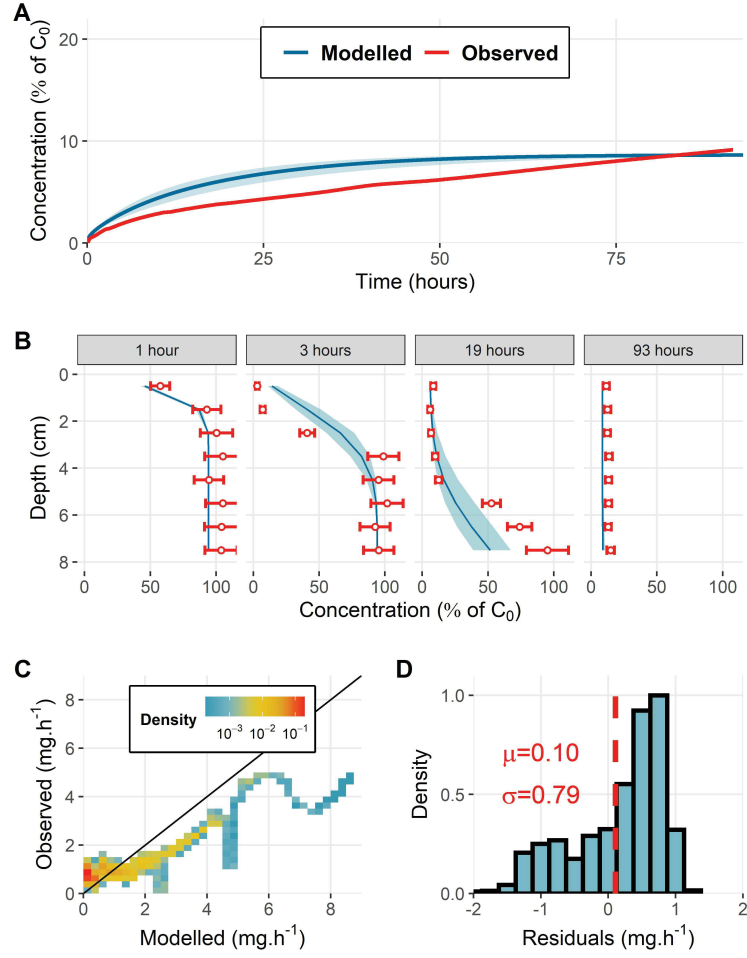


Figure III.3 – Experimental and modelled results for EHF_{NaCl} condition. A) Evolution of normalized tracer concentrations by the initial tracer concentration in the mixing beaker (C/C_0). Analytical uncertainties of NaCl concentration measurements are thinner than the line thickness. B) Observed and modelled tracer vertical distribution in the sediment bed. In A and B, the blue shaded areas correspond to the numerical confidence interval including the experimental uncertainties of K_0 and u^* . C) modelled (ϕ_M) and observed (ϕ_O) mass fluxes at the sediment-water interface (reported in $mg.h^{-1}$ of tracer and calculated at each time step from the evolution of concentrations within the mixing beaker) and D) residuals of the difference $\phi_O - \phi_M$ (μ and σ stand for the mean and the standard deviation of residual distribution).

by a spectrophotometric method may be a valuable alternative to NaCl. The experimental results were also highly sensitive to minor water height instabilities (± 2 mm)

under high flow which resulted in variations of the overlying water velocities. An automatic limitation of water height in the channel may be useful for future experiments. Although these experimental limitations punctually affected observations, they did not question the validity of the procedure as the overall tendencies were well reproduced.

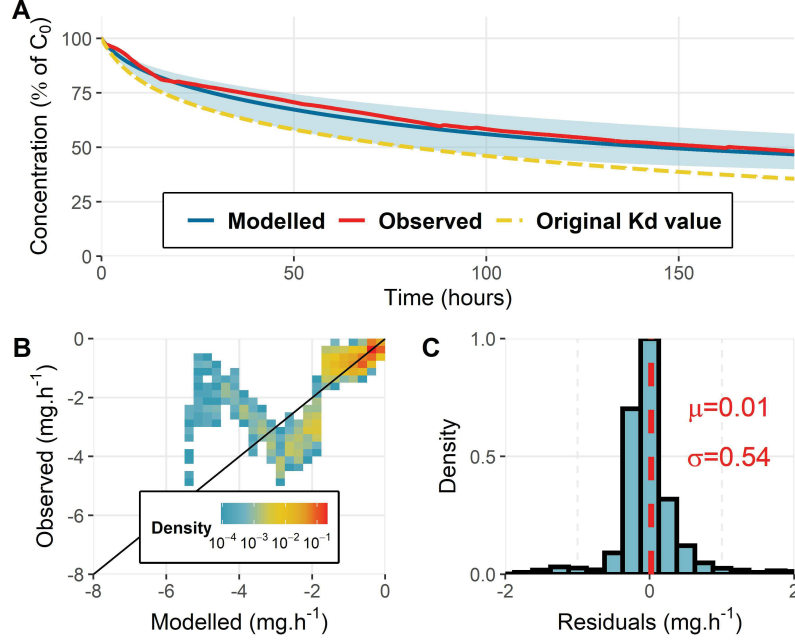


Figure III.4 – Experimental and modelled results for IHF_{FB291} . A) Evolution of normalized tracer concentration dynamic in the mixing beaker. Analytical uncertainties of FB291 concentration measurements are thinner than the line thickness. B) modelled (ϕ_M) and observed (ϕ_O) mass fluxes at the sediment-water interface and C) residuals of the difference $\phi_O - \phi_M$.

3.5 Pollutant transport at the sediment-water interface

3.5.1 Velocity field in the bench-scale river channel and transport processes

Understanding the velocity field is fundamental to interpret mass transport and exchange fluxes at the SWI, although experimental visualization of the velocity field is tedious. Numerical simulations can help revealing velocity variation across the domain, and identify dominant transport processes in the bench-scale river channel.

Distinct velocity patterns in the sediment bed occurred across the domain (Figure III.5B). In the overlying water, the model reproduced the log-law of wall profile with a non-null slip velocity at the interface [Nagaoka and Ohgaki, 1990, Rosti et al., 2015] (Text B.S7). Despite the small size of the experimental setup, the effect of surface tension on the sidewalls of the channel was considered negligible. The velocity profile prediction by the Navier-Stokes equation was assumed appropriate, although velocity was not directly measured [Malverti et al., 2008]. The simulated velocities in the transition layer abruptly dropped by several orders of magnitude and reached a value close to the Darcy velocity (v_{Darcy}) (see Text B.S8 for calculation details).

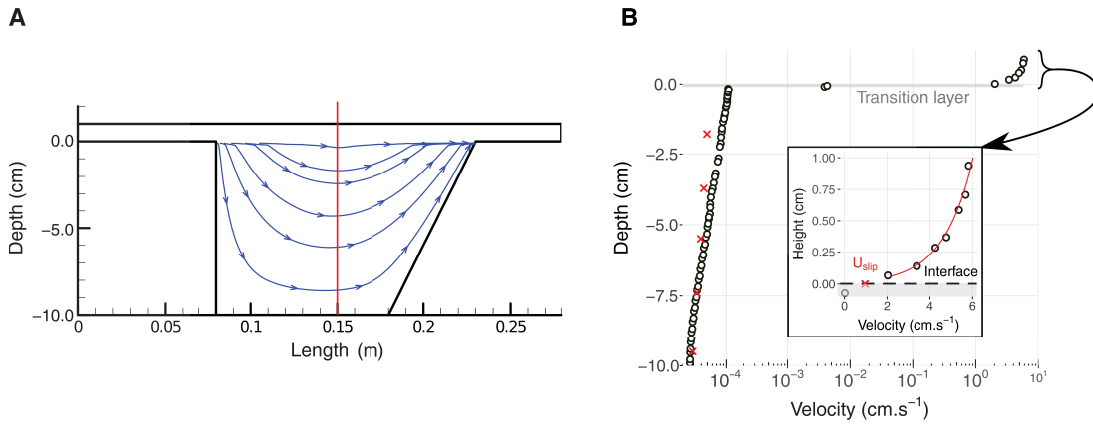


Figure III.5 – A) Streamlines in the domain showing the pumping effect that may be caused by bedforms in rivers. The vertical red line represents the axis where velocities were extracted in panel B. B) Modelled velocity profile (circles) and Darcy's velocities (red crosses). The grey shaded area represents the transition layer defined in the numerical domain. The black box zooms on the overlying water velocity profile and fitting results with the log-law of wall (solid red line).

The simulated velocities penetrated in the sediment bed over the thickness of the transition layer, corresponding to the maximum size of sediment grains, in agreement with previous observations from Goharzadeh et al. (2005) [Goharzadeh et al., 2005]. Hence, the model could reliably predict the velocity penetration depth in the sediment bed, without imposing any interface condition [Bars and Worster, 2006]. This observation is of great importance since the velocity pattern within the sediment bed controls mass exchange at the SWI [Nagaoka and Ohgaki, 1990, Voermans et al., 2017]. Below the transition layer, the hydrostatic pressure gradient at the interface mainly controlled

the water flow. This control indicates a minor effect of viscosity in the sediment bed. Considering the size of the experimental setup (15 *cm* long and 10 *cm* deep) and the control of flow within the sediment bed by pressure distribution alongside the interface, the system closely reproduced pumping flow induced by bed-forms in actual rivers [Cardenas and Wilson, 2007a, Kaufman et al., 2017]. Hence, the experimental setup and the developed model were suited to predict mass exchange driven by hydrodynamic (*e.g.* bed forms, rapid variations of water flow, inhomogeneity of sediment permeability, etc.) and hydrostatic (*e.g.* riverbed topography, meanders, etc.) forces, characterizing small and large scale rivers, respectively.

3.6 Transport processes governing mass exchange in the bench-scale river channel

Similar patterns of NaCl concentrations were observed in the sediment bed and the mixing beaker, regardless of the configurations (*i.e.* $ILF_{NaCL} \sim ELF_{NaCL}$ and $IHF_{NaCL} \sim EHF_{NaCL}$). Under similar flow conditions, the simulated times to reach 80% of equilibrium concentrations between export and incorporation cases were similar (Table III.1). Since the export and incorporation cases represent exact opposite experiments, a riverbed sediment would incorporate or release pollutants at equivalent rates. The proposed approach could then be applied in the future to investigate the transport of pollutants stemming either from the overlying water (*e.g.* diffuse or punctual contaminations) or from the riverbed sediment (*e.g.* groundwater or anterior contamination of the sediment bed), when pollutant sorption is insignificant.

The upper part of the sediment bed was rapidly and strongly affected by a concentration gradient imposed by the overlying water (Figure III.3B). Pollutant transport in the sediment bed decreases with increasing depth, as already reported in Chandler et al. (2016) [Chandler et al., 2016]. Hence, the deeper the pollutant is located in the sediment bed, the less it is expected to interact with the overlying water.

The results also emphasize that mass exchange at the SWI is sensitive to the overlying water velocity. Indeed, higher water flow increases Darcy's velocity and penetration of overlying water velocities into the sediment bed [Habel et al., 2002]. It is also worth noting that the velocity ratios between low and high flows were proportionally reflected on the simulated characteristic times ($t_{80\%}$) which were about 3-fold longer under low flow than high flow (Table III.1). Accordingly, the nature of the dominant transport

process (*i.e.* diffusion, dispersion or advection) governing the overall mass exchange may remain equivalent within the range of tested velocities (*i.e.* 1.4 to 4.7 cm.s^{-1} for NaCl). In addition, the contribution of diffusion to the overall transport may be modest: the rate of mass exchanged with time may remain unaffected by velocity changes as the magnitude of diffusion only depends on concentration gradients.

The nature of the dominant transport process can also be inferred from calculation of the Peclet number (Pe) over the depth as it expresses the ratio of advection over diffusion or dispersion [Chandler et al., 2016, Pinay et al., 2015]. Detailed calculation procedures for Pe and D_{eff} are provided in Text B.S9 and B.S10. The calculation of effective diffusivities (D_{eff}) as used in the diffusive models, also helped to characterize the overall dominant transport process. Indeed, the value of D_{eff} reflects the dominant transport process driving mass exchange at the SWI, being either diffusion ($D_{eff}/D_m \approx 1$) or dispersion and turbulent advection ($D_{eff}/D_m > 1$) [Grant et al., 2012, Voermans et al., 2018].

In our case, Pe from 5 to 100 (except at the very bottom of the sediment bed under low flow condition) confirmed the limited effect of diffusion over advection. In addition, calculation of the effective diffusivities for low and high flow conditions, revealed that diffusion was outranked by a factor of $D_{eff}/D_m = 3.8$ and $D_{eff}/D_m = 15.2$ by dispersion and/or advection in low and high flow, respectively. According to Voermans et al. (2017), these ratios feature dispersion dominated transport regimes [Voermans et al., 2017]. Finally, the proportionality between water flow and $t_{80\%}$ could not be related with the equivalent riverbed travel length ($L_{eq,80\%}(t) = u^* \cdot t_{80\%}$) which displayed rather constant values between low and high flows due to the similar dominant transport process (see Table III.1). The total mass of tracer exchanged per length unit of riverbed was thus independent from the overlying water velocities under these conditions. Thus, in the absence of degradation and/or sorption, the flow-independent exchange capacity of a river transect may be directly inferred from the physical characteristics of the riverbed (geometry and permeability).

3.6.1 Understanding and predicting the effect of sorption on mass exchange at the SWI

The sorption significantly increased the experimental duration. Equilibria were not reached in the experiment with FB291 (Figure III.4A), even after 7 and 4 times longer duration (for EHF_{FB291} and IHF_{FB291} , respectively) than in experiments with NaCl

under similar flow conditions. In the case of incorporation, this duration was attributed to sorption at the front edge of the tracer plume, which retarded its progression [Schaffer and Licha, 2015]. In the case of export, the slower desorption kinetics of FB291 likely delayed its release from the sediment bed [Ren and Packman, 2004b]. Partitioning between the aqueous phase and the sediment grain surfaces also decreased FB291 concentrations in the liquid phase. Although the equilibria were not fully established, it is estimated that up to 58% (EHF_{FB291}) and 42% (IHF_{FB291}) of the initial FB291 mass were sorbed to sediment at the end of the experiments with FB291. Overall, the sorption increased the amount of tracer incorporated into the sediment bed compared with NaCl, which limited the FB291 mobility in the overlying water.

Most importantly, the model predicted less FB291 sorption to the sediment under dynamic conditions than that observed in the batch characterization. In the export case, equilibrium was not reached but the FB291 concentrations emphasized that the amount of tracer released to the water column was larger than that derived from the C_{eq} value using $K_d = 7.7 \text{ mL.g}^{-1}$. In addition, predictions using the experimental K_d value excessively retarded the plume penetration compared to the observed penetration (data not shown). As exemplified by the dashed yellow line in Figure III.4A, the use of the experimental K_d value led to an overestimation of the decrease of FB291 concentration in the overlying water during IHF_{FB291} . At the opposite during EHF_{FB291} it led to a weaker FB291 release into the overlying water than that actually observed. Finally, accurate reproduction of export and incorporation configurations with the same calibrated K_d value suggest a reversible sorption isotherm for FB291 from quartz sand, as previously observed for metal ions [Eylers et al., 1995, Ren and Packman, 2004a]. Altogether, this isotherm validates the mathematical implementation of sorption in the FRT model.

The discrepancy between the calibrated and experimentally derived K_d values may be explained by the validity of the linear isotherm implemented in the model, although the laboratory characterization was unambiguous (see Text B.S3). A second explanation is the adsorption kinetic affecting the progression of the tracer plume [Eylers et al., 1995]. While the pseudo-first order kinetic implemented in the model is well suited for FB291 adsorption, the rate of 12 hours ($\alpha = 8.3 \cdot 10^{-5} \text{ s}^{-1}$), chosen as a maximal value ensuring complete equilibrium, is arguable as FB291 sorption on clay materials has been reported to take place in a few hours [Berez et al., 2016]. However, the interactions with clay material are potentially stronger than with sand surfaces,

favouring rapid sorption [Berez et al., 2014]. In addition, a quicker adsorption rate may further exacerbate the depletion of FB291 concentration in the mixing beaker and further delay FB291 penetration which is inconsistent with the observations (Figure III.6B). Finally, the constant shaking in the batch sorption equilibrium method largely differ from mixing occurring in packed sediment beds, which naturally limits pollutant exposure to sediment grain surfaces. This statement goes along with previous observations of enhanced sorption evidenced in stirred systems where sediment grinding resulted in an increase of available sorption sites while shaken systems did not [Shrestha et al., 2016].

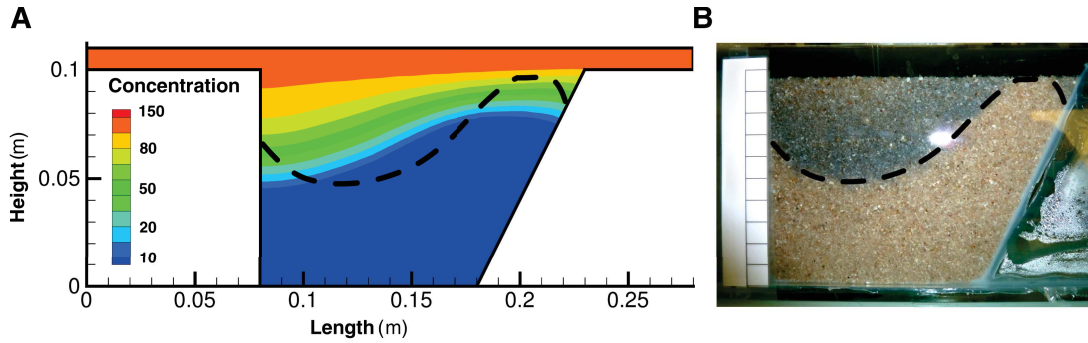


Figure III.6 – Numerical (A) and experimental (B) distribution of FB291 within the sediment bed after 12 hours under IHF_{FB291} conditions. The black dashed line in panel B corresponds to the limit of FB291 penetration observed and is reported in panel A for direct comparison with numerical results.

Altogether, the sorption increased pollutant incorporation, hampered export and decreased pollutant concentrations in pore water compared to conservative tracers. Accordingly, the role of sink of riverbed sediments is exacerbated for sorptive pollutants [Ren and Packman, 2004a]. Meanwhile, the sorption increases pollutant residence time within the riverbed by retarding its release to the overlying water [Eylers et al., 1995]. Sorption also limit pollutant penetration towards the deepest sediment layers [Liao et al., 2013].

3.7 Towards a comprehensive understanding of hyporheic process at the SWI

The experimental setup generally focused on the effect of overlying water dynamics to interpret mass exchange at the SWI and circumvent the relationship between the

river and groundwater. However, at the river scale, surface – ground water interactions also control hyporheic mass exchange as well as the nature and magnitude of biogeochemical processes [Byrne et al., 2014]. The effect of vertical hydraulic fluxes (*i.e.* upwelling or downwelling) on mass exchange at the SWI thus has to be considered when upscaling to reach scale [Lansdown et al., 2015]. While most of the diffusive and multi-domain models do not address vertical fluxes as detailed in the introduction, our model offers the opportunity to investigate the combined effect of overlying water velocity and vertical hydraulic gradient on mass exchange at the SWI.

To illustrate this combined effect, we examined a numerical test over a 1 *m* long (*L*) river reach with polluted overlying water ($C = 1 \text{ mg.L}^{-1}$) connected from below with a pristine groundwater ($C = 0 \text{ mg.L}^{-1}$). We considered 50 *cm* of sediment and 10 *cm* of overlying water which is in accordance with the actual scale of hyporheic processes [Boano et al., 2014]. The range of vertical fluxes tested was chosen to represent low Strahler order rivers ($v_{gw} \in [-0.10; 0.30]$ in m.d^{-1}) [Binley et al., 2013]. The overlying water velocities were chosen to satisfy the laminar flow assumption ($Re \in 500, 1000, 4000$ or $v_w \in 0.05, 0.01, 0.04$ in cm.s^{-1}) [Sparrow et al., 1973]. The effect of sorption strength was also tested to identify the typical behaviour of moderately to strongly hydrophobic pollutants ($K_d \in 0, 2, 7 \text{ mL.g}^{-1}$). The total pollutant mass flux (ϕ) was calculated alongside the 1 *m* long interface as the sum of advective (ϕ_{adv}) and dispersive (ϕ_{disp}) fluxes.

In the absence of vertical velocities (*i.e.* $v_{gw} = 0 \text{ m.d}^{-1}$), regardless the horizontal water flow, mass fluxes through the interface was driven by dispersion ($10^{-2} < \frac{\phi_{adv}}{\phi_{disp}} < 10^{-1}$). Contrarily to the bench-scale river channel, the absence of pressure gradients across the SWI (*e.g.* bedforms, instream obstacles, etc.) hampered the overlying water to penetrate the sediment bed, limiting advection driven transport. The vertical velocities thus strongly controlled mass fluxes through the SWI (see Figure III.7A). As a rule of thumb, suppression of pollutant penetration within the SWI was observed for dimensionless upwelling velocities about one order of magnitude higher than the dimensionless mass flux predicted for $v_{gw} = 0 \text{ m.d}^{-1}$ ($\hat{\phi}_0$). In contrast, for dimensionless downwelling velocities higher than about $\hat{\phi}_0$, the mass fluxes became exclusively driven by advection. In the latter case, pollutant mass flux through the interface can be estimated as the product $\phi = C_w \cdot v_{gw}$. This prediction is in line with previous observations demonstrating the existence of a threshold of $|v_{gw}|$ above which vertical fluxes are the dominant mechanism of water exchanges at the interface [Fox et al.,

2014].

The effect of sorption on pollutant penetration was remarkable even with K_d as low as 2 mL.g^{-1} (Figure III.7B). For instance, after 16 days of simulation with a downwelling flux $v_{gw} = 0.01 \text{ m.d}^{-1}$, while the non-sorptive pollutant reached the bottom of the numerical domain, sorptive pollutants with $K_d = 2.0$ and 7.0 mL.g^{-1} only penetrated the first 20 and 10 cm of sediment (see Figure III.7B). Accordingly, the propensity of a pollutant to sorb onto the sediment bed is an important feature to account for in actual riverine systems as it may significantly reduce the river contribution to groundwater pollution. It also highlights the fact that in riverbed, pollutant likely accumulates within the first cm of the sediment.

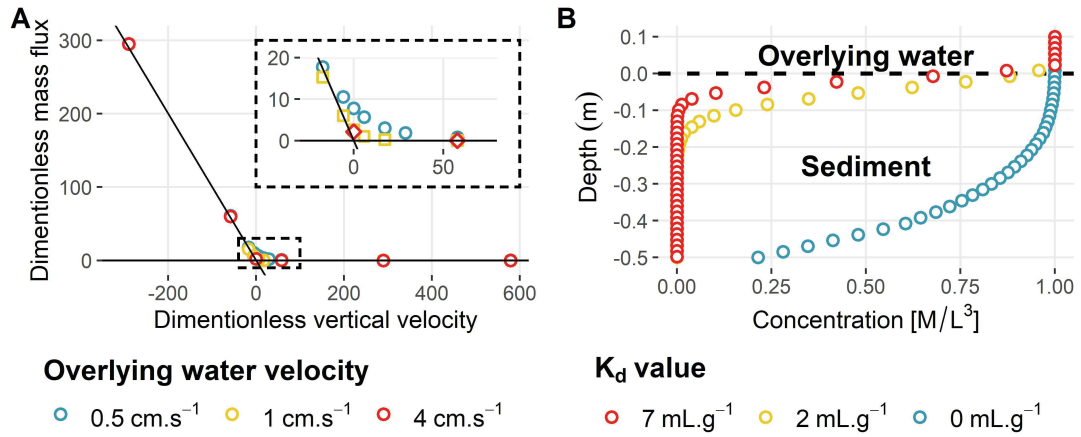


Figure III.7 – A) Modelled dimensionless mass flux ($\hat{\phi} = \frac{\phi}{L \cdot D_m \cdot C}$; y-axis) crossing the SWI under various upwelling (negative velocity) and downwelling (positive velocity) conditions ($\hat{v}_{gw} = \frac{v_{gw} \cdot L}{D_m}$; x-axis) and overlying water velocity (colours and legend). B) Modelled pollutant penetration within the sediment bed with $v_{gw} = 0.01 \text{ m.d}^{-1}$ and $v_w = 0.04 \text{ m.s}^{-1}$ and varying sorption strengths from sorptive (red) to non-sorptive (blue) pollutant (K_d in mL.g^{-1}).

Altogether, these observations confirm 1) the ability of the model to handle surface – groundwater interactions at the river scale (*i.e.* CPU time \approx 10 minutes for a 16 daylong simulated period), 2) the major control of vertical velocities on pollutant mass exchange at the SWI, and 3) the crucial role of sorption on pollutant penetration pace within the sediment bed.

3.8 Implication and perspectives for conservative and sorptive pollutant transport at the SWI

The variability of pollutant fluxes at the SWI is multifactorial and is still poorly addressed at large scale. In this context, experimental and numerical developments are required to improve the interpretation of pollutant fate at the river scale [Lewandowski et al., 2019]. This work showcased an experimental and model development for generic evaluation of pollutant transport at the SWI.

The experimental setup proved relevant to reproduce the transport of conservative and sorptive pollutants over riverbeds with bedforms. Thanks to advanced numerical techniques, the developed model brought advanced understanding of pollutant transport within the experimental setup. The experimental results fitted those of numerical simulations with a restrained calibration procedure (*i.e.* only the dispersion coefficients). The pollutant mass exchange at the SWI was positively correlated with the water flow regardless the origin of the pollutant (*i.e.* either from the overlying water or the sediment bed). Sorption of FB291 tracer retarded pollutant export downstream and strengthened the role of sink played by the sediment bed. The coupled procedure also brought up the idea that classical batch sorption experiments may not be suited to characterize sorption to riverbed sediment in dynamic conditions. Finally, to come up with a reliable methodology to investigate pollutant fate in actual riverine systems, we coupled river with upwelling/downwelling velocities over a 1 m long river reach. It highlighted the crucial role of bedforms and vertical velocities in driving mass exchange at the SWI. It also revealed the limited pollutant penetration in the sediment bed due to sorption.

Overall, these results may help in the future to improve interpretation of pollutant fate in riverine systems accounting for complex water fluxes originating from their surrounding environment (*e.g.* surface-groundwater fluxes). Further developments with this code are nonetheless needed to resolve pollutant transport in large rivers featuring turbulent flow. Indeed, while the laminar flow assumption holds for rivers with small currents, artificial ponds or lakes, vertical velocities generated by eddies may favour pollutant penetration within the SWI, even over flatbeds [Grant and Marusic, 2011] in rivers undergoing turbulent flow. In such a case, our model would underestimate the mass exchange rates [Cardenas and Wilson, 2007b]. The implementation of a turbulent closure scheme to the momentum equation would help to represent a large panel

of environmentally relevant riverine conditions. Overall, transient storage during flood events, the effect of varying sediment bed geometries or large-scale features such as dams or meanders on mass exchange rates, the relationship between organic matter cycling (*i.e.* sediment diagenesis) and pollutant degradation are examples of future researches that may benefit from these experimental and numerical developments.

3.9 Investigation of the influence of water flow on pollutant degradation

The coupled experimental bench-scale river channel and the FRT model developments helped to understand pollutant transport and phase partitioning at the SWI. The influence of water flow on pollutant degradation at the SWI can thus be more confidently addressed. Pollutant degradation at the SWI is often reported to occur within the oxic layer of the sediment bed [Kaufman et al., 2017]. As demonstrated with NaCl, water flow controls mass exchange rates at the SWI. Thus, the thickness of the oxic layer is expected to vary with water flow (*i.e.* enhanced oxygen incorporation during high flow than low flow). Consequently, as pollutant biodegradation is favoured under oxic conditions, one can hypothesize that pollutant degradation at the SWI is also controlled by water flow. While biodegradation, sorption and transport processes were separately investigated up to now, the objective of this study is to establish a proof of concept for the ability of the proposed coupled experimental and modelling procedure to assess pollutant degradation at the SWI. To that end, tracer experiments were conducted using caffeine as an anthropogenic model compound with properties similar to some of currently used pesticides (moderate hydrophobicity, $\log(K_{ow}) \approx 2$). Similarly to pesticides, caffeine is occurring worldwide in surface waters at $\sim \mu g.L^{-1}$ concentrations. While S-metolachlor revealed long biodegradation rates values in microcosms experiments (> 30 days), caffeine degrades quicker (≈ 1.5 day) which facilitates methodological developments with the bench-scale river channel [Korekar et al., 2020]. The FRT model was adapted to predict pollutant degradation and degradation-induced isotope fractionation.

As demonstrated with NaCl, water flow controls mass exchange rates at the SWI. Thus, the thickness of the oxic layer is expected to vary with water flow (*i.e.* enhanced oxygen incorporation during high flow than low flow), so would pollutant degradation rates. While oxic biodegradation as well as sorption and transport processes were separately investigated up to now, the objective of this section is to examine how the proposed coupled experimental and modelling procedure can support the investigation of pollutant degradation at the SWI. To that end, tracer experiments were conducted with caffeine as an anthropogenic model compound with chemical properties close to currently used pesticides ($\log(K_{ow}) < 1$, not volatile and $\log(K_{ow}) \approx 2$). The model was adapted to reproduce pollutant degradation and degradation-induced isotope fractionation.

3.9.1 Material and Methods

The same bench-scale river channel than for NaCl and FB291 was used with only minor adjustments presented below.

Adjustments to the bench-scale river channel

Sediment and water - The same pure quartz sand than previously used was mixed at a 95:5 ratio (w:w) with the Avenheimerbach riverbed sediment (France, 48°40'08"N, 7°33'50"E). The sediment was collected from the top 10 *cm* of the Avenheimerbach river, wet-sieved at 2 *mm* and stored wet at 4°C prior to the experiment. Effect of storage on soil microbial activity and community pattern was assumed to be negligible at this temperature [Lee et al., 2007]. The blend enabled microbial activity representative of real riverine systems in the sediment bed. Only 5% of sediment was blend with quartz sand to ensure sufficient water conductivity and allow the oxygen gradient to develop at least over the first centimetres of sediment. The final composition of the blend was characterized by NF/ISO method and is as follow: Clay 0.73% silt 3.1%, sand 96.2% and organic carbon (foc) 0.095%, with a constant porosity between experiment ($\Theta = 0.16 \pm 0.02$) and saturated conductivity $K_0 = 4.4 \pm 2.2 \cdot 10^{-4} m.s^{-1}$. Synthetic water was used to ensure stable and reproducible conditions over the experiments. Hydrochemistry between experiments were in average ($n = 4$; \pm standard deviation) in $mg.L^{-1}$: $Na^+ = 8.2 \pm 0.9$, $K^+ = 0.05 \pm 0.01$, $Mg^{2+} = 2.7 \pm 0.3$, $Ca^{2+} = 10 \pm 2$, $Cl^- = 9.7 \pm 0.5$, $NO_3^- = 21 \pm 1.5$, $SO_4^{2-} = 10.7 \pm 0.6$, $DOC = 0.8 \pm 0.3$ and $DIC = 4.5 \pm 0.1$.

Total suspended solid, hydrochemistry and dissolved oxygen quantification

- Nephelometric turbidity units (NTU) was recorded periodically with a turbidity meter (HI 88713, HANNA) and used as a proxy for the total suspended solid (TSS) present in the system. Prior the experiment a linear relationship between NTU and TSS was determined for our sediment. Hydrochemistry of the system was measured before each experiment, once in the middle of the experiment and at the end as follow: Cation-anion contents were measured from a sub-sample filtered at 0.45 μm with a cellulose-acetate filter by ionic chromatography (ICS-5000, Dionex/Thermo Fischer, US EPA 300.0). Dissolved organic/inorganic carbon (DOC/DIC) were analyzed by TOC analyzer (TOC-V-CPH Shimadzu, NF EN 1484). Dissolved oxygen concentrations in the sediment bed were continuously mapped alongside two vertical positions using 10 *mm* wide oxygen sensitive foils as depicted in Figure III.8 (SF-RPSU4, Vi-

siSens TD, PreSens®).

Hydraulic properties - The water height was adjusted to 2 *cm* instead of 1 *cm* because of tube clogging supposedly due to sediment transport. This resulted in higher water flow than with NaCl and FB291 but water velocities and Reynolds numbers remained consistent (Table III.2). The upside of the greater water height is that experimental results were less impacted by uncontrolled water height variations. 6 *L* of caffeine solution ($C_8H_{10}N_4O_2$, A.C.S.-grade reagents, $\geq 99\%$, Sigma–Aldrich) was used in total for each experiment, allowing successive sampling during the experiments.

Caffeine extraction, quantification and CSIA - Water samples were collected in the overlying water with a syringe at specific times for caffeine quantification and stable isotope composition analysis. Sampling volumes were adjusted over time to account for degradation. Water samples were frozen at $-20^\circ C$ up to 3 days prior extraction by SPE ($\eta = 110 \pm 10\%$). Caffeine was quantified by gas chromatography-mass spectrometry with an environmental quantification limit (QL) determined at 1 $\mu g.L^{-1}$ for the average experimental conditions (sampling volume of 30 *mL*). The analytical QL was determined on the signal over noise ratio (1:5) and normalized by the sampling volume leading to the environmental QL. Carbon isotope composition analysis were conducted by gas chromatography-isotope ratio mass spectrometry (GC-IRMS) within the $\delta^{13}C$ linearity range established elsewhere [Jochmann et al., 2006] between 8 and 300 *ng* for C (150 – 4500 *mV*). SPE did not induced significant isotope fractionation $\Delta\delta^{13}C = 0.22\text{‰}$. Pure caffeine isotopic signature was evaluated by the GC-IRMS directly to be $-30.3 \pm 0.2\text{‰}$ ($n = 3$). All analytical procedures and calculations provided above followed the methodologies reported in Section 2.1.

Experimental conditions

Three different water flows consistent with the previous tracer experiments with NaCl and FB291 were tested (see Table III.2). As an anthropogenic marker of human activity, caffeine occurs in rivers through waste-water discharges [Lim et al., 2017]. Accordingly, incorporation experiments with caffeine originating from the overlying water were conducted. Experiments were conducted under limited light exposition (UV filters and aluminium foils on every window of the experimental room) to avoid photolysis although caffeine direct photolysis is slow ($DT_{50} \approx 170$ *h*) and do not exhibit indirect photodegradation [Jacobs et al., 2012]. Before each experiment the channel was filled with a new amount of sediment (1.3 ± 0.1 *kg*) and synthetic water (same composition

than in the microcosm experiments). 24 hours of equilibrium time with water recirculating was left to the system before 6mL of caffeine stock solution in aqueous solution (10 g.L^{-1}) was added to the surface water near the sediment bed to obtain an initial concentration of $C_0 = 20 \text{ mg.L}^{-1}$ in the system.

Table III.2 – Hydraulic conditions tested and associated average hydrochemical conditions.

	Low flow	Medium flow	High flow
Water height (mm)	20 ± 2	20 ± 2	20 ± 2
Water velocity (cm.s^{-1})	1.1 ± 0.1	3.2 ± 0.1	4.8 ± 0.1
Reynold number	124 ± 25	352 ± 69	533 ± 93
pH	7.7 ± 0.2	7.5 ± 0.3	8.1 ± 0.3
Temperature ($^{\circ}\text{C}$)	20.2 ± 0.9	19.1 ± 0.4	20.7 ± 0.2
TSS (mg.L^{-1})	< 4.4	< 4.4	< 4.4

Adjustments to the FRT model

C isotope fractionation modelling – Normal kinetic isotope effect usually observed over contaminant degradation reflects the slightly faster degradation rates of molecules containing the most light isotopes (*i.e.* ^{12}C) as compared with the ones featuring the most abundant fraction of heavy isotopes (*i.e.* ^{13}C). The kinetic isotope fractionation factor (α_C) retrieved from laboratory degradation experiments expresses these kinetic differences. It relates the rates of disappearance of heavy to light molecules, namely isotopologues, according to Eq. III.7 [Hunkeler et al., 2008].

$$\begin{aligned}\alpha_C &= 1 + \frac{\epsilon_C}{1000} \\ &= \frac{r^{13\text{C}}}{r^{12\text{C}}}\end{aligned}\tag{III.7}$$

Thus, numerical modelling of isotope fractionation is enabled through separate computation of both isotopologues undergoing distinct degradation rates (*i.e.* $k^{12\text{C}}$ or $k^{13\text{C}}$ in d^{-1}) as in Eq. III.8 [Van Breukelen et al., 2005, Alvarez-Zaldívar et al., 2018].

$$k^{13C} = (1 + \epsilon_C) \cdot k^{12C} \quad (\text{III.8})$$

The total concentration of caffeine can be described as the sum of heavy and light isotopologues ($C_{tot} = {}^{12}C + {}^{13}C$). k^{12C} is assumed equal to the experimentally determined degradation rates as the natural abundance of ${}^{12}C$ over ${}^{13}C$ is about 99:1.

Oxygen consumption within the sediment – Oxygen consumption rate in the sediment (k_{O_2}) was determined 8 cm below the interface right after that the system was filled with fully oxygenated sediment. Oxygen consumption in the sediment bed was attributed to processing of organic matter and nutrients (*e.g.* ammonium, nitrates, etc.) contained in the Avenheimerbach sediment and the synthetic water [Akbarzadeh et al., 2018]. Oxygen consumption within the sediment was modelled by a single first-order reaction term $\left(\frac{d[O_2]}{dt} = k_{O_2} \cdot [O_2]\right)$ [Kaufman et al., 2017].

Oxygen controlled degradation – The preferential degradation of caffeine under oxic conditions is implemented via a hyperbolic formulation (Monod or Michaelis-Menten type), with a half-saturation constant for oxygen, K_M [$M.L^{-3}$] according to Eq. III.9. Since K_M was not available for caffeine oxic degradation $K_M = 1.0 \mu mol.L^{-1}$ was used as a default value often used in sediment diagenesis models for nitrification [Soetaert et al., 1996]. Considering the results presented below, simulations were not sensitive to this value. In this case, a simple first-order caffeine degradation without oxygen dependency would have led equivalent results [Vanderborght et al., 1977].

$$k_{oxic} = k_{max,oxic} \cdot \frac{[O_2]}{[O_2] + K_M} \quad (\text{III.9})$$

where $k_{max,oxic}$ [T^{-1}] refers to the experimentally determined oxic degradation rate (*i.e.* at 100% oxygen saturation), $[O_2]$ [$M.L^{-3}$] to the dissolved oxygen concentration. A first-order reaction term was used $\left(\frac{d[Caf]}{dt} = k_{oxic} \cdot [Caf]\right)$.

Model parameterization: Flow and transport parameters - Caffeine sorption coefficient (K_d) and oxic biodegradation rates were determined according to the procedures presented in section II. Two sediment:water ratios were tested (1:6 and 0.2:6, leading to TSS concentrations of 186 ± 13 and $4.53 \pm 0.06 g.l^{-1}$ respectively) for the batch oxic biodegradation experiment. The highest ratio was intended to reproduce oxic biodegradation in the sediment bed and the lowest, oxic biodegradation in the

overlying water. Caffeine biodegradation under anoxic condition was assumed null considering that caffeine catabolism in micro-organism is an oxidative pathway [Mazzafera, 2004]. Hydrolysis of caffeine was characterized negligible $< 5\%$ after 7 days. All parameters are summarized in Table A.S7.

Table III.3 – Hydraulic and reactive parameters for simulation of caffeine degradation in the bench-scale river channel.

Hydraulic Parameters - Flow and Transport	
K_0 ($m.s^{-1}$)	$(4.4 \pm 2.2) \cdot 10^{-4}$
Θ	0.16 ± 0.02
ρ_{bulk} ($g.cm^{-3}$)	2.29 ± 0.05
Caffeine diffusion coefficient ($m^2.s^{-1}$) [Price, 1989]	$3 \cdot 10^{-10}$
Reactive Parameters - Caffeine and Oxygen	
K_d ($L.kg^{-1}$)	1.21 ± 0.08
$k_{max,oxic}$ (h^{-1})	25.9 ± 2.4 (1:6) & 10.3 ± 1.4 (0.2:6)
ϵ_C ($\%$)	-0.59 ± 0.10 (1:6) & -0.69 ± 0.07 (0.2:6)
k_{O_2} (h^{-1})	1.3 ± 0.8
K_M ($\mu mol.L^{-1}$)	1

3.9.2 Results and discussion

Influence of water flow on the depth of the oxic sediment layer

Simulated oxygen gradients fitted well with the depth profile experimentally observed under low and high flow conditions (Figure III.8). This confirms the ability of the FRT model to reproduce the complex interplay between pollutant transport and degradation at the SWI. As hypothesized, the oxygen reached deeper sediment layers with increasing water flow. Under low flow condition, the oxic layer extended up to 1 *cm* below the sediment sediment-water interface (Figure III.8A). Under high flow condition, oxygen extended up to 2 to 3 *cm* below the sediment surface (Figure III.8A). Medium flow condition displayed an intermediate oxygen penetration. Interestingly, under high flow conditions, the shape of the oxic layer was not parallel to the sediment surface. Instead, oxygen penetration was enhanced at the entrance of the sediment bed. This is attributed to the flow regime characteristics in the bench-scale river channel, typical

of rivers with bedforms (*i.e.* pumping flow). While bedforms generally strengthen mass exchange at the SWI as demonstrated in section II, they can also locally favour deeper oxic sediment layers [Kaufman et al., 2017]. This effect may enhance pollutant degradation in rivers featuring instream structures by creating successive and multiple zones of increased oxygen penetration [Peter et al., 2019].

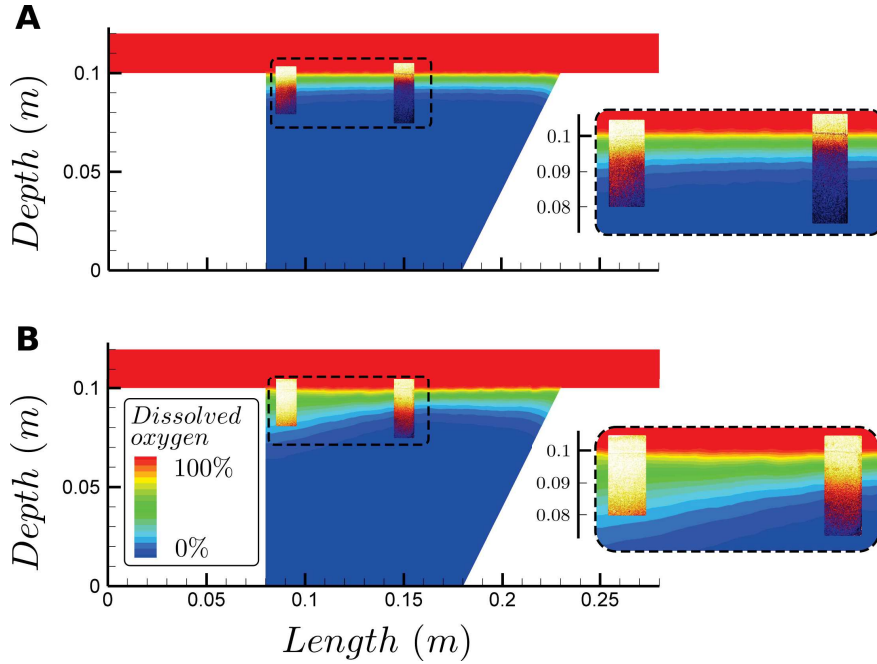


Figure III.8 – Observed (O_2 patches) and simulated (whole domain mapping) oxygen gradients in the sediment bed under low (A) and high (B) flow. For patches the color scale is yellow for $DO = 100\%$ and blue for $DO = 0\%$. For numerical simulations the color scale is presented on panel B. Color scales are voluntarily set different to help distinguishing between both observed and modelled data.

Influence of water flow on caffeine degradation at the SWI

Overlying water hydrochemistry remained constant under all flow conditions, suggesting a fairly stable system and minor changes in redox conditions within the sediment bed. It was also confirmed with oxygen penetration within the sediment bed, which only slightly fluctuated during the experiments. Equilibrium TSS concentrations were systematically below the detection limit $< 4.4 mg.L^{-1}$ in the overlying water.

Very similar caffeine degradation patterns were observed under all flow conditions

tested (Figure III.9). Observed time series could be decomposed in two main phases as depicted by the shaded areas and the associated segments in Figure III.9. During the first 1 to 2 days (phase 1) of each experiment, caffeine concentrations decreased slowly while carbon isotope composition remained fairly stable ($\approx C_0 = 20 \text{ mg.L}^{-1}$, and isotopic signature -30.3‰). Then, caffeine concentrations plummeted to 0 mg.L^{-1} and C isotope compositions increased from -30.3‰ to $-25.8 \pm 1.1\text{‰}$ in 1 to 2 days (phase 2).

A detailed analysis of caffeine degradation within the bench-scale river channel was complicated by the low temporal sampling resolution used during these experiments (about 1 day on average). Indeed, the rapid decrease of caffeine concentrations in phases 2 were only captured by one sampling point. Also, the FRT model, as currently implemented, could not reproduce the two successive phases of the experimentally observed caffeine dissipation with a single set of parameters. Nonetheless, using different model parameterizations for phase 1 (transport only, no degradation) and phase 2 (transport and degradation), the FRT model allowed to reproduce observed caffeine degradation and isotope composition time-series. As the two different set of parameters for in phases 1 and 2 reflected different underlying transport and degradation mechanisms, this analysis helped understanding and identifying factors controlling caffeine dissipation at the SWI.

Phase 1 highlighted the possible existence of a lag-phase of microbial activity at the beginning of the experiments. The slow concentration decrease observed during phase 1 emphasises caffeine penetration within the sediment and sorption without degradation. Indeed, it fitted with numerical simulations considering that caffeine did not undergo degradation during phase 1 (represented in the box "phase 1" of Figure III.9 with black dashed lines). Exception is made for the high flow condition where a manipulation error was thought responsible for the concentration peak occurring 1 day after the beginning of the experiment. The absence of significant isotopic fractionation further hints toward negligible degradation during phase 1. One explanation is that microorganisms in contact with new pollutants (caffeine was not quantified in the Avenheimerbach sediment and no waste-water discharge exists upstream the sampling points) do not immediately adapt and take time to acquire the ability to thrive on the new pollutant [Bertrand, 2019].

Consequently, as previously reported for atrazine degradation in soil columns, transient

pollution (< 1 day) punctually occurring would be likely not or slightly biodegraded in the river sediment [Cheyns et al., 2010]. The same work also suggests that pollutant fate modelling under transient conditions should use a Monod kinetic accounting for target microbial population growth/decay rather than a first-order pollutant biodegradation kinetics.

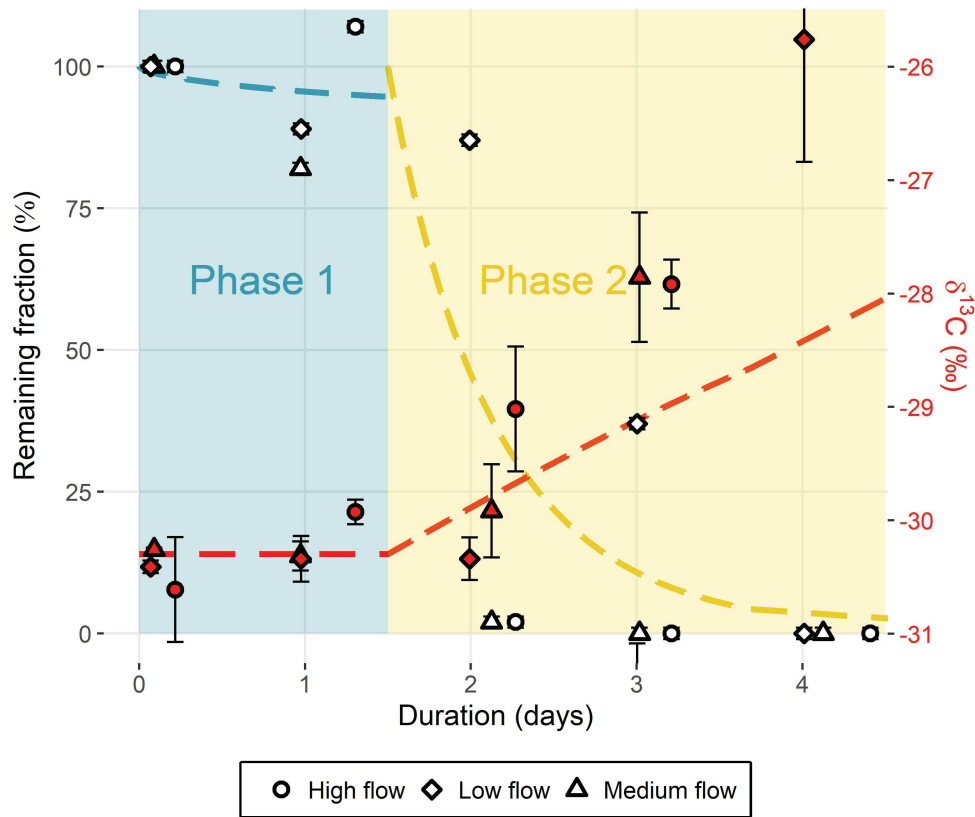


Figure III.9 – Observed (points) and simulated (dashed lines) caffeine concentrations and $\delta^{13}C$ for all flow conditions tested. Simulation results are provided for the medium flow condition and did not significantly change among tested conditions.

In contrast, the rapid decrease of caffeine concentrations during phase 2 emphasized that biodegradation predominated in the overlying water rather than in the oxic layer of the sediment as originally hypothesized.

According to simulation results, a complete degradation of caffeine of 1 to 2 days in the overlying water, irrespective of the flow conditions, can only be explained assuming

biodegradation in the overlying water (see the dashed line featured in the box "phase 2" of Figure III.9). Indeed, the shallow sediment oxic layer did not allow sufficient contact of caffeine with the reactive zone to explain a complete degradation in 1 to 2 days (15% predicted after 2 days when considering biodegradation to occur in the oxic part of sediment only). Furthermore, the best fit with experimental results was obtained with a degradation rate in the overlying water corresponding to the one derived from the batch experiment with the smallest sediment:water ratio. This is in agreement with the fact that the sediment:water ratio was the closest to the TSS concentrations measured during experiments within the bench-scale river channel. Caffeine degradation in phase 2 was also confirmed by the observed and simulated change of carbon isotopic signatures of caffeine, reflecting a degradation extent $> 97 \pm 1\%$ ($\epsilon_C = -0.69 \pm 0.07\text{‰}$) at the end of each experiment, as also reproduced by the FRT model. Biodegradation of caffeine may either be supported by the formation of a bacterial biofilm at the sediment surface or directly by biodegradation in the overlying water. On the one hand, biofilms developing at the SWI amplify biodegradation by retaining and concentrating highly diluted pollutant from the overlying water [Battin et al., 2016]. While biofilms may also develop around suspended particles, the low TSS concentrations measured in any flow conditions presumably not enabled that to occur. On the other hand, intra- (free bacteria) or extra-cellular enzyme activity may also directly promote biodegradation in the overlying water [Baltar, 2018]. In such conditions, extra-cellular activity seems to be preferred over intra-cellular as previously demonstrated by biodegradation tests of six antibiotics (amoxicillin, ampicillin, clindamycin, daptomycin, linezolid, and vancomycin) in waste water samples [Zumstein and Helbling, 2019].

Altogether, these observations undermine the initial assumption stating that increased water flow leads to increased oxic sediment layer and consequently enhanced caffeine degradation. It also highlights the need to numerically account for free-enzyme transport within the overlying water and for further investigations of the relationships between free-enzyme, TSS concentrations and pollutant degradation rates.

3.10 Implications and perspectives for pollutant degradation at the SWI

This preliminary analysis of experimental and numerical results emphasised no significant differences of degradation patterns under low and high flow conditions. In addition, caffeine degradation predominantly occurred in the overlying water, which

was first unexpected according to the literature [Jaeger et al., 2019]. Thus, the bench-scale river channel coupled with the FRT model proved suited to identify compartments of preferential degradation at the SWI. This observation also advocates for further experimental characterizations of microbial diversity, distribution and activity within the overlying water to understand factors controlling pollutant degradation at the SWI. Altogether, this suggests that caffeine degradation in rivers may be flow-independent.

The FRT model proved suited to reproduce the oxic gradient at the SWI. As oxygen is a major control of organic matter cycling at the SWI for instance [Akbarzadeh et al., 2018], this model may be further used in different contexts of research such as sediment diagenesis [Paraska et al., 2014]. Through discrete analysis of specific simulations (phase 1 - sorption and transport only, phase 2 - sorption, transport and degradation in the overlying water) the FRT model revealed main processes controlling caffeine degradation within the bench-scale river channel. However, the FRT model was not suited to reproduce in a raw the complete experiments. Caffeine degradation predominantly occurred after phase 1 (*i.e.* lag-phase) which could not be reproduced in the FRT model where degradation is implemented with a fixed rate. Providing the implementation of a bacterial population growth/decay module in the FRT model, it gives good confidence in the ability of the FRT model to reproduce pollutant degradation at the SWI.

Bibliography

- [Akbarzadeh et al., 2018] Akbarzadeh, Z., Laverman, A. M., Rezanezhad, F., Raimonet, M., Viollier, E., Shafei, B., and Van Cappellen, P. (2018). Benthic nitrite exchanges in the Seine River (France): An early diagenetic modeling analysis. *Science of The Total Environment*, 628-629:580–593.
- [Allen, 1965] Allen, J. (1965). Laminar and turbulent flow in open channels. *Nature*, 208(5016):1196–1197.
- [Alvarez-Zaldívar et al., 2018] Alvarez-Zaldívar, P., Payraudeau, S., Meite, F., Masbou, J., and Imfeld, G. (2018). Pesticide degradation and export losses at the catchment scale: Insights from compound-specific isotope analysis (CSIA). *Water Research*, 139:198–207.
- [Angot et al., 2017] Angot, P., Goyeau, B., and Ochoa-Tapia, J. A. (2017). Asymptotic modeling of transport phenomena at the interface between a fluid and a porous layer: Jump conditions. *Physical Review E*, 95(6).
- [Baltar, 2018] Baltar, F. (2018). Watch out for the “living dead”: cell-free enzymes and their fate. *Frontiers in Microbiology*, 8:2438.
- [Bars and Worster, 2006] Bars, M. L. and Worster, M. G. (2006). Interfacial conditions between a pure fluid and a porous medium: implications for binary alloy solidification. *Journal of Fluid Mechanics*, 550:149–173.
- [Battin et al., 2016] Battin, T. J., Besemer, K., Bengtsson, M. M., Romani, A. M., and Packmann, A. I. (2016). The ecology and biogeochemistry of stream biofilms. *Nature Reviews. Microbiology*, 14(4):251–263.
- [Berez et al., 2014] Berez, A., Ayari, F., Abidi, N., Schäfer, G., Trabelsi-Ayadi, M., and Ferrage, E. (2014). Adsorption-desorption processes of azo dye on natural bentonite: batch experiments and modelling. *Clay Minerals*, 49(5):747–763.

- [Berez et al., 2016] Berez, A., Schäfer, G., Ayari, F., and Trabelsi-Ayadi, M. (2016). Adsorptive removal of azo dyes from aqueous solutions by natural bentonite under static and dynamic flow conditions. *International Journal of Environmental Science and Technology*, 13(7):1625–1640.
- [Bertrand, 2019] Bertrand, R. L. (2019). Lag Phase Is a Dynamic, Organized, Adaptive, and Evolvable Period That Prepares Bacteria for Cell Division. *Journal of Bacteriology*, 201(7).
- [Binley et al., 2013] Binley, A., Ullah, S., Heathwaite, A. L., Heppell, C., Byrne, P., Lansdown, K., Trimmer, M., and Zhang, H. (2013). Revealing the spatial variability of water fluxes at the groundwater-surface water interface. *Water Resources Research*, 49(7):3978–3992.
- [Boano et al., 2014] Boano, F., Harvey, J. W., Marion, A., Packman, A. I., Revelli, R., Ridolfi, L., and Wörman, A. (2014). Hyporheic flow and transport processes: Mechanisms, models, and biogeochemical implications. *Reviews of Geophysics*, 52(4):603–679.
- [Briggs et al., 2014] Briggs, M. A., Lautz, L. K., and Hare, D. K. (2014). Residence time control on hot moments of net nitrate production and uptake in the hyporheic zone. *Hydrological Processes*, 28(11):3741–3751.
- [Burman and Hansbo, 2005] Burman, E. and Hansbo, P. (2005). Stabilized Crouzeix-Raviart element for the Darcy-Stokes problem. *Numerical Methods for Partial Differential Equations*, 21(5):986–997.
- [Byrne et al., 2014] Byrne, P., Binley, A., Heathwaite, A. L., Ullah, S., Heppell, C. M., Lansdown, K., Zhang, H., Trimmer, M., and Keenan, P. (2014). Control of river stage on the reactive chemistry of the hyporheic zone. *Hydrological Processes*, 28(17):4766–4779.
- [Cardenas and Wilson, 2007a] Cardenas, M. B. and Wilson, J. L. (2007a). Dunes, turbulent eddies, and interfacial exchange with permeable sediments. *Water Resources Research*, 43(8).
- [Cardenas and Wilson, 2007b] Cardenas, M. B. and Wilson, J. L. (2007b). Hydrodynamics of coupled flow above and below a sediment–water interface with triangular bedforms. *Advances in Water Resources*, 30(3):301–313.

- [Carman, 1997] Carman, P. C. (1997). Fluid flow through granular beds. *Chemical Engineering Research and Design*, 75:S32–S48.
- [Chandler et al., 2016] Chandler, I. D., Guymer, I., Pearson, J. M., and Egmond, R. v. (2016). Vertical variation of mixing within porous sediment beds below turbulent flows. *Water Resources Research*, 52(5):3493–3509.
- [Cheyns et al., 2010] Cheyns, K., Mertens, J., Diels, J., Smolders, E., and Springael, D. (2010). Monod kinetics rather than a first-order degradation model explains atrazine fate in soil mini-columns: Implications for pesticide fate modelling. *Environmental Pollution*, 158(5):1405–1411.
- [Downing, 2012] Downing, J. (2012). Global abundance and size distribution of streams and rivers. *Inland Waters*, 2(4):229–236.
- [Dwivedi et al., 2018] Dwivedi, D., Steefel, C. I., Arora, B., Newcomer, M., Moulton, J. D., Dafflon, B., Faybishenko, B., Fox, P., Nico, P., Spycher, N., Carroll, R., and Williams, K. H. (2018). Geochemical exports to river from the intramander hyporheic zone under transient hydrologic conditions: east river mountainous watershed, Colorado. *Water Resources Research*, 54(10):8456–8477.
- [Ehrhardt, 2012] Ehrhardt, M. (2012). *Progress in Computational Physics (PiCP) VOL:2 "Coupled Fluid Flow in Energy, Biology and Environmental Research"*. Bentham Science Publishers.
- [Eylers et al., 1995] Eylers, H., Brooks, N. H., and Morgan, J. J. (1995). Transport of adsorbing metals from stream water to a stationary sand-bed in a laboratory flume. *Marine and Freshwater Research*, 46(1):209–214.
- [Fahs et al., 2008] Fahs, M., Carrayrou, J., Younes, A., and Ackerer, P. (2008). On the efficiency of the direct substitution approach for reactive transport problems in porous media. *Water, Air, and Soil Pollution*, 193(1):299–308.
- [Fahs and Younes, 2014] Fahs, M. and Younes, A. (2014). A high-accurate fourier-galerkin solution for buoyancy-driven flow in a square cavity. *Numerical Heat Transfer, Part B: Fundamentals*, 65(6):495–517.
- [Fahs et al., 2011] Fahs, M., Younes, A., and Ackerer, P. (2011). An efficient implementation of the method of lines for multicomponent reactive transport equations. *Water, Air, & Soil Pollution*, 215(1):273–283.

- [Fernandez-Pascual et al., 2020] Fernandez-Pascual, E., Bork, M., Hensen, B., and Lange, J. (2020). Hydrological tracers for assessing transport and dissipation processes of pesticides in a model constructed wetland system. *Hydrology and Earth System Sciences*, 24(1):41–60.
- [Fox et al., 2014] Fox, A., Boano, F., and Arnon, S. (2014). Impact of losing and gaining streamflow conditions on hyporheic exchange fluxes induced by dune-shaped bed forms. *Water Resources Research*, 50(3):1895–1907.
- [Goharzadeh et al., 2005] Goharzadeh, A., Khalili, A., and Jørgensen, B. B. (2005). Transition layer thickness at a fluid-porous interface. *Physics of Fluids*, 17(5):057102.
- [Grant and Marusic, 2011] Grant, S. B. and Marusic, I. (2011). Crossing turbulent boundaries: interfacial flux in environmental flows. *Environmental Science & Technology*, 45(17):7107–7113.
- [Grant et al., 2012] Grant, S. B., Stewardson, M. J., and Marusic, I. (2012). Effective diffusivity and mass flux across the sediment-water interface in streams. *Water Resources Research*, 48(5).
- [Habel et al., 2002] Habel, F., Mendoza, C., and Bagtzoglou, A. C. (2002). Solute transport in open channel flows and porous streambeds. *Advances in Water Resources*, 25(4):455–469.
- [Harned and Hildreth, 1951] Harned, H. S. and Hildreth, C. L. (1951). The differential diffusion coefficients of lithium and sodium chlorides in dilute aqueous solution at 25°. *Journal of the American Chemical Society*, 73(2):650–652.
- [Hirthe and Graf, 2012] Hirthe, E. M. and Graf, T. (2012). Non-iterative adaptive time-stepping scheme with temporal truncation error control for simulating variable-density flow. *Advances in Water Resources*, 49:46–55.
- [Honti et al., 2018] Honti, M., Bischoff, F., Moser, A., Stamm, C., Baranya, S., and Fenner, K. (2018). Relating degradation of pharmaceutical active ingredients in a stream network to degradation in water-sediment simulation tests. *Water Resources Research*, 54(11):9207–9223.
- [Hunkeler et al., 2008] Hunkeler, D., Meckenstock, R. U., Sherwood Lollar, B., Schmidt, T. C., and Wilson, J. T. (2008). A guide for assessing biodegradation and source identification of organic ground water contaminants using Compound Specific Isotope Analysis (CSIA). page 82.

- [Jacobs et al., 2012] Jacobs, L. E., Weavers, L. K., Houtz, E. F., and Chin, Y.-P. (2012). Photosensitized degradation of caffeine: role of fulvic acids and nitrate. *Chemosphere*, 86(2):124–129.
- [Jada and Ait Akbour, 2014] Jada, A. and Ait Akbour, R. (2014). Adsorption and removal of organic dye at quartz sand-water interface. *Oil & Gas Science and Technology – Revue d’IFP Energies nouvelles*, 69(3):405–413.
- [Jaeger et al., 2019] Jaeger, A., Coll, C., Posselt, M., Mechelke, J., Rutere, C., Betterle, A., Raza, M., Mehrrens, A., Meinikmann, K., Portmann, A., Singh, T., Blaen, P. J., Krause, S., Horn, M. A., Hollender, J., Benskin, J. P., Sobek, A., and Lewandowski, J. (2019). Using recirculating flumes and a response surface model to investigate the role of hyporheic exchange and bacterial diversity on micropollutant half-lives. *Environmental Science: Processes & Impacts*, 21(12):2093–2108.
- [Jin et al., 2019] Jin, G., Chen, Y., Tang, H., Zhang, P., Li, L., and Barry, D. A. (2019). Interplay of hyporheic exchange and fine particle deposition in a riverbed. *Advances in Water Resources*, 128:145–157.
- [Jochmann et al., 2006] Jochmann, M. A., Blessing, M., Haderlein, S. B., and Schmidt, T. C. (2006). A new approach to determine method detection limits for compound-specific isotope analysis of volatile organic compounds. *Rapid communications in mass spectrometry: RCM*, 20(24):3639–3648.
- [Kaufman et al., 2017] Kaufman, M. H., Cardenas, M. B., Buttles, J., Kessler, A. J., and Cook, P. L. M. (2017). Hyporheic hot moments: Dissolved oxygen dynamics in the hyporheic zone in response to surface flow perturbations. *Water Resources Research*, 53(8):6642–6662.
- [Korekar et al., 2020] Korekar, G., Kumar, A., and Ugale, C. (2020). Occurrence, fate, persistence and remediation of caffeine: a review. *Environmental Science and Pollution Research*, 27(28):34715–34733.
- [Krause et al., 2017] Krause, S., Lewandowski, J., Grimm, N. B., Hannah, D. M., Pinay, G., McDonald, K., Martí, E., Argerich, A., Pfister, L., Klaus, J., Battin, T., Larned, S. T., Schelker, J., Fleckenstein, J., Schmidt, C., Rivett, M. O., Watts, G., Sabater, F., Sorolla, A., and Turk, V. (2017). Ecohydrological interfaces as hot spots of ecosystem processes. *Water Resources Research*, 53(8):6359–6376.

- [Lansdown et al., 2015] Lansdown, K., Heppell, C. M., Trimmer, M., Binley, A., Heathwaite, A. L., Byrne, P., and Zhang, H. (2015). The interplay between transport and reaction rates as controls on nitrate attenuation in permeable, streambed sediments. *Journal of Geophysical Research: Biogeosciences*, 120(6):1093–1109.
- [Lee et al., 2007] Lee, Y. B., Lorenz, N., Dick, L. K., and Dick, R. P. (2007). Cold storage and pretreatment incubation effects on soil microbial properties. *Soil Science Society of America Journal*, 71(4):1299–1305.
- [Lewandowski et al., 2019] Lewandowski, J., Arnon, S., Banks, E., Batelaan, O., Betterle, A., Broecker, T., Coll, C., Drummond, J. D., Gaona Garcia, J., Galloway, J., Gomez-Velez, J., Grabowski, R. C., Herzog, S. P., Hinkelmann, R., Höhne, A., Hollender, J., Horn, M. A., Jaeger, A., Krause, S., Löchner Prats, A., Magliozzi, C., Meinikmann, K., Mojarrad, B. B., Mueller, B. M., Peralta-Maraver, I., Popp, A. L., Posselt, M., Putschew, A., Radke, M., Raza, M., Riml, J., Robertson, A., Rutere, C., Schaper, J. L., Schirmer, M., Schulz, H., Shanafield, M., Singh, T., Ward, A. S., Wolke, P., Wörman, A., and Wu, L. (2019). Is the hyporheic zone relevant beyond the scientific community? *Water*, 11(11):2230.
- [Liao et al., 2013] Liao, Z., Lemke, D., Osenbrück, K., and Cirpka, O. A. (2013). Modeling and inverting reactive stream tracers undergoing two-site sorption and decay in the hyporheic zone. *Water Resources Research*, 49(6):3406–3422.
- [Lim et al., 2017] Lim, F. Y., Ong, S. L., and Hu, J. (2017). Recent advances in the use of chemical markers for tracing wastewater contamination in aquatic environment: a review. *Water*, 9(2):143.
- [Lācis and Bagheri, 2017] Lācis, U. and Bagheri, S. (2017). A framework for computing effective boundary conditions at the interface between free fluid and a porous medium. *Journal of Fluid Mechanics*, 812:866–889.
- [Malverti et al., 2008] Malverti, L., Lajeunesse, E., and Métivier, F. (2008). Small is beautiful: Upscaling from microscale laminar to natural turbulent rivers. *Journal of Geophysical Research: Earth Surface*, 113(F4).
- [Mazzafera, 2004] Mazzafera, P. (2004). Catabolism of caffeine in plants and microorganisms. *Frontiers in Bioscience: A Journal and Virtual Library*, 9:1348–1359.
- [Miller et al., 2013] Miller, C. T., Dawson, C. N., Farthing, M. W., Hou, T. Y., Huang, J., Kees, C. E., Kelley, C. T., and Langtangen, H. P. (2013). Numerical simulation

- of water resources problems: Models, methods, and trends. *Advances in Water Resources*, 51:405–437.
- [Munz et al., 2011] Munz, M., Krause, S., Tecklenburg, C., and Binley, A. (2011). Reducing monitoring gaps at the aquifer–river interface by modelling groundwater–surface water exchange flow patterns. *Hydrological Processes*, 25(23):3547–3562.
- [Nagaoka and Ohgaki, 1990] Nagaoka, H. and Ohgaki, S. (1990). Mass transfer mechanism in a porous riverbed. *Water Research*, 24(4):417–425.
- [Nield, 1983] Nield, D. A. (1983). The boundary correction for the Rayleigh-Darcy problem: limitations of the Brinkman equation. *Journal of Fluid Mechanics*, 128:37–46.
- [OECD, 2000] OECD (2000). *Test No. 106: Adsorption – Desorption Using a Batch Equilibrium Method*. Organisation for Economic Co-operation and Development, Paris.
- [Paraska et al., 2014] Paraska, D. W., Hipsey, M. R., and Salmon, S. U. (2014). Sediment diagenesis models: Review of approaches, challenges and opportunities. *Environmental Modelling & Software*, 61:297–325.
- [Peter et al., 2019] Peter, K. T., Herzog, S., Tian, Z., Wu, C., McCray, J. E., Lynch, K., and Kolodziej, E. P. (2019). Evaluating emerging organic contaminant removal in an engineered hyporheic zone using high resolution mass spectrometry. *Water Research*, 150:140–152.
- [Pinay et al., 2015] Pinay, G., Peiffer, S., De Dreuzzy, J.-R., Krause, S., Hannah, D. M., Fleckenstein, J. H., Sebilo, M., Bishop, K., and Hubert-Moy, L. (2015). Upscaling nitrogen removal capacity from local hotspots to low stream orders’ drainage basins. *Ecosystems*, 18(6):1101–1120.
- [Price, 1989] Price, W. E. (1989). Tracer caffeine diffusion in aqueous solutions at 298 K. The effect of caffeine self-association. *Journal of the Chemical Society, Faraday Transactions 1: Physical Chemistry in Condensed Phases*, 85(2):415–419.
- [Ren and Packman, 2004a] Ren, J. and Packman, A. I. (2004a). Modeling of simultaneous exchange of colloids and sorbing contaminants between streams and streambeds. *Environmental Science & Technology*, 38(10):2901–2911.

- [Ren and Packman, 2004b] Ren, J. and Packman, A. I. (2004b). Stream-subsurface exchange of zinc in the presence of silica and kaolinite colloids. *Environmental Science & Technology*, 38(24):6571–6581.
- [Rosti et al., 2015] Rosti, M. E., Cortelezzi, L., and Quadrio, M. (2015). Direct numerical simulation of turbulent channel flow over porous walls. *Journal of Fluid Mechanics*, 784:396–442.
- [Salim Joodi et al., 2010] Salim Joodi, A., Sizaret, S., Binet, S., Bruand, A., Albéric, P., and Lepiller, M. (2010). Development of a Darcy- Brinkman model to simulate water flow and tracer transport in a heterogeneous karstic aquifer (Val d’Orléans, France). *Hydrogeology Journal*, 18(2):295–309.
- [Santos et al., 2008] Santos, V., Morão, A., Pacheco, M. J., Ciríaco, L., and Lopes, A. (2008). Electrochemical degradation of azo dyes on bdd: effect of chemical structure and operating conditions on the combustion efficiency. page 13.
- [Schaffer and Licha, 2015] Schaffer, M. and Licha, T. (2015). A framework for assessing the retardation of organic molecules in groundwater: Implications of the species distribution for the sorption-influenced transport. *Science of The Total Environment*, 524-525:187–194.
- [Shrestha et al., 2016] Shrestha, P., Junker, T., Fenner, K., Hahn, S., Honti, M., Bakkour, R., Diaz, C., and Hennecke, D. (2016). Simulation studies to explore biodegradation in water–sediment systems: From OECD 308 to OECD 309. *Environmental Science & Technology*, 50(13):6856–6864.
- [Soetaert et al., 1996] Soetaert, K., Herman, P. M. J., and Middelburg, J. J. (1996). A model of early diagenetic processes from the shelf to abyssal depths. *Geochimica et Cosmochimica Acta*, 60(6):1019–1040.
- [Sousa et al., 2018] Sousa, J. C. G., Ribeiro, A. R., Barbosa, M. O., Pereira, M. F. R., and Silva, A. M. T. (2018). A review on environmental monitoring of water organic pollutants identified by EU guidelines. *Journal of Hazardous Materials*, 344:146–162.
- [Sparrow et al., 1973] Sparrow, E. M., Beavers, G. S., Chen, T. S., and Lloyd, J. R. (1973). Breakdown of the laminar flow regime in permeable-walled ducts. *Journal of Applied Mechanics*, 40(2):337–342.

- [Suga et al., 2010] Suga, K., Matsumura, Y., Ashitaka, Y., Tominaga, S., and Kaneda, M. (2010). Effects of wall permeability on turbulence. *International Journal of Heat and Fluid Flow*, 31(6):974–984.
- [Valdés-Parada et al., 2013] Valdés-Parada, F. J., Aguilar-Madera, C. G., Ochoa-Tapia, J. A., and Goyeau, B. (2013). Velocity and stress jump conditions between a porous medium and a fluid. *Advances in Water Resources*, 62:327–339.
- [Van Breukelen et al., 2005] Van Breukelen, B. M., Hunkeler, D., and Volkering, F. (2005). Quantification of sequential chlorinated ethene degradation by use of a reactive transport model incorporating isotope fractionation. *Environmental Science & Technology*, 39(11):4189–4197.
- [van Genuchten and Wagenet, 1989] van Genuchten, M. T. and Wagenet, R. J. (1989). Two-site/two-region models for pesticide transport and degradation: Theoretical development and analytical solutions. *Soil Science Society of America Journal*, 53(5):1303.
- [Vanderborght et al., 1977] Vanderborght, J.-P., Wollas, R., and Bitten, G. (1977). Kinetic models of diagenesis in disturbed sediments. Part 2. Nitrogen diagenesis. *Limnology and Oceanography*, 22(5):794–803.
- [Voermans et al., 2017] Voermans, J. J., Ghisalberti, M., and Ivey, G. N. (2017). The variation of flow and turbulence across the sediment–water interface. *Journal of Fluid Mechanics*, 824:413–437.
- [Voermans et al., 2018] Voermans, J. J., Ghisalberti Marco, and Ivey Gregory N. (2018). A model for mass transport across the sediment-water interface. *Water Resources Research*, 0(0).
- [Xu et al., 2018] Xu, Z., Hu, B. X., and Ye, M. (2018). Numerical modeling and sensitivity analysis of seawater intrusion in a dual-permeability coastal karst aquifer with conduit networks. *Hydrology and Earth System Sciences*, 22(1):221–239.
- [Younes et al., 2014] Younes, A., Makradi, A., Zidane, A., Shao, Q., and Bouhala, L. (2014). A combination of Crouzeix-Raviart, Discontinuous Galerkin and MPFA methods for buoyancy-driven flows. *International Journal of Numerical Methods for Heat & Fluid Flow*, 24(3):735–759.
- [Zumstein and Helbling, 2019] Zumstein, M. T. and Helbling, D. E. (2019). Biotransformation of antibiotics: Exploring the activity of extracellular and intracellular

enzymes derived from wastewater microbial communities. *Water Research*, 155:115–123.

Preface to Chapter IV

Rivers are intrinsically connected to their surrounding environment (*e.g.* groundwater, subsurface, riparian zone, etc.) and rivers display high spatial and temporal variabilities in terms of pollution source, apportionment and degradation potential. Knowledge derived from laboratory experiments in Chapter 4.1 and 4.1 were conducted under controlled and steady conditions and consequently lack of representativeness when extrapolated to actual river conditions. Transient hydraulic conditions during rainfall events or the effects of multiple-source apportionments could not be experimentally reproduced. Accordingly, in this chapter we present data from a 9 months monitoring campaign of S-metolachlor fate in a 2.2 *km* long low Strahler order river reach. Concentration, transformation products analysis and CSIA were analyzed together in the light of the previous experimental and numerical results to examine S-metolachlor fate within the studied river reach.

Hydrological (*i.e.* water flow and precipitations) and concentration data revealed preferential periods of S-Metolachlor entrance in the river reach. CSIA data supported the idea that the homogeneous input of S-Metolachlor under low flow conditions within the river reach. In line with concentration and flow data, CSIA suggested negligible S-Metolachlor degradation in the investigated river reach. Overall, this study highlights the potential of CSIA to identify pesticide degradation in long rivers and also clearly demonstrates the remaining analytical bottlenecks required for further investigations of pesticide fate in low Strahler order rivers.

Chapter IV

S-metolachlor dissipation alongside a river reach

4.1 Introduction

Pesticide pollution of agriculturally impacted surface waters is ubiquitous [Fenner et al., 2013], whereas knowledge of pesticide behaviour in rivers remains scarce. The hyporheic zone of rivers includes a reactive interface between the overlying water of the main river channel and the riverbed sediment, namely the sediment-water interface (SWI). The SWI is a unique interface sustaining intense and diverse key ecosystem functions, including pesticide transformation leading to water quality improvement [Lewandowski et al., 2019]. Dissipation of pesticides in rivers results from a complex interplay between transport and degradation processes occurring in the riverbed and the overlying water column [Krause et al., 2017]. Although the fate of point source pollutants discharged from waste water treatment plants in rivers have been intensively studied [Ward, 2016], less is known about the most commonly used pesticides in rivers which are non-point source.

The chloroacetanilide herbicide *S*-metolachlor ranks among the top five of most used active ingredients worldwide and is used in maize and sugar beet harvesting ‘ [Maggi et al., 2019]. It is frequently detected in surface waters, mainly due to its moderate solubility (490 mg l^{-1}) and sorption propensity (octanol-water partition coefficient: $\log(K_{ow}) = 3.05$; organic carbon-water partition coefficient in soil: $K_{oc} = 120 \text{ L.kg}^{-1}/\text{g}_{oc}.\text{g}^{-1}$). *S*-metolachlor degrades in agricultural soils with half-life values ranging from 12 to 34 days, and the non-degraded fraction and transformation products may be exported into rivers via runoff [Alvarez-Zaldívar et al., 2018, Lefrancq et al., 2017b]. However, to the best of our knowledge, *S*-metolachlor dissipation processes in

rivers have not been specifically studied so far.

In this context, Compound-Specific Isotope Analysis (CSIA) opens novel opportunities to follow-up pesticide persistence and degradation. CSIA is generally insensitive to non-destructive dissipation (*e.g.* dilution, sorption, volatilization) controlling environmental concentrations [Elsner and Imfeld, 2016]. In contrast, as lighter isotopes (*e.g.* ^{12}C) react faster than their heavier counterparts (*e.g.* ^{13}C) during pesticide biodegradation, it results in an enrichment of the heavier isotopologues in the non-degraded fraction of pesticides in environmental samples [Elsner, 2010]. In addition to the conventional monitoring approaches, pesticide CSIA may help to tease apart transport from degradation processes in opened agricultural catchments [Lutz et al., 2017]. Recent conceptual advances incorporating interpretation of CSIA data with numerical modelling allows examining pesticide transport and degradation in rivers [Alvarez-Zaldívar et al., 2018, Lutz et al., 2013]. While CSIA has been successfully used to evaluate degradation of legacy compounds at contaminated aquifers [Fischer et al., 2016], its application to evaluate the contribution of pesticide degradation and transport across distinct hydrological events in agriculturally impacted soils and surface waters is mostly lacking.

The purpose of this study was to evaluate the contribution of degradation and transport processes to *S*-metolachlor dissipation in a 2.2 km long river reach draining water from an agriculturally impacted catchment. The specific goals of this preliminary study were 1) to examine *S*-metolachlor transport and apportionment from agricultural fields into the river reach, 2) to evaluate the contribution of instream *S*-metolachlor degradation to overall pesticide dissipation at catchment scale, with emphasize on the role of the SWI, and 3) to discuss the applicability and limits of current analytical, experimental and numerical approaches to quantify the contribution of pesticide dissipation processes in rivers. *S*-metolachlor application dates and doses, concentrations and stable isotope composition, water discharges and hydrochemistry parameters were continuously followed-up from March 2019 to October 2019, upstream and downstream of the Avenheimerbach river (AVB - East of France). Data interpretation used ex-situ laboratory characterization of *S*-metolachlor biodegradation and photodegradation and numerical investigations of pollutant transport at the SWI presented in chapters and , respectively.

4.2 Material and methods

4.2.1 Study site

The studied river reach consisted in a 2.2 km long tributary draining a 3.6 km² catchment, which is part of the Avenheimerbach (AVB) headwater river (Strahler order 1) in North-East France (see Figure IV.1). The catchment has an average slope of 3.8%. The average annual rainfall depth measured 15 km away from the AVB river over the period 1949-2018 was 622 ± 102 mm (Météo France rain gauge - 48°32'58" N, 7°38'25" E). Conventional agriculture covered 91% of the total catchment area, urban or impervious areas 8%, while the remaining 1% consisted in riparian forests. The predominant landuse during the study was wheat (27%), maize (26%) and sugar beets (4%), the remaining 43% consisted in grassland and, to a minor extent, roads and river strip buffers. This landuse remained constant over time, with annual variations of landuse ratios below 2% from 2015 to 2018 according to the Land Parcel Identification System.

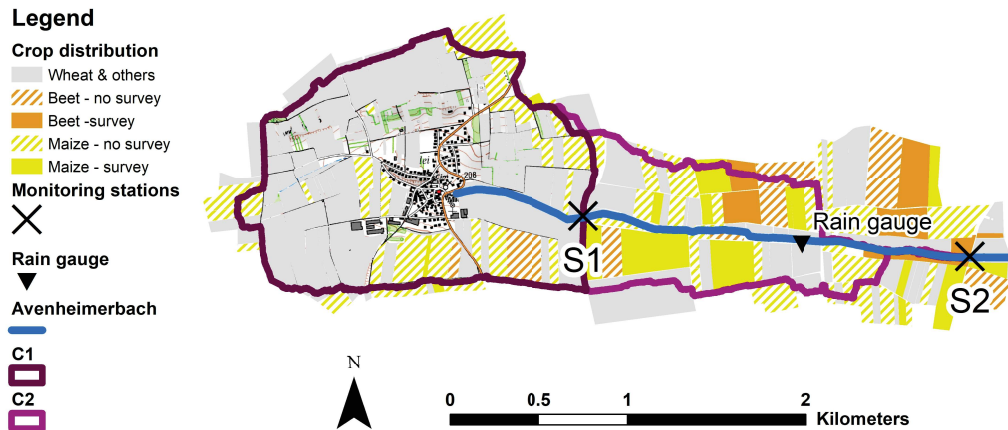


Figure IV.1 – Crop distribution and monitoring devices implemented in C1 and C2. Sugar beet (orange) and Maize (yellow) areas were filled with dashed lines when farmers did not provide *S*-metolachlor data. Grey areas are non-surveyed surfaces on which *S*-metolachlor was not applied.

Soil of the AVB catchment (< 20 m deep) mainly consisted of Pleistocene loess and loam and the AVB riverbed was characterized by silts with low clay and moderate sand contents (riverbed sediment texture presented in appendix C.S5) (Association pour la Relance Agronomique en Alsace, 2015). The AVB river has been extensively

straightened, and displays a tortuosity of 1.1. Waste water discharges from industrial, urban or impervious areas into the AVB were not observed. An artificial drainage system supporting maize harvesting presumably discharged into the AVB, with minor contribution to AVB discharged only locally observed at punctual occasions.

Two monitoring stations were deployed at the outlet of the 3.6 km^2 catchment (S2 - $48^\circ 39' 58.08''$ N, $07^\circ 35' 36.92''$ E) and 2.2 km upstream the AVB river (S1- $48^\circ 40' 09.60''$ N, $07^\circ 33' 51.18''$ E). This corresponded to two embedded catchments with similar land use characteristics, namely C1 and C2 (see Table IV.1).

Table IV.1 – Land-use for C1 and C2 catchments and estimated mass of applied *S*-metolachlor based on farmer surveys. Survey response rates were weighted by the corresponding land use percentage. Uncertainties associated with estimations of mass applied correspond to the propagation of standard deviations of average application rates to the whole catchment areas. *n.r.* stands for non-relevant for non-surveyed parcels.

Crop	Proportion of land use (%)		Survey response rate (%)		Extrapolated mass applied (kg)	
	C1 (2.3 km^2)	C2 (3.6 km^2)	C1	C2	C1	C2
Sugar beet	2	4	0	30	2.2 ± 0.7	6.8 ± 2.3
Maize	20	26	5	16	26.1 ± 8.1	63.0 ± 19.5
Wheat	28	27	<i>n.r.</i>	<i>n.r.</i>	<i>n.r.</i>	<i>n.r.</i>
Others	50	43	<i>n.r.</i>	<i>n.r.</i>	<i>n.r.</i>	<i>n.r.</i>

4.2.2 *S*-metolachlor application

The farmer survey covered 44% and 40% of the total maize and sugar beet surfaces of the study catchment, which was representative of agricultural practices in C1 and C2. Camix[®], Mercantor Gold[®], Dual Gold[®] and S-Metolastar[®] were the four *S*-metolachlor-based commercial products used in C1 and C2. The carbon isotope composition of *S*-metolachlor in the four commercial products was identical ($^{13}\text{C}_0 = -31.7 \pm 0.3$, $n = 4$).

Maize and sugar beet were the only cultures receiving *S*-metolachlor across the agricultural season. *S*-metolachlor was mainly used as pre- and post-emergence weed control on sugar beets (application histogram is provided in appendix C.S1). Three applications of *S*-metolachlor on sugar beet were reported from March 31 up to April 30 with a mean application rates of $330 \pm 110 \text{ g.ha}^{-1}$. A unique and massive application on

each maize field was reported with an average application rate of $775 \pm 240 \text{ g.ha}^{-1}$) from May 14 to May 23. Survey results were extrapolated to the entire C1 and C2 catchments to estimate applied mass of *S*-metolachlor. Accordingly, $9.0 \pm 3.0 \text{ kg}$ of *S*-metolachlor were applied on sugar beet and $89.1 \pm 27.6 \text{ kg}$ on maize (see Table IV.1).

4.2.3 Soil, water and sediment collection

The first 10 cm of field top soil were collected monthly at 4 different places in cultivated agricultural fields located in 100 m radius circle around S1 and S2, and pooled in a single composite sample per location. Calibrated multiparameter probes (Ponsel ODEON for S1 and HANNA HI 9289 for S2) continuously measured temperature, pH and conductivity. A ticking buckets rain gauge located between S1 and S2 ($48^\circ 40' 03'' \text{ N}$, $07^\circ 34' 51'' \text{ E}$) characterized precipitations over the whole catchment. A grab sample of 2 L was collected in the AVB at S2 on February 7 2019, before *S*-metolachlor applications, to characterize the initial concentration and isotope signature of *S*-metolachlor. Continuous flow measurements from Doppler flow meters (ISCO 2150 at S1 and IJINUS VLI H/V at S2, discharge accuracy $\pm 15 \%$) were used for flow-proportional water sampling by refrigerated auto-samplers (ISCO Avalanche, 4°C) in glass bottles every 70 and 155 m^3 , at S1 and S2, respectively. Different sampling volumes were set in S1 and S2 to account for increasing flow from up- to downstream and to ensure a sub-daily sampling frequency. Each glass bottle was filled with three successive samplings to increase the sampling frequency and representativeness (111 mL each, for a final 330 mL total). River water in glass bottles were pooled in composite samples in laboratory based on hydrological conditions and events (*i.e.* base-flow, rise or fall of event), to allow sufficient *S*-metolachlor concentration for CSIA measurements. The first centimeter of river sediment were collected monthly at S1 and S2 to evaluate change of *S*-metolachlor concentrations in sediment.

4.2.4 Chemical analyses

Water samples were filtered through $0.45 \mu\text{m}$ glass filters to quantify separately *S*-metolachlor dissolved in water and bound to total suspended solids (TSS). *S*-metolachlor in water was extracted by solid phase extraction (SPE) using SolEx C18 cartridges (Dionex[®], Sunnyvale, CA, USA) and an AutoTrace 280 SPE system (Dionex[®]). Particulate, sediment and soil samples were processed by liquid-liquid extraction, as described in chapter II, section 2.1. Hydrochemical composition of the AVB water was characterized from filtrated water sample by ion-chromatography (Dionex ICS-51000)

to quantify anions and cations, and by TOC analyser (Shimadzu TOC-V CPH) to quantify dissolved organic carbon (hydrochemistry presented in appendix C.S3). Sample extraction and analysis were carried out using procedures described in chapter II, section 2.1. GC-MS/MS was used to quantify *S*-metolachlor and GC-IRMS to measure its stable isotope composition.

Quantification limits (QLs) determined in chapter II, section 2.1 were normalized by sampled water volumes and sediment/soil mass. Depending on the amount of collected samples, averaged QLs were established as follows: $0.027 \mu\text{g.L}^{-1}$ in water ($\min = 0.003 \mu\text{g.L}^{-1}$, $\max = 0.093 \mu\text{g.L}^{-1}$), $32.6 \mu\text{g.kg}^{-1}$ in TSS ($\min = 0.7 \mu\text{g.kg}^{-1}$, $\max = 137.3 \mu\text{g.kg}^{-1}$), $1.4 \mu\text{g.kg}^{-1}$ in sediment ($\min = 0.4 \mu\text{g.kg}^{-1}$, $\max = 2.5 \mu\text{g.kg}^{-1}$) and $1.43 \mu\text{g.kg}^{-1}$ in soils ($\min = 0.4 \mu\text{g.kg}^{-1}$, $\max = 2.1 \mu\text{g.kg}^{-1}$). *S*-metolachlor was quantified in 127 water samples from March 5 to October 2 2019. *S*-metolachlor was not detected in TSS due to a systematically low amount of material. Sufficient amount of *S*-metolachlor for C-CSIA was achieved in 18 water samples. However, matrix effect hampered CSIA of *S*-metolachlor from soil samples and *S*-metolachlor $\delta^{13}\text{C}$ values presented later were predicted from *S*-metolachlor soil concentrations (see chromatogram in appendix C.S4).

Complementary, monthly pesticide and transformation product (TP) analysis using ISO/IEC 17025 certified laboratory procedures were carried out by the water agency (Agence de l'eau Rhin-Meuse) from water samples collected at the location of the rain gauge. This data set was used to evaluate the export of *S*-metolachlor and four of its TPs, namely metolachlor ethane sulfonic acid (ESA), metolachlor oxalonic acid (OXA), metolachlore CGA 357704 and metolachlore NOA 413173. These data were reported in mass equivalent loads of *S*-metolachlor (MEL_{SM}), as follows (Eq. IV.1):

$$MEL_{SM} = load(SM) + \sum_{TP_i} load(TP_i) \cdot \frac{MW_{SM}}{MW_{TP_i}} \quad (\text{IV.1})$$

where MW_{SM} and MW_{TP_i} correspond to the molar weight of *S*-metolachlor, and that of its TPs, respectively.

4.2.5 Data analysis

S-metolachlor loads in the AVB were estimated at a daily time-step according to Eq. IV.2. *S*-metolachlor concentrations in composite water samples were considered as representative mean values for the period starting at the first water collection sampling

time and ending at the sampling time of the last water collection.

$$M_{S_j,i} = \int_{i-1}^i Q_{S_j}(t) \cdot C_{S_j,i} \quad (\text{IV.2})$$

where $M_{S_j,i}$ stands for the exported load in station S_j during period i , $Q_{S_j}(t)$ for the instantaneous water flow at station S_j and $C_{S_j,i}$ the corresponding average S -metolachlor concentration over the period i .

Discharges and area normalized daily loads were used to compare S -metolachlor export in C1 and C2 [Shaw et al., 2019], since proportions of impervious areas were similar (11% and 8% for C1 and C2).

A detailed mass balance could not be established due to lacking water samples or flow measurements caused by acquisition failure following massive floods or severe weathers across the agricultural season. In total, 59% and 47% of the total monitoring period was covered by continuous flow and concentration time-series. Instream processes at the reach-scale were thus compared over 28 non-consecutive days using simultaneous records of S -metolachlor loads and water discharges at S1 and S2.

CSIA data may reflect both in-field and instream S -metolachlor degradation. In-field degradation can be evaluated based on temporal changes in the stable isotope ratio of S -metolachlor in field soil and runoff export, while instream degradation can be interpreted by comparing changes in stable isotope ratio of S -metolachlor in river water and sediment at S1 and S2. S -metolachlor degradation extent was estimated using the inverse form of the Rayleigh equation (Eq. IV.3).

$$\frac{\delta^{13}C_{S_j,i} + 1000}{\delta^{13}C_{S_j,0} + 1000} = \frac{C_{S_j,i}^{\frac{bulk}{1000}}}{C_{S_j,0}} \quad (\text{IV.3})$$

Since C1 and C2 did not fulfil the closed-system requirement, a corrected laboratory derived enrichment factor for S -metolachlor degradation in field soil ($\epsilon_C = -1.4 \pm 0.4\text{‰}$) was used to account for both dilution and degradation processes at catchment scale [Alvarez-Zaldívar et al., 2018]. Indeed, at catchment scale, hydrodynamic dispersion caused by long transport in subsurface may lead to an overestimation of pollutant degradation in field soils [Van Breukelen, 2007].

4.3 Results and discussion

Temporal and spatial patterns of *S*-metolachlor apportionment from export by surrounding fields should be accounted for when comparing *S*-metolachlor transport and degradation between S1 and S2. *S*-metolachlor sources were first evaluated by comparing area normalized discharges and *S*-metolachlor loads between S1 and S2 to ensure uniform *S*-metolachlor apportionment in C1 and C2. *S*-metolachlor chemographs and isotope signatures in S1 and S2 were then compared to evaluate *S*-metolachlor dissipation processes of *S*-metolachlor in the AVB.

4.3.1 Hydrological response and AVB hydrological functioning

From March 1st to October 31st, the total rainfall depth represented $76 \pm 8\%$ of the averaged precipitations of the preceding 69 years. The uncertainty accounts for missing data between May 2 to 12 due to rain gauge failure. During this period, values came from a nearby rain gauge located 7 km away from our station ($48^{\circ}37'56''$ N, $07^{\circ}37'02''$ E).

In total, 17 significant rainfall events (cumulative volume > 2 mm) separated by at least 24 hours were recorded (see Figure IV.2A and B). Long-lasting rainfall events (event 1 to 4) with low intensities ($I < 0.3$ mm.h⁻¹) prevailed from March to April 2019, while most intense events occurred from May to August 2019, with events 8 and 15 being the most intense ($I = 18.0$ mm.h⁻¹ and $I = 12.2$ mm.h⁻¹, respectively).

Hydrological responses of C1 and C2 were similar during the whole study period. Area normalized discharges in S1 and S2 ranged close to the 1:1 line (see Figure IV.3A), suggesting similar contributions of C1 and C2 to water apportionments in S1 and S2 [Shaw et al., 2019]. An absolute ratio of daily discharges between S1 and S2 higher than 1 indicated gaining conditions alongside the AVB river reach (see Figure IV.3A). Since no punctual water sources in between S1 and S2 were observed, vertical groundwater and lateral subsurface water likely fed the AVB river reach. During dry periods, water entering the stream likely only stemmed from groundwater. Higher conductivity in S1 than in S2 ($\sigma = 582 \pm 314$ and $\sigma = 1194 \pm 252$ $\mu S.cm^{-1}$ on average in S1 and S2) indicated gradual mixing of groundwater with surface water, since groundwater conductivity was $\sigma = 1331 \pm 63$ $\mu S.cm^{-1}$ in piezometers located 2 m away from the left and right riverbanks in S2 (on October 1st 2019).

In contrast, lateral subsurface flows presumably predominantly fed the AVB during wet periods. During rain events, an inverse and quasi-simultaneous response of flow and

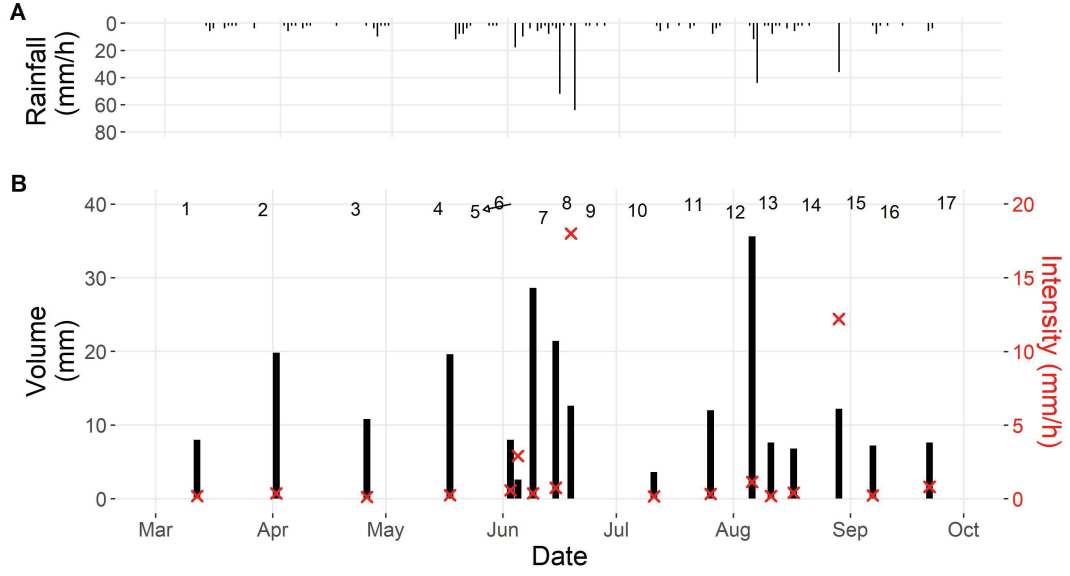


Figure IV.2 – Hyetograms used for rainfall event identification (A). Rainfall number, depth (mm) and intensity (red cross) (B).

conductivity in S1 and S2 suggested transport from fields to the AVB of fresh rainfall water with limited contact time with the soil matrix [Leu et al., 2004]. Fast transport from fields to the AVB was mainly attributed to lateral subsurface flow since surface runoff was unlikely according to the comparison of soil saturated conductivity (K_{sat}) and rainfall intensities over the agricultural season. As previously demonstrated for an agricultural catchment near the AVB river with similar top-soil properties (brown earth and calcic soils, equivalent to loess), the saturated water conductivity of field soils on maize crops ranges from $\approx 60 \text{ mm.h}^{-1}$ to $\approx 6 \text{ mm.h}^{-1}$ by the end of the agricultural season [Lefrancq et al., 2017a]. This temporal evolution is attributed to soil restructuration over rainfall events and tillage over the agricultural season. Accordingly, surface runoff presumably occurred only during events 8 and 15 as they displayed rainfall intensities higher than 6 mm.h^{-1} (other events systematically ranging below $\approx 3 \text{ mm.h}^{-1}$). In addition, event 8 generated an inverse trend of conductivity *vs* flow response in the AVB river. Also, event 8 fell in a wet period with 3 rainfall events closely preceding event 8 (see Figure IV.2).

Altogether, hydrological responses in S1 and S2 indicated the predominance of lateral subsurface flows, although surface runoff punctually occurred, resulting in similar *S*-metolachlor export from fields to the AVB in S1 and S2.

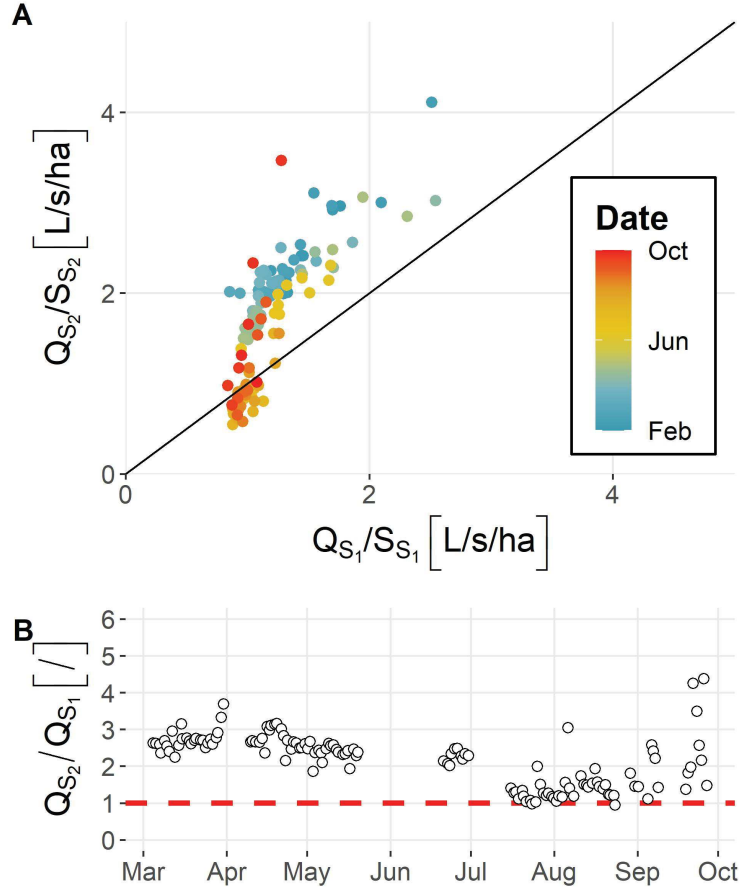


Figure IV.3 – Area normalized daily discharges in S1 vs S2 (A) and daily discharges ratios between S1 and S2 (B). Area normalized daily discharges at the beginning of the monitoring period range from blue to bright yellow. Colours get increasingly red later in the season, featuring a change from strong to light groundwater upwelling fluxes entering the AVB. The black line represents the 1:1 line.

4.3.2 *S*-metolachlor sources and export to the AVB

***S*-metolachlor degradation mainly occurred in field top-soil** – Since *S*-metolachlor isotope composition could not be measured in top soil due to matrix effect (reasons explained in appendix C.S4), the change in carbon stable isotope ratios ($\delta^{13}C$) of *S*-metolachlor in top-soil was modelled from measured *S*-metolachlor concentrations in top-soil as developed and validated in a similar agricultural headwater catchment [Alvarez-Zaldivar, 2018] (details on the procedure in appendix C.S6). Briefly,

the temporal evolution of topsoil *S*-metolachlor concentrations was fitted to a pseudo first-order degradation kinetic accounting for ambient soil moisture and temperature conditions. Then, the estimated degradation extent of *S*-metolachlor was reinjected in the Rayleigh equation (Eq. IV.3), resulting in estimations of *S*-metolachlor isotope composition in top-soil. It revealed that seasonal changes in $\delta^{13}C$ of dissolved *S*-metolachlor in the AVB river accurately followed values predicted in field top-soil. This strongly suggests that *S*-metolachlor degradation occurred in field top soils rather than during subsurface transport toward the AVB, in agreement with reported metolachlor biodegradation in anaerobic subsurface at least 10 times longer than in aerobic top soil (Accinelli et al., 2001). Furthermore, using Eq. IV.3 and considering a maximal change of isotope ratio of dissolved *S*-metolachlor in S1 and S2 of $\Delta\delta^{13}C = 2.8 \pm 0.1\text{‰}$ by the end of July (see figure IV.6), it was estimated that $87 \pm 2\%$ of the initial *S*-metolachlor mass was degraded in the top soil. This suggests that *S*-metolachlor predominantly degraded in field top soil at catchment scale. Worth noting, $\delta^{13}C$ values measured during long and intense rainfall events 12 to 15, close to the initial *S*-metolachlor $\delta^{13}C$ value suggested mobilization of undegraded fractions of *S*-metolachlor since no fresh applications were reported in August. Altogether, these observations confirm the ability of CSIA to trace pesticide stocks and degradation in agricultural soils as well as pesticide transport from agricultural soils to the river from measurements of $\delta^{13}C$ value in river water alone [Lutz et al., 2017, Torabi et al., 2020].

***S*-metolachlor export to the AVB by punctual surface runoff and quasi-continuous subsurface flow** – Overall, 0.08% (22 g) and 0.03% (18 g) of total *S*-metolachlor applied, respectively, on C1 and C2 were exported into the AVB during the study period. This estimation is likely underestimated because only 59% and 47% of the season duration was covered by continuous monitoring in S1 and S2, respectively. Nonetheless, it ranges within previously reported *S*-metolachlor export rates over entire agriculture seasons from 0.072% [Boithias et al., 2011] to 0.2% [Alvarez-Zaldívar et al., 2018]. *S*-metolachlor spray drift did not directly contributed to S1 and S2 *S*-metolachlor budget based on *S*-metolachlor concentrations in the AVB on the application dates reported by survey. The mandatory 5 m wide grass strip buffering the AVB river as well as the expectedly short drift of pesticide in the atmosphere (≈ 1 h and < 150 m) previously reported for alachlor (chloroacetanilide similar to *S*-metolachlor) also suggest limited direct contaminations by spray drift during the study period only from the fields directly linked to the AVB river [Felsot et al., 2010, Ravier

et al., 2005]. Hence, surface runoff or subsurface flow were assumed to be prevailing transport pathways of *S*-metolachlor toward the AVB.

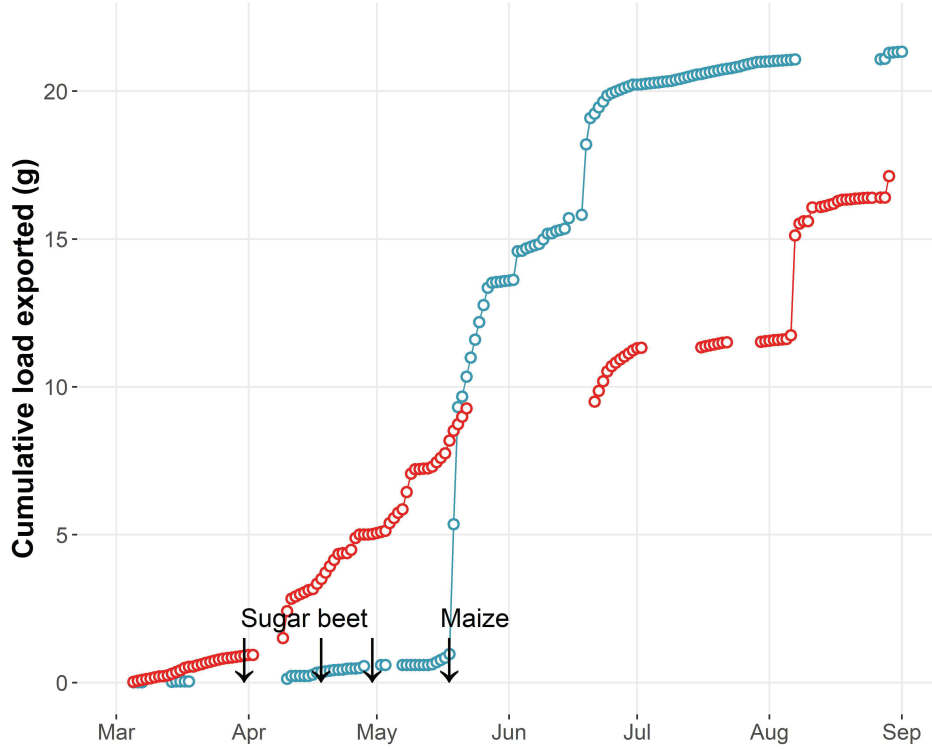


Figure IV.4 – Cumulative loads exported through S1 (blue) and S2 (red). Empty spaces stand for missing data. Mid-May is characterized by an event exporting

Fast transport by drainage and surface runoff resulted in massive *S*-metolachlor export across the investigation period (see Figure IV.4). Interestingly, a single rainfall event occurring 2 days after *S*-metolachlor applications on Maize (on May 18) exported 54% of the total *S*-metolachlor mass in S1, corresponding to a maximal concentration of $14.33 \mu\text{g.L}^{-1}$. *S*-metolachlor was likely transported by drainage rather than by surface runoff during this event, as previously observed during moderate rainfall events (10 to 16 mm.h^{-1}) occurring right after pesticide application [Lefrancq et al., 2017a]. Flash export in clayey soils by preferential flows in soil cracks may also explain the transient character of this event, as described for the herbicides bentazone and MCPA and other fungicides and insecticides [Kronvang et al., 2004].

Events 8 and 12 generated quick but massive export of *S*-metolachlor, corresponding to

a concentration of about $5 \mu\text{g.L}^{-1}$ in S1 and S2. These events accounted for 17.5% and 29.5% of the total mass export of *S*-metolachlor in S1 and S2, respectively. Although the likelihood of runoff occurrence during event 12 was considered low according to the analysis above, its cumulative volume being the largest of the season (36 mm) may have locally generate surface-runoff.

Constant slow subsurface transport also significantly contributed to about 28.5% and 70.5% of total *S*-metolachlor load discharged in S1 and S2, as estimated from moderate rainfall events (all events except events nr 8 and 15). While pesticide transport from field to rivers was larger during intense rainfall-events, subsurface transport also contributed to *S*-metolachlor export from field at a longer timescale.

***S*-metolachlor apportionment into the AVB river limits process investigation** – Instream *S*-metolachlor concentrations on March 12, prior *S*-metolachlor applications, were $0.054 \pm 0.002 \mu\text{g.L}^{-1}$ in S1 and $0.021 \pm 0.001 \mu\text{g.L}^{-1}$ in S2, corresponding to the remaining fraction of *S*-metolachlor applied in 2018. $\delta^{13}\text{C}$ values of dissolved *S*-metolachlor on April 16 (prior main applications on sugar beets) were $-27.3 \pm 0.5\text{‰}$ for S1 and S2, attributed to the remaining *S*-metolachlor applied in 2018. Using the reference enrichment factor for *S*-metolachlor biodegradation in soil ($\epsilon_C = -1.4 \pm 0.4\text{‰}$) [Alvarez-Zaldívar et al., 2018], and assuming that the $\delta^{13}\text{C}$ value of the commercial product mixture was identical in 2018 and 2019, it is estimated that $96 \pm 4\%$ of *S*-metolachlor applied in 2018 was degraded in April 16. The remaining mass of *S*-metolachlor applied in 2018 was negligible compared with *S*-metolachlor loads entering the AVB in 2019.

S-metolachlor was quantified earlier in S2 than S1 (beginning of April vs mid-May), presumably due to a larger contribution of sugar-beet plots in C2 (4% of the arable land) than in C1 (2%), and exclusive application of *S*-metolachlor from April to mid-May on sugar beet fields. By mid-May, *S*-metolachlor in S1 and S2 simultaneously became isotopically lighter (*i.e.* lower $\delta^{13}\text{C}$ values), with a maximal change in stable isotope ratios in S2 ($\Delta\delta^{13}\text{C} = 3.7 \pm 0.3\text{‰}$). From mid-May onwards, *S*-metolachlor isotopic composition of $\delta^{13}\text{C} = -31.5 \pm 0.3\text{‰}$ corresponded to that of the applied commercial products ($\delta^{13}\text{C} = -31.7 \pm 0.3\text{‰}$, see figure IV.6). Hence, comparison of *S*-metolachlor concentrations in S1 and S2 was only made possible from mid-May to the end of the agricultural season, when both catchment C1 and C2 received equivalent *S*-metolachlor loads and behaved similarly.

The dynamic of fast transport processes from fields to river significantly contributed to *S*-metolachlor export into the AVB and limited the simultaneous characterization of *S*-metolachlor apportionment in S1 and S2 [Sandin et al., 2018]. For instance, detection of *S*-metolachlor in S1 and not in S2 during event 4, indicated a transient and/or local contamination upstream S1 with a transfer time < 5 hours corresponding to the sampling frequency in S2 at that specific time (155 m^3). The analysis of *S*-metolachlor transport and dissipation was thus restricted to base flow conditions integrating small to moderate rainfall events exporting *S*-metolachlor through subsurface flow.

On the contrary, during small to moderate rainfall events, pesticide export to the AVB was proportional to C1 and C2 areas, as indicated by the majority of points ranging around the 1:1 line of the area normalized mass loads (see Figure IV.5). In addition, similar $\delta^{13}\text{C}$ values suggest that *S*-metolachlor homogeneously entered into the AVB between S1 and S2. Similar changes over time of *S*-metolachlor $\delta^{13}\text{C}$ in S1 and S2 suggest similar degradation and transport pathways acting at the scales of C1 and C2 catchments [Lutz et al., 2013, Lutz et al., 2017] (see appendix C.S7 for the $\delta^{13}\text{C}(t)$ slope equivalency test).

Knowledge of *S*-metolachlor export pathways and apportionment was a prerequisite to examine pesticide dissipation processes instream accounting for the input dynamics within the AVB. Overall, *S*-metolachlor concentration data emphasized periods of preferential input of *S*-metolachlor within the AVB through surface runoff and subsurface flow. Complementarily, CSIA data suggested homogeneous apportionment of *S*-metolachlor along the AVB during low flow periods.

4.3.3 *S*-metolachlor dissipation in the AVB: transport dominates over degradation

Instream degradation of *S*-metolachlor – The ratios of water flows between S1 and S2 (Q_{S1}/Q_{S2}) steadily decreased from 2.8 in March to ≈ 1.5 in October (see Figure IV.3), indicating that water flow alongside the river reach decreased over time. In the absence of punctual discharges alongside the river reach, $Q_{S1}/Q_{S2} > 1$ was attributed to upwelling and lateral water fluxes entering the AVB. Upwelling fluxes were estimated $> 0.10\text{ m}\cdot\text{d}^{-1}$ based on the geometry and the base-flow conditions described in Text S5. Under such hydrological conditions, the apportionment of dissolved species from the overlying water (*e.g.* dissolved oxygen, dissolved organic carbon and also pollutant)

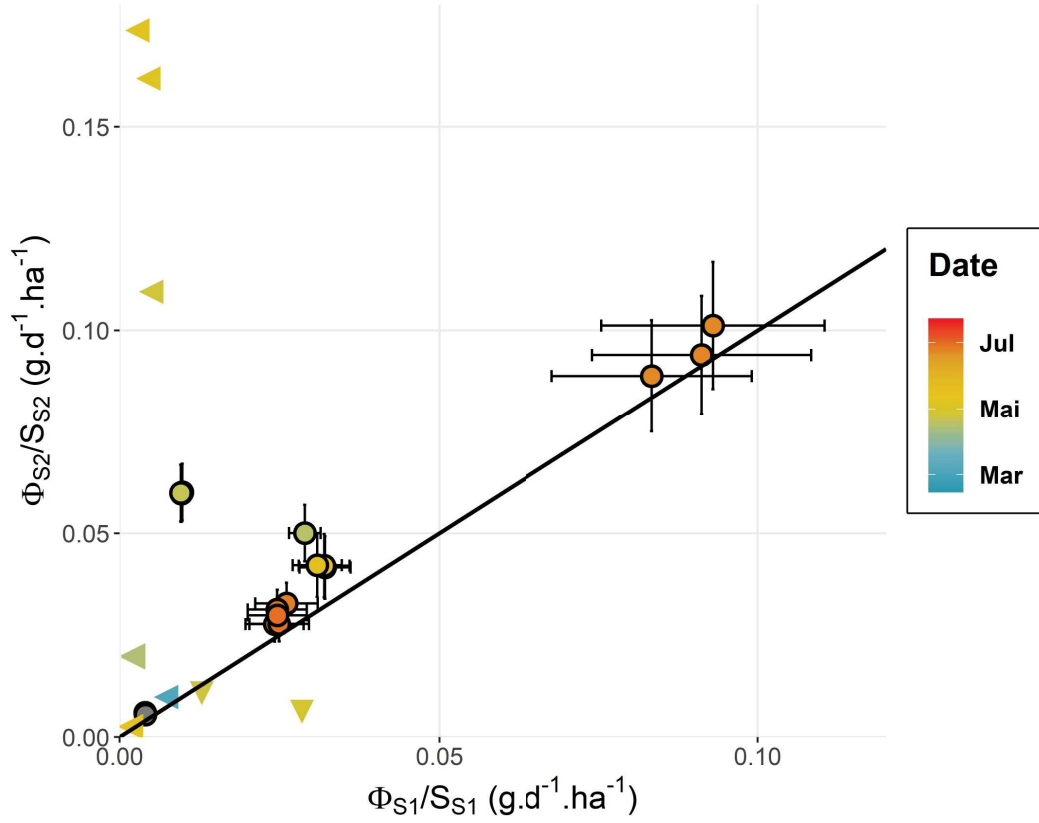


Figure IV.5 – Area normalized *S*-metolachlor mass loads in *S1* vs *S2*. All data were calculated when discharges and concentrations were simultaneously acquired during more than 19 hours per day (80% of a day duration). Values with concentrations in *S1* or *S2* lower than the quantification limits are depicted with triangles. The black line represents the 1:1 line. Points and triangles in green represent events during early *S*-metolachlor application on *C2* that are not reflected in *S1* (prior May 14).

into the riverbed sediment is limited, as confirmed by our FRT model (see section III) and observed in previous studies [Fox et al., 2014, Galloway et al., 2019]. Consequently, once *S*-metolachlor penetrates the overlying water of the AVB it is mainly transported downstream with limited interactions with the riverbed sediment. In addition, limited apportionment of dissolved species also alters redox gradients in the riverbed sediment, thereby limiting the diversity of microbial structures and possibly their ability to degrade pollutants [Krause et al., 2013, Nogaro et al., 2013, Zarnetske et al., 2011].

Consequently, even when pesticides are transported across the riverbed sediment to the AVB river reach (*i.e.* apportionment from subsurface flow), it may not be significantly degraded in the riverbed. Field observations reported that nitrates in upwelling NO_3^- rich groundwater with water velocities of about 0.15 m.d^{-1} were not degraded when crossing the riverbed sediment due to a lack of organic matter apportionment from the overlying water of a 200 m England river reach. Furthermore, limited instream geomorphic structures on the bottom of the AVB riverbed (*e.g.* debris, bed forms, dams, meanders, etc.) did not favour local dissolved species mixing in the riverbed. Instream geomorphic structures would have increased microbial activity as well as *S*-metolachlor residence time in the riverbed sediment, hence favouring its degradation alongside the AVB [Herzog et al., 2018, Hester and Doyle, 2008, Peter et al., 2019]. Worth noting, as no downwelling conditions, (*i.e.* river water crossing the riverbed sediment toward groundwater,) were observed during the study period, negligible pollution of groundwater from overlying river water are expected in our case [Fox et al., 2014]. Altogether, our results support the hypothesis of limited *S*-metolachlor degradation instream [Binley et al., 2013, Byrne et al., 2015].

Meanwhile, laboratory experiments, although hardly transferable to riverine conditions [Honti et al., 2018], advocate for negligible *S*-metolachlor degradation in the AVB river. Considering limited interactions with the riverbed sediment, photo- and bio-degradation between S1 and S2 would occur in the overlying water only. The combined effects of both photodegradation and biodegradation in the AVB is estimated less than 2%. This value was estimated using the laboratory derived half-lives for photodegradation and biodegradation and the Maning-Strickler relationship to estimate pollutant transit time from water velocity (transit time between 1.4 and 1.7 h, see calculation details in appendix C.S8). The considered half-lives were 6 days for *S*-metolachlor photodegradation under simulated sunlight irradiation with high nitrate concentrations (see section 3.9, value corresponding to an average water height of 15 cm), and 30 days for *S*-metolachlor oxic biodegradation (see Chapter II). Hydrolysis was excluded from this analysis since hydrolysis half-lives of *S*-metolachlor are far longer than the transit time in the AVB [Masbou et al., 2018].

CSIA data also support the idea that *S*-metolachlor degradation alongside the AVB river from May to June remained limited during the study period. Indeed, insignificant changes in *S*-metolachlor $\delta^{13}C$ values between S1 and S2 ($p = 0.04$, with $|\Delta_{S1-2}\delta^{13}C| = 0.6\text{‰}$, with measurement uncertainty of $|\Delta\delta^{13}C| = 0.4\text{‰}$, $n = 18$), suggested limited

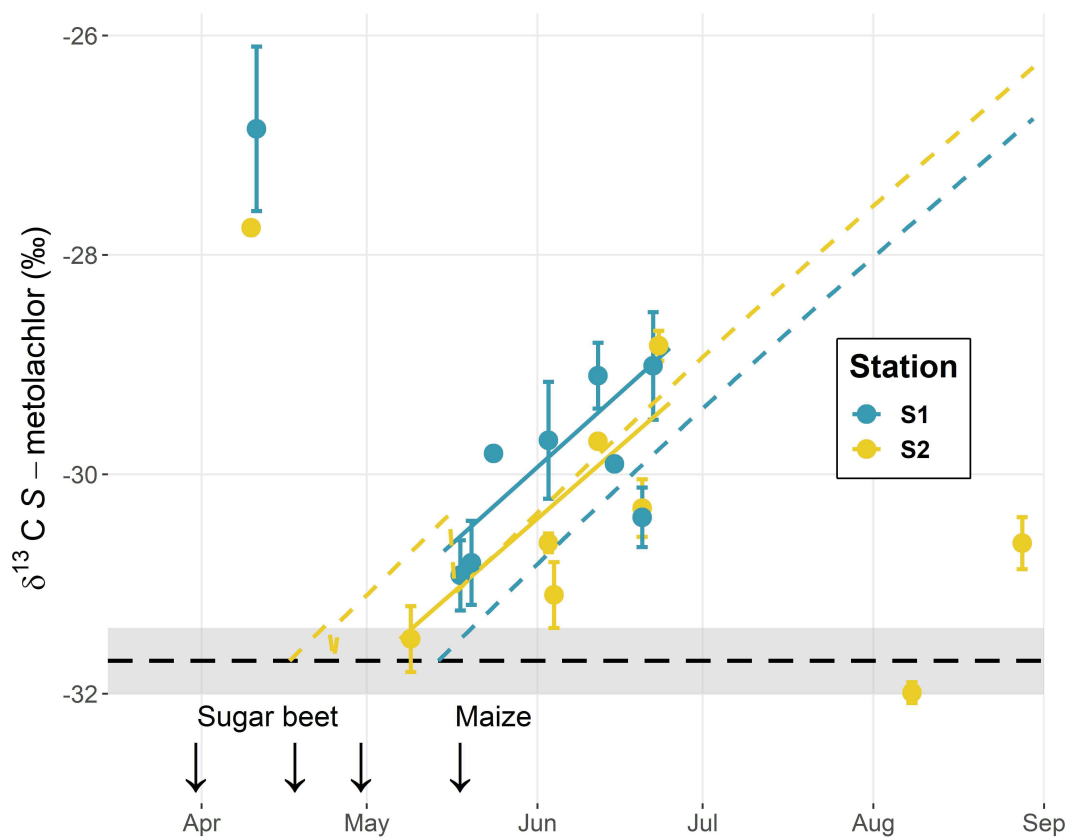


Figure IV.6 – Dissolved *S*-metolachlor $\delta^{13}\text{C}$ values in S1 and S2. Predicted *S*-metolachlor isotope compositions in soils (dashed lines). $\delta^{13}\text{C}$ values in April correspond to the remaining, non-degraded fraction of *S*-metolachlor of the 2018 agricultural season. Regression lines (solid lines) were obtained from ANCOVA analysis, assuming a fixed slope and highlight the insignificant differences in averaged isotope signatures evolution between S1 and S2.

S-metolachlor degradation during its transport alongside the AVB river (see appendix C.S7 for the $\delta^{13}\text{C}(t)$ origin equivalency test). Nonetheless, considering a minimal C isotope enrichment of 2‰ required to reliably attest for the occurrence of *S*-metolachlor degradation [Alvarez-Zaldívar et al., 2018], and that only biodegradation and not photodegradation may cause significant C isotope fractionation, instream biodegradation of *S*-metolachlor below 80% cannot be detected using C-CSIA.

***S*-metolachlor interactions with the riverbed sediment** – Although dominant upwelling conditions limited the riverbed sediment to act as a *S*-metolachlor sink, the sediment may also act as a *S*-metolachlor source in the AVB river, when it releases *S*-metolachlor to the overlying water. For instance, *S*-metolachlor concentrations in the AVB river was slightly higher than the base-flow value during a few days after event 8, although the low sampling resolution did not allow to ascertain it (see figure IV.7 and appendix C.S9). A long-lasting subsurface transport following this particularly wet period can be ruled out since flow rapidly converged back to the baseline value [Leu et al., 2004].

We hypothesized that soil-bounded *S*-metolachlor transported from the fields by surface runoff and deposited on the riverbed during event 8 progressively desorbed, thereby contributing to the long lasting *S*-metolachlor load in the AVB river [Jarsjö et al., 2017, Le Gall et al., 2016]. The TSS peak during event 8 indicated transport of soil particles within the AVB (see figure IV.7B). In addition, *S*-metolachlor was found at S1 and S2 within the top 1st cm of the riverine sediment following event 8 (July 17 - 1.7 ± 0.1 and $2.5 \pm 0.2 \mu\text{g} \cdot \text{kg}_{\text{sediment}}^{-1}$), whereas *S*-metolachlor concentrations were otherwise systematically below the quantification limit ($< 1.0 \mu\text{g} \cdot \text{kg}_{\text{sediment}}^{-1}$, see appendix C.S10). One exception to the above statement was attributed to an accidental contamination either in field or laboratory. Eroded soil particles likely carried fresh, undegraded *S*-metolachlor to the AVB river, as suggested by isotopically lighter *S*-metolachlor measured in water during event 8 ($\Delta\delta^{13}\text{C} = 1.4 \pm 0.8\text{‰}$) (see figure IV.7C). Soil particle-bound *S*-metolachlor entering the AVB river expectedly desorbed to equilibrate with the overlying water, either directly in the river or during the storage in the autosampler before sample extraction in laboratory, as it was previously found to have low affinity with the DOM fraction [Boithias et al., 2014]. This also indicates that for transient events carrying large amount of TSS, collected samples extraction in laboratory should be faster than the sorption equilibration time. Otherwise, the ratio of TSS bounded *S*-metolachlor over freely dissolved may be biased. This may explains that *S*-metolachlor was never quantified in TSS in this study, due to the weekly sample collection longer than the equilibration time of pesticide sorption generally assumed around 24 hours [OECD, 2000]. This is further supported by the fact that *S*-metolachlor sorption coefficient K_d on the souffel sediment was found close to zero (non-significant regression with the batch sorption experiment presented in Chapter II, section 2.1).

S-metolachlor contributed more significantly to the MEL_{SM} (21%) in the eight days following event 8 (June 27), whereas TPs dominated ($> 95\%$ of the MEL_{SM} - ESA and OXA - see figure IV.7D) in the previous (May 31) and following (July 25) periods. The predominance of ESA and OXA under low flow conditions in May 31 and July 25 is consistent with the prevailing transport of *S*-metolachlor and its TPs by subsurface flow. This was previously related to the lower K_{oc} values and higher solubilities of ESA and OXA than *S*-metolachlor (see appendix C.S2) [Lefrancq et al., 2017b]. In addition, the predominance of ESA vs OXA further advocates for subsurface transport processes as ESA has a lower affinity with the solid phase than OXA [Rose et al., 2018]. Comparatively, larger contribution of *S*-metolachlor to the MEL_{SM} was generally observed during direct input from runoff following intense or long rainfall events [Lefrancq et al., 2017b, Leu et al., 2004]. Hence, larger contribution of *S*-metolachlor to the MEL_{SM} during the tailing period following event 8 can be attributed to fresh *S*-metolachlor released from the riverbed sediment itself and not from direct field contribution.

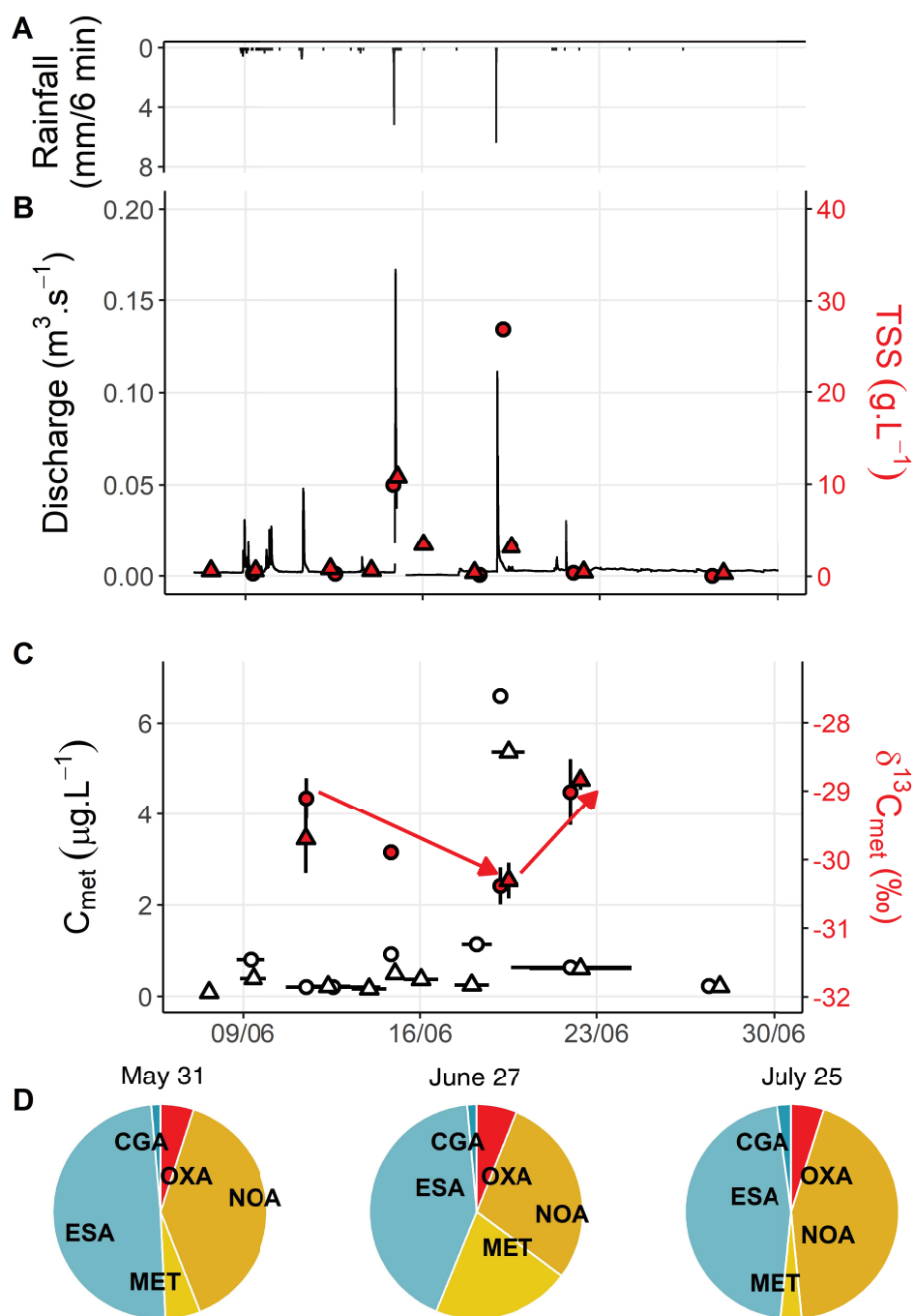


Figure IV.7 – Rainfall (A), river discharge in S1 and TSS concentrations in S1 (red circles) and S2 (red triangles) (B), S-metolachlor concentration and stable isotope signatures for rainfall-runoff events 5 to 9 in S1 (circles) and S2 (triangles), horizontal black lines express the periods covered by each sample (C) and relative contribution of S-metolachlor and its TPs to the MEL_{SM} (D)

4.4 Environmental significance and outlook for CSIA use in rivers

This study evaluated pesticide transport and dissipation in the AVB river, and highlights the potential and limits of using CSIA in the rivers. CSIA proved useful to evaluate the apportionment of non-point source pollution under dynamic hydrological conditions [Ouyang et al., 2017]. Hydrological and *S*-metolachlor concentration data suggested a homogeneous apportionment alongside the AVB river reach during low flow conditions. CSIA data suggested similar degradation extent in soil of C1 and C2 catchments ($87 \pm 2\%$, ≈ 4 months after applications) and transport pathways toward the AVB river. This further supported the idea of a homogeneous *S*-metolachlor apportionment alongside the AVB river reach during low flow conditions.

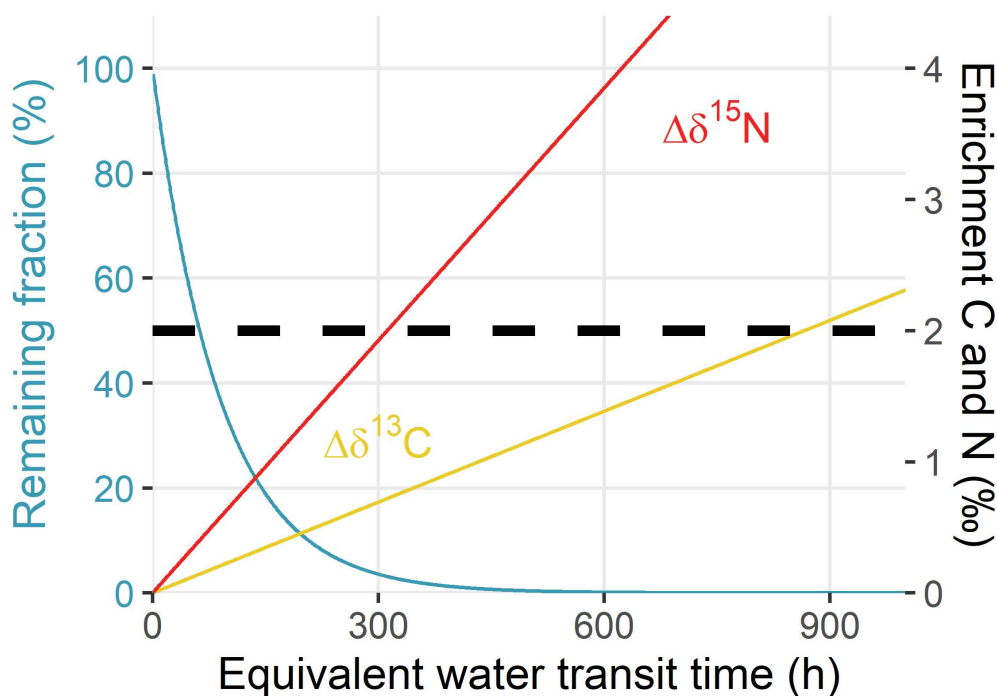


Figure IV.8 – Predicted C and N enrichment during *S*-metolachlor degradation with increasing water transit time. The black dashed line corresponds to the analytical uncertainty $\Delta\delta^{13}\text{C} = \Delta\delta^{15}\text{N} = 2.0\text{‰}$ reported for this work.

Along with analysis of *S*-metolachlor loads between S1 and S2, CSIA data suggested

that *S*-metolachlor persisted in the AVB river. This was predominantly attributed to the upwelling fluxes in the AVB river, hampering *S*-metolachlor interactions with the riverbed sediment and favouring its rapid transport downstream. The slight *S*-metolachlor degradation in the AVB ($< 2\%$) estimated using results of laboratory experiments did not significantly alter the isotope composition of *S*-metolachlor ($\Delta\delta^{13}C < 0.6\text{‰}$). Using laboratory derived degradation rates, it is possible to estimate the *S*-metolachlor minimum residence time above which CSIA data would allow to quantify degradation extent instream when interactions between *S*-metolachlor and the riverbed sediment are favoured. Considering the photodegradation and biodegradation half-lives of *S*-metolachlor of 6 and 30 days, respectively, and enrichment factors of $\epsilon_N = -0.7 \pm 0.4\text{‰}$ for photodegradation and $\epsilon_C = -1.2 \pm 0.4\text{‰}$ for biodegradation (see Chapter II), a residence time in rivers exceeding 800 *h* would be required to measure significant C isotope fractionation (see figure IV.8). The minimal C isotope fractionation reflecting instream degradation is considered to be $\Delta\delta^{13}C = 2.0\text{‰}$ as previously suggested in Alvarez-Zaldívar et al. (2018) [Alvarez-Zaldívar et al., 2018]. Considering a maximal pollutant retardation in the river of two as compared with water transit time, caused by interactions with the riverbed sediment or instream vegetation [Liao et al., 2013, Salehin et al., 2003], CSIA may be used in rivers with equivalent water transit time (*i.e.*, $\tau_{eq} = v_{water}/L_{river}$ with v_{water} and L_{river} being the overlying water velocity and the river length respectively) of about 400 *h* (≈ 17 days) (see figure IV.8 and calculation details in appendix C.S11). Considering the same threshold for $\Delta\delta^{15}N = 2.0\text{‰}$, N-CSIA would more easily reflect instream degradation with residence time of about 300 *h* only (≈ 12 days). However, N-CSIA faces analytical challenges with environmental samples (*e.g.* matrix effects and lower fraction of N atoms than C atoms in *S*-metolachlor leading to less sensitive analysis at equivalent *S*-metolachlor concentrations), and was not possible in this study. This advocates for further developments on N-CSIA for future research. Further analytical developments may also help increasing the sampling temporal resolution required to obtain a sufficient pesticide amount for C- and N- CSIA. In this study, C-CSIA of *S*-metolachlor in transient events was not possible. As rapid changes in hydrological regimes in rivers may alter the river degradation potential due to exchange at the SWI [Byrne et al., 2014], event-based analysis with higher temporal resolution monitoring should also be attempted with CSIA to confirm the absence of degradation in the AVB river. Altogether, this highlights the potential of CSIA to evaluate instream pesticide degradation in large rivers with long transit time, where the occurrence of micro-pollutant degradation is still debated in the literature [Honti et al., 2018].

Overall, our results suggest that *S*-metolachlor transport and dissipation at catchment scale is mainly controlled by degradation in field top-soil. Once in rivers, *S*-metolachlor is transported downstream with limited mass reduction, leading to downstream contamination of water resources. Hence, preventing pesticides to enter into rivers is a key lever to limit pesticide contamination of water resources.

Bibliography

- [Alvarez-Zaldívar et al., 2018] Alvarez-Zaldívar, P., Payraudeau, S., Meite, F., Masbou, J., and Imfeld, G. (2018). Pesticide degradation and export losses at the catchment scale: Insights from compound-specific isotope analysis (CSIA). *Water Research*, 139:198–207.
- [Alvarez-Zaldívar, 2018] Alvarez-Zaldívar, P. (2018). *Pesticide degradation and transport at catchment scale*. PhD thesis.
- [Binley et al., 2013] Binley, A., Ullah, S., Heathwaite, A. L., Heppell, C., Byrne, P., Lansdown, K., Trimmer, M., and Zhang, H. (2013). Revealing the spatial variability of water fluxes at the groundwater-surface water interface. *Water Resources Research*, 49(7):3978–3992.
- [Boithias et al., 2014] Boithias, L., Sauvage, S., Merlina, G., Jean, S., Probst, J.-L., and Sánchez Pérez, J. M. (2014). New insight into pesticide partition coefficient K_d for modelling pesticide fluvial transport: Application to an agricultural catchment in south-western France. *Chemosphere*, 99:134–142.
- [Boithias et al., 2011] Boithias, L., Sauvage, S., Taghavi, L., Merlina, G., Probst, J.-L., and Sánchez Pérez, J. M. (2011). Occurrence of metolachlor and trifluralin losses in the Save river agricultural catchment during floods. *Journal of Hazardous Materials*, 196:210–219.
- [Byrne et al., 2014] Byrne, P., Binley, A., Heathwaite, A. L., Ullah, S., Heppell, C. M., Lansdown, K., Zhang, H., Trimmer, M., and Keenan, P. (2014). Control of river stage on the reactive chemistry of the hyporheic zone. *Hydrological Processes*, 28(17):4766–4779.
- [Byrne et al., 2015] Byrne, P., Zhang, H., Ullah, S., Binley, A., Heathwaite, A. L., Heppell, C. M., Lansdown, K., and Trimmer, M. (2015). Diffusive equilibrium in thin films provides evidence of suppression of hyporheic exchange and large-scale nitrate transformation in a groundwater-fed river. *Hydrological Processes*, 29(6):1385–1396.

- [Elsner, 2010] Elsner, M. (2010). Stable isotope fractionation to investigate natural transformation mechanisms of organic contaminants: principles, prospects and limitations. *Journal of Environmental Monitoring*, 12(11):2005–2031.
- [Elsner and Imfeld, 2016] Elsner, M. and Imfeld, G. (2016). Compound-specific isotope analysis (CSIA) of micropollutants in the environment — current developments and future challenges. *Current Opinion in Biotechnology*, 41:60–72.
- [Felsot et al., 2010] Felsot, A. S., Unsworth, J. B., Linders, J. B., Roberts, G., Rautman, D., Harris, C., and Carazo, E. (2010). Agrochemical spray drift; assessment and mitigation—A review*. *Journal of Environmental Science and Health, Part B*, 46(1):1–23.
- [Fenner et al., 2013] Fenner, K., Canonica, S., Wackett, L. P., and Elsner, M. (2013). Evaluating Pesticide Degradation in the Environment: Blind Spots and Emerging Opportunities. *Science*, 341(6147):752–758.
- [Fischer et al., 2016] Fischer, A., Manefield, M., and Bombach, P. (2016). Application of stable isotope tools for evaluating natural and stimulated biodegradation of organic pollutants in field studies. *Current Opinion in Biotechnology*, 41:99–107.
- [Fox et al., 2014] Fox, A., Boano, F., and Arnon, S. (2014). Impact of losing and gaining streamflow conditions on hyporheic exchange fluxes induced by dune-shaped bed forms. *Water Resources Research*, 50(3):1895–1907.
- [Galloway et al., 2019] Galloway, J., Fox, A., Lewandowski, J., and Arnon, S. (2019). The effect of unsteady streamflow and stream-groundwater interactions on oxygen consumption in a sandy streambed. *Scientific Reports*, 9(1):19735.
- [Herzog et al., 2018] Herzog, S. P., Higgins, C. P., Singha, K., and McCray, J. E. (2018). Performance of Engineered Streambeds for Inducing Hyporheic Transient Storage and Attenuation of Resazurin. *Environmental Science & Technology*, 52(18):10627–10636.
- [Hester and Doyle, 2008] Hester, E. T. and Doyle, M. W. (2008). In-stream geomorphic structures as drivers of hyporheic exchange. *Water Resources Research*, 44(3).
- [Honti et al., 2018] Honti, M., Bischoff, F., Moser, A., Stamm, C., Baranya, S., and Fenner, K. (2018). Relating degradation of pharmaceutical active ingredients in a stream network to degradation in water-sediment simulation tests. *Water Resources Research*, 54(11):9207–9223.

- [Jarsjö et al., 2017] Jarsjö, J., Chalov, S. R., Pietroni, J., Alekseenko, A. V., and Thorslund, J. (2017). Patterns of soil contamination, erosion and river loading of metals in a gold mining region of northern Mongolia. *Regional Environmental Change*, 17(7):1991–2005.
- [Krause et al., 2017] Krause, S., Lewandowski, J., Grimm, N. B., Hannah, D. M., Pinay, G., McDonald, K., Martí, E., Argerich, A., Pfister, L., Klaus, J., Battin, T., Larned, S. T., Schelker, J., Fleckenstein, J., Schmidt, C., Rivett, M. O., Watts, G., Sabater, F., Sorolla, A., and Turk, V. (2017). Ecohydrological interfaces as hot spots of ecosystem processes. *Water Resources Research*, 53(8):6359–6376.
- [Krause et al., 2013] Krause, S., Tecklenburg, C., Munz, M., and Naden, E. (2013). Streambed nitrogen cycling beyond the hyporheic zone: Flow controls on horizontal patterns and depth distribution of nitrate and dissolved oxygen in the upwelling groundwater of a lowland river. *Journal of Geophysical Research: Biogeosciences*, 118(1):54–67.
- [Kronvang et al., 2004] Kronvang, B., Strøm, H., Hoffmann, C., Laubel, A., and Friberg, N. (2004). Subsurface tile drainage loss of modern pesticides: field experiment results. *Water Science and Technology*, 49(3):139–148.
- [Le Gall et al., 2016] Le Gall, M., Evrard, O., Foucher, A., Laceby, J. P., Salvador-Blanes, S., Thil, F., Dapigny, A., Lefèvre, I., Cerdan, O., and Ayrault, S. (2016). Quantifying sediment sources in a lowland agricultural catchment pond using ^{137}Cs activities and radiogenic $^{87}\text{Sr}/^{86}\text{Sr}$ ratios. *Science of The Total Environment*, 566–567:968–980.
- [Lefrancq et al., 2017a] Lefrancq, M., Dijk, P. V., Jetten, V., Schwob, M., and Payraudeau, S. (2017a). Improving runoff prediction using agronomical information in a cropped, loess covered catchment. *Hydrological Processes*, 31(6):1408–1423.
- [Lefrancq et al., 2017b] Lefrancq, M., Payraudeau, S., Guyot, B., Millet, M., and Imfeld, G. (2017b). Degradation and Transport of the Chiral Herbicide S-Metolachlor at the Catchment Scale: Combining Observation Scales and Analytical Approaches. *Environmental Science & Technology*, 51(22):13231–13240.
- [Leu et al., 2004] Leu, C., Singer, H., Stamm, C., Müller, S. R., and Schwarzenbach, R. P. (2004). Simultaneous Assessment of Sources, Processes, and Factors Influencing Herbicide Losses to Surface Waters in a Small Agricultural Catchment. *Environmental Science & Technology*, 38(14):3827–3834.

- [Lewandowski et al., 2019] Lewandowski, J., Arnon, S., Banks, E., Batelaan, O., Betterle, A., Broecker, T., Coll, C., Drummond, J. D., Gaona Garcia, J., Galloway, J., Gomez-Velez, J., Grabowski, R. C., Herzog, S. P., Hinkelmann, R., Höhne, A., Hollender, J., Horn, M. A., Jaeger, A., Krause, S., Löchner Prats, A., Magliozzi, C., Meinikmann, K., Mojarrad, B. B., Mueller, B. M., Peralta-Maraver, I., Popp, A. L., Posselt, M., Putschew, A., Radke, M., Raza, M., Riml, J., Robertson, A., Rutere, C., Schaper, J. L., Schirmer, M., Schulz, H., Shanafield, M., Singh, T., Ward, A. S., Wolke, P., Wörman, A., and Wu, L. (2019). Is the hyporheic zone relevant beyond the scientific community? *Water*, 11(11):2230.
- [Liao et al., 2013] Liao, Z., Lemke, D., Osenbrück, K., and Cirpka, O. A. (2013). Modeling and inverting reactive stream tracers undergoing two-site sorption and decay in the hyporheic zone. *Water Resources Research*, 49(6):3406–3422.
- [Lutz et al., 2017] Lutz, S. R., van der Velde, Y., Elsayed, O. F., Imfeld, G., Lefrancq, M., Payraudeau, S., and van Breukelen, B. M. (2017). Pesticide fate at catchment scale: conceptual modelling of stream CSIA data. *Hydrol. Earth Syst. Sci. Discuss.*, 2017:1–30.
- [Lutz et al., 2013] Lutz, S. R., van Meerveld, H. J., Waterloo, M. J., Broers, H. P., and van Breukelen, B. M. (2013). A model-based assessment of the potential use of compound-specific stable isotope analysis in river monitoring of diffuse pesticide pollution. *Hydrol. Earth Syst. Sci.*, 17(11):4505–4524.
- [Maggi et al., 2019] Maggi, F., Tang, F. H. M., Cecilia, D. I., and McBratney, A. (2019). PEST-CHEMGRIDS, global gridded maps of the top 20 crop-specific pesticide application rates from 2015 to 2025. *Scientific Data*, 6(1):1–20.
- [Masbou et al., 2018] Masbou, J., Drouin, G., Payraudeau, S., and Imfeld, G. (2018). Carbon and nitrogen stable isotope fractionation during abiotic hydrolysis of pesticides. *Chemosphere*, 213:368–376.
- [Nogaro et al., 2013] Nogaro, G., Datry, T., Mermillod-Blondin, F., Foulquier, A., and Montuelle, B. (2013). Influence of hyporheic zone characteristics on the structure and activity of microbial assemblages. *Freshwater Biology*, 58(12):2567–2583.
- [OECD, 2000] OECD (2000). *Test No. 106: Adsorption – Desorption Using a Batch Equilibrium Method*. Organisation for Economic Co-operation and Development, Paris.

- [Ouyang et al., 2017] Ouyang, W., Gao, X., Wei, P., Gao, B., Lin, C., and Hao, F. (2017). A review of diffuse pollution modeling and associated implications for watershed management in China. *Journal of Soils and Sediments*, 17(6):1527–1536.
- [Peter et al., 2019] Peter, K. T., Herzog, S., Tian, Z., Wu, C., McCray, J. E., Lynch, K., and Kolodziej, E. P. (2019). Evaluating emerging organic contaminant removal in an engineered hyporheic zone using high resolution mass spectrometry. *Water Research*, 150:140–152.
- [Ravier et al., 2005] Ravier, I., Haouisee, E., Clément, M., Seux, R., and Briand, O. (2005). Field experiments for the evaluation of pesticide spray-drift on arable crops. *Pest Management Science*, 61(8):728–736.
- [Rose et al., 2018] Rose, C. E., Coupe, R. H., Capel, P. D., and Webb, R. M. T. (2018). Holistic assessment of occurrence and fate of metolachlor within environmental compartments of agricultural watersheds. *Science of The Total Environment*, 612:708–719.
- [Salehin et al., 2003] Salehin, M., Packman, A. I., and Wörman, A. (2003). Comparison of transient storage in vegetated and unvegetated reaches of a small agricultural stream in Sweden: seasonal variation and anthropogenic manipulation. *Advances in Water Resources*, 26(9):951–964.
- [Sandin et al., 2018] Sandin, M., Piikki, K., Jarvis, N., Larsbo, M., Bishop, K., and Kreuger, J. (2018). Spatial and temporal patterns of pesticide concentrations in streamflow, drainage and runoff in a small Swedish agricultural catchment. *Science of The Total Environment*, 610-611:623–634.
- [Shaw et al., 2019] Shaw, S., Beslity, J., and Colvin, M. (2019). Working Toward a More Holistic Set of Hydrologic Principles to Teach Non-Hydrologists: Five Simple Concepts Within Catchment Hydrology. *Hydrological Processes*, page hyp.13485.
- [Torabi et al., 2020] Torabi, E., Wiegert, C., Guyot, B., Vuilleumier, S., and Imfeld, G. (2020). Dissipation of S-metolachlor and butachlor in agricultural soils and responses of bacterial communities: Insights from compound-specific isotope and biomolecular analyses. *Journal of Environmental Sciences*, 92:163–175.
- [Van Breukelen, 2007] Van Breukelen, B. M. (2007). Quantifying the Degradation and Dilution Contribution to Natural Attenuation of Contaminants by Means of an Open System Rayleigh Equation. *Environmental Science & Technology*, 41(14):4980–4985.

- [Ward, 2016] Ward, A. S. (2016). The evolution and state of interdisciplinary hyporheic research. *WIREs Water*, 3(1):83–103.
- [Zarnetske et al., 2011] Zarnetske, J. P., Haggerty, R., Wondzell, S. M., and Baker, M. A. (2011). Labile dissolved organic carbon supply limits hyporheic denitrification. *Journal of Geophysical Research: Biogeosciences*, 116(G4).

Chapter V

General conclusions

5.1 Introduction

The intrinsic complexity of pesticide fate in surface waters - Pesticides are ubiquitous in surface waters, threatening biodiversity and public health [de Souza et al., 2020]. Their occurrence is likely to be increasingly frequent over the next decade [Maggi et al., 2019]. Accordingly, understanding pesticide fate in soils and water is a topical issue which has already been addressed at catchment scale [Alvarez-Zaldívar et al., 2018, Chen et al., 2017b] or in specific environmental compartments with the objective to examine and improve attenuation and remediation options (*e.g.* riparian or river buffer zones) [Dollinger et al., 2019, Feld et al., 2018]. While rivers are the intrinsic outlet of all catchments, their degradation potential with respects to pesticides is poorly known. In either dynamic or static surface waters (*e.g.* rivers or ponds), the sediment-water interface (SWI) was already demonstrated as a highly reactive area where pollutants processing (*e.g.* macro-pollutants; nitrates, organic matter – micro-pollutants; pharmaceuticals) may control water quality [Krause et al., 2017]. The strong inter-connectivity of surface waters with their surrounding environment, as well as their high spatial and temporal dynamic limit a thorough examination of mechanisms and factors influencing their reactivities [Boano et al., 2014, Lansdown et al., 2015, Ward, 2016]. Current gaps of knowledge arising from this complexity and motivating the present thesis can be summarized as follows:

- I. Individual degradation processes at stake in surface waters are not well characterized for pesticides. The main factors controlling the extent and distribution of pesticides across the SWI still need to be identified [Katagi, 2016];
- II. Although modes of pollutant transport at the SWI are well described in the literature, the interplay between transport and degradation processes is poorly

understood, especially under highly spatial (*e.g.* vertical/lateral fluxes) and temporal (*e.g.* transient low/high flow) conditions [Boano et al., 2014];

- III. The pesticide degradation potential of rivers is only postulated from analogy with research focusing on nutrient processing at the SWI, but remains poorly characterized and mechanistically understood [Lewandowski et al., 2019].

Current methodological shortcomings - From a methodological point of view, a major bottleneck to achieve great advances in understanding pesticide fate in surface waters, is the segregation of approaches focusing either on laboratory microcosms experiments, mesocosms tracer experiments, river scale investigations with or without numerical modelling [Lewandowski et al., 2019]. Microcosm experiments allow to investigate individual processes and are easy to conduct with replications but may only partly reflect processes at stake in field [Katagi, 2016]. Mesocosm tracer experiments are conceptually between field investigations and microcosm experiments, and allow basic investigations on the interplay between transport and degradation processes but at the expense of a higher experimental effort [Jaeger et al., 2019]. Modelling used in combination with most complex experimental works can address non-measurable and intertwined processes, including individual contributions of degradation and transport mechanisms to the global dissipation, provided accurate and suited mathematical formulations [Liao et al., 2013]. A key way of improvements underscored in most recent reviews on pollutant processing at the SWI is to combine several of these approaches from multi-disciplinary and -scale perspectives [Krause et al., 2017, Lewandowski et al., 2019, Ward, 2016]. This is expected to strengthen knowledge acquired from individual methodologies, thus overcoming their intrinsic limits and allowing for a more systematic understanding of pesticide processing at the SWI [Jaeger et al., 2019].

Research approach - In this context, we developed a consistent set of simple, interdisciplinary and robust experimental and modelling procedures, to improve the understanding of the SWI functioning. The ultimate goal of such conceptualization was to provide an easily up-scalable knowledge of pesticide fate at the SWI of static and dynamic surface waters. First, individual characterizations of hydrolysis, photodegradation and biodegradation at the SWI brought elementary descriptions of main degradation processes expected at the SWI (Chapter II). The distribution and the interplay of these processes across the SWI were investigated using a second experimental step including a semi-integrative bench-scale river channel mimicking typical transport processes occurring in river systems (Chapter III). In parallel, to improve the inter-

pretation of laboratory data and initiate the projection towards field-scale studies, a comprehensive mathematical framework was built. This framework is original because it captured and revealed the interplay of degradation and transport processes under all theoretical hydrological conditions typical of surface water. Finally, a first attempt for upscaling laboratory and numerical insights at river scale was attempted and disclosed main analytical, monitoring and numerical locks still holding (Chapter IV). Altogether, this work unveiled the potential of building a bottom to top multi-disciplinary approach toward a more systematic and thorough understanding of pesticide fate in surface waters.

Outline — Here we first discuss the relevance of the proposed experimental setup for the characterization of individual degradation processes under static and dynamic conditions. Experimental insights are then discussed with respects to the best suited mathematical formulation. As a complementary line of evidence, CSIA has the potential to provide unconditional information on pesticide degradation at the SWI, and we review accordingly, its emerging perspectives and limitations. Knowledge from this thesis work may serve future methodological research and help sharpening monitoring campaigns of pesticide dissipation in surface waters. Finally, as an operational research project, I provide some guidelines to the water resource stakeholders based on lessons learned from this thesis. These may be implemented in the future to follow river water quality and meet quality standards.

5.2 Laboratory testing procedures to understand pesticide fate in surface waters

5.2.1 General discussion

To date, thousands of synthetic pollutants display trace concentrations ($pg.L^{-1}$ to $ng.L^{-1}$) in surface waters. The persistence of these diversified pollutants (*e.g.* pesticides, pharmaceuticals, industrial chemicals and by-products) depends on their hydrophobicity and their propensity to partition with the organic matter (*i.e.* particulate, colloids or dissolved), affecting their bioavailability and transport in environmental compartments [Wenning and Martello, 2014]. Accordingly, predicting the fate of these pollutants in the environment, requires to understand underlying transport, sorption and degradation mechanisms across relevant environmental compartments. Although recent advances in quantitative structure-activity relationships (QSARs) proved re-

liable to predict main properties governing organic pollutant fate in homogeneous phases (*e.g.* adsorption/desorption coefficient, biotic and abiotic degradation rates), this method still struggles to predict pollutant behaviour in complex, heterogeneous and biological systems (see the special issue on this topic for recent information [Fenner and Tratnyek, 2017]). Accordingly, in complex environmental systems, only heuristic and statistical approaches are available with somehow high degree of uncertainties [Servien et al., 2014]. Accordingly, **laboratory tests in microcosms remain to date an efficient tool to acquire mechanistic understanding on factors governing pesticide degradation, as well as molecule-specific dissipation indicators for environmental risk assessment** [Katagi, 2016]. However, improperly designed experimental procedures may hamper the extrapolation of laboratory derived indicators to actual environmental systems [Honti et al., 2018].

To address this issue, a minimal but robust serie of laboratory tests dedicated to the assessment of pollutant fate at the SWI was designed and tested on S-metolachlor. Hydrolysis, photodegradation and biodegradation were separately investigated. The first interest of developing a complete serie of laboratory tests is the possibility to **ensure strong consistency between distinct experimental setups, hence strengthening experimental reproducibility**. For instance, the use of synthetic freshwaters mimicking the ionic composition of typical soft surface waters [Smith et al., 2002, Katagi, 2016] allowed to investigate all degradation processes with a minimal variability and to compare results among experimental setups. Second, hydrochemical parameters controlling degradation mechanisms can be precisely and individually studied over a wide range of relevant environmental conditions. For instance, typical hydrochemistry of agriculturally impacted surface waters only required to adjust nitrate and DOC concentrations to the original synthetic freshwater. In this way, although photodegradation was known to be greatly influenced by the presence of nitrates and DOM, experimental data with high nitrate concentrations and moderate DOC (*i.e.* $[NO_3^-] > 20 \text{ mg.L}^{-1}$ and $DOC = 5 \text{ mg}_C.\text{L}^{-1}$) were critically lacking in the literature so far [Remucal, 2014].

A second originality of the experimental test procedure developed in this thesis is that along with the usual batch biodegradation experiments (*i.e.* OECD 308) marred by experimental inaccuracies and limited field of validity (*i.e.* static surface waters – lakes, ponds, etc.), we went one step further with a dynamic biodegradation experiment. This experiment taking place in a recirculated flume allowed to assess the relationship

between transport and degradation processes inherent of dynamic surface waters (*e.g.* rivers, stormwater ponds, etc.). Upsides associated with such approach are numerous:

I. Aerobic and strictly anaerobic conditions represent both extreme cases that may either be found in the first mm of sediment bed (*i.e.* fully oxic sediment layer) or much lower once all electron acceptors are consumed (*i.e.* below 10 cm deep) [Akbarzadeh et al., 2018]. However, intermediate anaerobic conditions (*i.e.* nitrates, manganese, iron, sulphate reductions) are much less considered and studied (see the rapid decrease of potential final electron acceptors during the strictly anaerobic biodegradation experiment). However, pesticide biodegradation in such conditions is largely unknown, and potentially occurring through different mechanisms and at different associated rates [Ghattas et al., 2017, Sims and Kanissery, 2019]. By contrast, the 10 cm deep sediment bed reproduced within the bench-scale river channel allowed to observe the effect of this progressively shifting redox gradient with depth as witnessed by the oxic gradient developing across the SWI. In contrast, since caffeine mostly degraded within the overlying water, it revealed insensitive to the oxygen gradient developing at the SWI. Thus, this also confirms the potential to identify favourable hydrochemical conditions where degradation may predominate at the SWI with recirculated flume experiments.

II. When aiming at characterizing sorption in river systems, **evaluation of pollutant sorption coefficient within the recirculated flume brings more accurate and robust values of phase partitioning coefficients.** Continuous shacking typically applied during biodegradation microcosm experiments is likely to modify pesticide sorption properties and affect biodegradation rates. Harsh shacking in similar systems was previously hold responsible for sediment grinding resulting in freshly exposed sediment surfaces and subsequent enhanced sorption [Shrestha et al., 2016]. Over-estimation of the experimentally determined Foron Blue 291 adsorption coefficient under continuous shaking (*i.e.* batch sorption experiment undergoing similar shacking than biodegradation microcosms) as compared with the numerically calibrated value within the bench-scale river channel confirmed the experimental bias arising from microcosms experiments.

III. **The complex interplay between degradation, sorption and transport mechanisms arising at the SWI of rivers is reflected within the recirculated flume.** As described in Chapter II, successively conducting conservative (*i.e.* NaCl), sorptive (*i.e.* Foron Blue 291) and reactive tracer experiments (*i.e.* caffeine) within the recirculated flume, can precisely inform on pollutant penetration rate (*i.e.*

conservative), sorption within the sediment bed (*i.e.* sorptive) as well as pinpoint compartments of preferential degradation at the SWI (*i.e.* reactive) [Fernandez-Pascual et al., 2020]. Furthermore, by replacing the sediment (*e.g.* high *vs* low permeability) and varying water flows, the interplay between transport and degradation can be tested for a wide panel of environmentally representative conditions. Thus, in contrast to half-life values derived from batch experiments (*i.e.* DT_{50} in temporal unit such as days) which are hardly extrapolated to environmental systems [Honti et al., 2018], degradation rates observed within the recirculated flume more accurately reflect river conditions. Accordingly, they may be normalized by the river length (*i.e.* DD_{50} half-life distances in river length unit such as kilometers) as proposed in Kunkel et al. (2008), which constitute a more robust representation of actual river systems [Kunkel and Radke, 2008].

Although no DD_{50} were derived for S-metolachlor with the recirculated flume, a summary of experimental results obtained from batch experiments is presented below. This complete dataset provides a global overview of S-metolachlor degradation at the SWI (see Figure V.1). It may be further used as a set of parameters for risk assessment and fate modelling as described in Section 5.3.

On the one hand, abiotic degradation processes were dominated by sunlight mediated degradations. Both direct and indirect photodegradation processes quickly degraded S-metolachlor with half-life values < 4 days. While direct photodegradation may vary over space and time (*e.g.* water chemistry, solar spectrum variations, etc.), indirect photodegradation is likely more consistent in surface waters with high nitrate concentrations (*i.e.* $> 20 \text{ mg.L}^{-1}$). By contrast, under typical river conditions with $pH < 9$ and $T < 30^\circ\text{C}$, abiotic hydrolysis was negligible with half-life values > 200 days. Also, the absence of degradation in the sterile anoxic control conducted in parallel of the biodegradation experiment confirmed the negligible effect of chemical reactions with abiotic catalysts such as (poly)sulfides that may occur in low redox environments [Fenner et al., 2013, Loch et al., 2002]. On the other hand, biodegradation prevailed under oxic conditions, with a degradation half-life of S-metolachlor ≈ 30 days (> 200 days under anoxic conditions). Accordingly, only the first mm of sediment bed displaying oxic conditions are expected to be particularly reactive as regards to pesticide degradation. Then, instream structures favouring oxygen penetration within the sediment bed (*e.g.* water falls) would favour pesticide degradation at the SWI. On the contrary, oxygen depletion in both the overlying water and the sediment bed subsequent to river eutrophication would significantly hamper pesticide degradation. It may also

be expected that pesticides entering the river from the bottom of the sediment bed (*i.e.* from groundwater under upwelling conditions or subsurface flow) is likely not degraded across the SWI as anoxic upwelling waters drastically limit the extension of the oxic layer at the SWI [Galloway et al., 2019].

Sorption mainly controlled pesticide dissipation at the SWI. Indeed, the effective degradation rate of S-metolachlor during aerobic dissipation was inferred twice higher than actually reflected in the two-phase system (dissipation half-life ≈ 60 days). Sorption depleted the available dissolved fraction of S-metolachlor within sediment porewater, hence limiting degradation rates [Honti et al., 2018]. In addition, in the recirculated flume, about half of the initial Foron Blue 291 mass was sorbed within the sediment bed by the end of the experiments, hence limiting the dissolved concentrations. Conversely, as observed when comparing the modelled pollutant penetration with (*i.e.* Foron Blue 291) and without (*i.e.* saline solution) sorption, it limited pollutant penetration within the upper layer of the sediment bed where pesticide degradation is the most likely occurring (*i.e.* oxic layer). Thus, while sorption proved to slow down pesticide degradation due to depletion of dissolved concentrations, it may also increase pesticide residence time within the highly reactive oxic layer of the sediment bed. Although not tested with S-metolachlor within the recirculated bench-scale river channel (mostly due to its long degradation rates observed in microcosms experiments that would have hamper methodological developments in the bench-scale river channel), this experimental setup revealed the crucial role played by sorption on S-metolachlor dissipation at the SWI of rivers.

5.2.2 Implications and perspectives

Overall, the methodology developed in this thesis was suited to retrieve environmentally relevant persistence indicators of S-metolachlor. It may be further implemented and improved in future studies with other pesticides or micropollutants. To that end, one should pay particular attention to the use of sunlight analogues (*e.g.* Xenon lamp) instead of UV lamps when aiming at deriving environmentally relevant photodegradation characteristics for organic micropollutants. In agriculturally impacted surface waters, indirect photodegradation is expected to dominate pesticide photodegradation. The use of a UV lamp may thus lead to overestimating the role direct and nitrate mediated mechanisms at the expense of DOM mediated photodegradation [Apell and McNeill, 2019]. Second, environmentally relevant kinetics can only be derived under sunlight analogue conditions [Zeng and Arnold, 2013]. Third, patterns of transforma-

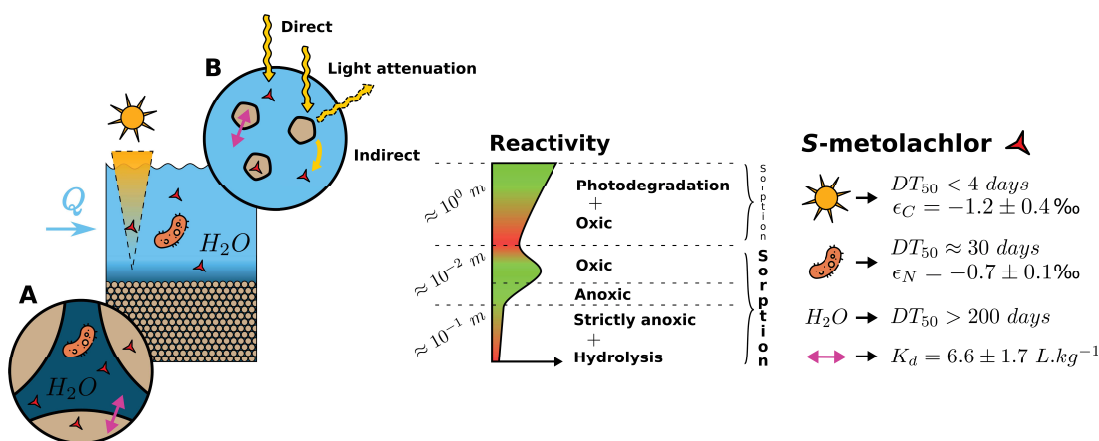


Figure V.1 – Schematic representation of the SWI functioning (left) and reactivity (middle). Panel A focuses on the porous sediment bed. Panel B focuses on the overlying water and represents suspended solids. Although not represented here, sorption to dissolved organic matter is equivalent to suspended solids. *S-metolachlor* is partitioned between liquid and solid phases and degradation processes are distributed within the compartments where they are expected to occur according to this work. Typical degradation rates and sorption strength are summarized in the legend (right)

tion products and stable isotope fractionation revealed distinct between UV lights and sunlight analogue. Accordingly, misinterpretation of environmental sample measurements may arise even when CSIA and transformation product analysis are combined to infer degradation extent from experimental values derived with UV lights.

The use of a recirculated flume experiment mimicking dynamic conditions typical of rivers in addition to the microcosm setups is also advised to derive molecule-specific patterns of degradation. Indeed, while degradation of organic pollutants were previously identified within the oxic part of the sediment layer [Posselt et al., 2020], caffeine unexpectedly degraded within the overlying water. Nonetheless, this experimental setup presumably remains suited to study the impact of the oxygen layer thickness for slowly degrading molecules within the overlying water.

However, the recirculated flume faces shortcomings. First, experiments with caffeine revealed the need for additional microbial characterizations within the sediment and the overlying water. Indeed, a "lag-phase" hardly rationalized apart from a microbiological point of view was observed for caffeine degradation within the recirculating

flume. In addition, degradation within the overlying water could only be inferred from numerical evidences but not confirmed and understood from a mechanistic point of view. Genomic DNA with real-time PCR of 16s rRNA to characterize species richness, Shannon diversity and bacterial activity or even protein-stable isotope probing (protein-SIP) may help understanding microbial response within the recirculated flume and assess their relevance in actual rivers [Iribar et al., 2008, Jehmlich et al., 2016, Posselt et al., 2020]. Second, the small volume of water ($\approx 2\text{ L}$) within the experimental setup forced us to work with high pollutant concentrations ($\sim \text{mg.L}^{-1}$, typical caffeine concentrations in surface water $\sim \mu\text{g.L}^{-1}$ [Korekar et al., 2020]). Such concentrations may directly affect the aquatic life (*i.e.* algal, fungal species or bacteria) which develop within the bench-scale river channel and provides biodegradation potential [Staley et al., 2015]. This may results in biased observations and conclusions about pesticide degradation in rivers. Online monitoring of pollutant concentrations with a spectrofluorometer would help reducing pollutant concentrations spiked by adjusting sampling frequencies and volumes to periods of increased interest (*e.g.* strong degradation extents). Study with pesticides in the bench-scale river channel may also benefit from spectrofluorometric techniques as pesticides display specific and distinct excitation-emission spectra [Hassoun et al., 2017].

Overall, recirculated bench-scale river channels have a strong potential not only for hydraulic research, but also for simplified laboratory investigations of biogeochemical processing at the SWI that reflect actual river conditions. First, it allows for a reproducible, fast and simple testing strategy. Second, thanks to its conception, distinguishing between lumped transport and degradation processes at the SWI is achievable by spatially distributed monitoring and balanced sampling frequencies, which is rather hampered in batch microcosm experiments for instance [Honti et al., 2016]. Third, it may benefit to plenty of additional fields of research investigating SWI processes such as sediment early diagenesis [Paraska et al., 2014] or analysis of microbial structure and activity at the SWI [Nogaro et al., 2013, Posselt et al., 2020]. As called by the most recent reviews on pollutant fate at the SWI, this experimental setup perfectly suit to interdisciplinary developments aiming at deriving first holistic knowledge of micropollutant fate at the SWI [Krause et al., 2017, Lewandowski et al., 2019, Ward, 2016].

Altogether, a mechanistic understanding of pesticide fate at the SWI requires to account for the oxic zonation as well as sorption within the sediment bed. In well homogenized systems, direct observations individually reflect these processes. In contrastst, for

transient conditions within complex environmental compartments (*e.g.* bi-phasic sediment bed) a mathematical framework capable of distinguishing between co-occurring and potentially antagonistic degradation, phase partitioning and transport processes is required

5.3 A robust and parsimonious mathematical framework tailored to the studied system

5.3.1 General discussion

River systems are complex compartments where pesticides undergo spatially and temporally variable transport and degradation processes [Fenner et al., 2013]. As a consequence, the direct interpretation of experimental data and the acquisition of compartment and process specific persistence indicators further used for risk assessment or environmental fate investigations, is challenging [Honti and Fenner, 2015]. Within the bench-scale river channel, the potentially antagonist effect of sorption described above would hardly be interpreted from direct observation of experimental data. A major postulate of my thesis is that deepening and upscaling the understanding of the SWI functioning from the simplistic static microcosms to the dynamic bench-scale river channel and ultimately to actual river systems requires developing specific mathematical frameworks [Wang et al., 2019]. To do so, developing and validating flow reactive transport (FRT) models along with laboratory experiments are advised [Krause et al., 2017]. However, to ensure model robustness and avoid over-parametrization, the right level of complexity should be pursued and physically-based models favoured over empirical and conceptual schemes [Her and Chaubey, 2015]. In particular, simulated processes as well as their mathematical formulations should suit the actually investigated environmental compartment. Accordingly, the previously described experimental procedure was used to develop a parsimonious and holistic mathematical framework tailored to predict the interplay between pesticide transport and degradation at the SWI.

In a two phases system, a first challenge in converging toward the best suited mathematical representation is the occurrence of pollutant partitioning (*i.e.* sorption in the case of the SWI) greatly influencing both degradation and transport mechanisms as demonstrated in the previous section. Pollutant sorption onto sediment grain may show varying properties depending on the biogeochemical and hydrological conditions and the molecule physico-chemical properties [Ciffroy, 2018]. Amongst others are the sorption strength controlling the ratio of dissolved *vs* bounded pollutant mass, sorption kinetics and reversibility, respectively governing short and long term pollutant transport and bioavailability at the SWI:

I. At trace concentrations ($< \mu\text{g}.L^{-1}$) pesticide sorption onto riverbed sedi-

ment at the SWI displayed a linear isotherms. Dependency of pollutant affinity with a sorbent matrix (*e.g.* sediment) is related to pollutant molecular properties and nature of the organic fraction of the sorbent matrix itself [Mamy et al., 2014]. This affinity influences the shape of the sorption isotherm determining whether a sorption site saturation should be accounted for (*e.g.* Freundlich, Langmuir, BET, etc.) or not (*i.e.* linear) [Limousin et al., 2007]. Within the Avenheimerbach sediment, sorption isotherms of the herbicides acetochlor, atrazine, S-metolachlor and terbutryn as well as of the fungicide metalaxyl revealed linear up to 10 mg.L^{-1} spiked in water. Another study also demonstrated quasi-linear sorption of 15 pesticides onto riverbed sediment (*i.e.* good fit with both linear and Freundlich isotherms with $n \approx 1$) [Radović et al., 2016]. Altogether, it advocates for the use of a linear isotherm to reproduce pesticide sorption onto river sediment.

II. Pesticide sorption onto riverbed sediment may be, in a first effort of simplification, considered as time-independent and reversible. Pesticide sorption onto unsaturated soils has been reported to be time-dependant with an increase of partitioning coefficient values due to micropore and diffusion in the intra-organic matter [Gulkowska et al., 2016]. This fraction is often considered as non-bioavailable and accordingly requires a two-site – one rate modelling approach to be accounted for [van Genuchten and Wagenet, 1989, Shrestha et al., 2016]. However, in the absence of specific studies on this phenomenon for pesticides on saturated riverbed sediments, we suggest that this effect is negligible in aquatic sediments. Indeed, constant partitioning coefficients of pesticides within the 300 days of the biodegradation microcosm experiments were observed. In addition, within the recirculated flume, Foron Blue 291 revealed a perfectly reversible sorption behaviour.

III. Finally, as rivers are highly dynamic systems, event-based modelling of pesticide fate requires implementation of a kinetic sorption formalism and should be accompanied with the appropriate experimental procedure. Conversely, pesticide fate in ponds or lakes may better rely on the less parameterized equilibrium formulation. Most water quality models including pollutant fate assume that partitioning between sediment porewater and sediment particles is instantaneously equilibrated [Ciffroy, 2018]. While this assumption is valid under static conditions involving slow (*i.e.* diffusion) or no transport processes (*i.e.* fully homogeneous systems) [Honti et al., 2016] it is disputable for highly dynamic systems [Eylers et al., 1995, Liao et al., 2013]. For instance, the linear equilibrium sorption successfully used to interpret S-metolachlor biodegradation data within the

microcosm experiments, proved not suited to reproduce Foron Blue 291 penetration within the recirculated flume sediment layer. In the latter case, instantaneous sorption led to over-estimation of Foron Blue 291 sorption and an excessive retardation of its penetration within the sediment bed. Thus, kinetic sorption had to be considered to account for fast transport under dynamic conditions. However, this formulation introduces a supplementary parameter (*i.e.* sorption characteristic time - set to 24 hours for Foron Blue 291) that requires experimental determination by examining time-dependant sorption of the studied pollutant [Berez et al., 2016].

However, the ability of FB291 to mimic pesticide sorption is disputable. Indeed, while FB291 desorption proved fully reversible in our case, other authors reported partial reversibility of pesticide sorption in saturated forest buffer zone or wetland sediments [Passeport et al., 2011, Passeport et al., 2014]. FB291 sorption originates from the electrostatic interaction forces between its cationic form and the negatively charge surface of the sand sediment [Jada and Ait Akbour, 2014]. Nonetheless, while pesticides are slightly ionizable molecules (high pK_a), their sorption on natural organic matter involves different mechanisms such as covalent bonding to groups present at the surface of the organic material [Schwarzenbach et al., 2003]. Alternatively, the dye sulforhodamine B may be envisaged as it was previously observed to accurately mimic sorption of moderately [Lange et al., 2018] to strongly [Dollinger et al., 2017] hydrophilic pesticides on field soils.

Accordingly, seeking for **the most suited mathematical formalism for sorption is increasingly important when moving toward investigations of pollutant fate in river systems influenced by hydraulic forcing from surrounding compartments**. In most cases, conceptual or empirical modelling frameworks (*e.g.* black-box models [Jaeger et al., 2019] or conceptual arrangement of small boxes [Liao et al., 2013]) are used to interpret data from tracer experiments in laboratory flumes or directly from *in situ* tracer experiments that are featuring typical but non variable river conditions [Knapp et al., 2018, Ward, 2016]. Consequently, the use of non-physical or conceptual parameters that lump the interplay between transport, sorption and degradation processes hampers the systematic extrapolation of results to a representative panel of hydraulic forcing limiting further uses in larger and more complex environmental systems [Fox et al., 2014, Liao et al., 2013]. In line with the previous paragraph, it advocates for a systematic reconsideration of the best suited formalism for sorption.

A fine and two dimensional discretization of the SWI is necessary to capture small scale processes at a mechanistic level. Most current modelling frameworks

focus on reproducing the overall mass exchange at the SWI [Voermans et al., 2018]. In such conditions, capturing small scale vertical variations of degradation potential caused by millimetre wide inhomogeneities (*e.g.* redox gradients, hydraulic short-circuit generated by wood debris on the riverbed) is hampered. Consequently, at river scale, predicting and identifying hot-spots of pollutant degradation caused by instream geomorphologic structures is unabled. To tackle this issue, we fully discretized the SWI across two dimensions alongside the SWI, and explicitly treated separately transport, sorption and degradation processes. As a proof of concept, with only minor calibration steps, oxygen diffusion was well reproduced for varying overlying water flows. Altogether, it highlights the strong potential of the modelling approach developed in this thesis to physically reproduce degradation processes at a vertical mm scale and over long horizontal scales (*i.e.* tested for a 1 m long river reaches).

An additional level of complexity arises from the control of surface/groundwater exchanges on pollutant fate in actual river systems [Byrne et al., 2014]. As confirmed by the comparison of flow and S-metolachlor mass loads across the Avenheimerbach river reach, surface/groundwater exchanges likely controlled the extent of pollutant processing at the SWI of rivers [Byrne et al., 2015]. However, this feature is barely captured by current FRT models. In contrast, **the FRT model developed here allowed to integrate surface/groundwater exchanges without additional parameterization**. Numerical simulations confirmed the suppression of pollutant incorporation by the sediment bed under upwelling conditions. In other words, the developed FRT model mechanistically accounts for both horizontal and vertical hydraulic forcing which constitutes a major breakthrough toward a deepened understanding of the influence of surface/groundwater exchanges on pollutant processing at the SWI [Flipo et al., 2014].

5.3.2 Implications and perspectives

One major achievement of these parallel numerical and experimental developments is the ability to refine current persistence indicators at the SWI for a wide panel of pollutants and conditions (*i.e.* static – ponds, lakes, etc. or dynamic – rivers, stormwater ponds, etc.). Indeed, the slow increase in complexity offered by the successive batch and recirculated experiments allows to build the most suited mathematical framework for each molecule. In addition, it offers a normalized and environmentally relevant option to acquire and process data to derive persistence indicators with minimal extra experimental work as compared with current OECD procedures. Subject to the implementation of the validation steps described in section 5.2, such a procedure may

largely benefit the European pesticide registration procedures [Honti et al., 2018]. As a first step, half-life values and partitioning coefficients derived from the batch experiments (*i.e.* slightly modified from the OECD 308 and 106 protocols) may be directly used as input parameters for the FRT model over a normalized numerical SWI domain (see Figure V.2) to **automatically convert DT_{50} to the more environmentally relevant DD_{50} as a function of hydrological forcing and geomorphologic properties of rivers (*e.g.* sediment permeability, bedforms)**. As compared with the current OECD serie of batch experiments required for pesticide registration, only one additional experiment in the recirculated flume would be required to ensure indicator robustness (see Figure V.2). One may even think that for analog series of molecules (*e.g.* amides, organophosphorus, traizine, etc.), similar mathematical framework for sorption and biodegradation may be used, reducing again the experimental labour required.

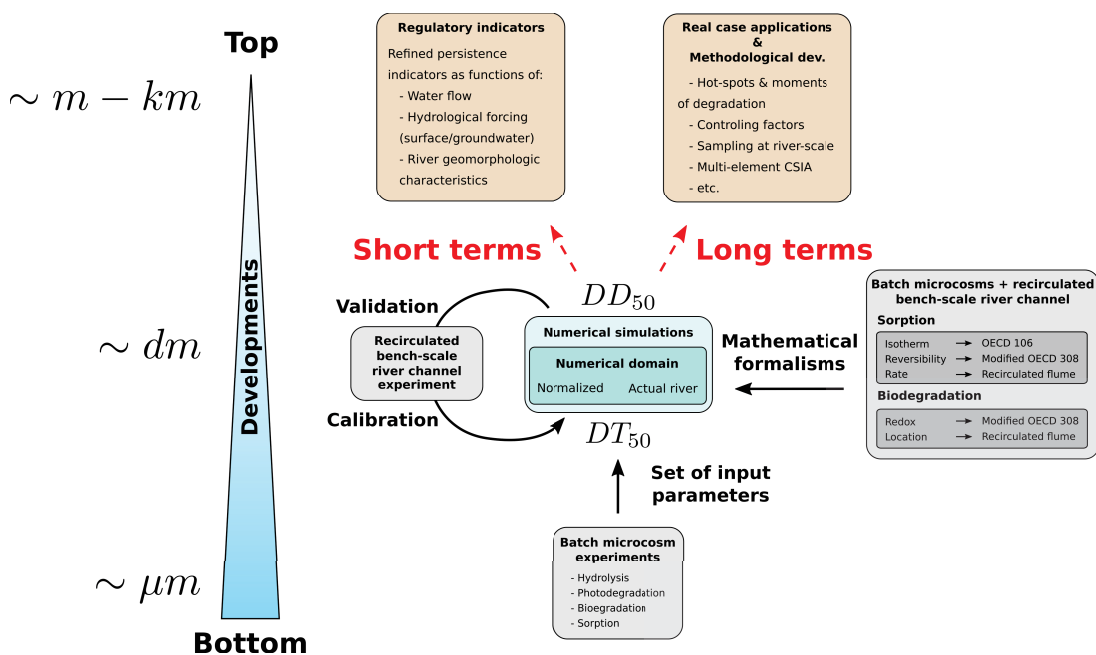


Figure V.2 – Representation of the bottom to top and micro to macro scale methodologies applied in this thesis work. From simplistic laboratory scale experiments (grey boxes), pollutant fate in surface waters is understood and predicted via a coupling between bench-scale river channel and numerical modelling (green box). In this way, DT_{50} are converted to DD_{50} . Red and discontinuous arrows represent short term and long term perspectives partly achieved in this work.

This mechanistic conceptualization also paves the way for a more systematic investigation of the hierarchical order of factors controlling pollutant fate at the SWI from small scales (*i.e.* $\sim 10\text{ cm}$ to 1 m , bed-forms, redox gradients, etc.) to catchment scales (*i.e.* up to 100 km^2 , meanders, dams, regional groundwater, etc.) [Flipo et al., 2014]. To do so, complementary in-house numerical models accurately reproducing pesticide transport from field to rivers [Alvarez-Zaldivar, 2018] and surface/subsurface hydrological forcing at catchment scale [Jeannot et al., 2018] should be coupled with the SWI model presented in this thesis [Boano et al., 2014, Lewandowski et al., 2019]. Such a perspective would nonetheless requires further developments to account for additional transport and degradation processes relevant when studying the river at catchment scale:

I. For pollutants mostly degraded in the sediment bed, a more **complete representation of redox zonation would be necessary to account for the contribution of aerobic and (strictly) anaerobic biodegradation processes.** The same applies to batch biodegradation experiments that should also be conducted under intermediate and controlled anaerobic conditions. Numerically speaking, that may be achieved by implemented in our FRT model the most recent sediment diagenesis mathematical frameworks including anammox and dissimilatory nitrate reduction to ammonium (DNRA) [Akbarzadeh et al., 2018]. Doing so, the FRT model would also become a relevant alternative to the current sediment diagenesis models relying on simplified representations of transport processes at the SWI [Paraska et al., 2014].

II. Numerically reproducing sediment re-suspension is also required for catchment scale applications. The substantial pollutant sorption to sediment observed in the biodegradation microcosms and the bench-scale river channel, suggests that re-suspended sediment may carry significant fractions of pesticide downstream. This is all the more important since total suspended solids (TSS) ranked high in the Avenheimerbach during the monitoring campaign (up to 50 g.L^{-1}). The same applies to dissolved organic matter particles sizing between 0.22 and $0.45\text{ }\mu\text{m}$ that are believed to carry significant share of sorbed pesticides when abundant in rivers [Wang et al., 2019]. To that purpose, the recently published generalized Engelund–Hansen relationship could be implemented to accurately predict fine-grained sediment re-suspension and TSS concentrations [Ma et al., 2019]. An explicit account for sediment deposition is also of great importance as fine sediment deposition clogs riverbeds, affecting biogeochemical processing at the SWI [Jin et al., 2019]. Coupling predictions of sediment re-suspension alongside rivers with sediment apportionment from fields would also be

relevant at catchment scale to further explain variations of sorption properties observed with increasing suspended solid concentrations in rivers [Boithias et al., 2014].

5.4 CSIA from molecular to river scales to characterize pesticide fate at the SWI: potential, limits and perspectives.

While the coupling between experimental and modelling developments already constitute a robust methodology, in complex environmental systems where pollutant undergo co-occurring transport and degradation processes, assessing pesticide fate becomes challenging and predictions highly skewed [Elsner and Imfeld, 2016]. Although several studies achieved experimental estimations of pollutant fate in river systems they mostly focused on point source pollutions discharged at well identified rates and location within rivers [Knapp et al., 2018, Kunkel and Radke, 2011, Lewandowski et al., 2011]. This constitutes an essential difference with pesticide pollutions which are non-point source. Indeed, for non-point source pollutions, rivers constitute a “second order compartment” where pesticide inputs are greatly influenced by prior transport and degradation processes occurring in fields [Chen et al., 2017a]. Accordingly, the identification of pesticide inputs into river systems is more difficult, further complicating the identification of their instream degradation at catchment scale. CSIA recently proved helpful in identifying pesticide sources in rivers [Alvarez-Zaldívar et al., 2018, Lutz et al., 2017]. Nonetheless, the question remains open on its potential to identify and even better quantify the respective role of involved degradation mechanisms in rivers. Relying on these recent insights, pesticide CSIA was used at every step of the development of this thesis to eventually produce a clear overview of its current and future potential to assess pesticide fate at the SWI and more prospectively, in river systems.

From a molecular scale perspective, CSIA revealed its potential to directly evaluate pesticide instream degradation. The joint analysis of enrichment factors derived for S-metolachlor biodegradation and photodegradation, revealed that multi-element C and N CSIA may help distinguishing between individual degradation processes at the SWI. Indeed, contrasted and complementary enrichment patterns were observed for biodegradation ($\epsilon_C = -1.2 \pm 0.4\text{‰}$ and $\epsilon_N \approx 0\text{‰}$) and indirect photodegradation ($\epsilon_C \approx 0\text{‰}$ and $\epsilon_N = -0.7 \pm 0.1\text{‰}$). Extrapolating to river scale, this confirms that punctual comparisons of C and N pesticide isotopic composition from two distant sampling points alongside a river reach could provide a direct line of evidence of instream bio- or photodegradation, provided that sufficient instream degradation occurred ($> 30\%$ and $> 50\%$ for bio- and photodegradation considering analytical uncertainties of $\Delta\delta^{13}C = 0.4\text{‰}$ and $\Delta\delta^{15}N = 0.5\text{‰}$). Conversely, the absence of iso-

topic enrichment on both or either atoms would evidence no or low extent of instream degradation, pointing out pollutant persistence. Accordingly, it gives good confidence for similar analysis with other widely used and ubiquitous chloroacetanilides in surface waters with long residence time (*e.g.* high Strahler order rivers, wetlands, stormwater ponds, etc.), among which for instance, acetochlor or alachlor are representative chloroacetanilides [de Souza et al., 2020].

At river scale, CSIA also proved valuable to locate and quantify pesticide inputs alongside a studied river reach, making it a useful tool to address non-point pollution problems. Identifying locations of pesticide inputs within river systems is of great importance since pollutant crossing the SWI from subsurface or groundwater may undergo different degradation mechanisms than pollutant entering from the overlying water directly [Byrne et al., 2015]. As previously demonstrated by Lutz et al. (2017), $\delta^{13}C$ values closely related to soil isotopic signatures hint towards pesticide inputs within the river from subsurface (*i.e.* deepest subsurface layers of soil or groundwater). On the contrary, $\delta^{13}C$ values closer to the initial commercial product signatures hints towards an increasing penetration of pesticides from the surface (*i.e.* shallow subsurface flow or surface runoff, which nonetheless also tend to be depleted with time) [Lutz et al., 2017]. In this way, the comparison of long-term temporal evolution of instream and soil isotopic compositions can be used to delineate boundaries crossed by pesticides at the SWI. For instance, in the case of the Avenheimerbach river, pesticide predominantly entered into the river from subsurface or groundwater as $\delta^{13}C$ values measured in the river along the monitoring season closely followed the predicted soil isotopic signatures.

CSIA may also help evaluating homogeneity of pesticide inputs alongside the studied river reach when assessing instream degradation. Indeed, hydraulic shortcuts caused by cracks in clayey soils for examples and discharging at the middle of the studied river reach may significantly bias the estimated mean transit time of pesticides [Kronvang et al., 2004]. Also, uneven pesticide degradation in field caused by spatial variations of soil permeability, riparian vegetation [Feld et al., 2018] or land-use [Dollinger et al., 2019] may hamper a direct comparison of $\delta^{13}C$ values in the river from up- to downstream. In this context, a similar evolution from up- to downstream of long-term trends as well as similar responses of $\delta^{13}C$ values to rain events can help confirming negligible effects of spatially variable infield conditions on the observed instream degradation.

The absence of significant differences in S-metolachlor isotopic composition under low

and high flow conditions within the Avenheimerbach ($\Delta\delta^{13}C < 0.6\text{‰}$) from up- to downstream may reflect negligible instream degradation (estimated $\approx 1.5\%$ in the Avenheimerbach) and consequently the pesticide persistence. In our case, this indicates that pesticide fate in headwater catchments is mainly controlled by degradation in field soils rather than in the river. Small rivers displaying comparable geomorphologic features than the Avenheimerbach (*i.e.* flat bed, low tortuosity and clayey sediment bed) are likely solely transport vectors for pesticides. Altogether, it emphasizes the crucial role of soil conservation strategies to enhance pesticide degradation in fields and limit pollutions of water resources [Joko et al., 2017].

On the other hand, these results also highlighted the current limitations of CSIA to monitor pesticide degradation instreams and the most imminent methodological development required.

I. The typical analytical uncertainties of C- and N-CSIA and the slight bulk enrichment factors measured for S-metolachlor hamper the identification of biodegradation and photodegradation lower than $\approx 45\%$ and $\approx 75\%$, respectively, but track pesticide persistence. Thus, pesticide CSIA would reveal more suited to quantify instream degradation in longer rivers or in shorter rivers characterized by intense pesticide degradation. However, for higher Strahler order rivers, additional pesticide pollution originating from urban or industrial amenities with distinct isotopic signatures than from agricultural areas would potentially blur the direct analysis of CSIA data from upstream to downstream [Masiol et al., 2018]. Alternatively, at equivalent river length, strong pollutant interactions with the sediment bed would favour higher pollutant residence transit time, degradation and isotopic fractionation [Briggs et al., 2014]. Future methodological developments may benefit from studies of fast degrading pharmaceuticals that already displayed similar isotopic behaviour than S-metolachlor as regards to photodegradation, biodegradation and hydrolysis in rivers [Maier et al., 2016]. Multi-element CSIA may further help decreasing the threshold below which degradation is not reflected by shifts in isotopic compositions. Cl and H atoms are good candidate to target. For instance, indirect photodegradation-induced H isotope fractionation of atrazine with proxies of DOM and nitrates displays strong enrichment factors of $\epsilon_H = -51.2 \pm 2.5\text{‰}$ and $\epsilon_H = -25.3 \pm 1.7\text{‰}$ [Hartenbach et al., 2008]. Similarly, the phenylurea herbicide isoproturon featured strong H isotope fractionation during biodegradation $< -20.8 \pm 2.2\text{‰}$ whereas ϵ_C and ϵ_N values were almost negligible [Penning et al., 2010]. Although analytical uncertainties associated with H-CSIA are generally higher than for C- and N-CSIA ($\pm 5\text{‰}$) [Penning et al.,

2010], significant degradation would be reflected from 18% and 21% for nitrate mediated atrazine photodegradation and isoproturon biodegradation in rivers. Cl-CSIA is also promising as nucleophilic substitution at the $C - Cl$ bond of chloroacetanilides and leading to S-metolachlor OXA was evidenced for all degradation mechanisms studied in this work. In addition, as chloroacetanilides have a unique Cl heteroatom, no “dilution” effects leading to smaller bulk enrichment factors would occur [Elsner et al., 2005]. Finally, the rapid emergence of succinate dehydrogenase inhibitors (SDHIs) fungicides [Reilly et al., 2012] often carrying fluorine atoms should also guide future methodological developments toward F-CSIA [Renpenning et al., 2017]. Since SDHIs have low to moderate mobility in soils and are persistence [Gulkowska et al., 2014], they may display similar behaviour in the environment than S-metolachlor. Accordingly, extensive pollution of water resources with SDHI may be anticipated by understanding their interactions in the environment following a similar methodology than developed in this thesis, provided that suited analytical methods are available.

II. Although high S-metolachlor concentrations (median $0.17 \mu g.L^{-1}$) were measured within the Avenheimerbach, N-CSIA was not possible, hampering the identification of photodegradation. N-CSIA is intrinsically more challenging than C-CSIA. Indeed, while C atoms constitute 63.5% of the total S-metolachlor mass, N atoms barely account for 5% and N-CSIA requires higher concentrations to be achieved (for $3 \mu L$ injected, S-metolachlor concentration required $> 314 mg.L^{-1}$, see Chapter II, Section 2.1) [Elsner and Imfeld, 2016]. In order to keep a sufficient temporal resolution to capture rainfall event responses of the Avenheimerbach, sampled volumes were limited to up to $2.8 L$ during low flow conditions. However, considering the median S-metolachlor concentration in the Avenheimerbach, water samples of $5.5 L$ would have been necessary to perform N-CSIA. Since S-metolachlor concentrations revealed highly variable within the Avenheimerbach, this value may only be used as a lower bound value enabling N-CSIA for half of the collected samples. In this context, once again, targeting pharmaceuticals with higher proportions of heteroatoms may also help near future methodological developments as they may more easily allow for N-, H- or Cl-CSIA (*e.g.* Metformin - $C_4H_{11}N_5$ – widely found in waste water treatment plant discharges [Posselt et al., 2020]).

III. Matrix effect due to organic material contained in environmental samples significantly limited the amount of water or soil/sediment extractable without precluding the chromatographic resolution of the GC-IRMS analysis. For instance, although the solid phase extraction of water samples led to quantitative ex-

traction of S-metolachlor (*i.e.* $\approx 100\%$), samples containing high content of dissolved organic carbon generated excessive matrix effect. This was characterised by a large analytical background (*i.e.* higher background than the pesticide peak or of the same order of magnitude) hampering reliable isotopic signature measurements. The same was observed for all soil samples. Accordingly, methodological developments focusing on improvements of pesticide extraction methodologies are required. Developments of molecularly imprinted polymers (MIPs) is a valuable way to explore as it allows for a selective clean-up of environmental samples and does not affect isotopic composition of the targeted compounds [Bakkour et al., 2018]. Preparative high performance liquid chromatography (HPLC) or case-specific selection of sorbent used for SPE extractions may also help to isolate the targeted compound although it may not reduce the background in the same extent as MIPs [Torrentó et al., 2019].

5.5 Perspectives

The results presented in this thesis highlight the potential of the developed methodology to investigate pesticide fate at the SWI under both static and dynamic conditions. Nonetheless, over this work several shortcomings arose from laboratory to field scale when attempting to observe, infer and predict pesticide fate at the SWI. Accordingly, results presented in this work are promising but still require experimental and numerical confirmations. Although pesticides are undoubtedly environmentally relevant molecules to study, their persistence somehow challenges methodological developments. Experimental characterizations of individual degradation pathways of S-metolachlor were very long (> 300 days for biodegradation, about 6 months of irradiation for photodegradation, > 200 days for hydrolysis at environmental pH due to high pK_a). As a consequence, studying pesticide degradation within the recirculated flume was uncertain and not attempted in the first instance and S-metolachlor degradation alongside the Avenheimerbach negligible. In my opinion, these shortcomings could be addressed at laboratory and field scales by the use of a fast degrading probe compound over the whole procedure presented in this thesis. On this basis, both scientific and operational aims could be achieved together (see red arrows in Figure V.2). First, from an operational point of view, one may confirm the validity of the procedure to shift from the less environmentally representative DT_{50} to the more suited DD_{50} (left pathway in Figure V.2). Eventually, a submission to the OECD of an advanced standardized protocol to assess pesticide degradation in surface waters could be envisaged. Second, from a scientific perspective, improvements of sampling strategies, analytical performances and modelling efficiencies may be achieved. This would benefit the understanding of pesticide fate in rivers in rivers at a higher spatial and temporal resolution than achieved here (right pathway in Figure V.2).

I. As a short-term perspectives (6 months internship), I would conduct again the complete serie of experimental procedures with the less persistent probe compound to derive DT_{50} and DD_{50} . To that end, the organic tracer resazurin appears as a good candidate as it is known to degrade in ≈ 1 hour in river sediments [Knapp et al., 2018] and to partition similarly to pesticides onto river sediments (linear sorption isotherm with $K_d \approx 1 \text{ mL.g}^{-1}$ reported for river sediment with $f_{oc} \approx 1\%$ [Lemke et al., 2014]). Then, quantitative comparisons of DT_{50} from batch experiments and DD_{50} experimentally derived in the recirculated flume and predicted would definitively demonstrate the validity of the proposed procedure to derive environmentally relevant persistence indicators. Furthermore, as resazurin is fast degraded at the SWI, it would be more

likely to rule out design flaws from the experimental and numerical frameworks. For instance, as it degrades up to 1000 times faster in sediment than in overlying water [Haggerty et al., 2009], it may confirm that caffeine degradation observed within the overlying water did not originate from experimental bias (*e.g.* biofilm formation on channel sides or tubing, excessive biomass in the overlying water due to rapid recirculation, etc.). From a scientific point of view, it may also reveal the crucial control of water flow pushing pollutant across the sediment bed in pollutant fate at the SWI, which was missed with caffeine.

II. Long-term perspectives (3 years - research proposal) may subsequently rely on the use of resazurin at larger scale. For low Strahler order rivers with short transit times (\sim hours), pesticide persistence hampered the direct quantification of instream degradation from combined concentration, transformation products and CSIA data analysis. Considering the current analytical limitations, the threshold of directly quantifiable instream degradation is rather high ($\approx 50\%$). Consequently, mechanistic investigations of pesticide degradation at river-scale is still hardly accessible from direct measurements in rivers. While analytical developments are advised to lower this threshold, numerical developments allowing to infer instream degradation solely from laboratory insights would be a complementary way to pursue. A serie of tracer experiments in the Avenheimerbach river with resazurin (non toxic) under different hydrological conditions (*e.g.* low *vs* high flow, upwelling *vs* downwelling conditions) would reveal different patterns of degradation, sorption and transport [Knapp and Cirpka, 2017]. Alternatively, one may also rely on a previously derived benchmark dataset of pharmaceutical degradations within a 12.5 km long river reach under favorable degradation conditions [Kunkel and Radke, 2012]. One may rely on numerical modelling to reproduce and explain these patterns solely from laboratory insight (short term perspectives). Doing so, factors controlling pollutant fate in rivers may be identified at high spatial and temporal resolution. As a consequence, such results would allow for systematic extrapolation of pollutant fate predictions for a large panel of pollutant and environmental conditions. Furthermore, it would shed light on promising sampling (*e.g.* passive *vs* active samplers, continuous *vs* flow-controlled discrete samplings, sampling locations and frequencies, etc.) and analytical methods (*e.g.* elements to target with CSIA, system- and period-specific analysis, etc.). While developments are still needed at laboratory and small river reach scales, as a very long term perspective (> 3 years), the coupling between the validated SWI FRT model with pesticide fate and hydrogeological models at catchment scale may be a promising way to better understand the fate of anthropogenic chemicals throughout all environmental compartments. Main

targets would be the achievements of systematic and accurate predictions of pollutant inputs (time and locations) and surface-groundwater exchanges.

5.6 Implications for water resource managers

The PolISO project was initially built to bring advanced knowledge on pesticide behaviour within the Avenheimerbach catchment and provide the water resource manager with the most relevant technical guidelines to meet the EU demand in terms of water quality conservation. Water resource managers often focus on the preservation and the increase of biodiversity to achieve good water quality but rarely consider the role played by the SWI [Lewandowski et al., 2019]. Although our results suggest that the Avenheimerbach has a limited pesticide degradation potential, these results also suggest that there is scope for progress.

I. Water residence time within the Avenheimerbach river should be increased as much as possible to favour instream degradation. One may think about recreating meanders which are completely absent for now (*i.e.* tortuosity of 1.1). However, even with a doubled residence time thanks to meanders, only limited water quality improvements are expected ($< 3\%$ degradation on the basis of the estimations developed in Chapter IV). Nonetheless, associated with the creation of meanders forming loops is the apparition of intra-meander hyporheic [Revelli et al., 2008]. It significantly increases pollutant residence time and degradation potential by forcing pollutant across meanders which display oxic and anoxic (nitrate- and iron- reducing) redox conditions favourable to pesticide degradation [Dwivedi et al., 2018]. Finally, river bank vegetation should be conserved as much as possible as it increases pollutant residence time within the river and act as a barrier limiting pesticide input from spray drift and surface runoff [Salehin et al., 2003].

II. Water and pollutant exchanges at the SWI should be forced to enable pesticide processing within the sediment bed. While the Avenheimerbach river faces upwelling water fluxes most of the time, only instream structures (*e.g.* wood debris, bedforms, obstacles, etc.) may help creating pumping flow alternatively entering and exiting the sediment bed [Boano et al., 2014]. Worth of note, enhanced exchanges at the SWI would not increase the risk of groundwater pollution from surface waters as the dominant upwelling conditions would hamper pollutant to cross the sediment bed. Artificial instream structures and engineered riverbed recently proved very efficient in reducing organic pollutant masses with rates $> 50\%$ [Herzog et al., 2018, Peter et al., 2019]. From a very local perspective, restoring the continuity of the sediment load currently broken by the presence of a nozzle upstream the investigated river reach, may also help increasing pollutant exchanges within the Avenheimerbach by increasing the

sediment hydraulic conductivity. Indeed, fine particle deposition is known to reduce by several times water and pollutant penetration within river sediment bed which may be counterbalanced by a strong sediment turnover [Jin et al., 2019].

III. From the observation of dominant subsurface transport of pesticides toward the Avenheimerbach river, we may also suggest the creation of buffering (*e.g.* vegetated strips) and riparian zones enabling S-metolachlor degradation before it enters the Avenheimerbach river [Dollinger et al., 2019, Feld et al., 2018].

However, although well described in the literature, the reported efficiencies of the proposed engineering actions are site-specific and cannot be directly extrapolated to the Avenheimerbach. Nonetheless, to date, the FRT model could directly provide order of magnitudes of efficiencies of the actions proposed in the river prior their implementation on the sole basis of the experimental characterizations of S-metolachlor degradation pathways.

In a nutshell, although less than 0.1% of the total applied *S*-metolachlor was exported toward the Avenheimerbach river, measured *S*-metolachlor concentrations often exceeded the national regulatory threshold level for surface waters of $2 \mu\text{g.L}^{-1}$ for a single pesticide. Furthermore, considering that the 2019 season was rather dry (*i.e.* $76 \pm 8\%$ of the averaged precipitations of the preceding 69 years), the Avenheimerbach river presents a high risk of pollution by pesticides. Then, reducing the use of *S*-metolachlor on this specific catchment is particularly advised. To that end, one may rely on agricultural scenarios including changes in land use, farming systems, and practices which efficiencies may be assessed by recently presented modelling tools [Vernier et al., 2017].

Bibliography

- [Akbarzadeh et al., 2018] Akbarzadeh, Z., Laverman, A. M., Rezanezhad, F., Raimonet, M., Viollier, E., Shafei, B., and Van Cappellen, P. (2018). Benthic nitrite exchanges in the Seine River (France): An early diagenetic modeling analysis. *Science of The Total Environment*, 628-629:580–593.
- [Alvarez-Zaldívar et al., 2018] Alvarez-Zaldívar, P., Payraudeau, S., Meite, F., Masbou, J., and Imfeld, G. (2018). Pesticide degradation and export losses at the catchment scale: Insights from compound-specific isotope analysis (CSIA). *Water Research*, 139:198–207.
- [Alvarez-Zaldivar, 2018] Alvarez-Zaldivar, P. (2018). *Pesticide degradation and transport at catchment scale*. PhD thesis.
- [Apell and McNeill, 2019] Apell, J. N. and McNeill, K. (2019). Updated and validated solar irradiance reference spectra for estimating environmental photodegradation rates. *Environmental Science: Processes & Impacts*, 21(3):427–437.
- [Bakkour et al., 2018] Bakkour, R., Bolotin, J., Sellergren, B., and Hofstetter, T. B. (2018). Molecularly Imprinted Polymers for Compound-Specific Isotope Analysis of Polar Organic Micropollutants in Aquatic Environments. *Analytical Chemistry*, 90(12):7292–7301.
- [Berez et al., 2016] Berez, A., Schäfer, G., Ayari, F., and Trabelsi-Ayadi, M. (2016). Adsorptive removal of azo dyes from aqueous solutions by natural bentonite under static and dynamic flow conditions. *International Journal of Environmental Science and Technology*, 13(7):1625–1640.
- [Boano et al., 2014] Boano, F., Harvey, J. W., Marion, A., Packman, A. I., Revelli, R., Ridolfi, L., and Wörman, A. (2014). Hyporheic flow and transport processes: Mechanisms, models, and biogeochemical implications. *Reviews of Geophysics*, 52(4):603–679.

- [Boithias et al., 2014] Boithias, L., Sauvage, S., Merlina, G., Jean, S., Probst, J.-L., and Sánchez Pérez, J. M. (2014). New insight into pesticide partition coefficient K_d for modelling pesticide fluvial transport: Application to an agricultural catchment in south-western France. *Chemosphere*, 99:134–142.
- [Briggs et al., 2014] Briggs, M. A., Lautz, L. K., and Hare, D. K. (2014). Residence time control on hot moments of net nitrate production and uptake in the hyporheic zone. *Hydrological Processes*, 28(11):3741–3751.
- [Byrne et al., 2014] Byrne, P., Binley, A., Heathwaite, A. L., Ullah, S., Heppell, C. M., Lansdown, K., Zhang, H., Trimmer, M., and Keenan, P. (2014). Control of river stage on the reactive chemistry of the hyporheic zone. *Hydrological Processes*, 28(17):4766–4779.
- [Byrne et al., 2015] Byrne, P., Zhang, H., Ullah, S., Binley, A., Heathwaite, A. L., Heppell, C. M., Lansdown, K., and Trimmer, M. (2015). Diffusive equilibrium in thin films provides evidence of suppression of hyporheic exchange and large-scale nitrate transformation in a groundwater-fed river. *Hydrological Processes*, 29(6):1385–1396.
- [Chen et al., 2017a] Chen, H., Luo, Y., Potter, C., Moran, P. J., Grieneisen, M. L., and Zhang, M. (2017a). Modeling pesticide diuron loading from the San Joaquin watershed into the Sacramento-San Joaquin Delta using SWAT. *Water Research*, 121:374–385.
- [Chen et al., 2017b] Chen, Z., Chen, Y., Vymazal, J., Kule, L., and Koželuh, M. (2017b). Dynamics of chloroacetanilide herbicides in various types of mesocosm wetlands. *Science of The Total Environment*, 577(Supplement C):386–394.
- [Ciffroy, 2018] Ciffroy, P. (2018). Modelling the Fate of Chemicals in Surface Waters. In Ciffroy, P., Tediosi, A., and Capri, E., editors, *Modelling the Fate of Chemicals in the Environment and the Human Body*, pages 77–99. Springer International Publishing, Cham.
- [de Souza et al., 2020] de Souza, R. M., Seibert, D., Quesada, H. B., de Jesus Bassetti, F., Fagundes-Klen, M. R., and Bergamasco, R. (2020). Occurrence, impacts and general aspects of pesticides in surface water: A review. *Process Safety and Environmental Protection*, 135:22–37.
- [Dollinger et al., 2017] Dollinger, J., Dagès, C., and Voltz, M. (2017). Using fluorescent dyes as proxies to study herbicide removal by sorption in buffer zones. *Environmental Science and Pollution Research*, 24(12):11752–11763.

- [Dollinger et al., 2019] Dollinger, J., Lin, C.-H., Udawatta, R. P., Pot, V., Benoit, P., and Jose, S. (2019). Influence of agroforestry plant species on the infiltration of S-Metolachlor in buffer soils. *Journal of Contaminant Hydrology*, 225:103498.
- [Dwivedi et al., 2018] Dwivedi, D., Steefel, C. I., Arora, B., Newcomer, M., Moulton, J. D., Dafflon, B., Faybishenko, B., Fox, P., Nico, P., Spycher, N., Carroll, R., and Williams, K. H. (2018). Geochemical exports to river from the intramainder hyporheic zone under transient hydrologic conditions: east river mountainous watershed, Colorado. *Water Resources Research*, 54(10):8456–8477.
- [Elsner and Imfeld, 2016] Elsner, M. and Imfeld, G. (2016). Compound-specific isotope analysis (CSIA) of micropollutants in the environment — current developments and future challenges. *Current Opinion in Biotechnology*, 41:60–72.
- [Elsner et al., 2005] Elsner, M., Zwank, L., Hunkeler, D., and Schwarzenbach, R. P. (2005). A new concept linking observable stable isotope fractionation to transformation pathways of organic pollutants. *Environmental Science & Technology*, 39(18):6896–6916.
- [Eylers et al., 1995] Eylers, H., Brooks, N. H., and Morgan, J. J. (1995). Transport of adsorbing metals from stream water to a stationary sand-bed in a laboratory flume. *Marine and Freshwater Research*, 46(1):209–214.
- [Feld et al., 2018] Feld, C. K., Fernandes, M. R., Ferreira, M. T., Hering, D., Ormerod, S. J., Venohr, M., and Gutiérrez-Cánovas, C. (2018). Evaluating riparian solutions to multiple stressor problems in river ecosystems — A conceptual study. *Water Research*, 139:381–394.
- [Fenner et al., 2013] Fenner, K., Canonica, S., Wackett, L. P., and Elsner, M. (2013). Evaluating Pesticide Degradation in the Environment: Blind Spots and Emerging Opportunities. *Science*, 341(6147):752–758.
- [Fenner and Tratnyek, 2017] Fenner, K. and Tratnyek, P. G. (2017). QSARs and computational chemistry methods in environmental chemical sciences. *Environmental Science. Processes & Impacts*, 19(3):185–187.
- [Fernandez-Pascual et al., 2020] Fernandez-Pascual, E., Bork, M., Hensen, B., and Lange, J. (2020). Hydrological tracers for assessing transport and dissipation processes of pesticides in a model constructed wetland system. *Hydrology and Earth System Sciences*, 24(1):41–60.

- [Flipo et al., 2014] Flipo, N., Mouhri, A., Labarthe, B., Biancamaria, S., Rivière, A., and Weill, P. (2014). Continental hydrosystem modelling: the concept of nested stream–aquifer interfaces. *Hydrology and Earth System Sciences*, 18(8):3121–3149.
- [Fox et al., 2014] Fox, A., Boano, F., and Arnon, S. (2014). Impact of losing and gaining streamflow conditions on hyporheic exchange fluxes induced by dune-shaped bed forms. *Water Resources Research*, 50(3):1895–1907.
- [Galloway et al., 2019] Galloway, J., Fox, A., Lewandowski, J., and Arnon, S. (2019). The effect of unsteady streamflow and stream-groundwater interactions on oxygen consumption in a sandy streambed. *Scientific Reports*, 9(1):19735.
- [Ghattas et al., 2017] Ghattas, A.-K., Fischer, F., Wick, A., and Ternes, T. A. (2017). Anaerobic biodegradation of (emerging) organic contaminants in the aquatic environment. *Water Research*, 116:268–295.
- [Gulkowska et al., 2014] Gulkowska, A., Buerge, I. J., and Poiger, T. (2014). Online solid phase extraction LC–MS/MS method for the analysis of succinate dehydrogenase inhibitor fungicides and its applicability to surface water samples. *Analytical and Bioanalytical Chemistry*, 406(25):6419–6427.
- [Gulkowska et al., 2016] Gulkowska, A., Buerge, I. J., Poiger, T., and Kasteel, R. (2016). Time-dependent sorption of two novel fungicides in soils within a regulatory framework. *Pest Management Science*, 72(12):2218–2230.
- [Haggerty et al., 2009] Haggerty, R., Martí, E., Argerich, A., von Schiller, D., and Grimm, N. B. (2009). Resazurin as a “smart” tracer for quantifying metabolically active transient storage in stream ecosystems. *Journal of Geophysical Research: Biogeosciences*, 114(G3).
- [Hartenbach et al., 2008] Hartenbach, A. E., Hofstetter, T. B., Tentscher, P. R., Canonica, S., Berg, M., and Schwarzenbach, R. P. (2008). Carbon, Hydrogen, and Nitrogen Isotope Fractionation During Light-Induced Transformations of Atrazine. *Environmental Science & Technology*, 42(21):7751–7756.
- [Hassoun et al., 2017] Hassoun, H., Lamhasni, T., Foudeil, S., El Bakkali, A., Ait Lyazidi, S., Haddad, M., Choukrad, M., and Hnach, M. (2017). Total Fluorescence Fingerprinting of Pesticides: A Reliable Approach for Continuous Monitoring of Soils and Waters. *Journal of Fluorescence*, 27(5):1633–1642.

- [Her and Chaubey, 2015] Her, Y. and Chaubey, I. (2015). Impact of the numbers of observations and calibration parameters on equifinality, model performance, and output and parameter uncertainty. *Hydrological Processes*, 29(19):4220–4237.
- [Herzog et al., 2018] Herzog, S. P., Higgins, C. P., Singha, K., and McCray, J. E. (2018). Performance of Engineered Streambeds for Inducing Hyporheic Transient Storage and Attenuation of Resazurin. *Environmental Science & Technology*, 52(18):10627–10636.
- [Honti et al., 2018] Honti, M., Bischoff, F., Moser, A., Stamm, C., Baranya, S., and Fenner, K. (2018). Relating degradation of pharmaceutical active ingredients in a stream network to degradation in water-sediment simulation tests. *Water Resources Research*, 54(11):9207–9223.
- [Honti and Fenner, 2015] Honti, M. and Fenner, K. (2015). Deriving Persistence Indicators from Regulatory Water-Sediment Studies – Opportunities and Limitations in OECD 308 Data. *Environmental Science & Technology*, 49(10):5879–5886.
- [Honti et al., 2016] Honti, M., Hahn, S., Hennecke, D., Junker, T., Shrestha, P., and Fenner, K. (2016). Bridging across OECD 308 and 309 Data in Search of a Robust Biotransformation Indicator. *Environmental Science & Technology*, 50(13):6865–6872.
- [Iribar et al., 2008] Iribar, A., Sánchez-Pérez, J. M., Lyautey, E., and Garabétian, F. (2008). Differentiated free-living and sediment-attached bacterial community structure inside and outside denitrification hotspots in the river–groundwater interface. *Hydrobiologia*, 598(1):109–121.
- [Jada and Ait Akbour, 2014] Jada, A. and Ait Akbour, R. (2014). Adsorption and removal of organic dye at quartz sand-water interface. *Oil & Gas Science and Technology – Revue d’IFP Energies nouvelles*, 69(3):405–413.
- [Jaeger et al., 2019] Jaeger, A., Coll, C., Posselt, M., Mechelke, J., Rutere, C., Betterle, A., Raza, M., Mehrtens, A., Meinikmann, K., Portmann, A., Singh, T., Blaen, P. J., Krause, S., Horn, M. A., Hollender, J., Benskin, J. P., Sobek, A., and Lewandowski, J. (2019). Using recirculating flumes and a response surface model to investigate the role of hyporheic exchange and bacterial diversity on micropollutant half-lives. *Environmental Science: Processes & Impacts*, 21(12):2093–2108.

- [Jeannot et al., 2018] Jeannot, B., Weill, S., Eschbach, D., Schmitt, L., and Delay, F. (2018). A low-dimensional integrated subsurface hydrological model coupled with 2-D overland flow: Application to a restored fluvial hydrosystem (Upper Rhine River – France). *Journal of Hydrology*, 563:495–509.
- [Jehmlich et al., 2016] Jehmlich, N., Vogt, C., Lünsmann, V., Richnow, H. H., and von Bergen, M. (2016). Protein-SIP in environmental studies. *Current Opinion in Biotechnology*, 41:26–33.
- [Jin et al., 2019] Jin, G., Chen, Y., Tang, H., Zhang, P., Li, L., and Barry, D. A. (2019). Interplay of hyporheic exchange and fine particle deposition in a riverbed. *Advances in Water Resources*, 128:145–157.
- [Joko et al., 2017] Joko, T., Anggoro, S., Sunoko, H. R., and Rachmawati, S. (2017). Pesticides Usage in the Soil Quality Degradation Potential in Wanasari Subdistrict, Brebes, Indonesia. ISSN: 1687-7667 Library Catalog: www.hindawi.com Pages: e5896191 Publisher: Hindawi Volume: 2017.
- [Katagi, 2016] Katagi, T. (2016). Pesticide behavior in modified water-sediment systems. *Journal of Pesticide Science*, 41(4):121–132.
- [Knapp and Cirpka, 2017] Knapp, J. L. A. and Cirpka, O. A. (2017). Determination of hyporheic travel time distributions and other parameters from concurrent conservative and reactive tracer tests by local-in-global optimization. *Water Resources Research*, 53(6):4984–5001.
- [Knapp et al., 2018] Knapp, J. L. A., González-Pinzón, R., and Haggerty, R. (2018). The Resazurin-Resorufin System: Insights From a Decade of “Smart” Tracer Development for Hydrologic Applications. *Water Resources Research*, 54(9):6877–6889.
- [Korekar et al., 2020] Korekar, G., Kumar, A., and Ugale, C. (2020). Occurrence, fate, persistence and remediation of caffeine: a review. *Environmental Science and Pollution Research*, 27(28):34715–34733.
- [Krause et al., 2017] Krause, S., Lewandowski, J., Grimm, N. B., Hannah, D. M., Pinay, G., McDonald, K., Martí, E., Argerich, A., Pfister, L., Klaus, J., Battin, T., Larned, S. T., Schelker, J., Fleckenstein, J., Schmidt, C., Rivett, M. O., Watts, G., Sabater, F., Sorolla, A., and Turk, V. (2017). Ecohydrological interfaces as hot spots of ecosystem processes. *Water Resources Research*, 53(8):6359–6376.

- [Kronvang et al., 2004] Kronvang, B., Strøm, H., Hoffmann, C., Laubel, A., and Friberg, N. (2004). Subsurface tile drainage loss of modern pesticides: field experiment results. *Water Science and Technology*, 49(3):139–148.
- [Kunkel and Radke, 2008] Kunkel, U. and Radke, M. (2008). Biodegradation of Acidic Pharmaceuticals in Bed Sediments: Insight from a Laboratory Experiment. *Environmental Science & Technology*, 42(19):7273–7279.
- [Kunkel and Radke, 2011] Kunkel, U. and Radke, M. (2011). Reactive Tracer Test To Evaluate the Fate of Pharmaceuticals in Rivers. *Environmental Science & Technology*, 45(15):6296–6302.
- [Kunkel and Radke, 2012] Kunkel, U. and Radke, M. (2012). Fate of pharmaceuticals in rivers: Deriving a benchmark dataset at favorable attenuation conditions. *Water Research*, 46(17):5551–5565.
- [Lange et al., 2018] Lange, J., Olsson, O., Sweeney, B., Herbstritt, B., Reich, M., Alvarez-Zaldivar, P., Payraudeau, S., and Imfeld, G. (2018). Fluorescent tracers to evaluate pesticide dissipation and transformation in agricultural soils. *Science of The Total Environment*, 619-620:1682–1689.
- [Lansdown et al., 2015] Lansdown, K., Heppell, C. M., Trimmer, M., Binley, A., Heathwaite, A. L., Byrne, P., and Zhang, H. (2015). The interplay between transport and reaction rates as controls on nitrate attenuation in permeable, streambed sediments. *Journal of Geophysical Research: Biogeosciences*, 120(6):1093–1109.
- [Lemke et al., 2014] Lemke, D., González-Pinzón, R., Liao, Z., Wöhling, T., Osenbrück, K., Haggerty, R., and Cirpka, O. A. (2014). Sorption and transformation of the reactive tracers resazurin and resorufin in natural river sediments. *Hydrology and Earth System Sciences*, 18(8):3151–3163.
- [Lewandowski et al., 2019] Lewandowski, J., Arnon, S., Banks, E., Batelaan, O., Betterle, A., Broecker, T., Coll, C., Drummond, J. D., Gaona Garcia, J., Galloway, J., Gomez-Velez, J., Grabowski, R. C., Herzog, S. P., Hinkelmann, R., Höhne, A., Hollender, J., Horn, M. A., Jaeger, A., Krause, S., Löchner Prats, A., Magliozzi, C., Meinikmann, K., Mojarrad, B. B., Mueller, B. M., Peralta-Maraver, I., Popp, A. L., Posselt, M., Putschew, A., Radke, M., Raza, M., Riml, J., Robertson, A., Rutere, C., Schaper, J. L., Schirmer, M., Schulz, H., Shanafield, M., Singh, T., Ward, A. S., Wolke, P., Wörman, A., and Wu, L. (2019). Is the hyporheic zone relevant beyond the scientific community? *Water*, 11(11):2230.

- [Lewandowski et al., 2011] Lewandowski, J., Putschew, A., Schwesig, D., Neumann, C., and Radke, M. (2011). Fate of organic micropollutants in the hyporheic zone of a eutrophic lowland stream: Results of a preliminary field study. *Science of The Total Environment*, 409(10):1824–1835.
- [Liao et al., 2013] Liao, Z., Lemke, D., Osenbrück, K., and Cirpka, O. A. (2013). Modeling and inverting reactive stream tracers undergoing two-site sorption and decay in the hyporheic zone. *Water Resources Research*, 49(6):3406–3422.
- [Limousin et al., 2007] Limousin, G., Gaudet, J. P., Charlet, L., Szenknect, S., Barthès, V., and Krimissa, M. (2007). Sorption isotherms: A review on physical bases, modeling and measurement. *Applied Geochemistry*, 22(2):249–275.
- [Loch et al., 2002] Loch, A. R., Lippa, K. A., Carlson, D. L., Chin, Y. P., Traina, S. J., and Roberts, A. L. (2002). Nucleophilic Aliphatic Substitution Reactions of Propachlor, Alachlor, and Metolachlor with Bisulfide (HS-) and Polysulfides (Sn2-). *Environmental Science & Technology*, 36(19):4065–4073.
- [Lutz et al., 2017] Lutz, S. R., van der Velde, Y., Elsayed, O. F., Imfeld, G., Lefrancq, M., Payraudeau, S., and van Breukelen, B. M. (2017). Pesticide fate at catchment scale: conceptual modelling of stream CSIA data. *Hydrol. Earth Syst. Sci. Discuss.*, 2017:1–30.
- [Ma et al., 2019] Ma, H., Nittrouer, J. A., Wu, B., Lamb, M. P., Zhang, Y., Mohrig, D., Fu, X., Naito, K., Wang, Y., Moodie, A. J., Wang, G., Hu, C., and Parker, G. (2019). Universal relation with regime transition for sediment transport in fine-grained rivers. *Proceedings of the National Academy of Sciences*.
- [Maggi et al., 2019] Maggi, F., Tang, F. H. M., Cecilia, D. I., and McBratney, A. (2019). PEST-CHEMGRIDS, global gridded maps of the top 20 crop-specific pesticide application rates from 2015 to 2025. *Scientific Data*, 6(1):1–20.
- [Maier et al., 2016] Maier, M. P., Prasse, C., Pati, S. G., Nitsche, S., Li, Z., Radke, M., Meyer, A., Hofstetter, T. B., Ternes, T. A., and Elsner, M. (2016). Exploring Trends of C and N Isotope Fractionation to Trace Transformation Reactions of Diclofenac in Natural and Engineered Systems. *Environmental Science & Technology*, 50(20):10933–10942.
- [Mamy et al., 2014] Mamy, L., Patureau, D., Barriuso, E., Bedos, C., Bessac, F., Louchart, X., Martin-laurent, F., Miegé, C., and Benoit, P. (2014). Prediction of the

Fate of Organic Compounds in the Environment From Their Molecular Properties:
A Review. *Critical Reviews in Environmental Science and Technology*.

- [Masiol et al., 2018] Masiol, M., Gianni, B., and Prete, M. (2018). Herbicides in river water across the northeastern Italy: occurrence and spatial patterns of glyphosate, aminomethylphosphonic acid, and glufosinate ammonium. *Environmental Science and Pollution Research*, pages 1–11.
- [Nogaro et al., 2013] Nogaro, G., Datry, T., Mermillod-Blondin, F., Foulquier, A., and Montuelle, B. (2013). Influence of hyporheic zone characteristics on the structure and activity of microbial assemblages. *Freshwater Biology*, 58(12):2567–2583.
- [Paraska et al., 2014] Paraska, D. W., Hipsey, M. R., and Salmon, S. U. (2014). Sediment diagenesis models: Review of approaches, challenges and opportunities. *Environmental Modelling & Software*, 61:297–325.
- [Passeport et al., 2011] Passeport, E., Benoit, P., Bergheaud, V., Coquet, Y., and Tournebize, J. (2011). Selected pesticides adsorption and desorption in substrates from artificial wetland and forest buffer. *Environmental Toxicology and Chemistry*, 30(7):1669–1676.
- [Passeport et al., 2014] Passeport, E., Richard, B., Chaumont, C., Margoum, C., Liger, L., Gril, J.-J., and Tournebize, J. (2014). Dynamics and mitigation of six pesticides in a “Wet” forest buffer zone. *Environmental Science and Pollution Research*, 21(7):4883–4894.
- [Penning et al., 2010] Penning, H., Sørensen, S. R., Meyer, A. H., Aamand, J., and Elsner, M. (2010). C, N, and H Isotope Fractionation of the Herbicide Isoproturon Reflects Different Microbial Transformation Pathways. *Environmental Science & Technology*, 44(7):2372–2378.
- [Peter et al., 2019] Peter, K. T., Herzog, S., Tian, Z., Wu, C., McCray, J. E., Lynch, K., and Kolodziej, E. P. (2019). Evaluating emerging organic contaminant removal in an engineered hyporheic zone using high resolution mass spectrometry. *Water Research*, 150:140–152.
- [Posselt et al., 2020] Posselt, M., Mechelke, J., Rutere, C., Coll, C., Jaeger, A., Raza, M., Meinikmann, K., Krause, S., Sobek, A., Lewandowski, J., Horn, M. A., Hollender, J., and Benskin, J. P. (2020). Bacterial Diversity Controls Transformation of Wastewater-Derived Organic Contaminants in River-Simulating Flumes. *Environmental Science & Technology*, 54(9):5467–5479.

- [Radović et al., 2016] Radović, T. T., Grujić, S. D., Kovačević, S. R., Laušević, M. D., and Dimkić, M. A. (2016). Sorption of selected pharmaceuticals and pesticides on different river sediments. *Environmental Science and Pollution Research*, 23(24):25232–25244.
- [Reilly et al., 2012] Reilly, T. J., Smalling, K. L., Orlando, J. L., and Kuivila, K. M. (2012). Occurrence of boscalid and other selected fungicides in surface water and groundwater in three targeted use areas in the United States. *Chemosphere*, 89(3):228–234.
- [Remucal, 2014] Remucal, C. K. (2014). The role of indirect photochemical degradation in the environmental fate of pesticides: a review. *Environmental Science-Processes & Impacts*, 16(4):628–653.
- [Renpenning et al., 2017] Renpenning, J., Schimmelmann, A., and Gehre, M. (2017). Compound-specific hydrogen isotope analysis of fluorine-, chlorine-, bromine- and iodine-bearing organics using gas chromatography–chromium-based high-temperature conversion (Cr/HTC) isotope ratio mass spectrometry. *Rapid Communications in Mass Spectrometry*, 31(13):1095–1102.
- [Revelli et al., 2008] Revelli, R., Boano, F., Camporeale, C., and Ridolfi, L. (2008). Intra-meander hyporheic flow in alluvial rivers. *Water Resources Research*, 44(12).
- [Salehin et al., 2003] Salehin, M., Packman, A. I., and Wörman, A. (2003). Comparison of transient storage in vegetated and unvegetated reaches of a small agricultural stream in Sweden: seasonal variation and anthropogenic manipulation. *Advances in Water Resources*, 26(9):951–964.
- [Schwarzenbach et al., 2003] Schwarzenbach, R. P., Gschwend, P. M., Imboden, D. M., and Imboden, M. (2003). *Environmental Organic Chemistry / Edition 2*.
- [Servien et al., 2014] Servien, R., Mamy, L., Li, Z., Rossard, V., Latrille, E., Bessac, F., Patureau, D., and Benoit, P. (2014). TyPol – A new methodology for organic compounds clustering based on their molecular characteristics and environmental behavior. *Chemosphere*, 111:613–622.
- [Shrestha et al., 2016] Shrestha, P., Junker, T., Fenner, K., Hahn, S., Honti, M., Bakkour, R., Diaz, C., and Hennecke, D. (2016). Simulation studies to explore biodegradation in water–sediment systems: From OECD 308 to OECD 309. *Environmental Science & Technology*, 50(13):6856–6864.

- [Sims and Kanissery, 2019] Sims, G. K. and Kanissery, R. G. (2019). Anaerobic Biodegradation of Pesticides. In Arora, P. K., editor, *Microbial Metabolism of Xenobiotic Compounds*, Microorganisms for Sustainability, pages 33–54. Springer, Singapore.
- [Smith et al., 2002] Smith, E. J., Davison, W., and Hamilton-Taylor, J. (2002). Methods for preparing synthetic freshwaters. *Water Research*, 36(5):1286–1296.
- [Staley et al., 2015] Staley, Z. R., Harwood, V. J., and Rohr, J. R. (2015). A Synthesis of the Effects of Pesticides on Microbial Persistence in Aquatic Ecosystems. *Critical reviews in toxicology*, 45(10):813–836.
- [Torrentó et al., 2019] Torrentó, C., Bakkour, R., Glauser, G., Melsbach, A., Ponsin, V., Hofstetter, T. B., Elsner, M., and Hunkeler, D. (2019). Solid-phase extraction method for stable isotope analysis of pesticides from large volume environmental water samples. *The Analyst*, 144(9):2898–2908.
- [van Genuchten and Wagenet, 1989] van Genuchten, M. T. and Wagenet, R. J. (1989). Two-site/two-region models for pesticide transport and degradation: Theoretical development and analytical solutions. *Soil Science Society of America Journal*, 53(5):1303.
- [Vernier et al., 2017] Vernier, F., Leccia-Phelpin, O., Lescot, J.-M., Minette, S., Miralles, A., Barberis, D., Scordia, C., Kuentz-Simonet, V., and Tonneau, J.-P. (2017). Integrated modeling of agricultural scenarios (IMAS) to support pesticide action plans: the case of the Coulange drinking water catchment area (SW France). *Environmental Science and Pollution Research*, 24(8):6923–6950.
- [Voermans et al., 2018] Voermans, J. J., Ghisalberti Marco, and Ivey Gregory N. (2018). A model for mass transport across the sediment-water interface. *Water Resources Research*, 0(0).
- [Wang et al., 2019] Wang, R., Yuan, Y., Yen, H., Grieneisen, M., Arnold, J., Wang, D., Wang, C., and Zhang, M. (2019). A review of pesticide fate and transport simulation at watershed level using SWAT: Current status and research concerns. *Science of The Total Environment*, 669:512–526.
- [Ward, 2016] Ward, A. S. (2016). The evolution and state of interdisciplinary hydrogeic research. *WIREs Water*, 3(1):83–103.

- [Wenning and Martello, 2014] Wenning, R. J. and Martello, L. (2014). Chapter 8 - POPs in Marine and Freshwater Environments. In O’Sullivan, G. and Sandau, C., editors, *Environmental Forensics for Persistent Organic Pollutants*, pages 357–390. Elsevier, Amsterdam.
- [Zeng and Arnold, 2013] Zeng, T. and Arnold, W. A. (2013). Pesticide Photolysis in Prairie Potholes: Probing Photosensitized Processes. *Environmental Science & Technology*, 47(13):6735–6745.

Appendix A

Supporting information to chapter II

A.S1 Photodegradation

A.S1.1 List of chemicals

Pesticides: *S*-metolachlor (2-chloro-*N*-(2-ethyl-6-methylphenyl)-*N*-((2*S*)-1-methoxypropan-2-yl)acetamide), atrazine (6-chloro-4-*N*-ethyl-2-*N*-propan-2-yl-1,3,5-triazine-2,4-diamine) and metolachlor d11 were analytical grade (Pestanal, > 99.9%, Sigma-Aldrich®, St Louis, MO, USA).

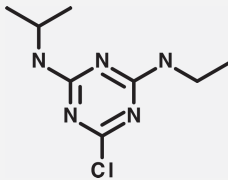
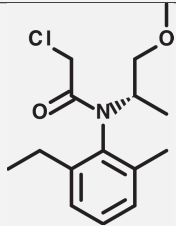
Transformation products of *S*-metolachlor and atrazine: *S*-metolachlor ethanesulfonic acid (ESA - sodium 2-((2-ethyl-6-methylphenyl)(1-methoxy-2-propenyl)amino)-2-oxoethanesulfonate), *S*-metolachlor oxanilic acid (OXA - 2-(2-ethyl-*N*-(1-methoxypropan-2-yl)-6-methylanilino)-2-oxoacetic acid), metolachlor CGA 37735 (*N*-(2-ethyl-6-methylphenyl)-2-hydroxyacetamide), 2-hydroxy-atrazine (A-OH - 2-(ethylamino)-6-(propan-2-ylamino)-1*H*-1,3,5-triazin-4-one), desethylatrazine (DEA; 6-chloro-2-*N*-propan-2-yl-1,3,5-triazine-2,4-diamine), desisopropylatrazine (DIA; 6-chloro-2-*N*-ethyl-1,3,5-triazine-2,4-diamine), atrazine-desethyl-2-hydroxy (A-DOH - (6*Z*)-4-Imino-6-(isopropylimino)-1,4,5,6-tetrahydro-1,3,5-triazin-2-ol) were analytical grade (> 98%, Sigma-Aldrich® St Louis, MO, USA). Hydroxy-metolachlor (Met-OH - *N*-(2-ethyl-6-methylphenyl)-2-hydroxy-*N*-(1-methoxypropan-2-yl)acetamide) was purchased as reference standard for GC in ACN from LGC Standards (Molsheim, France).

Actinometer: *p*-nitroanisole (PNA) and pyridine (anhydrous, > 99.8%) were analytical grade (> 97%).

Solvents and other chemicals: The solvents dichloromethane (DCM), acetonitrile (ACN) and ethyl acetate (EtOAc) were HPLC grade purity ($> 99.9\%$). All the pre-cited chemicals as well as magnesium sulfate heptahydrate (BioUltra, $\geq 99.5\%$), calcium chloride hexahydrate (BioUltra, $\geq 99.0\%$), calcium nitrate tetrahydrate ($\geq 99.0\%$), potassium phosphate monobasic (BioUltra, $\geq 99.5\%$) and sodium phosphate dibasic (BioUltra, $\geq 99.5\%$) used for buffer solution and synthetic fresh water preparation were purchased from Sigma-Aldrich® (St Louis, MO, USA).

A.S1.2 Main Properties of Selected Pesticides and Origin of the Substances Used

Table A.S1 – Main properties of atrazine and *S*-metolachlor and literature references addressing their photodegradation

Molecule	atrazine	<i>S</i> -metolachlor
Use	Herbicide	Herbicide
Chemical properties		
Chemical family	Triazine	Chloroacetanilide
Chemical structure		
Chemical formula	$C_8H_{14}ClN_5$	$C_{15}H_{22}ClNO_2$
Molar mass ($g.mol^{-1}$)	215.68	283.79
Studies relating photolytic behaviour		
References	[Hartenbach et al., 2008, Héquet et al., 2001, Hessler et al., 1993, Karpuzcu et al., 2016, Sharpless et al., 2003, Torrents et al., 1997, Zeng and Arnold, 2013]	[Dimou et al., 2005, Gutowski et al., 2015a, Gutowski et al., 2015b, Kochany and Maguire, 1994, Zeng and Arnold, 2013]

Note: For additional studies on atrazine and/or *S*-metolachlor photodegradation see Remucal et al.(2014) [Remucal, 2014].

A.S1.3 Chemical Composition of Irradiation Solutions

Table A.S2 – Chemical composition of irradiation solutions

Parameter	Unit	Value ^a	Analytical method	Irradiation solution
pH	/	7.9 ± 0.2	Glass electrode	All
DOC ^b	$mg_C.L^{-1}$	5.4 ± 0.2	TOC analyzer	SRFA & TOT
Cations				
NH_4^+	$mg.L^{-1}$	<i>n.p.</i>	IC	NIT & TOT
Na^+		9.9 ± 0.5	IC	NIT & TOT
K^+		0.71 ± 0.04	IC	NIT & TOT
Mg^{2+}		1.47 ± 0.07	IC	NIT & TOT
Ca^{2+}		13.4 ± 0.7	IC	NIT & TOT
Anions				
Cl^-	$mg.L^{-1}$	12.0 ± 0.6	IC	NIT & TOT
NO_3^-		20.5 ± 1.0	IC	NIT & TOT
SO_4^{2-}		5.6 ± 0.3	IC	NIT & TOT

^a Analytical uncertainties reported correspond to one standard deviation over triplicate measurements.

^b DOC concentrations measured in UW were $< 0.2 mg_C.L^{-1}$, which limited any effect of dissolved organic matter in direct photodegradation experiments (DIR and DIR254). *n.p.* stands for not present and DOC for dissolved organic carbon.

A.S1.4 Organic Matter Photobleaching

DOM photoirradiation reduces its light absorbance properties. The control experiment showed that the decrease of light absorbance at $\lambda = 254 \text{ nm}$ was less than 20% after > 310 hours of irradiation. SRFA photosensitizing and light absorption effects were thus assumed constant across the experiments in TOT solutions. Also, the composition of SRFA did not change over irradiation as evidenced by its steady absorption spectrum.

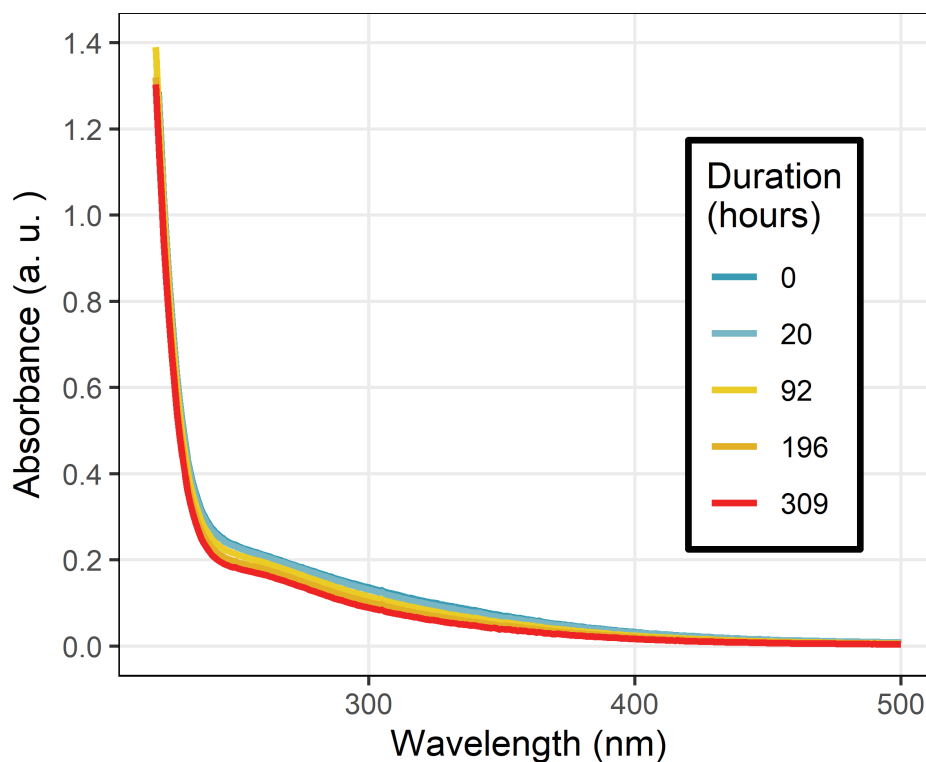


Figure A.S1 – Temporal changes of absorbance of the TOT solution caused by organic matter photobleaching.

A.S1.5 PNA/Pyr Actinometer System

A PNA (30 μM)/pyridine (10 mM) actinometer system was used to measure mean light intensity during experiments [Dulin and Mill, 1982, Laszakovits et al., 2017]. Values of wavelength independent quantum yields (Θ_{PNA}) of $3.19 \cdot 10^{-3} \text{ mol.einstein}^{-1}$ were used from Laszakovits et al. (2017) [Laszakovits et al., 2017]. To account for a closed irradiation system (*i.e.* aluminium foil covering the quartz vial walls and assumed to reflect light without absorption), it was assumed that chemicals absorbed all of the incident light and the decay of PNA as expressed in Eq. A.S1: [Schwarzenbach et al., 2003]

$$\frac{dC_{PNA}}{dt}(\lambda) = \frac{\epsilon(\lambda)}{\sum_{\lambda} \epsilon(\lambda)} \cdot \Theta_{PNA} \cdot F_W(\lambda) \quad (\text{A.S1})$$

with $\frac{dC_{PNA}}{dt(\lambda)}$ the observed pseudo first-order decaying rate of PNA, Θ_{PNA} the wavelength independent PNA quantum yield, $\frac{\epsilon(\lambda)}{\sum_{\lambda} \epsilon(\lambda)}$ the relative fraction of light absorbed by PNA at wavelength λ also provided by Laszakovits et al. (2017) and $F_W(\lambda)$ the relative photon irradiance of the lamp at wavelength λ [Laszakovits et al., 2017].

$$\frac{dC_{PNA}}{dt} = \sum_{\lambda} \left(\frac{\epsilon(\lambda)}{\sum_{\lambda} \epsilon(\lambda)} \cdot \Theta_{PNA} \cdot F_W(\lambda) \right) \quad (\text{A.S2})$$

Eq. A.S2 and $F_W(\lambda)$ and $\frac{\epsilon(\lambda)}{\sum_{\lambda} \epsilon(\lambda)}$ were computed over the range of validity for the PNA/Pyr system $\lambda \in [290, 400] \text{ nm}$.

A.S1.6 Irradiation conditions and correction of degradation rates

Table A.S3 – Irradiation conditions with the Xenon arc lamp and correction factors used to estimate photodegradation rates

Light interval ^a ($\Delta\lambda$)	VIS ($360 < \lambda < 830 \text{ nm}$)		UVA ($320 < \lambda < 400 \text{ nm}$)		UVB ($280 < \lambda < 320 \text{ nm}$)		Total (I_{tot})	Correction factor ^b
Experiment	Absolute $mW.cm^{-2}$	Relative %	Absolute $mW.cm^{-2}$	Relative %	Absolute $mW.cm^{-2}$	Relative %	Absolute $mW.cm^{-2}$	
ATZ - DIR	16.4	68.4	6.8	28.3	0.8	3.4	24	0.63
ATZ - TOT	12.9	64.1	6.7	33.4	0.5	2.5	20.2	0.75
ATZ - NIT	8.5	66.3	4	31.1	0.3	2.6	12.8	1.18
ATZ - DOM	7.1	68.4	3	28.7	0.3	2.9	10.4	1.45
SMET - DIR	13.1	68	5.6	28.9	0.6	3.1	19.3	0.78
SMET - TOT	6.9	69.2	2.8	27.8	0.3	3	10.8	1.40
SMET - NIT	6.2	70.5	2.4	27.1	0.2	2.4	9.9	1.52
SMET - DOM	9.6	66.9	4.2	29.6	0.5	3.5	13.3	1.14
Mean irradiation	10.1	67.7	4.4	29.4	0.4	2.9	15.1	
Standard deviation	3.7	2	1.8	2	0.2	0.4	5.3	

^a Light intensities are reported as the arithmetic mean of light measurements at the beginning and the end of the respective experiments. Relative light intensities stand for the contribution of each wavelength interval (VIS, UVA, UVB) to the whole irradiation, $I_{relative} = \frac{I_{\lambda}}{\sum_{i \in (VIS, UVA, UVB)} I_{\lambda_i}}$.

^b Correction of degradation rates were performed according to the correction factors with the averaged total light intensity $\overline{I_{tot}} = 15.1 \text{ mW.cm}^{-2}$ as the reference value divided by individual total light intensities, $F_k = \overline{I_{tot}}/I_{tot}$.

A.S1.7 Light Spectrum Homogeneity within the Light-proof Box

Light homogeneity within the light-proof box varied between 80 and 120% of relative irradiation intensity taking the mean intensity value as a reference. The LP Hg lamp was temporarily replaced by Medium Pressure Hg lamp emitting at $\lambda = 365 \text{ nm}$ and was used to irradiate 11 beakers filled with 50 mL of PNA (30 μM)/Pyridine (10 μM) actinometers and evenly distributed within the light-proof box. After four hours, the remaining concentration of PNA was measured in each beaker and the variations in the irradiation intensity were retrieved by comparing the mean value of k_{pE} with individual values computed from Eq. A.S3. [Dulin and Mill, 1982, Laszakovits et al., 2017]

$$\ln \left(\frac{[PNA]_t}{[PNA]_0} \right) = k_{pE} \cdot t \quad (\text{A.S3})$$

k_{pE} stands for the pseudo first order reaction rate of PNA and is linearly proportional to the incident irradiance.

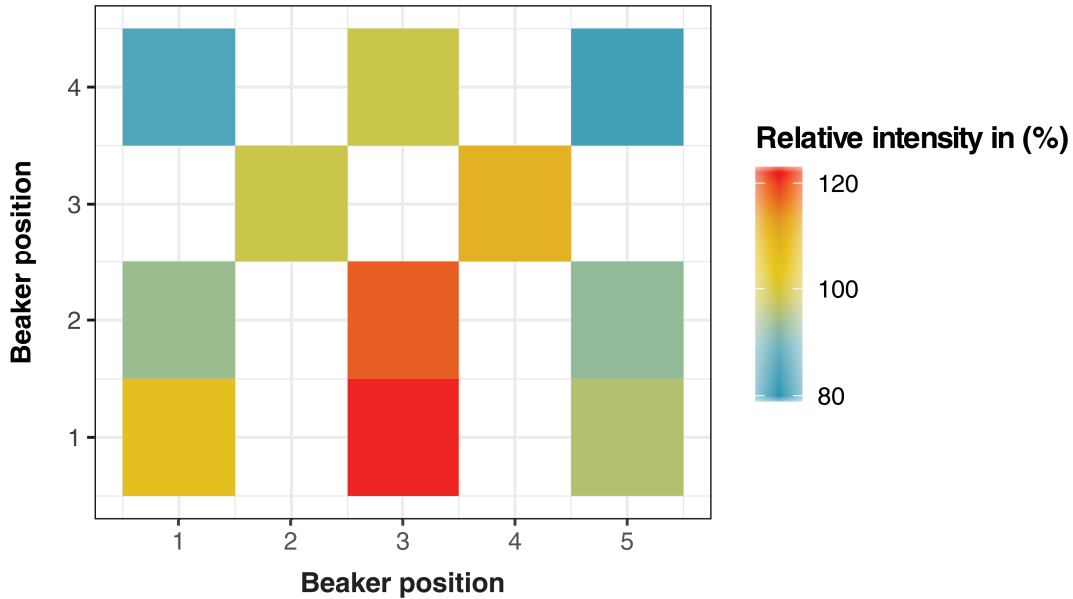


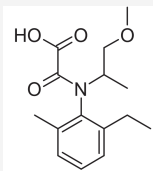
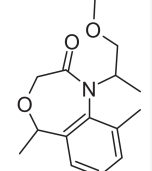
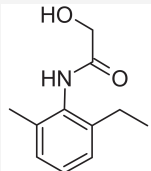
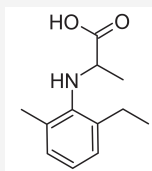
Figure A.S2 – Spatial distribution of irradiation intensity within the light-proof box. Transparent places correspond to empty spaces where the irradiation intensity was not measured within the light-proof box

A.S1.8 Atrazine and *S*-metolachlor transformation products

Table A.S4 – Atrazine transformation products and corresponding structures

Transformation product	Desisopropyl atrazine	Desethyl atrazine	Hydroxy-atrazine	Desethyl 2 hydroxy atrazine
Abbreviation	DIA	DEA	A-OH	A-DOH
Parent compound	Atrazine	Atrazine	Atrazine	Atrazine
Chemical structure				
Chemical formula	$C_5H_8ClN_5$	$C_6H_{10}ClN_5$	$C_8H_{15}N_5O$	$C_6H_{11}N_5O$
Molar mass ($g.mol^{-1}$)	173.6	187.6	197.2	169.2
Analytical standard available	Yes	Yes	Yes	Yes

Table A.S5 – *S*-metolachlor transformation products and corresponding structures

Transformation product	Metolachlor oxalinic acid	MET-GLui	Metolachlor CGA 37735	Metolachlor CGA 50267
Abbreviation	OXA	/	/	/
Parent compound	<i>S</i> -metolachlor	<i>S</i> -metolachlor	<i>S</i> -metolachlor	<i>S</i> -metolachlor
Chemical structure				
Chemical formula	$C_{15}H_{21}NO_4$	$C_{15}H_{21}NO_2$	$C_{11}H_{15}NO_2$	$C_{12}H_{17}NO_2$
Molar mass ($g.mol^{-1}$)	279.3	248.4	193.2	207.3
Analytical standard available	Yes	No	Yes	No

A.S1.9 Optical properties of chemicals and irradiation solutions

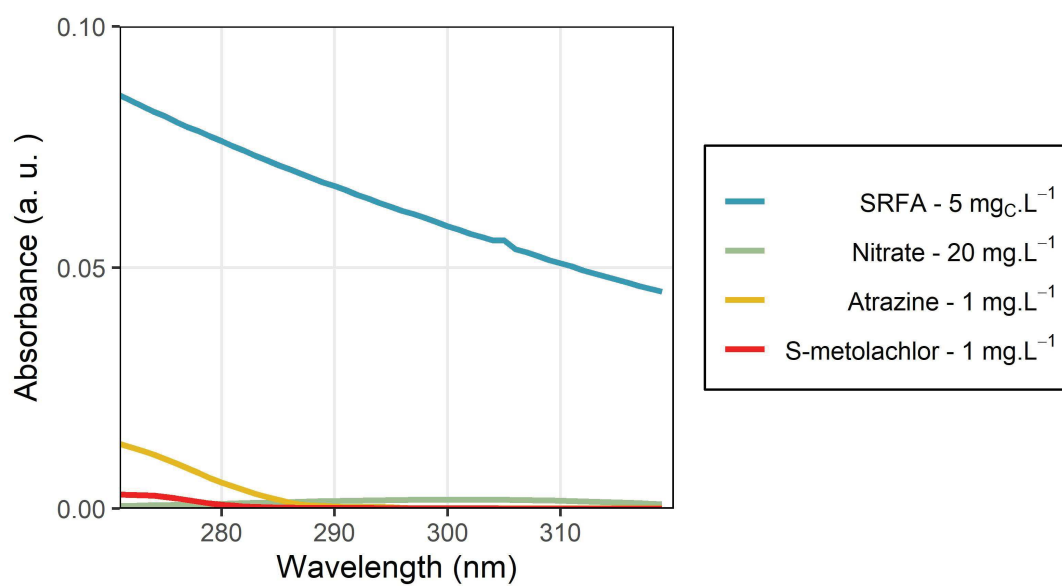


Figure A.S3 – Adsorption spectra of atrazine, *S*-metolachlor, nitrates and SRFA at experimental concentrations. The absorption spectra for nitrates was extracted from Gaffney et al. (1992) [Gaffney et al., 1992].

A.S1.10 Simulated sunlight characteristics

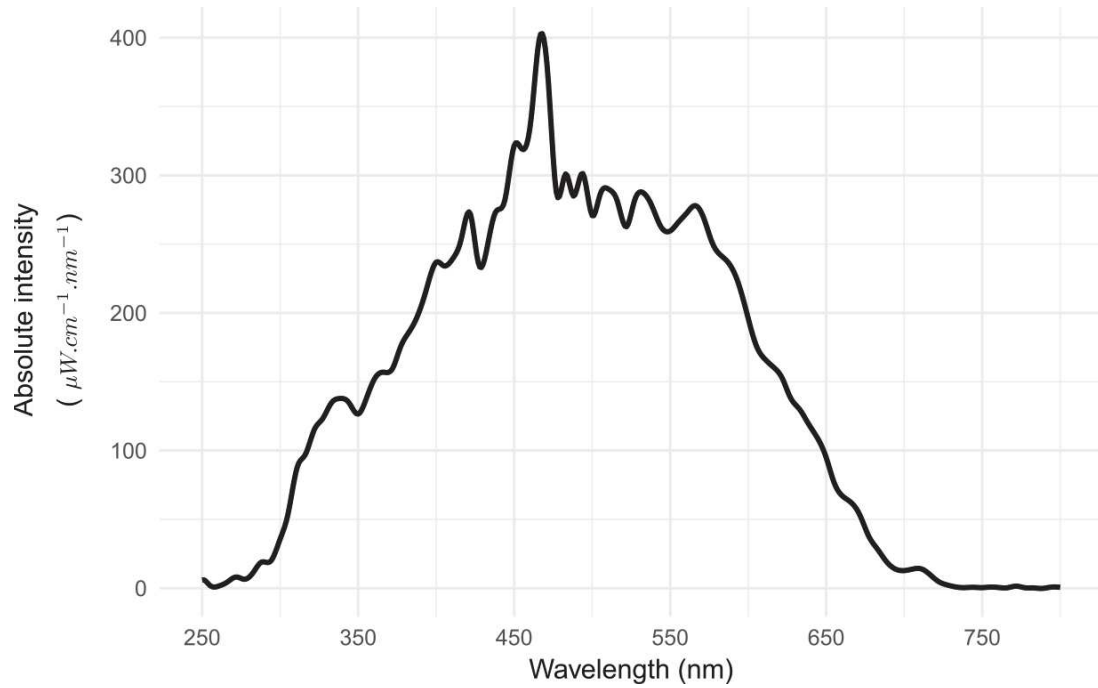


Figure A.S4 – Absolute light intensity as a function of the wavelength for the Xenon Arc Lamp as measured in the quartz tube after the liquid light guide¹.

¹ The light spectrum was characterized with a calibrated spectroradiometer ILT 900C (International Light®) at a wavelength resolution of 1 nm. Significant irradiation (i.e. $I(\lambda) > 0.1 \cdot I_{mean}$) ranged from [270; 720] nm.

A.S1.11 Prediction of Degradation Rates and Identification of Dominant Photodegradation Mechanisms

General methodology

The effective contribution of nitrates and DOM as photosensitizers can be inferred from Eq. A.S5. The observed degradation rates were composed of the sum of elemental photo-oxidation processes (*e.g.* direct, HO^\bullet and ${}^3DOM^*$ mediated) [Bodrato and Vione, 2014, Janssen et al., 2014, Zeng and Arnold, 2013]. The contribution of carbonate radicals $CO_3^{\bullet-}$ as potential relevant photosensitizer was not included here because Vionne et al. (2009) highlighted the limited oxidation of atrazine and anilines with $CO_3^{\bullet-}$ under sunlight irradiation even in carbonate rich waters (sum of $[HCO_3^-]$ and $[CO_3^{2-}] \approx 10$ times higher than in our conditions) [Vione et al., 2009]. Accordingly, Eq. A.S5 can be simplified to Eq. A.S6. However, carbonates were considered as significant quenchers of HO^\bullet radicals [Zeng and Arnold, 2013].

$$\frac{\partial C}{\partial t} = -k_{obs} \cdot t \quad (A.S4)$$

$$\frac{\partial C}{\partial t} = - (k_{dir} + k_{HO^\bullet} \cdot [HO^\bullet]_{SS} + k_{{}^3DOM^*} \cdot [{}^3DOM^*]_{SS} + k_{{}^1O_2} \cdot [{}^1O_2]_{SS} + k_{CO_3^{\bullet-}} \cdot [CO_3^{\bullet-}]_{SS}) \quad (A.S5)$$

$$\frac{\partial C}{\partial t} = - (k_{dir} + k_{HO^\bullet} \cdot [HO^\bullet]_{SS} + k_{{}^3DOM^*} \cdot [{}^3DOM^*]_{SS} + k_{{}^1O_2} \cdot [{}^1O_2]_{SS}) \quad (A.S6)$$

C stands for pesticide concentration, k_{obs} for the observed degradation rate [T^{-1}], which is expressed as the sum of direct (k_{dir}) and selected indirect processes (k_{HO^\bullet} , $k_{{}^3DOM^*}$ and $k_{{}^1O_2}$). The latter degradation rates are second order and depend on the steady state concentrations of the associated short-lived reactive intermediates ($[HO^\bullet]_{SS}$, $[{}^3DOM^*]_{SS}$ and $[{}^1O_2]_{SS}$).

Calculation of Short-lived Reactive Intermediates Steady State Concentrations

Estimating the steady state concentrations of short-lived reactive intermediates requires identification of the main photosensitizers promoting and scavenging radicals and short-lived species and to determine the amount of light absorbed by each photosensitizers. The latter step accounts for competition for light irradiance between the different light-absorbing dissolved species as well as corrections for light attenuation.

Identification of Main Photosensitizers

Main short-lived reactive intermediates involved in pesticide photodegradation (HO^\bullet , $^3DOM^*$ and 1O_2) were formed through irradiation of fulvic substances and nitrates [Remucal, 2014]. $^3DOM^*$ and 1O_2 originate from irradiation of DOM and HO^\bullet from irradiation of DOM and nitrates [Schwarzenbach et al., 2003]. Fulvic acids such as SRFA also have the ability to scavenge HO^\bullet [Westerhoff et al., 2007] and 1O_2 [Cory et al., 2009]. These species are short-lived and their concentrations in water are balanced by their ratio of production over quenching as expressed in Eq. A.S7, A.S8 and A.S9 [Schwarzenbach et al., 2003].

$$[HO^\bullet]_{SS} = S(\lambda) \cdot \frac{\Phi_{HO^\bullet, NO_3^-} \cdot k_{a, NO_3^-} \cdot [NO_3^-] + \Phi_{HO^\bullet, DOM} \cdot k_{a, DOM} \cdot [DOM]}{k_{HO^\bullet, DOM} \cdot [DOM] + k_{HO^\bullet, HCO_3^-} \cdot [HCO_3^-] + k_{HO^\bullet, CO_3^{2-}} \cdot [CO_3^{2-}]} \quad (A.S7)$$

$$[^1O_2]_{SS} = S(\lambda) \cdot \frac{\Phi_{^1O_2, DOM} \cdot k_{a, ^1O_2} \cdot [DOM]}{k_{d, ^1O_2}} \quad (A.S8)$$

$$[^3DOM^*]_{SS} = S(\lambda) \cdot \frac{\Phi_{^3DOM^*, DOM} \cdot k_{a, DOM} \cdot [DOM]}{k_{^3DOM^*, O_2} \cdot [O_2]} \quad (A.S9)$$

$\Phi_{R, Sens}$ refers to the quantum yield of formation of short-lived reactive intermediates (R) by the photosensitizer (Sens) expressed in $mol.einstein^{-1}$, $k_{a, Sens}$ stands for the rate constant of light absorption by Sens over the whole light spectrum considered and is expressed in $einstein.mol^{-1}.s^{-1}$ and $k_{R, Sens}$ is the second-order rate constant of consumption of R by Sens in $mol^{-1}.L.s^{-1}$. $k_{d, ^1O_2}$ refers to the first-order reaction rate of 1O_2 with water and is expressed in s^{-1} . $[O_2]$ was set to $2.4 \cdot 10^{-4} M$ corresponding to the aqueous saturation at $20^\circ C$. Most parameters could be found in Janssen et al. (2014) [Janssen et al., 2014]. However, updated values were used instead when they could be found in recent literature (see Table A.S6).

Although it is in principle possible to evaluate $[^3DOM^*]_{SS}$ using eq. A.S9, there are some uncertainties in the literature about the value of $\Phi_{^3DOM^*, DOM}$. We chose to evaluate $[^3DOM^*]_{SS}$ using the following expression: $[^3DOM^*]_{SS} \approx [^1O_2]_{SS} / f_\Delta$, where f_Δ is the fraction of $^3DOM^*$ that produces 1O_2 . We chose a value of 0.34 for f_Δ based on data for a Suwannee River natural organic matter isolate from the IHSS [Schmitt et al., 2017].

Second-order rate constant for the reaction between atrazine or S-metolachlor and $^3DOM^*$ can be found in Zeng et al. (2013) [Zeng and Arnold, 2013]. They were determined by multiplying measured pseudo-first order reaction constant by the estimated

$[^3DOM^*]_{SS}$. As the $[^3DOM^*]_{SS}$ reported in Zeng et al. (2013) were manifestly underestimated (it does not follow the expression $[^3DOM^*]_{SS} \approx [^1O_2]_{SS}/f_{\Delta}$), it was necessary to correct the reported constant by recalculating them. We achieved that by recalculating $[^3DOM^*]_{SS}$ in Zeng et al. (2013). Then we calculated the corrected second-order rate between atrazine or S-metolachlor and $^3DOM^*$ as the reported second-order rate constant divided by the recalculated $[^3DOM^*]_{SS}$ and multiplied by the reported $[^3DOM^*]_{SS}$.

Table A.S6 – Kinetic parameters for formation and consumption of short-lived reactive intermediates

Quenching rates		Units	Reference	Comments
$k_{HO^{\bullet}, DOM}$	$1.6 \cdot 10^8$	$M^{-1}.s^{-1}$	[Westerhoff et al., 2007]	Most recent values as in [Janssen et al., 2014]
$k_{HO^{\bullet}, HCO_3^-}$	10^7	$M^{-1}.s^{-1}$	[Buxton et al., 1988, Vione et al., 2009]	
$k_{HO^{\bullet}, CO_3^{2-}}$	$4 \cdot 10^8$	$M^{-1}.s^{-1}$	[Buxton et al., 1988, Vione et al., 2009]	
$k_{^3DOM^*, O_2}$	$2 \cdot 10^9$	$M^{-1}.s^{-1}$	[Janssen et al., 2014]	
$k_{d, ^1O_2} (s^{-1})$	$2.5 \cdot 10^5$	s^{-1}	[Appiani et al., 2017, Cory et al., 2009, Janssen et al., 2014]	A recent work also reported a lower value of $4.5 \cdot 10^4$ as estimated from a DOM proxy (<i>i.e.</i> furfuryl alcohol) [Appiani et al., 2017]

Quantum yield of formation				
$\Phi_{HO\bullet, NO_3^-}$	$1 \cdot 10^{-2}$	/	[Dong and Rosario-Ortiz, 2012]	$(0.95\text{--}1.65) \cdot 10^{-5}$ Value chosen after an automatic procedure aiming at reducing discrepancies between observed and predicted values
$\Phi_{HO\bullet, DOM}$	$1.65 \cdot 10^{-5}$	/	[Cawley et al., 2015]	
$\Phi_{3DOM^*, DOM}$	$4.2 \cdot 10^{-4}$	/	[Cawley et al., 2015]	$(2.09\text{--}4.20) \cdot 10^{-4}$
$\Phi_{1O_2, DOM}$	$6.54 \cdot 10^{-2}$	/	[Cawley et al., 2015]	$(2.74 - 6.54) \cdot 10^{-2}$
Second-Order Rate Constants for Reactions of Target Pesticides with Short-lived Reactive Intermediates, All values available in [Zeng and Arnold, 2013]				
Atrazine				
$k_{HO\bullet}$	$2.7 \cdot 10^9$	$M^{-1}.s^{-1}$	k_{3DOM^*} was recalculated	
k_{1O_2}	$2.0 \cdot 10^5$			
k_{3DOM^*}	$1.0 \cdot 10^4$			
S-metolachlor				
$k_{HO\bullet}$	$6.9 \cdot 10^9$	$M^{-1}.s^{-1}$	k_{3DOM^*} was recalculated	
k_{1O_2}	$4.4 \cdot 10^5$			
k_{3DOM^*}	$8.1 \cdot 10^5$			

Calculation of Light Absorption Rates and Screening Factors

Calculations were performed over the spectral range $\lambda \in [270 - 320 \text{ nm}]$ as it corresponds to the range of significant absorbance for all dissolved species with respect to the emission spectrum of the Xenon arc lamp. As the light path length changed over repetitive samplings, an average path length of 15 *cm* was chosen as representative across the experiments. Changes in the actual path length would only significantly affect the absolute predicted degradation rates while the relative contribution of different processes would remain unaffected. The screening factor was computed in its wavelength dependant form. We assumed the light to travel straight through the quartz vial and to be insensitive to light scattering as in Eq. A.S10 [Wenk et al., 2011]. Depending on the water composition, $Sens_i$ referred to a combination of DOM, NO_3^- , atrazine and S-metolachlor. We introduced $S(\lambda)$ to calculate the rate of light absorption as shown in Eq. A.S11 [Bodrato and Vione, 2014].

$$S(\lambda) = \frac{1 - e^{-2.303 \cdot \sum (\epsilon_i(\lambda) \cdot [sens_i]) \cdot l}}{2.303 \cdot \sum (\epsilon_i(\lambda) \cdot [sens_i])} \quad (\text{A.S10})$$

$$k_{a,Sens} = \sum S(\lambda) \cdot \frac{A_i(\lambda)}{A_{tot}(\lambda)} \cdot E_0 \cdot \left(1 - 10^{-A_{tot}(\lambda)}\right) \quad (\text{A.S11})$$

Detailed Results

Predicted degradation rates and relative contributions of each short-lived reactive intermediates to the overall photodegradation are provided in Table A.S7. The prediction generally fitted with the observation of a systematic decrease in degradation rates in the presence of DOM, although predicted values of absolute degradation rates were more uncertain. The predicted degradation rates proved extremely sensitive to the average path length while the relative contribution of each photodegradation pathways was left completely unaffected by this parameter. The best fit to experimental data was obtained with an average path length of 8 *cm* (relatively lower than the actual value estimated at 15 *cm*). Predicted data were only compared with each other. Note that k_{dir} was not computed and that we used the observed values of degradation rates in UW instead. Indeed, k_{dir} strongly depends on the experimental setup, as shown by the wide range of reaction quantum yield for direct photodegradation gathered in Zeng et Arnold (2013) for atrazine and *S*-metolachlor with different light sources [Zeng and Arnold, 2013].

Table A.S7 – Comparison of predicted and observed degradation rates and presentation of the predicted contribution of each short-lived reactive intermediates to the overall photodegradation

Pesticide	Condition	Predicted contribution (%)				Predicted	Observed	Observed / Predicted (%)
		Direct	HO^\bullet	1O_2	$^3DOM^*$	$K_{deg} (d^{-1})$		
atrazine	DIR	100	0	0	0	0.57	0.57	100
	SRFA	34	22	2	42	0.14	0.12	164
	TOT	17	62	1	20	0.3	0.15	144
	NIT	25	75	0	0	0.46	0.94	58
<i>S</i> -metolachlor	DIR	100	0	0	0	0.28	0.28	100
	SRFA	8	54	4	33	0.09	0.1	144
	TOT	3	87	1	9	0.11	0.21	74
	NIT	5	95	0	0	0.28	5.11	8

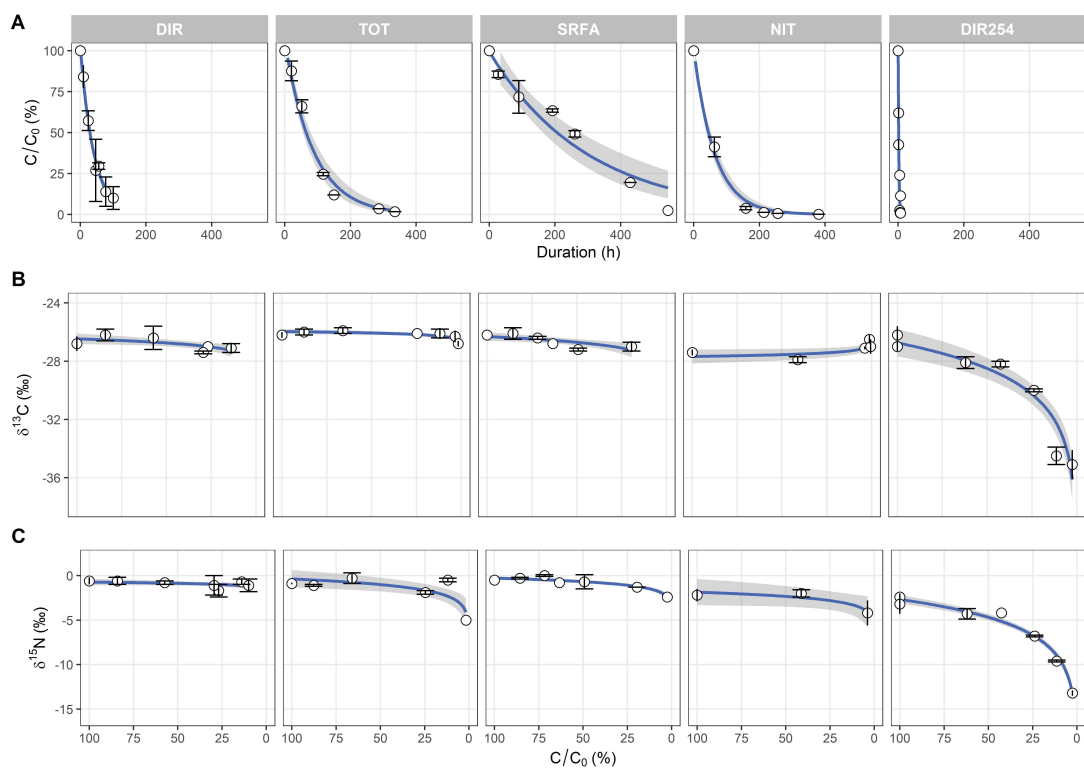


Figure A.S5 – Observed degradation kinetics (A) and Rayleigh plots for carbon (B) and nitrogen (C) for atrazine.

A.S1.12 Presentation of Experimental Datasets

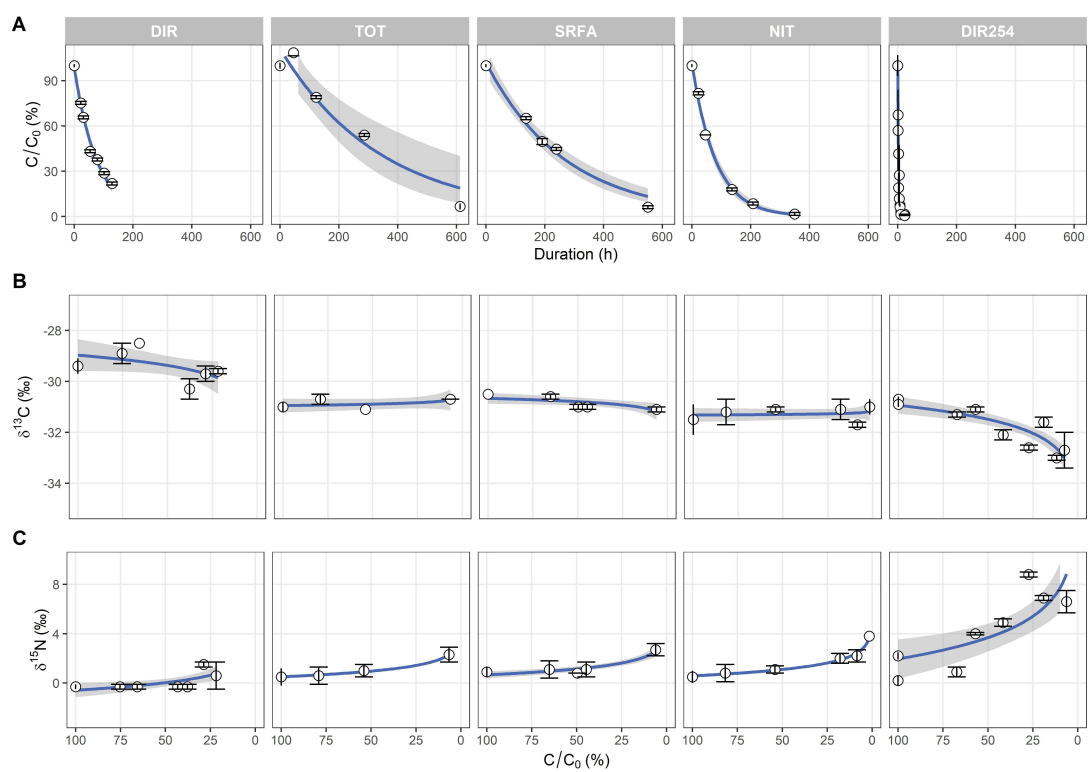


Figure A.S6 – Observed degradation kinetics (A) and Rayleigh plots for carbon (B) and nitrogen (C) for *S*-metolachlor.

A.S1.13 Comparison of C and N isotope fractionation during atrazine photodegradation, biodegradation and abiotic hydrolysis

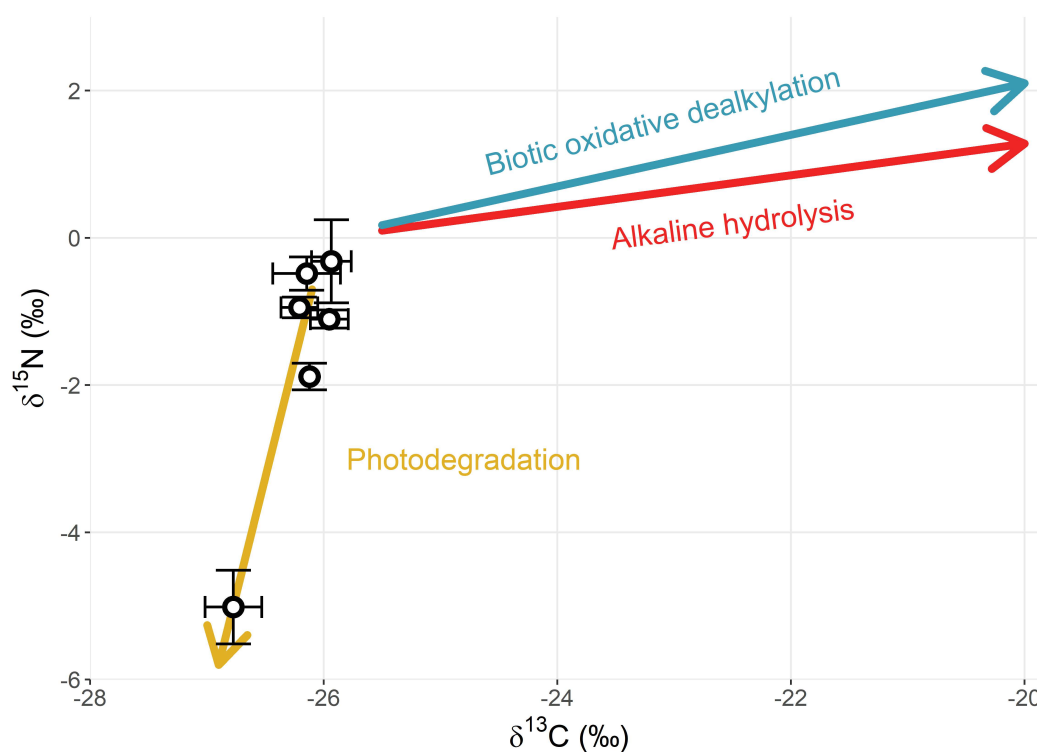


Figure A.S7 – Dual C and N isotope plot for atrazine reflecting contrasted enrichment patterns between biotic oxidative dealkylation by the bacterial strain *Rhodococcus* sp. NI86/21 [Meyer and Elsner, 2013], abiotic alkaline hydrolysis at pH 12 [Masbou et al., 2018] and photodegradation in agriculturally impacted surface waters, with points representing the C and N enrichments observed in the presence of nitrates and DOM.

Atrazine photodegradation footprint is mainly carried by changes in N stable isotope composition, whereas the others degradative processes occurring in surface waters are mostly reflected by changes of C stable isotope composition [Fenner et al., 2013].

Bibliography

- [Appiani et al., 2017] Appiani, E., Ossola, R., Latch, D. E., Erickson, P. R., and McNeill, K. (2017). Aqueous singlet oxygen reaction kinetics of furfuryl alcohol: effect of temperature, pH, and salt content. *Environmental Science: Processes & Impacts*, 19(4):507–516.
- [Bodrato and Vione, 2014] Bodrato, M. and Vione, D. (2014). APEX (Aqueous Photochemistry of Environmentally occurring Xenobiotics): a free software tool to predict the kinetics of photochemical processes in surface waters. *Environmental Science. Processes & Impacts*, 16(4):732–740.
- [Buxton et al., 1988] Buxton, G. V., Greenstock, C. L., Helman, W. P., and Ross, A. B. (1988). Critical Review of rate constants for reactions of hydrated electrons, hydrogen atoms and hydroxyl radicals (OH/O in Aqueous Solution. *Journal of Physical and Chemical Reference Data*, 17(2):513–886.
- [Cawley et al., 2015] Cawley, K. M., Korak, J. A., and Rosario-Ortiz, F. L. (2015). Quantum Yields for the Formation of Reactive Intermediates from Dissolved Organic Matter Samples from the Suwannee River. *Environmental Engineering Science*, 32(1):31–37.
- [Cory et al., 2009] Cory, R. M., Cotner, J. B., and McNeill, K. (2009). Quantifying Interactions between Singlet Oxygen and Aquatic Fulvic Acids. *Environmental Science & Technology*, 43(3):718–723.
- [Dimou et al., 2005] Dimou, A. D., Sakkas, V. A., and Albanis, T. A. (2005). Metolachlor Photodegradation Study in Aqueous Media under Natural and Simulated Solar Irradiation. *Journal of Agricultural and Food Chemistry*, 53(3):694–701.
- [Dong and Rosario-Ortiz, 2012] Dong, M. M. and Rosario-Ortiz, F. L. (2012). Photochemical Formation of Hydroxyl Radical from Effluent Organic Matter. *Environmental Science & Technology*, 46(7):3788–3794.

- [Dulin and Mill, 1982] Dulin, D. and Mill, T. (1982). Development and evaluation of sunlight actinometers. *Environmental Science & Technology*, 16(11):815–820.
- [Fenner et al., 2013] Fenner, K., Canonica, S., Wackett, L. P., and Elsner, M. (2013). Evaluating Pesticide Degradation in the Environment: Blind Spots and Emerging Opportunities. *Science*, 341(6147):752–758.
- [Gaffney et al., 1992] Gaffney, J. S., Marley, N. A., and Cunningham, M. M. (1992). Measurement of the absorption constants for nitrate in water between 270 and 335 nm. *Environmental Science & Technology*, 26(1):207–209.
- [Gutowski et al., 2015a] Gutowski, L., Baginska, E., Olsson, O., Leder, C., and Kümmerer, K. (2015a). Assessing the environmental fate of S-metolachlor, its commercial product Mercantor Gold® and their photoproducts using a water–sediment test and in silico methods. *Chemosphere*, 138(Supplement C):847–855.
- [Gutowski et al., 2015b] Gutowski, L., Olsson, O., Leder, C., and Kümmerer, K. (2015b). A comparative assessment of the transformation products of S-metolachlor and its commercial product Mercantor Gold(®) and their fate in the aquatic environment by employing a combination of experimental and in silico methods. *The Science of the Total Environment*, 506-507:369–379.
- [Hartenbach et al., 2008] Hartenbach, A. E., Hofstetter, T. B., Tentscher, P. R., Canonica, S., Berg, M., and Schwarzenbach, R. P. (2008). Carbon, Hydrogen, and Nitrogen Isotope Fractionation During Light-Induced Transformations of Atrazine. *Environmental Science & Technology*, 42(21):7751–7756.
- [Hessler et al., 1993] Hessler, D. P., Gorenflo, V., and Frimmel, F. H. (1993). Degradation of Aqueous Atrazine and Metazachlor Solutions by UV and UV/H₂O₂ — Influence of pH and Herbicide Concentration Abbau von Atrazin und Metazachlor in wäßriger Lösung durch UV und UV/H₂O₂ — Einfluß von pH und Herbizid-Konzentration. *Acta hydrochimica et hydrobiologica*, 21(4):209–214.
- [Héquet et al., 2001] Héquet, V., Gonzalez, C., and Le Cloirec, P. (2001). Photochemical processes for atrazine degradation: methodological approach. *Water Research*, 35(18):4253–4260.
- [Janssen et al., 2014] Janssen, E. M.-L., Erickson, P. R., and McNeill, K. (2014). Dual Roles of Dissolved Organic Matter as Sensitizer and Quencher in the Photooxidation of Tryptophan. *Environmental Science & Technology*, 48(9):4916–4924.

- [Karpuzcu et al., 2016] Karpuzcu, M. E., McCabe, A. J., and Arnold, W. A. (2016). Phototransformation of pesticides in prairie potholes: effect of dissolved organic matter in triplet-induced oxidation. *Environmental Science: Processes & Impacts*, 18(2):237–245.
- [Kochany and Maguire, 1994] Kochany, J. and Maguire, R. J. (1994). Sunlight Photodegradation of Metolachlor in Water. *Journal of Agricultural and Food Chemistry*, 42(2):406–412.
- [Laszakovits et al., 2017] Laszakovits, J. R., Berg, S. M., Anderson, B. G., O’Brien, J. E., Wammer, K. H., and Sharpless, C. M. (2017). p-Nitroanisole/Pyridine and p-Nitroacetophenone/Pyridine Actinometers Revisited: Quantum Yield in Comparison to Ferrioxalate. *Environmental Science & Technology Letters*, 4(1):11–14.
- [Masbou et al., 2018] Masbou, J., Drouin, G., Payraudeau, S., and Imfeld, G. (2018). Carbon and nitrogen stable isotope fractionation during abiotic hydrolysis of pesticides. *Chemosphere*, 213:368–376.
- [Meyer and Elsner, 2013] Meyer, A. H. and Elsner, M. (2013). $^{13}\text{C}/^{12}\text{C}$ and $^{15}\text{N}/^{14}\text{N}$ Isotope Analysis To Characterize Degradation of Atrazine: Evidence from Parent and Daughter Compound Values. *Environmental Science & Technology*, 47(13):6884–6891.
- [Remucal, 2014] Remucal, C. K. (2014). The role of indirect photochemical degradation in the environmental fate of pesticides: a review. *Environmental Science-Processes & Impacts*, 16(4):628–653.
- [Schmitt et al., 2017] Schmitt, M., Erickson, P. R., and McNeill, K. (2017). Triplet-State Dissolved Organic Matter Quantum Yields and Lifetimes from Direct Observation of Aromatic Amine Oxidation. *Environmental Science & Technology*, 51(22):13151–13160.
- [Schwarzenbach et al., 2003] Schwarzenbach, R. P., Gschwend, P. M., Imboden, D. M., and Imboden, M. (2003). *Environmental Organic Chemistry / Edition 2*.
- [Sharpless et al., 2003] Sharpless, C. M., Seibold, D. A., and Linden, K. G. (2003). Nitrate photosensitized degradation of atrazine during UV water treatment. *Aquatic Sciences*, 65(4):359–366.

- [Torrents et al., 1997] Torrents, A., Anderson, B. G., Billboulain, S., Johnson, W. E., and Hapeman, C. J. (1997). Atrazine Photolysis: Mechanistic Investigations of Direct and Nitrate-Mediated Hydroxy Radical Processes and the Influence of Dissolved Organic Carbon from the Chesapeake Bay. *Environmental Science & Technology*, 31(5):1476–1482.
- [Vione et al., 2009] Vione, D., Maurino, V., Minero, C., Carlotti, M. E., Chiron, S., and Barbati, S. (2009). Modelling the occurrence and reactivity of the carbonate radical in surface freshwater. *Comptes Rendus Chimie*, 12(8):865–871.
- [Wenk et al., 2011] Wenk, J., von Gunten, U., and Canonica, S. (2011). Effect of Dissolved Organic Matter on the Transformation of Contaminants Induced by Excited Triplet States and the Hydroxyl Radical. *Environmental Science & Technology*, 45(4):1334–1340.
- [Westerhoff et al., 2007] Westerhoff, P., Mezyk, S. P., Cooper, W. J., and Minakata, D. (2007). Electron Pulse Radiolysis Determination of Hydroxyl Radical Rate Constants with Suwannee River Fulvic Acid and Other Dissolved Organic Matter Isolates. *Environmental Science & Technology*, 41(13):4640–4646.
- [Zeng and Arnold, 2013] Zeng, T. and Arnold, W. A. (2013). Pesticide Photolysis in Prairie Potholes: Probing Photosensitized Processes. *Environmental Science & Technology*, 47(13):6735–6745.

A.S2 Biodegradation

A.S2.1 Appendices for material and methods

List of chemicals

Pesticides: atrazine, acetochlor, metalaxyl, S-metolachlor, metolachlor-d11 and terbutryn were purchased in highest available purity (> 99%; Pestanal®), Sigma–Aldrich, St. Louis, USA).

Commercially available transformation products of pesticides: carboxylic acid metalaxyl, demethylmetalaxyl, S-metolachlor ethanesulfonic acid (MET ESA), S-metolachlor oxanilic acid (MET OXA), acetochlor ethanesulfonic acid (ACE ESA), 2-hydroxy-atrazine (HA), desethylatrazine (DEA), desisopropylatrazine (DIA), atrazine-desethyl-2-hydroxy, metolachlor CGA 37913, metolachlor CGA 37735, metolachlor MFCD01034341 were purchased in A.C.S-grade reagents (> 98%) from Sigma–Aldrich (USA). Acetochlor oxanilic acid, deethylterbutryn, terbutylazine-2-hydroxy, terbutryn sulfoxide, desethylhydroxyterbutryne were purchased in highest available purity (> 99%) from TechLab (Metz, France). Terbutryn sulfoxide was purchased in highest available purity (> 97%) from MicroCombiChem (Wiesbaden, Germany). 2-hydroxy-acetochlor, metolachlor CGA 40919 and hydroxy-metolachlor were purchased as reference standard for GC in ACN from LGC Standards (Molsheim, France).

Solvent and reagents: dichloromethane (DCM), acetonitrile (ACN), ethanol (EtOH), ethylacetate (EtOAc) and pentane in HPLC grade purity (> 99.9%), anhydrous magnesium sulphate (MgSO₄; technical grade reagent, > 97%), calcium nitrate tetrahydrate (Ca(NO₃)₂·4H₂O), magnesium sulfate heptahydrate (MgSO₄·7H₂O), calcium chloride dihydrate (CaCl₂·2H₂O), sodium bicarbonate (NaHCO₃), potassium dihydrogen phosphate (KH₂PO₄), disodium hydrogen phosphate (Na₂HPO₄) were purchased in A.C.S-grade reagents (≥ 99%) were purchased from Sigma–Aldrich. Primary-secondary amine (PSA; P/N 52738, bonded silica) was purchased from Supelco (Bellefonte, USA). All aqueous solutions were prepared with ultrapure water (> 18 M.cm⁻¹).

Sediment sampling and characteristics

The 10 first centimetres of sediment were collected from an experimental stormwater wetland (Rouffach, France, 47°57'43" N, 7°17'26" E). A total of ten sub-samples, each

of 2 *kg* per location, were successively collected with a shovel cleaned with ultrapure water, acetone and wiped at 10 random spots. The ten sub-samples were then pooled together and homogenized with the shovel.

Physico-chemical parameters were measured following standard analytical procedures (NF/ISO) from homogenized sediment samples dried at 105°C and sieved at 2 *mm*. Residual humidity (RH) was measured by mass difference after drying to constant mass (ISO 11465). pH was measured in a 1:5 (w/w) sediment:ultrapure water ratio. Cation exchange capacity (CEC) was measured by the cobaltihexamine chloride extraction method (ISO 23470). Bulk density (BD) was measured using the core method (ISO 11272) from a core sample of soil with a known volume cylinder (48 cm^3) collected from field and weighted. Total carbon and organic carbon content for the sediment (f_{oc}) were measured by combustion on a CHN elementary analyzer (FLASH 2000 NC-Thermo Fisher Scientific; ISO 10694) with a precision of $\pm 2\%$. Before organic carbon measurement, the sediment was decarbonated by acid fumigation. (Ramnarine et al. 2011) Organic matter was measured by the weight loss on ignition method at 375°C during 16 hours (in house method). Particle size distribution was measured by laser diffraction methods in water mode (LS230, Beckmann Coulter; ISO 13320) and converted into three texture class contents following the World Reference Base (WRB) of soil: (IUSS working group WRB 2015) clay $< 2\text{ }\mu\text{m}$, silt from 2 to $50\text{ }\mu\text{m}$, and sand from 50 to $2000\text{ }\mu\text{m}$. First, several phases were sequentially removed by solid-liquid extraction: i) organic matter was extracted by proportion of 1:3 (v/v) H_2O_2 at 60°C , ii) flocculants cation was extract by proportion of KCl 1:50 (v/v) or HCl 1:20 (v/v) depending if the sample contain carbonate or no carbonate, iii) desegregation of particle was made by adding a 1:1 (v/v) solution of natrium hexametaphosphate 0.55%. Major elements (*Si*, *Al*, *Mg*, *Ca*, *Fe*, *Mn*, *Na*, *K*) were measured on a dried and powdered sediment using an agate disk mill ($< 250\text{ }\mu\text{m}$). Samples were prepared following: alkaline fusion procedure (NF ISO 14869-2) followed by a total dissolution in nitric acids:glycerol solution ($0.7 : 4\text{ mol.L}^{-1}$) and measurements by inductively coupled plasma optical emission spectrometry (ICP-OES, ICAP6500, Thermo Fisher Scientific).

Hydrochemistry characterization

Cation-anion contents were measured from a sub-sample filtered at $0.2\ \mu m$ with a CA filter of the water phase by ionic chromatography (ICS-5000, Dionex/Thermo Fischer, US EPA 300.0). DOC/DIC, COD and UV-Visible light absorbance measurements were performed using a separate sample filtered at $0.45\ \mu m$ with a CA filter. DOC/DIC were analyzed at selected sampling times (0, 15, 200 and 300 days) by TOC analyzer (TOC-V-CPH Shimadzu, NF EN 1484). COD was measured photometrically using test kit (P/N 985036, Nanocolor, range between 3 to $150\ mg.L^{-1}\ O_2$ Macherey-Nagel) at days 0 and 300 for oxic and anoxic conditions. The anoxic sample was prepared and transferred into the photometrically tube under Argon ($< 0.2\ ppm\ O_2$) using glovebox (GP[concept], Jacomex).

Batch sorption isotherm

Batch sorption experiments were conducted at room temperature ($20 \pm 5^\circ C$) and in the dark to avoid photolysis, following OECD Guideline 106: Adsorption - Desorption Using a Batch Equilibrium Method [OECD, 2000]. Batch sorption were carried out with the sediment used for biodegradation experiments. Three conditions were tested (i) sorption on non-autoclaved sediment with the pesticide mixture, (ii) sorption on autoclaved sediment with the pesticide mixture, and (iii) sorption on non-autoclaved sediment with individual pesticides. The differences between (i) and (ii) enabled to evaluate the effect of autoclaving on sorption properties in abiotic control experiments. Differences between (i) and (iii) enabled to assess the effect of pesticide mixture on sorption compared with sorption of a single pesticide. Sediment was dried at $40^\circ C$, sieved at 2 mm and stored in dark before sorption experiments. In a 50 mL polypropylene (PP) centrifuge tube, 5 g of dried sediment were mixed with 30 mL of $CaCl_2$ (0.01M) and vortex 20 seconds. Tubes were spiked with the pesticide mixture to obtained initial pesticide concentrations of 0.75, 1, 2.5, 5, 7.5 and 10 $mg.L^{-1}$ and flushed with N_2 until complete ACN evaporation. Centrifuge tubes were shaken (orbital shaker 80 rpm) for 24 hours. Tubes were then centrifuged at 2400 RCF for 20 minutes. The water phase was collected and filtered successively through 0.45 μm and 0.2 μm CA syringe filter. Pesticide extraction, quantification and CSIA were carried out as for the biodegradation experiment. Control experiments without TSS showed no sorption (> 95% of recovery) on the PP centrifuge tube within the range of concentrations at the time scale of the sorption experiments. Sorption experiments were best fitted with a linear model following:

$$P_s = K_d \cdot P_w \quad (A.S12)$$

Sorption was compared among experiments under the assumption that organic carbon content is directly related to pesticide sorption capacity. The sediment organic carbon-water partitioning coefficient (K_{oc}) were calculated for each experiment following:

$$K_{oc} = k_d \cdot f_{oc}^{-1} \quad (A.S13)$$

Mass balance accounting for the phase-transfer process

A pesticide mass balance was established from the two-phase conceptual model to detangle destructive and non-destructive processes contributing to pesticide dissipation in a water–sediment system with two phases. First, the pesticide mass balance was used to estimate the half-life of degradation ($DegT_{50}$) from the observed half-life of dissipation (DT_{50}) for each phase. Then, the conceptual model was used to evaluate how the isotopic fractionation factor (ϵ) was affected by desorption of isotopically lighter, non-degraded, pesticide from the sediment phase to the water phase.

Estimation of the Rate Constant of the Degradation - The pesticide mass balance relies on nine mathematical assumptions described below which set the boundaries of the developed framework. As compared with previous studies [Honti and Fenner, 2015, Shrestha et al., 2016, Honti et al., 2016] we closed the mass balance only for the pesticide itself as the other species (*i.e.* non-extractable residues - NER, formation of CO_2 over mineralization, sum of TPs) were not quantified in our study.

- I. The system is closed and the initial pesticide mass is conserved.
- II. The water–sediment system with two phases is defined similarly as in a previous study [Honti et al., 2016]; the water phase (subscript w) is assumed to contain only the aqueous freely dissolved species (P_w), and the sediment phases (subscript s) contains the bounded fraction of the studied species (*i.e.* particulate and dissolved organic carbon - P_s).
- III. Species are bounded (*i.e.* sorbed) only to organic carbon because the studied pesticides are not charge at the experimental pH (*i.e.* no ionic charge interactions with minerals). (Schwarzenbach, Gschwend, and Imboden 2016) Accordingly, pesticides may sorb to organic carbon present in the dissolved (DOC) and particulate (POC) forms.
- IV. Sorption on DOC and POC were assumed equivalent with sediment organic carbon-water partitioning coefficient (K_{oc}) and assumed to remain unaffected by the type of organic matter as well as the pH of the water phase. (Bronner and Goss 2011)
- V. As regards to the experimental durations, the system is assumed under steady state condition. This is supported by two aspects:

- (a) We observed a constant $P_s : P_w$ ratio all along the experiment which corresponded to K_d values obtained in a separate batch isotherm experiments (Table A.S2.2). It advocates for a fully established sorption equilibrium at any time.
- (b) The hydrochemistry was fairly stable during the experiment, suggesting constant water redox condition over the experiment.

- VI. The sum of all transformation products (TPs) is considered as a single species.
- VII. System shaking is assumed sufficient to maintain fully mixed conditions (*i.e.* the dissipation processes are homogeneous in the system over space and time). This is supported by a volume ratio between the total (V_{tot}) and by the water phase (V_w) close to one (0.96).
- VIII. Pesticide degradation in the sediment phase is negligible during the experiment. This is supported by the isotope signature showing no significant isotope fractionation in the sediment phase (Figure II.4), which follow the general assumption that sorbed species are not or less available for degradation (Schwarzenbach , Gschwend , and Imboden 2016). Consequently, species should be fully dissolved to be bio-available for microorganisms [Gadd, 2010]
- IX. Hydrolysis does not occur at the experimental pH for the species of interest [Masbou et al., 2018].

The pesticide mass balance equation (Eq. A.S14) writes:

$$m_{p,system} = m_{p,w} + m_{p,s} \quad (\text{A.S14})$$

The degradation during the experiment ($\frac{dm_{p,system}}{dt}$) is assumed to fit to a pseudo first-order degradation kinetic in the water phase (Eq. A.S15),

$$\frac{dm_{p,system}}{dt} = -k_{deg,w} \cdot t \cdot V_w \quad (\text{A.S15})$$

Under steady state condition, $m_{p,s}$ is expressed by the partitioning between the two phases following Eq. A.S12 and can be re-written as Eq. A.S16 ,

$$m_{p,s} = K_d \cdot m_{p,w} \cdot TSS \quad (\text{A.S16})$$

Which leads to Eq. A.S17 once reinjected in Eq. A.S14

$$m_{p,system} = m_{p,w} \cdot (1 + K_d \cdot m_{p,w} \cdot TSS) \quad (A.S17)$$

Then, the variation of pesticide mass in the sediment phase can be expressed as a function of $f_{oc,s}$ (Eq. A.S13) and the total organic carbon concentration (eq. A.S18; TOC) as the sum of particulate and dissolved species,

$$TOC = POC + DOC = f_{oc,s} \cdot TSS + DOC \quad (A.S18)$$

Eq. A.S17 becomes A.S19,

$$m_{p,system} = m_{p,w} \cdot [1 + K_{oc} \cdot (f_{oc,s} \cdot TSS + DOC)] \quad (A.S19)$$

Finally, assuming the observed dissipation of the pesticide in the water phase to follow a pseudo first-order reaction (Eq. A.S20):

$$\frac{dm_{p,s}}{dt} = -k_{obs,w} \cdot t \cdot V_w \quad (A.S20)$$

We get Eq. A.S21:

$$\frac{dm_{p,system}}{dt} = \frac{dm_{p,s}}{dt} \cdot [1 + K_{oc} \cdot (f_{oc,s} \cdot TSS + DOC)] \quad (A.S21)$$

Which brings the relationship between effective ($k_{deg,w}$) and observed ($k_{obs,w}$) degradation rates presented in Eq. A.S22, when combining Eq. A.S15 and A.S19:

$$k_{deg,w} = k_{obs,w} \cdot [1 + K_{oc} \cdot (f_{oc,s} \cdot TSS + DOC)] \quad (A.S22)$$

However, as in our system DOC and POC originated from the same source of sediment (*i.e.* DOC dissolved from POC), the sum of POC and DOC remained constant over time which agrees with observations (see section above). Additionally, DOC was negligible because i) it accounts for only 0.3% (DOC/POC in w/w) of the sediment phase, which is equivalent to 0.002% of the total sorbed pesticide mass of the system, ii) accounting for DOC would propagate a variance of $\pm 0.1 d^{-1}$ over the $k_{deg,w}$ which is far below the uncertainty associated to the calculation of the $k_{obs,w}$ which is $\pm 11 d^{-1}$, iii) TSS losses during the extraction process, less than 2%, are higher than the fraction of DOC contained within the system. By consequence we used the simplified Eq. A.S23:

$$k_{deg,w} = k_{obs,w} \cdot [1 + K_{oc} \cdot f_{oc,s} \cdot TSS] \quad (A.S23)$$

Impact of Phase Transfer on Isotopic Enrichment Factor Following the same assumptions and the water–sediment system conceptual model developed above for the degradation, we calculated a corrected isotopic enrichment factor ($\epsilon_{bulk,corr}$) accounting for degradation on the water phase only. As observed, the sorbed fraction of acetochlor and S-metolachlor was attributed to a constant isotope signature over time equal to $\delta^{13}C_0$, reflecting the absence of degradation within the sediment phase.

Under closed system assumption, experimental ϵ_{bulk} values for an element E is determined following the Raleigh equation (Eq. A.S24) [Van Breukelen, 2007]:

$$\ln \left(\frac{\delta^h E(t) + 1}{\delta^h E_0 + 1} \right) = \epsilon_{bulk} \cdot \ln \left(\frac{m_{p,w}}{m_{p,w_0}} \right) \quad (\text{A.S24})$$

Where m_{p,w_0} and $m_{p,w}$ are the initial and the remaining masses of pesticide. In the water–sediment system with two phases, $m_{p,w}$ corresponds to the freely dissolved fraction and m_{p,w_0} the initial dissolved pesticide mass at the equilibrium:

$$m_{p,w} = m_{p,system} - m_{p,s} \quad (\text{A.S25})$$

$$\ln \left(\frac{\delta^h E(t) + 1}{\delta^h E_0 + 1} \right) = \epsilon_{bulk} \cdot \ln \left(\frac{m_{p,system} - m_{p,s}}{m_{p,w_0}} \right) \quad (\text{A.S26})$$

Accordingly, ϵ_{bulk} is not linearly correlated to $\ln \left(\frac{m_{p,w}}{m_{p,w_0}} \right)$ anymore and cannot be derived from a simple linear regression. ϵ_{bulk} could not be analytically expressed as a function of $m_{p,w}$ either. By consequence, we used a stepwise calculation expressing $m_{p,system} - m_{p,s}$ according to the equivalent pesticide mass remaining in the water phase, that actually undergone degradation. This calculation accounts for the mass of pesticide desorbed from the sediment ($m_{p,s \rightarrow w}(t)$) and the mass of pesticide remaining in the water phase at each time step ($m_{p,w}(t)$) which can be expressed as the fraction of pesticide ($f_{p,s \rightarrow w}$) desorbing from the sediment over time, as follow:

$$f_{p,s \rightarrow w} = \frac{m_{p,s \rightarrow w}(t)}{m_{p,s \rightarrow w}(t) + m_{p,w}(t)} \quad (\text{A.S27})$$

Iterative correction scheme is necessary as $m_{p,s \rightarrow w}(t)$ at time t depends on the t-1 values (Eq. A.S28),

$$m_{p,s \rightarrow w}(t) = m_{p,s \rightarrow w}(t-1) - m_{p,deg} \quad (\text{A.S28})$$

where the theoretical pesticide mass degraded in water phase ($m_{p,deg}$) is recalculated based on a pseudo first-order k_{deg} previously derived.

Theoretically, isotope signatures follow additive properties. (Kendall and Caldwell 1998)
 At each time step the measured $\delta^h E_{meas}$ corresponds to a mix $\delta^h E$ values present in the water phase and that of the pesticide pool desorbed from the sediment (Eq. A.S29):

$$\delta^h E_{meas} = f_{p,s \rightarrow w} \cdot \delta^h E_s + (1 - f_{p,s \rightarrow w}) \cdot \delta^h E_w \quad (\text{A.S29})$$

As no degradation was observed in the sediment phases, $\delta^h E_s$ was assumed constant over time and equal to the $\delta^h E_0$. By using the system of equations A.S24 to A.S29 we expressed the modified Rayleigh equation as:

$$\ln \left(\frac{\delta^h E(t) + 1}{\delta^h E_0 + 1} \right) = \epsilon_{bulk,corr} \cdot (-k_{deg} \cdot t) \quad (\text{A.S30})$$

A.S2.2 Appendices for results and discussion

Sediment characteristics

The sediment texture (Table A.S8) could be classified as silt loam (Ditzler, Scheffe, and Monger 2017) with a low content of organic carbon and carbonate [OECD, 2002]. The C/N ratio of the sediment suggests a carbon limitation environment for microbial growth. (Demoling, Figueroa, and Bååth 2007; Hessen et al. 2004) Elemental composition analysis emphasizes that silica was the main constituent followed by calcium.

Table A.S8 – Wetland sediment characteristics

	Day 0		Day 300
	non- autoclaved	autoclaved	non- autoclaved
Residual humidity (w/w)	0.37 ± 0.03		
pH_{H2O}	7.5 ± 0.5		
pH_{CaCl2}	7.2 ± 0.5		
CEC (cmol g⁻¹)	14.3 ± 2.8		
BD (g cm⁻³)	1.7 ± 0.1		
Clay (< 2µm; %)	21.2 ± 2.5		19.3
Silt (2 - 50 µm; %)	67.4 ± 2.5		65.5
Sand (50 - 2000 µm; %)	11.4 ± 4.3		15.2
f_{oc} (%)¹	2.3 ± 2.1	1.2	2.0
C/N^a	7.2 ± 1.5	9.3	7.0
C_{min} (%)¹	3.9 ± 0.5	4.9	4.0
OM (%)	17.0		
SiO₂ (%)	52.9		
Al₂O₃ (%)	7.4		
MgO (%)	1.5		
CaO (%)	13.4		
Fe₂O₃ (%)	2.9		
MnO (%)	0.076		
TiO₂ (%)	0.44		
Na₂O (%)	1.0		
K₂O (%)	1.7		
P₂O₅ (%)	0.30		

¹ Measurements of f_{oc} , C/N and C_{min} are associated with an analytical uncertainty of 2%. Elementary analysis by ICP-OES measurements are reported for the most abundant oxide form.

Hydrochemistry

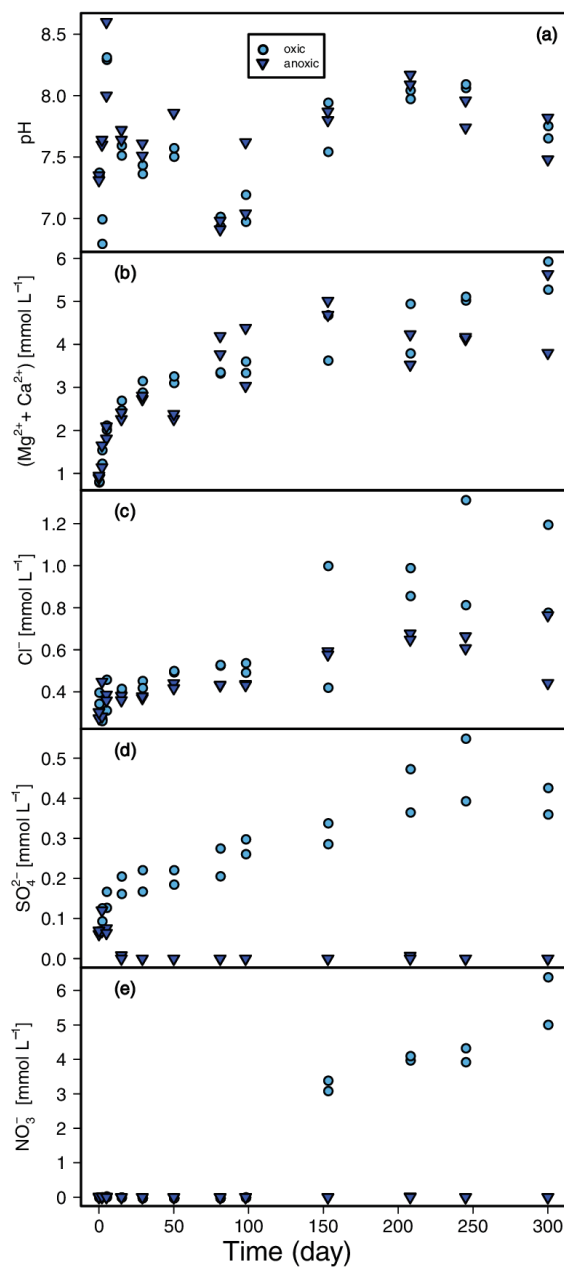


Figure A.S8 – Changes in hydrochemistry during biodegradation experiments. (a) pH, (b) magnesium-calcium ($Mg^{2+} + Ca^{2+}$), (c) chloride (Cl^-), (d) sulfate (SO_4^{2-}) and (e) nitrate (NO_3^-) concentrations.

Control experiments

Table A.S9 – Changes from days 0 to 300 of the Pesticide Remaining Fractions ($P(t)/P_0$) and Carbon Isotope Signatures ($\delta^{13}C$) in the Control Experiment. *w*: water phase, *s*: sediment phase, n.m.: not measured. CSIA of pesticides in the autoclaved sediment was associated with large matrix effect which did not enable the measurement. Uncertainties correspond to the standard deviations of *n* samples collected over time.

	atrazine	terbutryn	acetochlor	S-metolachlor	metalaxyl
oxic autoclaved (<i>n</i>=8)					
$\Delta(P(t)/P_0)_w$	1.01 ± 0.11	1.13 ± 0.25	1.15 ± 0.14	1.07 ± 0.09	1.11 ± 0.11
$\Delta(P(t)/P_0)_s$	1.04 ± 0.12	0.87 ± 0.12	0.95 ± 0.11	0.93 ± 0.07	1.09 ± 0.22
$\Delta\delta^{13}C_w$ (‰)	0.22 ± 0.81	-0.58 ± 0.51	0.81 ± 2.17	-0.63 ± 0.78	-1.56 ± 0.31
$\Delta\delta^{13}C_s$ (‰)	n.m.	n.m.	n.m.	n.m.	n.m.
anoxic autoclaved (<i>n</i>=8)					
$\Delta(P(t)/P_0)_w$	1.13 ± 0.14	1.56 ± 0.38	1.20 ± 0.19	1.11 ± 0.20	1.05 ± 0.11
$\Delta(P(t)/P_0)_s$	0.98 ± 0.07	0.82 ± 0.20	0.90 ± 0.08	0.95 ± 0.05	0.96 ± 0.17
$\Delta\delta^{13}C_w$ (‰)	-0.10 ± 0.36	0.05 ± 2.98	-1.12 ± 0.12	-0.54 ± 2.11	-2.05 ± 0.31
$\Delta\delta^{13}C_s$ (‰)	n.m.	n.m.	n.m.	n.m.	n.m.
hydrolysis autoclaved (pH=8; <i>n</i>=10)					
$\Delta(P(t)/P_0)_w$	0.88 ± 0.10	0.83 ± 0.12	0.94 ± 0.08	0.94 ± 0.11	1.23 ± 0.42

Batch sorption experiments

Table A.S10 – Comparison of Pesticide Sediment Partitioning Coefficients as Derived from the Batch Sorption Experiment and Observed During the Biodegradation Experiments. Uncertainties correspond to the 95% confidence interval (C.I.) from n replicate measurements.

Batch sorption experiments (OECD 106)		Biodegradation experiment	
	K_d (L kg ⁻¹) ¹	P_s - P_w ratio (L kg ⁻¹)	
Sediment non-autoclaved and pesticide in mixture			
<i>(n</i> = 11; pH=7.5)		oxic (<i>n</i> = 10)	anoxic (<i>n</i> = 10)
atrazine	4.1 ± 5.7	1.4 ± 0.9	0.8 ± 0.4
terbutryn	21.6 ± 5.8	12.9 ± 9.0	13.3 ± 11.1
acetochlor	5.8 ± 2.3	4.3 ± 3.4	2.4 ± 1.3
<i>S</i> -metolachlor	6.6 ± 1.7	3.8 ± 2.3	2.6 ± 0.8
metalaxyl	0.6 ± 0.4	1.3 ± 0.8	0.6 ± 0.3
Sediment non-autoclaved and one pesticide at the time			
<i>(n</i> = 8; pH=7.5)			
atrazine	2.1 ± 1.4		
terbutryn	15.7 ± 2.0		

¹ The coefficient of determination (R^2) of linear K_d fitting ranged from 0.66 to 1.00.

Pesticide dissipations

Dissipation in water were 2 to 6 times faster under oxic conditions than under anoxic conditions, although acetochlor dissipation rate constant did not differ among conditions (Figure A.S9). Dissipation rate constants in water and sediment were similar, under the same conditions, on the basis of the 95% C.I. However, dissipation of S-metolachlor under oxic condition was faster in water, whereas dissipations of atrazine and metalaxyl under anoxic conditions were faster in the sediment.

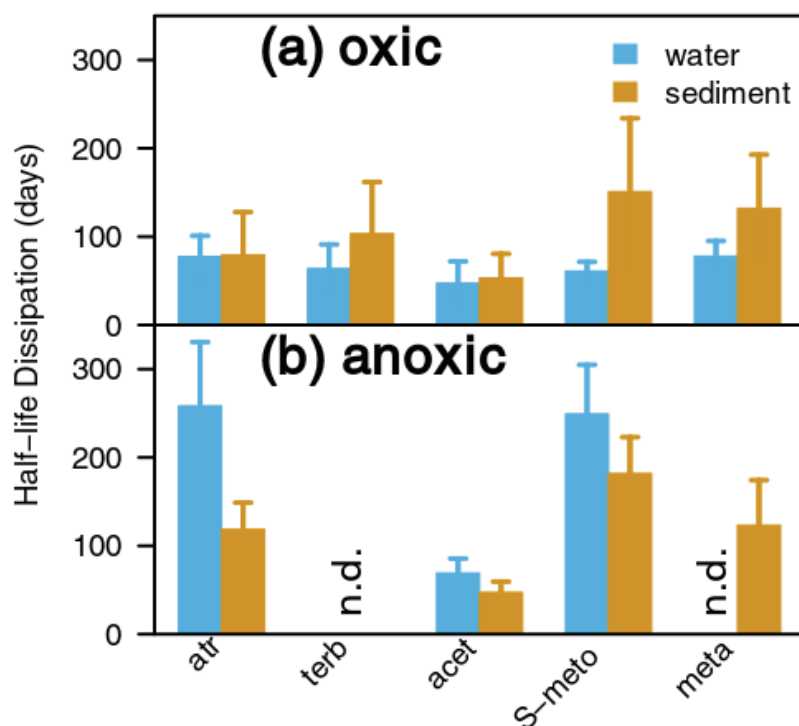


Figure A.S9 – Half-life dissipation (DT_{50}) for atrazine (atr), terbutryn (terb), acetochlor (acet), S-metolachlor (S-meto) and metalaxyl (meta) under (a) oxic and (b) anoxic conditions in the water and the sediment phases. Metalaxyl did not follow a strict pseudo first-order kinetics (goodness on linear fit $R^2 = 0.6$) in both phases. n.d.: not determined due to not enough degradation ($P(t)/P_0 > 0.5$) to calculate a DT_{50} .

Insignificant changes in carbon stable isotope signature were observed (obs) in wa-

ter and sediment after 300 days for atrazine ($\Delta\delta^{13}C_{obs} < 1.0\text{‰}$) and metalaxyl ($\Delta\delta^{13}C_{obs} < 0.7\text{‰}$). Terbutryn was mainly found in the sediment, and low concentration in the water phase hampered CSIA measurements. By consequence, CSIA data obtained for atrazine, terbutryn and metalaxyl were not further analyzed. **Only data for acetochlor and S-metolachlor are further analyzed.**

Bibliography

- [Gadd, 2010] Gadd, G. M. (2010). Metals, minerals and microbes: geomicrobiology and bioremediation. *Microbiology*, 156(3):609–643.
- [Honti and Fenner, 2015] Honti, M. and Fenner, K. (2015). Deriving Persistence Indicators from Regulatory Water-Sediment Studies – Opportunities and Limitations in OECD 308 Data. *Environmental Science & Technology*, 49(10):5879–5886.
- [Honti et al., 2016] Honti, M., Hahn, S., Hennecke, D., Junker, T., Shrestha, P., and Fenner, K. (2016). Bridging across OECD 308 and 309 Data in Search of a Robust Biotransformation Indicator. *Environmental Science & Technology*, 50(13):6865–6872.
- [Masbou et al., 2018] Masbou, J., Drouin, G., Payraudeau, S., and Imfeld, G. (2018). Carbon and nitrogen stable isotope fractionation during abiotic hydrolysis of pesticides. *Chemosphere*, 213:368–376.
- [OECD, 2000] OECD (2000). *Test No. 106: Adsorption – Desorption Using a Batch Equilibrium Method*. Organisation for Economic Co-operation and Development, Paris.
- [OECD, 2002] OECD (2002). *OECD Guidelines for the Testing of Chemicals / OECD Series on Testing and Assessment Report of the OECD/UNEP Workshop on the Use of Multimedia Models for Estimating Overall Environmental Persistence and Long Range Transport in the Context of PBTS/POPS Assessment*. OECD Publishing.
- [Shrestha et al., 2016] Shrestha, P., Junker, T., Fenner, K., Hahn, S., Honti, M., Bakkour, R., Diaz, C., and Hennecke, D. (2016). Simulation studies to explore biodegradation in water–sediment systems: From OECD 308 to OECD 309. *Environmental Science & Technology*, 50(13):6856–6864.
- [Van Breukelen, 2007] Van Breukelen, B. M. (2007). Quantifying the Degradation and Dilution Contribution to Natural Attenuation of Contaminants by Means of an Open System Rayleigh Equation. *Environmental Science & Technology*, 41(14):4980–4985.

Appendix B

Supporting information to chapter III

B.S1 Current developments at the SWI

The following table summarizes main studies targeting pollutant transport at the SWI with a coupled approach between experimental and numerical developments. On average, the laboratory flumes were $\approx 5\text{ m}$ long, recirculated and allowed for studying the effects of riverbed forms on transport. Conservative, sorptive and reactive tracers have all already been actively studied. Among the works referenced here, only one [Kaufman et al., 2017] attempted a physically-based discretization of the SWI with a multi-domain transport model. Most of the other works focused on diffusive type model with additional pumping or advective equations.

Table B.S1 – Short review of current numerical and experimental developments at the SWI (Continued on the two next pages)

Reference	Purpose	Tracer	Physico-chemical properties	Flume size (m)	Flume type	Riverbed geometry	Flow characteristics	Sediment grain size <i>mm</i>	Model type
[Kaufman et al., 2017]	Transport & reactivity	Dissolved oxygen	Degrading	5	Recirculated	Bed forms	Turbulent	Quartz sand $\Phi_{50} = 1.5 + 0.05\%$ finely crushed walnut shells	Multi-domain (2D vertical)-continuity of pressure at the interface
[Trauth et al., 2013]	Flow	/	/	10	Numerical test case	Bed forms	Turbulent	sandy sediment	Multi-domain (3D - Open-FOAM) - continuity of pressure at the interface
[Nagaoka and Ohgaki, 1990]	Flow visualisation & transport	<i>NaCl</i>	Conservative	3	Recirculated	Flat	Turbulent	Ceramic balls $19 < \Phi_{50} < 40$	Diffusive
[Marion et al., 2002]	Transport	<i>NaCl</i>	Conservative	25	Recirculated	Bed forms	Turbulent	Quartz sand $\Phi_{50} = 0.85$	Diffusive pumping model

Reference	Purpose	Tracer	Physico-chemical properties	Flume size (m)	Flume type	Riverbed geometry	Flow characteristics	Sediment grain size <i>mm</i>	Model type
[Elliott and Brooks, 1997]	Transport	7-amino, 1,3 naphthalene disulphonic acid (CAS: 86-65-7) & Brilliant Sulphafavin (CAS: 2391-30-2)	Conservative	5	Recirculated	Flat and bed form	Turbulent	Sand $\Phi_{50} = 0.47$ and $\Phi_{50} = 0.13$	Diffusive pumping model +
[Fox et al., 2014]	Transport (horizontal & vertical fluxes)	Brilliant Blue FCF (CAS: 3844-45-9)	Conservative	6.4	Recirculated	Bed forms	Turbulent	Quartz sand $\Phi_{50} = 0.384$	Pumping model + advective term
[Eylers et al., 1995]	Transport & sorption	Zinc & Lithium	Sorptive	4.34	Recirculated	Bed forms	Turbulent	Quartz sand $\Phi_{50} = 0.500$ and $\Phi_{50} = 0.195$	Pumping model
[Ren and Packman, 2004]	Transport & sorption (colloids)	<i>NaCl</i> & Zinc	Conservative & sorptive	2.5	Recirculated	Bed forms	Turbulent	Quartz sand $\Phi_{50} = 0.500$ & Colloids (silica + kaolinite)	Diffusive pumping model +

Reference	Purpose	Tracer	Physico-chemical properties	Flume size (m)	Flume type	Riverbed geometry	Flow characteristics	Sediment grain size <i>mm</i>	Model type
[Liao et al., 2013]	Transport & reactivity & sorption	fluorescein (CAS: 2321-07-5) & resazurin (CAS: 62758-13-8) & resorufin (CAS: 635-78-9)	Conservative & degrading	River scale 200	Flow through	Actual riverbed	Turbulent	Coarse sand & gravels	1D advection dispersion with travel time distribution
This work	Transport & sorption	<i>NaCl</i> & Foron Blue 291	Conservative & sorptive	Bench scale - 0.15	Recirculated	Flatbed (~ bed-forms)	Laminar (potential for mild turbulent)	Quartz sand $\Phi_{50} = 0.493$	Fully coupled multi-domain (2D vertical) - continuity of all variables

B.S2 Sand characterization

The sand used was from Kaltenhouse (France, Alsace). Its particle size distribution was determined with a Beckmann-Coulter laser particle size analyser (Table B.S2). The sand was thoroughly washed in a rotatory shaker for 3 times 24 hours in renewed Ultrapur water. Its composition was characterized from ICP-OES measurement assuming that an element is present in its most abundant oxide form and is reported in Table B.S3. The sand saturated conductivity was determined with the constant-head method to be $K_0 = 7.4 \pm 2.2 \cdot 10^{-4} \text{ m.s}^{-1}$.

Table B.S2 – Sand particle size distribution

Quartile	Size (μm)
Φ_5	310
Φ_{10}	340
Φ_{16}	373
Φ_{25}	410
Φ_{30}	450
Φ_{50}	494
Φ_{60}	542
Φ_{75}	595
Φ_{84}	653
Φ_{90}	717
Φ_{95}	787

Table B.S3 – Sand relative composition

Parameter	Proportion (%)
OM	0.06
SiO ₂	98.7
Al ₂ O ₃	0.38
MgO	0.043
CaO	0.26
Fe ₂ O ₃	< 0.03
MnO	< 0.0002
TiO ₂	0.015
Na ₂ O	< 0.07
K ₂ O	< 0.1
P ₂ O ₅	< 0.004

B.S3 Characterization of FB291 adsorption from the batch equilibrium method – OECD 106

Around 5 g of washed sand was equilibrated in 30 mL of 0.01 M $CaCl_2$ solution, spiked with FB291 at 5 different concentrations from 0 to $200\text{mg}\cdot\text{L}^{-1}$ and shaken for 24 hours at room temperature ($T = 20 \pm 2\text{ }^\circ\text{C}$). Afterwards, the remaining concentration in the liquid phase was quantified and assumed to be the equilibrium concentration. The experiment was duplicated. Assuming a closed mass balance (degradation $< 5\%$ after 48h), calculation of phase partitioning allowed us to derive the adsorption isotherm and the associated K_d value. Linear isotherm proved to be the most suited in this case with $K_d = 7.7 \pm 0.2\text{ mL}\cdot\text{g}^{-1}$ for FB291 as represented in Figure B.S1.

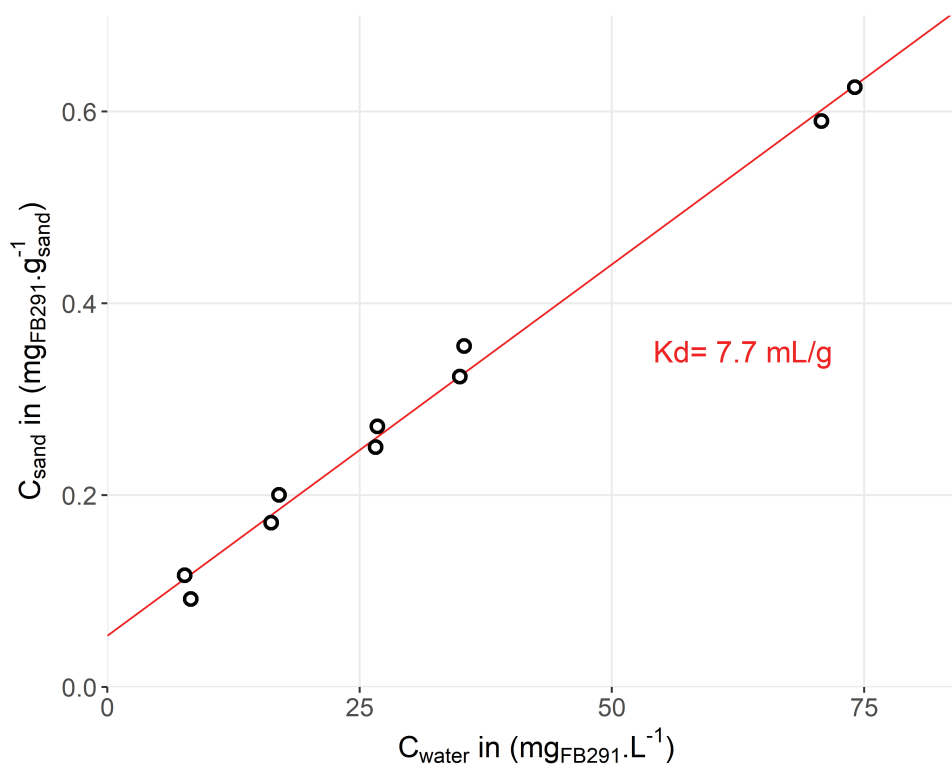


Figure B.S1 – Sorption isotherm of FB291 with dissolved concentrations of FB291 plotted versus solid concentrations at equilibrium and linear regression performed to derive K_d .

B.S4 Compensation of tracer concentrations for evaporation and ion release

Evaporation and ion release from sand were observed during tracer experiments. A beaker full of water with similar shape than the mixing beaker was placed along with the channel and weighted over time to account for evaporation. Blank experiments were also conducted for low and high flow without tracer to quantify any unexpected release of ions from sand, potentially increasing the measured conductivity. The latter correction only concerned tracer experiments with NaCl as the spectrophotometric measure of FB291 was not impacted by ion release. All along the experiments, evaporation was pretty constant and was estimated at $\approx 0.5 \text{ mL.h}^{-1}$ (except for ELF_{NaCl} where a failure of the air conditioning happened and the evaporation raised up to $\approx 5 \text{ mL.h}^{-1}$). Evaporation effect was accounted for by applying a dilution formula to the measured concentration ($C_{measured}$), knowing the rate of evaporation (R_{evap}) and reporting it to the initial water volume (V_0) as in Equation B.S1. The influence of ion release was estimated to account for a final shift in the measured NaCl concentration comprised between 5% to 20% of the equilibrium concentration. The measured conductivity in blank experiment ($blank$) was subtracted to the measured conductivity in tracer experiment ($measured$) at each time step and further converted to NaCl concentrations as in Equation B.S2.

$$C_{measured} \cdot (V_0 - R_{evap}) = C_{compensated} \cdot V_0 \quad (\text{B.S1})$$

$$\sigma_{compensated} = \sigma_{measured} - \sigma_{blank} \quad (\text{B.S2})$$

Altogether, these uncertainties make the analysis of the absolute values of NaCl concentrations within the mixing beaker relatively sensitive to experimental bias. Nevertheless, measurements within the sediment bed were less sensitive to these bias as they reacted with a longer timescale. At the opposite, as measurements of FB291 was not sensitive to ion release, the method was much more reliable. Altogether, it would advocate to replace NaCl by another conservative tracer for further use (*e.g.* fluorescein although photosensitive), which could even be simultaneously detected with FB291 by a fluorimeter.

B.S5 Scaling methodology of concentrations for inter-comparison of experiments

To allow for inter-comparison of different experiments, measured concentrations (C_b) were scaled by the theoretical equilibrium value (C_{eq}) observed when the equilibrium is fully reached as in (3):

$$C^*(t) = \frac{C_b(t)}{C_{eq}} \cdot 100 \quad \text{in \%} \quad (\text{B.S3})$$

$$C_{eq} = \begin{cases} \frac{C_0 \cdot V_b}{(V_b + V_p) + K_d \cdot M_s} & \text{For incorporation} \\ \frac{C_0 \cdot V_p}{(V_b + V_p) + K_d \cdot M_s} & \text{For export} \end{cases} \quad (\text{B.S4})$$

Where $C^*(t)$ is the normalized concentration, C_0 the initial tracer concentration spiked either in the overlying water or within the sediment bed, V_p and V_b the pore water and the overlying water volume in the system, M_s the mass of sediment constituting the river bed and K_d the adsorption capacity of the tracer ($K_d = 0 \text{ mL.g}^{-1}$ for NaCl). Eq. B.S4 stands for the incorporation and Eq. B.S5 for the export configurations. Accordingly, phase partitioning due to adsorption ($K_d > 0$) is expected to exacerbate the differences between C_0 and C_{eq} during incorporation and to lower the potential release during export.

B.S6 Mesh sensitivity analysis

Flow and transport dependency to mesh size has been tested with 2 different meshes of decreasing element size; coarse \rightarrow 5606 elements, $\delta_L \approx 3 - 4 \text{ mm}$ and fine \rightarrow 9406 elements, $\delta_L \approx 1 - 2 \text{ mm}$. The analysis was conducted with the highest experimentally tested velocity ($u^* = 5.4 \cdot 10^{-2} \text{ m.s}^{-1}$) as it revealed the maximum error with mesh size. Tracer was initially in the sediment and released toward the flowing water. To avoid inaccuracies arising from large time steps, Δt_{max} was set at 0.13 s . Velocities dropped from 5 orders of magnitude between the NS and the DB domain ($5 \cdot 10^{-2}$ to $1 \cdot 10^{-7} \text{ m.s}^{-1}$) with a minor sensibility to mesh size of about $\Delta u = 1 \cdot 10^{-8} \text{ m.s}^{-1}$. However, it did not significantly impact transport processes and both solutions converged toward the same equilibrium (see Figure B.S2A and B.S2B). In both cases, the amount of mass within the system remained constant ($\Delta_m \pm 0.05\%$ in the end of the simulation) indicating a closed mass balance. As a consequence, a millimetric element size at the interface and within the porous domain is prescribed for further simulations, which is consistent with previous studies using similar element sizes [Gualtieri, 2010, Kaufman et al., 2017]. The coarse mesh was further used for the model validation.

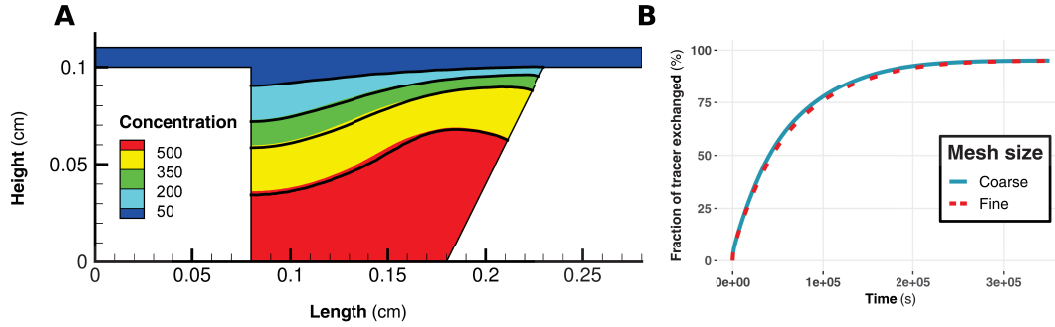


Figure B.S2 – A) Comparison of predicted tracer distribution at $t=3$ hours within the porous medium with coarse (solid lines) and fine (coloured area) mesh, B) Mesh size effect on the predicted tracer mass exchange as measured within the mixing beaker.

B.S7 Fit of modelled velocities with the log-law profile

Velocity distribution in channels with impermeable walls is well established and described by the log-law of wall (Eq. B.S6) with no slip velocity at the wall [Grant and Marusic, 2011, Nikuradse, 1950].

$$\frac{\bar{u}}{u^*} = \frac{1}{k} \ln \left(\frac{y}{y_0} \right) + b \quad (\text{B.S6})$$

with \bar{u} the horizontal velocity at depth y , u^* the shear velocity characterizing the shear stress at the boundary, y_0 the characteristic roughness indicating whether under fixed flow conditions the logarithmic profile is impacted by the bed roughness and finally, $k \approx 0.41$ and $B \approx 5$ are the empirical Von Karman constant assumed universal [Grant and Marusic, 2011]. With a permeable wall (*i.e.* sediment bed), a non-null slip velocity is observed but the shape of the velocity profile remains unaffected and the log-law of wall can be revised as in Eq. B.S7 [Nagaoka and Ohgaki, 1990, Rosti et al., 2015].

$$\frac{\bar{u} - u_i}{u^*} = \frac{1}{k} \cdot \ln \left(\frac{y}{y_0} \right) + b \quad (\text{B.S7})$$

with u_i the interface horizontal velocity estimated at $y = 0$.

In this context, we tested our simulations against Eq. B.S7 to confirm the ability of the model to accurately and physically reproduce water flow within the overlying water. As Eq. B.S7 is only valid above the viscous sub-layer (*i.e.* where the velocity profile is linear) the fit to Eq. B.S7 with our simulations was performed with points lying far enough from the sediment bed and from the surface of the overlying water. Consequently, the two points the closest to the interface were excluded as they may lie in the viscous sublayer as well as the points the closest to the water surface as it may be influenced by the air-water interface. Thus, the fit was performed on the five intermediate points.

The slip velocity $u_i = 0.96 \text{ cm.s}^{-1}$ was determined using the closest velocities computed above and below the interface (Eq. B.S8). $u^* = 0.55 \text{ cm.s}^{-1}$ was evaluated using two points of the logarithmic zone (P3 and P6) according to Eq. B.S9. $y_0 = 0.22 \text{ cm}$ corresponds to the origin of the regression line in Figure III.5B. Finally, the modelled velocity followed Eq. B.S7 parameterized as in Eq. B.S10 and represented by the red line in Figure III.5B.

$$u_i = u^+ - \frac{u^+ - u^-}{y^+ - y^-} \cdot y^+ \quad (\text{B.S8})$$

$$u^* = \frac{k}{2.3} \cdot \frac{u_{P6} - u_{P3}}{\log_{10}(y_{P6}) - \log_{10}(y_{P3})} \quad (\text{B.S9})$$

$$\frac{\bar{u} - 0.96}{0.55} = \frac{1}{0.40} \cdot \ln\left(\frac{y}{0.22}\right) + 5.50 \quad (\text{B.S10})$$

B.S8 Darcy's velocities calculation

Darcy's velocities were computed at several depths within the sediment bed. Streamtraces similar to those plotted in Figure III.5A were used to approximate the water path length (ΔL) within the sediment bed. Note that streamtraces revealed quasi-horizontal velocities around $X = 0.15 \text{ cm}$, making Darcy's velocities comparable with the horizontal component of the velocity plotted in Figure III.5B at the same horizontal position. At the sediment water interface, pressure steadily decreased from positions ($X = 0.08 \text{ m}$, $Y = 0.10 \text{ m}$) to (0.23 m , 0.10 m) leading to a maximal pressure gradient of $\Delta P_0 = 1.1 \text{ Pa.m}^{-1}$. The pressure gradient associated to each streamtrace was calculated as $\Delta P = \Delta P_0 \cdot \frac{\Delta X}{\Delta X_0}$, with ΔX being the difference between the horizontal positions where a streamtrace penetrates and exits the sediment bed. Finally, Darcy's velocities were computed according to Eq. B.S11 and the head gradient (∇H) alongside a streamtrace from Eq. B.S12 .

$$v_{Darcy} = -K_0 \nabla H \quad (\text{B.S11})$$

$$\nabla H = \frac{\Delta P}{\rho \cdot g \cdot \Delta L} \quad (\text{B.S12})$$

B.S9 Characterization of the transport regime with Pe

The nature of the locally dominant transport process was retrieved from calculation of the Peclet number (Pe) over depth, see Eq. B.S13.

$$Pe(z) = \frac{\overline{u_i u_j} \left(\frac{L_c}{2}, z \right) \cdot L_c}{D_m} \quad (\text{B.S13})$$

where L_c is the characteristic length of the system, taken as $L_c = 0.15 \text{ m}$ corresponding to the SWI length. $\overline{u_i u_j} \left(\frac{L_c}{2}, z \right)$ is the averaged velocity magnitude on horizontal and vertical directions at depth z and at middle length of the channel. Pe was computed at the centre of meshes as the code provides u_i and u_j at these positions. $Pe \gg 1$ is indicative of an advection driven transport regime while when Pe comes close to 1 or below, diffusion becomes more prominent on the overall transport.

B.S10 Characterization of the transport regime with D_{eff}

Mass exchanges at the SWI can be represented by an equivalent diffusivity with the help of a 1D Fickian type transport equation (see Eq. B.S14) [Grant et al., 2012]:

$$\frac{\partial C}{\partial t} = D_{eff} \cdot \frac{\partial^2 C}{\partial z^2} \quad (\text{B.S14})$$

where z [L] and t [T] represent the vertical position within the sediment bed and the time, C [$M.L^{-3}$] the concentration of the dissolved species and D_{eff} [$L^2.T^{-1}$] the effective diffusivity accounting for molecular ($D_m = 2.0 \cdot 10^{-9} \text{ m}^2.s^{-1}$ for NaCl), dispersive (D_{disp} [$L^2.T^{-1}$]) and turbulent (D_{turb} [$L^2.T^{-1}$]) diffusivities.

The ratio D_{eff}/D_m is an accurate proxy to determine whether the dominating transport process at the interface is purely diffusive, dispersive or caused by turbulences penetrations within the sediment bed [Voermans et al., 2018].

Determination of D_{eff} in the case of a recirculated experimental flume with tracer coming from the overlying water can be done with Eq. B.S15 [Grant et al., 2012].

$$C^*(t) = 1 - 2 \cdot \frac{A_s}{V_w} \cdot \sqrt{\frac{D_{eff}}{\pi}} \cdot t \quad (\text{B.S15})$$

Here, $C^*(t)$ stands for the ratio $C(t)/C(t=0)$, A_s the area of the SWI ($A_s = 7.5 \cdot 10^{-3} \text{ m}^2$) and V_w the volume of overlying water. A plot of $C^*(t)$ versus \sqrt{t} then yields to a affine relationship of slope $2 \cdot \frac{A_s}{V_w} \cdot \sqrt{\frac{D_{eff}}{\pi}}$. Eq. B.S15 stands for a semi-infinite sediment bed with no influence of the sediment bottom along the tracer experiment. This assumption was believed sufficient with decametric deep sediment beds as in the case of Nagaoka and Ohgaki (1990) for example [Nagaoka and Ohgaki, 1990]. Thus, as our experimental setup has similar vertical extent, Eq. B.S15 applies. However, as edge effects arose by the end of the experiments (once the tracer reached the bottom), we only considered the linear part of the plot $C^*(t)$ versus \sqrt{t} for the regression (see Figure S4).

D_{eff} was determined from numerical results for the configurations ILF_{NaCl} and IHF_{NaCl} . Figure B.S3 shows the plots $C^*(t)$ versus \sqrt{t} in each cases. In addition, as export and incorporation conditions yielded similar results, so the values of D_{eff} were assumed equivalent for EL and EH. Finally, we get $\left\{ \frac{D_{eff}}{D_m} \right\}_{HF} = 15.2$ ($D_{eff_{HF}} = 3.0 \cdot 10^{-8} \text{ m}^2.s^{-1}$) and $\left\{ \frac{D_{eff}}{D_m} \right\}_{LF} = 3.8$ ($D_{eff_{LF}} = 7.7 \cdot 10^{-9} \text{ m}^2.s^{-1}$). These values

are in accordance with dispersion driven transport processes according to Voermans et al. (2018) ($10^0 < \frac{D_{eff}}{D_m} < 10^3$).

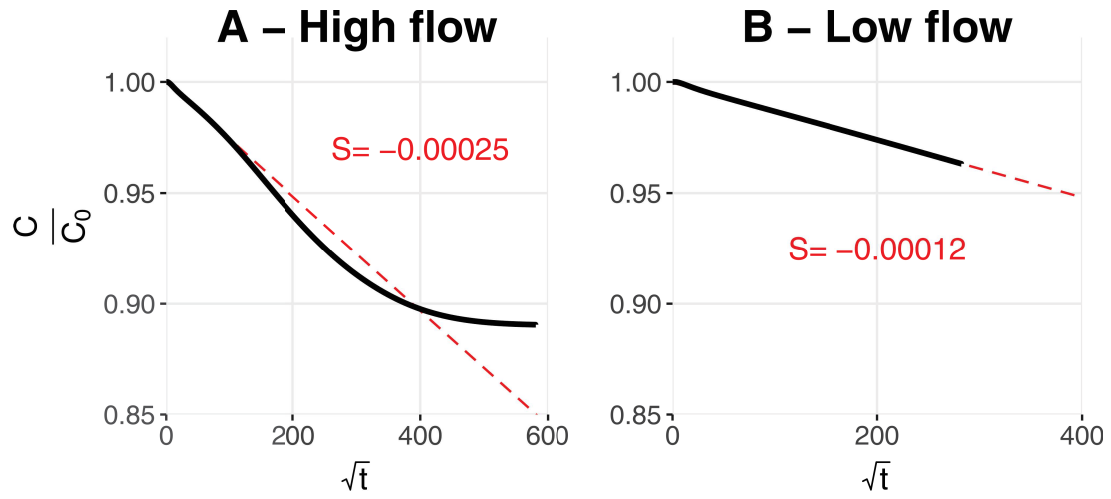


Figure B.S3 – Regression plot for the determination of S according to Eq. B.S15 in the case of IHF_{NaCl} (A) and ILF_{NaCl} (B).

Bibliography

- [Elliott and Brooks, 1997] Elliott, A. H. and Brooks, N. H. (1997). Transfer of non-sorbing solutes to a streambed with bed forms: Theory. *Water Resources Research*, 33(1):123–136.
- [Eylers et al., 1995] Eylers, H., Brooks, N. H., and Morgan, J. J. (1995). Transport of adsorbing metals from stream water to a stationary sand-bed in a laboratory flume. *Marine and Freshwater Research*, 46(1):209–214.
- [Fox et al., 2014] Fox, A., Boano, F., and Arnon, S. (2014). Impact of losing and gaining streamflow conditions on hyporheic exchange fluxes induced by dune-shaped bed forms. *Water Resources Research*, 50(3):1895–1907.
- [Grant and Marusic, 2011] Grant, S. B. and Marusic, I. (2011). Crossing turbulent boundaries: interfacial flux in environmental flows. *Environmental Science & Technology*, 45(17):7107–7113.
- [Grant et al., 2012] Grant, S. B., Stewardson, M. J., and Marusic, I. (2012). Effective diffusivity and mass flux across the sediment-water interface in streams. *Water Resources Research*, 48(5).
- [Gualtieri, 2010] Gualtieri, C. (2010). Numerical simulation of transition layer at a fluid-porous interface. In *Materials Science*, Ottawa, Canada.
- [Kaufman et al., 2017] Kaufman, M. H., Cardenas, M. B., Buttles, J., Kessler, A. J., and Cook, P. L. M. (2017). Hyporheic hot moments: Dissolved oxygen dynamics in the hyporheic zone in response to surface flow perturbations. *Water Resources Research*, 53(8):6642–6662.
- [Liao et al., 2013] Liao, Z., Lemke, D., Osenbrück, K., and Cirpka, O. A. (2013). Modeling and inverting reactive stream tracers undergoing two-site sorption and decay in the hyporheic zone. *Water Resources Research*, 49(6):3406–3422.

- [Marion et al., 2002] Marion, A., Bellinello, M., Guymer, I., and Packman, A. (2002). Effect of bed form geometry on the penetration of nonreactive solutes into a streambed. *Water Resources Research*, 38(10):27–1–27–12.
- [Nagaoka and Ohgaki, 1990] Nagaoka, H. and Ohgaki, S. (1990). Mass transfer mechanism in a porous riverbed. *Water Research*, 24(4):417–425.
- [Nikuradse, 1950] Nikuradse, J. (1950). Laws of Flow in Rough Pipes.
- [Ren and Packman, 2004] Ren, J. and Packman, A. I. (2004). Stream-subsurface exchange of zinc in the presence of silica and kaolinite colloids. *Environmental Science & Technology*, 38(24):6571–6581.
- [Rosti et al., 2015] Rosti, M. E., Cortelezzi, L., and Quadrio, M. (2015). Direct numerical simulation of turbulent channel flow over porous walls. *Journal of Fluid Mechanics*, 784:396–442.
- [Trauth et al., 2013] Trauth, N., Schmidt, C., Maier, U., Vieweg, M., and Fleckenstein, J. H. (2013). Coupled 3-D stream flow and hyporheic flow model under varying stream and ambient groundwater flow conditions in a pool-riffle system. *Water Resources Research*, 49(9):5834–5850.
- [Voermans et al., 2018] Voermans, J. J., Ghisalberti Marco, and Ivey Gregory N. (2018). A model for mass transport across the sediment-water interface. *Water Resources Research*, 0(0).

Appendix C

Supporting information to chapter IV

C.S1 *S*-metolachlor applications

The surveyed area was slightly wider than C1 and C2 catchments. Half of the farmer answers fell in the outside edges of C1 and C2, which limited catchment surfaces represented in the survey. However, surface depressions on the edges of C2, alongside the AVB and heightened river banks restricted the actual catchment area during extraction from GIS by surface flux accumulation analysis. A comprehensive and visual field investigation conducted in May 2019 precisely mapped crop distribution over the entire catchment, which allowed extrapolating survey results to missing areas.

S-metolachlor was applied first on sugar beets and then on maize. Three main application periods were identified from surveys while applications on Maize were mostly concomitant with nonetheless two minor applications reported on June 3.

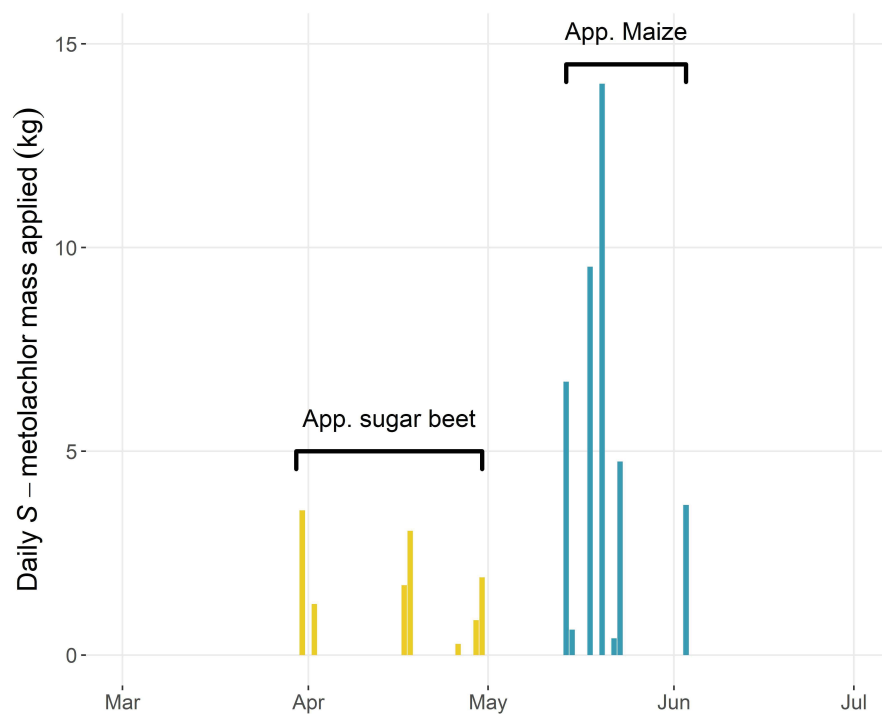
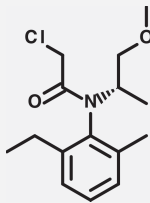


Figure C.S1 – Graphical summary of S-metolachlor application dates reported by farmers revealing three separated applications on sugar beets (yellow) and one major application over a 14 days long window on Maize (blue).

C.S2 *S*-metolachlor and main TPs summary of physico-chemical properties

Table C.S1 – Physicochemical properties of *S*-metolachlor (SM) and its major transformation products, metolachlor oxanilic acid (OXA) and metolachlor ethane sulfonic acid (ESA).

Active substance	<i>S</i> -metolachlor	OXA	ESA
Use			
Usage ¹	Herbicide	-	-
Approved/not in France ²	Approved	-	-
Crops	Maize and Sugar beet	-	-
General properties			
Chemical family	Chloroacetamide	-	-
Chemical structure		-	-
Chemical formula	$C_{15}H_{22}ClNO_2$	$C_{15}H_{21}NO_4$	$C_{15}H_{21}NO_5S$
Molecular mass ($g \cdot mol^{-1}$)	283.8	279.3	329.1
Water solubility ($g \cdot L^{-1}$)	480	-	-
Phase partitioning (K_{oc} - $mg \cdot g^{-1}$) ¹⁻³	190	17 -39	2 - 9
DT_{50} water-sediment system (d^{-1})	47.5	-	-
Degradation			
Pathways ⁴	Microbial (glutathione), hydrolysis, photolysis	-	-
Major transformation products ⁵	Metolachlor oxanilic acid (OXA), metolachlor ethane sulfonic acid (ESA)	-	-
Isotope composition			
CSIA of parent pesticide ($\delta^{13}C$ / $\delta^{15}N$) ⁶	Possible	-	-

- 1 - PPDB, 2020 (<http://sitem.herts.ac.uk/aeru/ppdb/>)
- 2 - E-phy (<https://ephy.anses.fr/>)
- 3 - (Capel et al., 2008) [Capel et al., 2008]
- 4 - (Katagi, 2006) [Katagi, 2006]
- 5 - (Fenner et al., 2013) [Fenner et al., 2013]
- 6 - (Elsayed et al., 2014; Elsner Imfeld, 2016) [Elsayed et al., 2014, Elsner and Imfeld, 2016]

C.S3 Hydrochemistry of the AVB river measured at S1 and S2

Hydrochemistry was characterized during grab samples only for major ions and DOC (n=7 and n=8 for S1 and S2). TSS are reported for grab and continuous samples (n=58 and n=69 for S1 and S2). Conductivity and temperatures are averaged values from continuous monitoring.

Table C.S2 – *Hydrochemistry over the entire monitoring campaign measured in S1 and S2 (continued over the two next pages).*

Station	S1	S2
TSS ($mg.L^{-1}$)		
Mean (SD)	2299.3 (7631.7)	1055.9 (2199.9)
Median (Q1, Q3)	230.0 (67.1, 642.8)	455.5 (93.6, 679.8)
Min - Max	1.9 - 49605.3	2.2 - 10998.2
pH		
Mean (SD)	8.6 (1.0)	8.6 (0.9)
Median (Q1, Q3)	8.6 (7.9, 9.4)	8.4 (8.0, 9.4)
Min - Max	7.1 - 9.9	7.6 - 9.7
Conductivity ($\mu S.cm^{-1}$)	(n=52 000)	(n=13 813)
Mean (SD)	582 (314)	1194 (252)
Median (Q1, Q3)	504 (438, 835)	1261 (1101, 1370)
Min - Max	/ - 10422	/ - 2925
Temperature ($^{\circ}C$)	(n=191 084)	(n=13 813)
Mean (SD)	13.7 (3.2)	13.2 (3.8)
Median (Q1, Q3)	14.1 (11.3, 16.3)	13.6 (10.3, 16.1)
Min - Max	/ - 22.3	/ - 21.8
DOC ($mg_C.L^{-1}$)		
Mean (SD)	2.2 (0.8)	3.8 (1.9)
Median (Q1, Q3)	1.8 (1.7, 2.6)	3.3 (2.4, 4.6)
Min - Max	1.3 - 3.7	2.0 - 7.4
Ammonium ($mg.L^{-1}$)		
Mean (SD)	0.8 (1.9)	0.2 (0.5)
Median (Q1, Q3)	0.0 (0.0, 0.2)	0.0 (0.0, 0.1)
Min - Max	0.0 - 5.0	0.0 - 1.2

Sodium ($mg.L^{-1}$)		
Mean (SD)	12.2 (1.0)	11.1 (2.6)
Median (Q1, Q3)	12.1 (11.5, 12.7)	11.0 (10.8, 13.0)
Min - Max	11.0 - 13.8	5.9 - 13.3
Potassium ($mg.L^{-1}$)		
Mean (SD)	4.5 (1.4)	3.7 (0.8)
Median (Q1, Q3)	4.1 (4.0, 4.1)	3.5 (3.2, 4.1)
Min - Max	3.8 - 7.6	2.9 - 4.9
Magnesium ($mg.L^{-1}$)		
Mean (SD)	69.0 (13.1)	63.7 (16.1)
Median (Q1, Q3)	68.9 (65.1, 78.6)	68.6 (58.7, 75.1)
Min - Max	43.9 - 82.5	32.1 - 77.9
Calcium ($mg.L^{-1}$)		
Mean (SD)	154.5 (25.7)	138.9 (42.6)
Median (Q1, Q3)	165.4 (149.1, 169.4)	161.2 (124.4, 168.7)
Min - Max	103.9 - 175.5	54.8 - 170.4
Chlorine ($mg.L^{-1}$)		
Mean (SD)	33.5 (3.5)	38.1 (11.8)
Median (Q1, Q3)	34.7 (32.9, 35.4)	42.8 (38.4, 44.1)
Min - Max	26.1 - 36.7	12.3 - 46.4
Nitrate ($mg.L^{-1}$)		
Mean (SD)	69.0 (13.1)	63.7 (16.1)
Median (Q1, Q3)	68.9 (65.1, 78.6)	68.6 (58.7, 75.1)
Min - Max	43.9 - 82.5	32.1 - 77.9
Sulfate ($mg.L^{-1}$)		
Mean (SD)	185.9 (36.9)	144.5 (51.3)
Median (Q1, Q3)	186.6 (181.8, 208.8)	139.7 (132.1, 180.5)
Min - Max	110.5 - 222.9	46.5 - 200.2
Phosphate ($mg.L^{-1}$)		
Mean (SD)	0.0 (0.0)	0.0 (0.0)
Median (Q1, Q3)	0.0 (0.0, 0.0)	0.0 (0.0, 0.0)
Min - Max	0.0 - 0.0	0.0 - 0.0
Hydrogenocarbonate ($mg.L^{-1}$)		
Mean (SD)	369.7 (124.2)	344.2 (145.7)
Median (Q1, Q3)	333.3 (303.8, 477.2)	286.4 (256.8, 431.6)
Min - Max	176.2 - 516.9	168.3 - 578.0

Carbonate ($mg.L^{-1}$)		
Mean (SD)	52.8 (65.3)	55.9 (68.4)
Median (Q1, Q3)	22.9 (3.8, 86.5)	14.6 (5.3, 96.7)
Min - Max	0.7 - 165.8	1.9 - 171.1
Nitrite ($mg.L^{-1}$)		
Mean (SD)	0.4 (1.2)	0.0 (0.0)
Median (Q1, Q3)	0.0 (0.0, 0.0)	0.0 (0.0, 0.0)
Min - Max	0.0 - 3.1	0.0 - 0.0
Total iron ($mg.L^{-1}$)		
Mean (SD)	0.0 (0.0)	0.0 (0.0)
Median (Q1, Q3)	0.0 (0.0, 0.0)	0.0 (0.0, 0.0)
Min - Max	0.0 - 0.0	0.0 - 0.0

C.S4 Example of GC-IRMS chromatogram with soil sample

Example of GC-IRMS chromatogram on soil sample (S1 on May 21 with $[S - met] = 107 \mu g.kg^{-1}$). Although the peak of *S*-metolachlor clearly ranks higher than others it is drawn in several preceding and following peaks responsible for a high background value slightly lower than 1000 mV. These peaks presumably originated from carbon of soil extracted during the liquid-solid extraction procedure. Consequently, proper integration of heavy and light *S*-metolachlor peaks were hampered. The liquid-solid extraction procedure was presumably too harsh for soil samples constituting complex soil matrices. Although this did not impact measurements of *S*-metolachlor concentrations by GC-MS (ionization in selected ion mass), as the GC-IRMS burns all carbons entering the oven, soil carbon likely mixed to *S*-metolachlor.

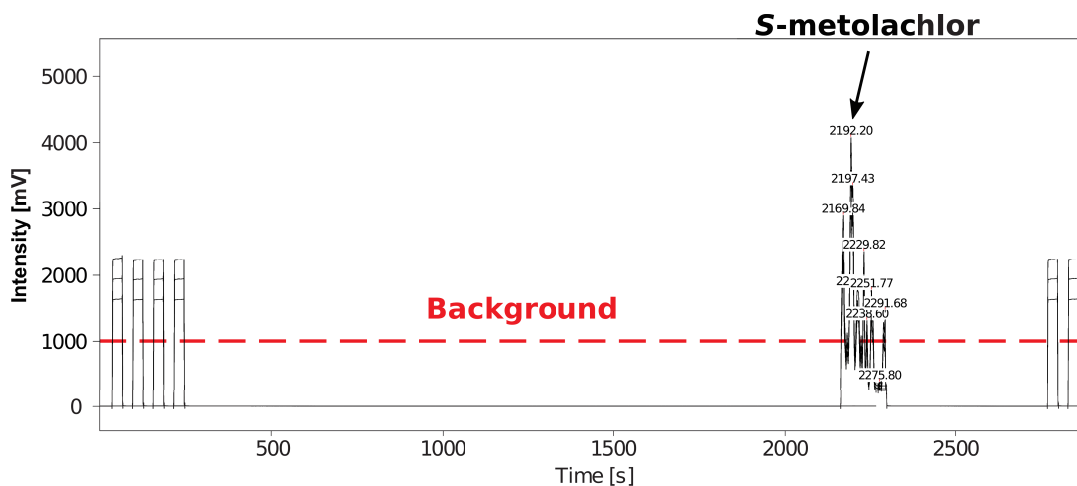


Figure C.S2 – Example of GC-IRMS chromatogram from soil sample in S1.

C.S5 Riverbed sediment texture

The AVB riverbed sediment consists in a very silty material (from 40 to 80%) with relatively low organic carbon content ($2.8 \pm 0.8\%$). Spatial heterogeneities alongside the AVB river reach occasionally led to riverbed sediment enriched with sand fractions up to 55%. Sediment permeability was not measured but estimated at $K = 3.2 \cdot 10^{-6} \text{ m.s}^{-1}$ from the Carman-Kozeny equation (Eq. C.S1 - [Carman, 1997]) considering the average median particle size $\phi_{50} = 33 \text{ }\mu\text{m}$ and porosity $\epsilon = 0.32$. Although sand explained in some cases more than 50% of the total sediment composition, the remaining fraction of silts is expected to be responsible for the low sediment permeability. Indeed, the maximal ϕ_{50} value was estimated at $82 \text{ }\mu\text{m}$.

$$K = \frac{\epsilon^3}{180 \cdot (1 - \epsilon)^2} \cdot \phi_{50}^2 \quad (\text{C.S1})$$

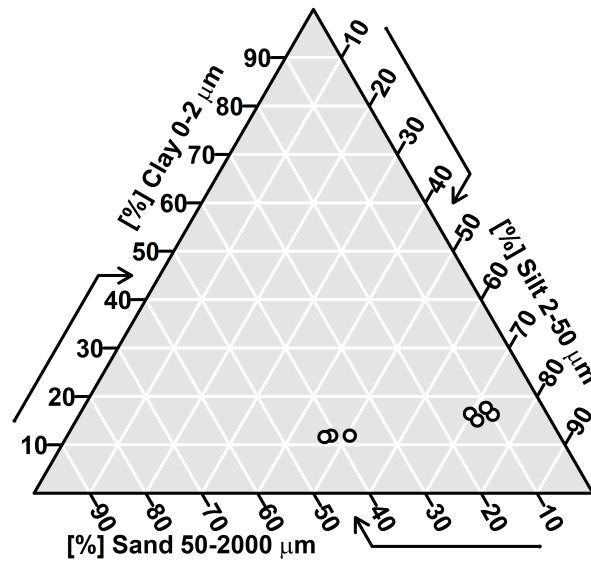


Figure C.S3 – Texture triangle of 7 riverbed sediment collected randomly alongside the Avenheimerbach river reach. Two main groups exist with 1) a quasi-exclusive dominance of silt materials and 2) a half-half mix of silt and sand materials. No spatial correlation from up to downstream was observed though.

C.S6 Temporal evolution of *S*-metolachlor concentrations within top soils surrounding S1 and S2.

As isotopic signatures of *S*-metolachlor could not be measured in soil samples, *S*-metolachlor soil stocks and its extent of degradation could not be directly deduced from the Rayleigh equation. However, according to a previously tested and validated methodology relying on laboratory characterizations of *S*-metolachlor biodegradation in agricultural clayey soils, one can accurately predict *S*-metolachlor degradation in field [Alvarez-Zaldívar et al., 2018]. To so, *S*-metolachlor degradation in soils is calculated according to Eq. C.S2 with a first-order kinetic ($k_{Dynamic} - [T^{-1}]$) controlled by soil temperature and moisture [N. Jarvis and M. Larsbo, 2012]:

$$k_{Dynamic} = k_{Ref} \cdot F_T \cdot F_{\Theta} \quad (C.S2)$$

where F_T stands for the soil temperature and F_{Θ} for soil water content.

The dependency on soil temperature complies with the Arrhenius law as in Eq. C.S3 [Walker, 1987]:

$$F_T = \begin{cases} 0 & \text{if, } T_C \leq 0 \\ \frac{T_{K,obs} - 273.15}{5} \cdot e^{\frac{E_a}{R} \cdot (\frac{1}{T_{K,ref}} - \frac{1}{T_{K,obs}})} & \text{if, } 0 < T_C \leq 5 \\ e^{\frac{E_a}{R} \cdot (\frac{1}{T_{K,ref}} - \frac{1}{T_{K,obs}})} & \text{if, } T_C > 5 \end{cases} \quad (C.S3)$$

where T_K and T_C are soil temperatures in Kelvin and Celsius, respectively and $T_{K,ref}$ is the reference temperature at 293.15 *K*. E_a is the *S*-metolachlor activation energy ($23.91 \cdot 10^3 \text{ J.mol}^{-1}$) and R is the gas constant ($8.314 \text{ L.mol}^{-1} \cdot \text{K}^{-1}$) [Jaikaew et al., 2017].

The dependency on soil water content follows Eq. C.S4 [Walker, 1987]:

$$F_{\Theta} = \min \left[1.0, \frac{\theta_t}{\theta_{ref}}^{\beta_{\theta}} \right] \quad (C.S4)$$

where β_{θ} is a calibration constant and θ_{ref} the reference water content, which was set constant over the season at 0.2 [L^3/L^3]. θ_t and $T_{K,obs}$ were computed at a 8 *km* spatial resolution by the national weather service with a soil water budget model first introduced in Noilhan Planton (1989) [Noilhan and Planton, 1989].

Initial *S*-metolachlor concentrations in soils were estimated from reported application rates. *S*-metolachlor doses were assumed to distribute within the top 10 cm of soils [Silva et al., 2019, Silva et al., 2020]. Bulk soil density was set at 1.2 g.cm^{-3} according to a long term monitoring within the catchment. This estimation likely introduces uncertainties on absolute *S*-metolachlor concentrations as bulk soil density may significantly increase (hence decreasing the predicted *S*-metolachlor concentrations) over the agricultural season while soil is tilled for instance [Alletto and Coquet, 2009, Kool et al., 2019]. As isotopic signatures could not be measured in soils, they were estimated from the predictions of *S*-metolachlor degradation in soils, according to the Rayleigh equation with $\epsilon_C = -1.4\text{‰}$ calibrated from a previous infield study close to our study catchment [Alvarez-Zaldívar et al., 2018] (see Figure C.S4).

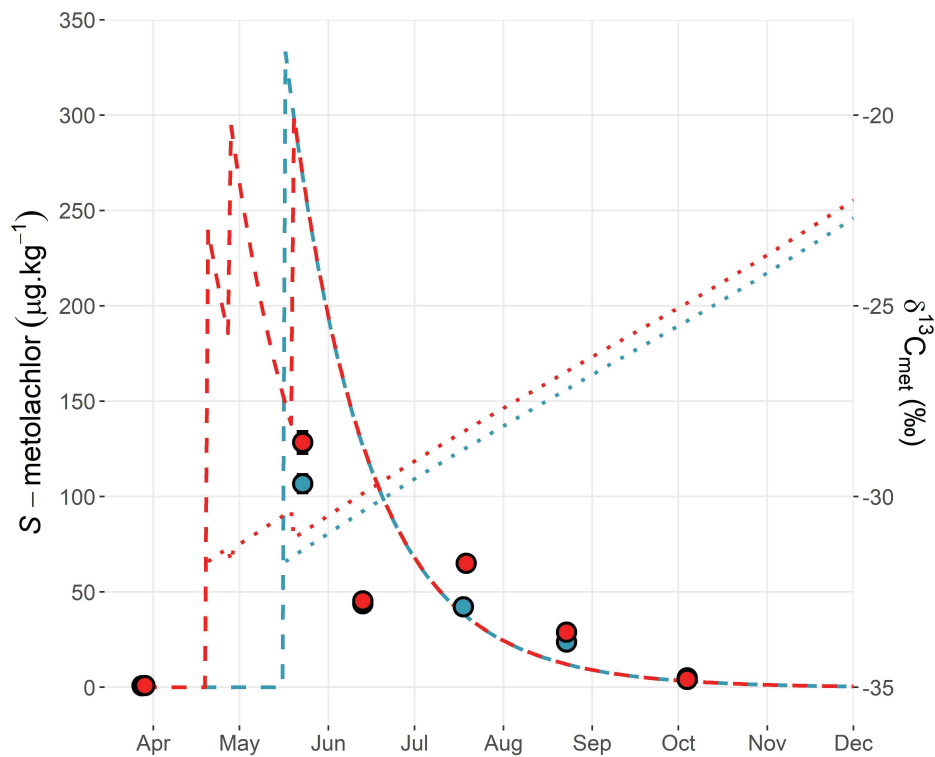


Figure C.S4 – Comparison of measured and predicted *S*-metolachlor soil concentrations around S1 (blue) and S2 (red). Points stand for the measured and dashed lines for the predicted concentrations. Dotted lines correspond to the predicted isotope fractionation accounting.

C.S7 Test of isotopic signatures shift within the AVB river reach

To test whether instream degradation may be inferred from changes in *S*-metolachlor isotopic signatures in between S1 and S2 (H_1 : Significant variations of *S*-metolachlor isotopic signatures caused by instream degradation are measured between S1 and S2, H_0 : Variations of *S*-metolachlor isotopic signatures between S1 and S2 are negligible) an analysis of covariance (ANCOVA) was performed. To do so, ANCOVA was applied with monitoring stations S1 and S2 as qualitative variables representing the group of populations to be compared and $\delta^{13}C$ as quantitative variable. ANCOVA is traditionally used in clinical studies aiming at inferring treatment effect from the difference between a treated and untreated group (*i.e.* qualitative variable) on a quantitative variable (*e.g.* blood pressure) also considering the influence of a covariate (*e.g.* baseline - pre-test blood pressure) [Van Breukelen, 2006]. The effect of the covariate in-field degradation (temporal evolution of $\delta^{13}C$ corresponding to the analysis baseline) was eliminated from the influencing factors by comparing intercepts of temporal regressions of $\delta^{13}C$ *vs* time. The procedure developed here follows guidelines published in Leppink (2018) [Leppink, 2018].

Only *S*-metolachlor isotopic signatures characteristic of subsurface transport processes are included in the statistical analysis here, as during rainfall runoff event 8, $\delta^{13}C$ values were proved to reflect punctual mobilization of undegraded fractions.

- I. Linear relationships were tested independently for both groups (*i.e.* S1 and S2) and revealed significant with $p < 0.05$ in each case (see Figure C.S5 and C.S6).
- II. Homogeneity of regression slopes (called “interaction terms”) is tested to ensure the ANCOVA to be performed without effects from the covariate. To do so a t-test is performed with the null hypothesis H_0 , stating that $Slope_1 = Slope_2$, *i.e.* $Slope_1 - Slope_2 = 0$ and the complementary hypothesis H_1 , that $Slope_1 \neq Slope_2$, *i.e.* $Slope_1 - Slope_2 \neq 0$. In this case $p = 0.05$ and we cannot reject H_0 validating the homogeneity of slopes (*i.e.* slopes are considered equal).
- III. Finally, we test similarities of the intercepts, the same way we did for slopes and conclude to debatable differences in regression intercepts with a threshold of 5% ($|\Delta_{S1-2}\delta^{13}C| = 0.6\text{‰}$, $p = 0.04$). However, the observed more negative values in S2 than S1 are inconsistent with the expected normal isotopic shift occurring

over biodegradation and the value of $|\Delta_{S1-2}\delta^{13}C|$ is close to the analytical limit. On these basis, we conclude to no significant instream degradation alongside the studied AVB river reach.

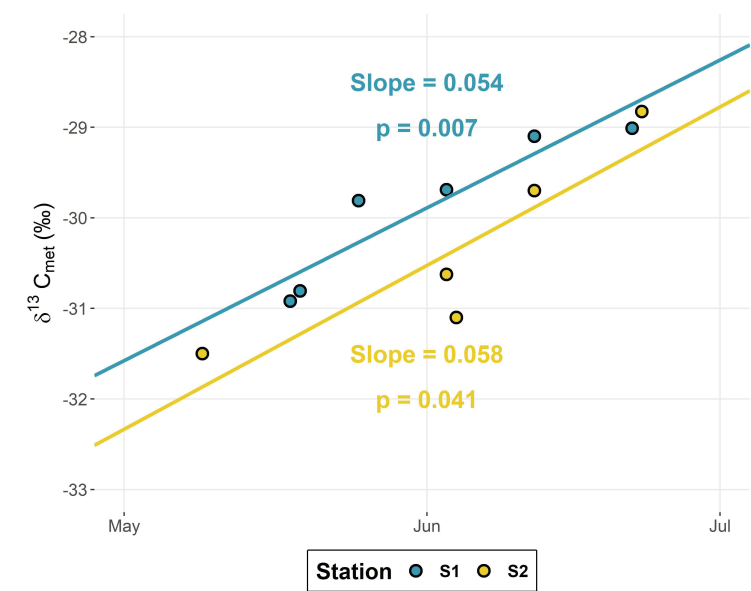


Figure C.S5 – Linear regressions for S1 and S2 on $\delta^{13}C$ values vs time.

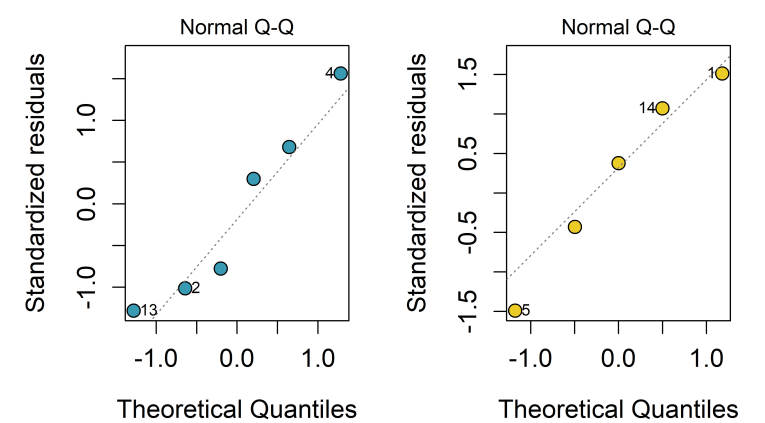


Figure C.S6 – Validation of the normal distribution of the regression residuals. This condition is necessary for the next steps testing equalities of slopes and intercepts.

C.S8 Averaged transit time and degradation within the AVB river reach

Considering no retardation effects in accordance with limited interactions of *S*-metolachlor with the sediment riverbed [Lemke et al., 2013], the average transit time of dissolved species within the AVB river reach in between S1 and S2 is associated to the water travel time. As exemplified in Figure C.S7, a V-shape channel geometry of averaged width 6.5 *m* and depth 1.5 *m* ($m = 6,5/1.5 = 4.3$ the channel bank slope) can be considered as representative of the whole AVB river reach. Under uniform and steady state conditions, the normal water height in the river can be estimated with the Manning-Strickler relationship (Eq. C.S5) [Akan, 2006]. For clayey river beds a Manning roughness (*n*) of 0.030 is indicated [Akan, 2006].

$$Q_n = K_s \cdot S \cdot n R_h^{2/3} \cdot \sqrt{I} \quad (\text{C.S5})$$

where Q_n [L^3/T] refers to the normal velocity, K_s [$L^{1/3}/T$] to the Strickler coefficient and equals $K_s = 1/n$, R_h [*L*] to the hydraulic radius defined as $R_h = S/P$ with P [*L*] being the wetted perimeter and S [L^2] the cross-sectional area, and I [L/L] to the averaged channel slope.

Under low flow conditions, considering an averaged water flow in between S1 and S2 to range between $5 \cdot 10^{-3}$ and $10 \cdot 10^{-3} \text{ m}^3 \cdot \text{s}^{-1}$, one can determine the normal water height (h_n [*L*]) to lie between 6 and 8 *cm* within the channel according to numerical application of Eq. C.S5. Thus, applying Eq. C.S6, the average velocity (v_n) under low flow conditions is estimated between 33 and 40 *cm.s*⁻¹. Finally, considering the total length of the AVB river reach of 2200 *m*, under low flow conditions, *S*-metolachlor transit time within the AVB is estimated between 1.4 and 1.7 *h*.

$$Q_n = \frac{v_n}{S} = \frac{v_n}{m \cdot h_n^2} \quad (\text{C.S6})$$

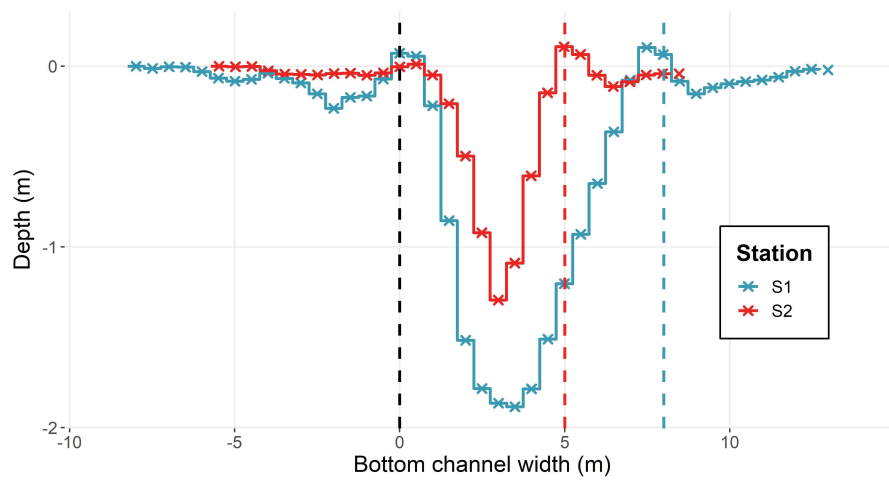


Figure C.S7 – Cross section profiles near S1 and S2 revealing a V shaped channel of depth comprised between 1.2 and 1.9 m and width between 5 and 8 m.

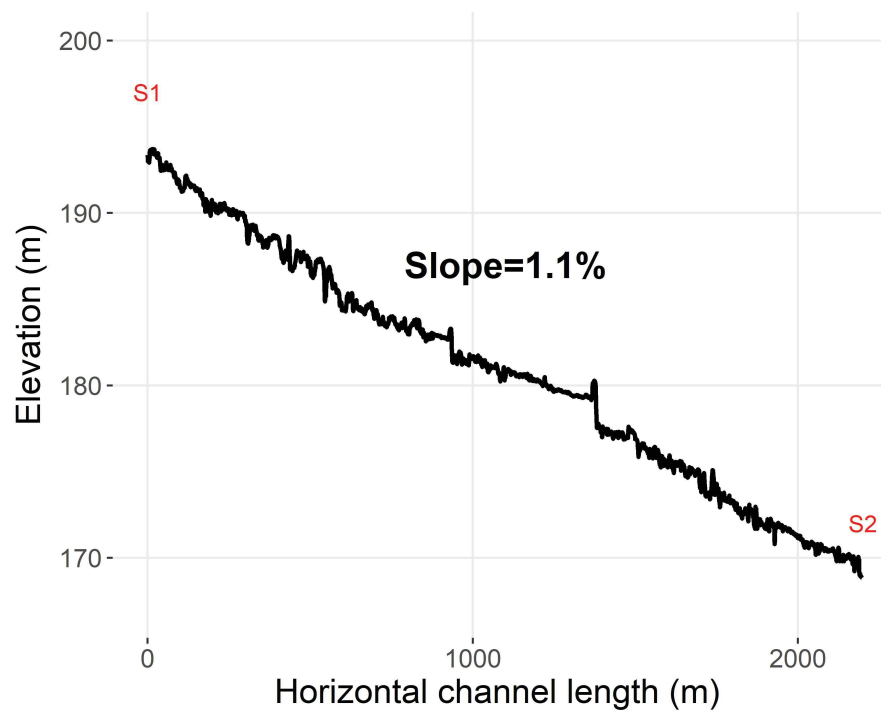


Figure C.S8 – Elevation profile of the AVB transect in between S1 and S2. Mean slope is 1.1%.

C.S9 Evidences of *S*-metolachlor release from the riverbed from monitoring of the regional water agency

Grab samples punctually conducted by the regional water agency reinforce the analysis of event 8. Punctual *S*-metolachlor measurements all along the monitoring season revealed *S*-metolachlor concentrations $< 0.11 \mu\text{g.L}^{-1}$ (right after applications during high flow conditions on April 5) except 8 days after event 8 (June 27) where *S*-metolachlor peaked at $0.3 \mu\text{g.L}^{-1}$ (see Figure C.S9). During rainfall event such a peak would have been easily explained by enhanced *S*-metolachlor transport from field to the river. However, on June 27 low flow conditions were already established for a few days and *S*-metolachlor was not likely originating from field but more from the riverbed itself.

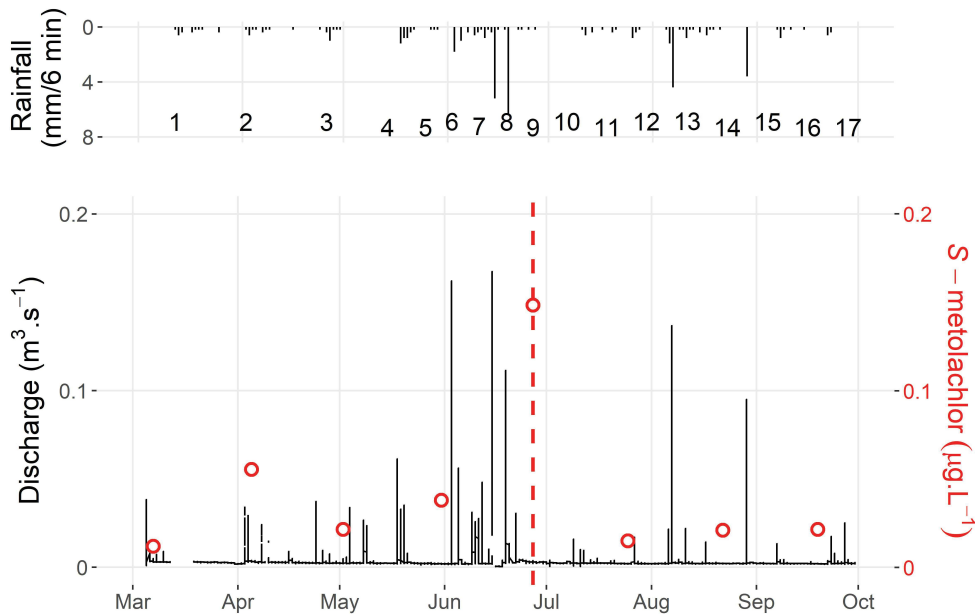


Figure C.S9 – Temporal evolution of *S*-metolachlor concentrations as measured by the regional water agency. Rainfall events and their number are reminded in the upper panel while *S*-metolachlor concentrations are plotted along with the S1 hydrogram in the bottom panel. The red dashed line locates the sampling time (June 27) on the hydrogram and clearly show the long established low flow conditions at that time

C.S10 Temporal evolution of *S*-metolachlor concentrations in the riverbed sediment

S-metolachlor concentrations in the riverbed sediment almost systematically ranged below the quantification limit (see Figure C.S10). Nonetheless, in April 2nd a punctual and huge contamination of $11.9 \pm 0.5 \mu\text{g.kg}_{\text{sediment}}^{-1}$ was measured in S1 sediments which cannot easily be rationalized in the absence of water measurements of *S*-metolachlor at that time. One may assume accidental pollution consecutive to the first *S*-metolachlor applications or laboratory mishandling. On July 17, although almost 1 month after the runoff event, *S*-metolachlor residues seemed to remained within the sediment bed with *S*-metolachlor exceptionally ranging slightly above the quantification limit.

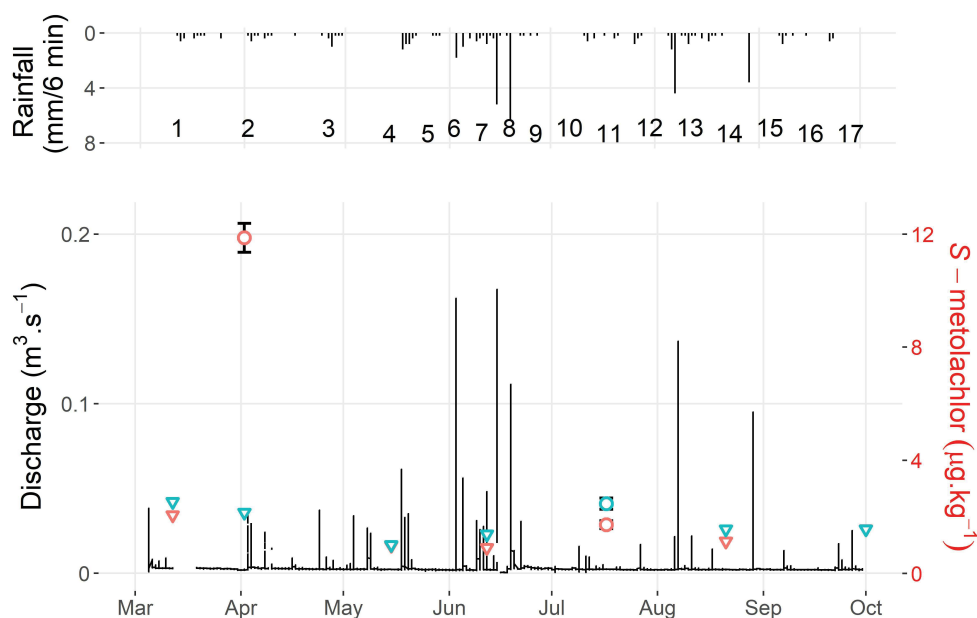


Figure C.S10 – Temporal evolution of *S*-metolachlor concentrations within the riverbed sediment in S1 (orange) and S2 (blue). Rainfall events and their number are reminded in the upper panel. In the bottom panel, circles refer to *S*-metolachlor concentrations measured higher than the quantification limit while are used when *S*-metolachlor were not quantifiable and stand for the quantification limit. Discharge refer to S1.

C.S11 Excepted isotope fractionation with increasing residence time

Despite the negligible enrichment observed in the AVB, CSIA may prove useful for larger rivers displaying significantly longer residence time. In addition, for longer river reach the retardation caused by pollutant penetration and sorption into the sediment bed may further exacerbate instream degradation. Although retardation factors are very case- and molecule-specific a higher-bound value of 2 may be considered for testing the potential of CSIA to quantify instream degradation over long rivers [Liao et al., 2013, Salehin et al., 2003]. The laboratory derived photodegradation and biodegradation half-lives of *S*-metolachlor of 6 and 30 days and enrichment factors of $\epsilon_N = -0.7 \pm 0.4\text{‰}$ for photodegradation and $\epsilon_C = -1.2 \pm 0.4\text{‰}$ for biodegradation were considered. As photodegradation and biodegradation co-occur in rivers, the Rayleigh equation was corrected according to Van Breukelen et al. (2007) [Van Breukelen, 2007] (Eq. C.S7):

$$\epsilon_{eff} = \frac{k_{photo} \cdot \epsilon_{photo} + k_{biodeg} \cdot \epsilon_{biodeg}}{k_{photo} + k_{biodeg}} \quad (\text{C.S7})$$

with ϵ_{eff} the effective enrichment factor to be re-injected in the Rayleigh equation.

Accordingly, for *S*-metolachlor, isotope enrichment in C higher than the threshold of $\Delta\delta^{13}C = 2.0\text{‰}$ is expected to be achieved for rivers with equivalent water transit time > 400 hours. No equivalent river length is expressed as long equivalent transit times like this one correspond to high Strahler order rivers with water flows and velocities varying at each confluence.

Bibliography

- [Akan, 2006] Akan, A. O. (2006). 3 - Normal flow. In Akan, A. O., editor, *Open Channel Hydraulics*, pages 67–96. Butterworth-Heinemann, Oxford.
- [Alletto and Coquet, 2009] Alletto, L. and Coquet, Y. (2009). Temporal and spatial variability of soil bulk density and near-saturated hydraulic conductivity under two contrasted tillage management systems. *Geoderma*, 152(1):85–94.
- [Alvarez-Zaldívar et al., 2018] Alvarez-Zaldívar, P., Payraudeau, S., Meite, F., Masbou, J., and Imfeld, G. (2018). Pesticide degradation and export losses at the catchment scale: Insights from compound-specific isotope analysis (CSIA). *Water Research*, 139:198–207.
- [Capel et al., 2008] Capel, P. D., McCarthy, K. A., and Barbash, J. E. (2008). National, Holistic, Watershed-Scale Approach to Understand the Sources, Transport, and Fate of Agricultural Chemicals. *Journal of Environmental Quality*, 37(3):983–993.
- [Carman, 1997] Carman, P. C. (1997). Fluid flow through granular beds. *Chemical Engineering Research and Design*, 75:S32–S48.
- [Elsayed et al., 2014] Elsayed, O. F., Maillard, E., Vuilleumier, S., Nijenhuis, I., Richnow, H. H., and Imfeld, G. (2014). Using compound-specific isotope analysis to assess the degradation of chloroacetanilide herbicides in lab-scale wetlands. *Chemosphere*, 99:89–95.
- [Elsner and Imfeld, 2016] Elsner, M. and Imfeld, G. (2016). Compound-specific isotope analysis (CSIA) of micropollutants in the environment — current developments and future challenges. *Current Opinion in Biotechnology*, 41:60–72.
- [Fenner et al., 2013] Fenner, K., Canonica, S., Wackett, L. P., and Elsner, M. (2013). Evaluating Pesticide Degradation in the Environment: Blind Spots and Emerging Opportunities. *Science*, 341(6147):752–758.

- [Jaikaew et al., 2017] Jaikaew, P., Malhat, F., Boulange, J., and Watanabe, H. (2017). Aspect of the degradation and adsorption kinetics of atrazine and metolachlor in andisol soil. *Hellenic Plant Protection Journal*, 10(1):1–14.
- [Katagi, 2006] Katagi, T. (2006). Behavior of Pesticides in Water-Sediment Systems. In Ware, G. W., Albert, L. A., Voogt, P. d., Gerba, C. P., Hutzinger, O., Knaak, J. B., Mayer, F. L., Morgan, D. P., Park, D. L., Tjeerdema, R. S., Whitacre, D. M., Yang, R. S. H., and Gunther, F. A., editors, *Reviews of Environmental Contamination and Toxicology*, number 187 in Reviews of Environmental Contamination and Toxicology, pages 133–251. Springer New York.
- [Kool et al., 2019] Kool, D., Tong, B., Tian, Z., Heitman, J. L., Sauer, T. J., and Horton, R. (2019). Soil water retention and hydraulic conductivity dynamics following tillage. *Soil and Tillage Research*, 193:95–100.
- [Lemke et al., 2013] Lemke, D., Liao, Z., Wöhling, T., Osenbrück, K., and Cirpka, O. A. (2013). Concurrent conservative and reactive tracer tests in a stream undergoing hyporheic exchange. *Water Resources Research*, 49(5):3024–3037.
- [Leppink, 2018] Leppink, J. (2018). Analysis of Covariance (ANCOVA) vs. Moderated Regression (MODREG): Why the Interaction Matters. *Health Professions Education*, 4(3):225–232.
- [Liao et al., 2013] Liao, Z., Lemke, D., Osenbrück, K., and Cirpka, O. A. (2013). Modeling and inverting reactive stream tracers undergoing two-site sorption and decay in the hyporheic zone. *Water Resources Research*, 49(6):3406–3422.
- [N. Jarvis and M. Larsbo, 2012] N. Jarvis and M. Larsbo (2012). MACRO (v5.2): Model Use, Calibration, and Validation. *Transactions of the ASABE*, 55(4):1413–1423.
- [Noilhan and Planton, 1989] Noilhan, J. and Planton, S. (1989). A Simple Parameterization of Land Surface Processes for Meteorological Models. *Monthly Weather Review*, 117(3):536–549.
- [Salehin et al., 2003] Salehin, M., Packman, A. I., and Wörman, A. (2003). Comparison of transient storage in vegetated and unvegetated reaches of a small agricultural stream in Sweden: seasonal variation and anthropogenic manipulation. *Advances in Water Resources*, 26(9):951–964.

- [Silva et al., 2020] Silva, V., Gonzalez-Pelayo, O., Abrantes, N., Keizer, J. J., Mol, H., Ritsema, C., and Geissen, V. (2020). Pesticide residues in vineyard soils and water-eroded sediments - predictions versus observations. 22:10656.
- [Silva et al., 2019] Silva, V., Mol, H. G. J., Zomer, P., Tienstra, M., Ritsema, C. J., and Geissen, V. (2019). Pesticide residues in European agricultural soils – A hidden reality unfolded. *Science of The Total Environment*, 653:1532–1545.
- [Van Breukelen, 2007] Van Breukelen, B. M. (2007). Quantifying the Degradation and Dilution Contribution to Natural Attenuation of Contaminants by Means of an Open System Rayleigh Equation. *Environmental Science & Technology*, 41(14):4980–4985.
- [Van Breukelen, 2006] Van Breukelen, G. J. (2006). ANCOVA versus change from baseline had more power in randomized studies and more bias in nonrandomized studies. *Journal of Clinical Epidemiology*, 59(9):920–925.
- [Walker, 1987] Walker, A. (1987). Evaluation of a simulation model for prediction of herbicide movement and persistence in soil. *Weed Research*, 27(2):143–152.

